The influence of surface roughness on runoff generation and soil erosion in semi-arid Environments

Mark Smith

The Influence of Surface Roughness on Runoff Generation and Soil Erosion in Semi-Arid Environments

Mark Smith

MSc

Department of Geography

University of Durham

September 2005

Acknowledgements

First and foremost, I would like to thank my supervisors Dr Louise Bracken and Dr Nick Cox for their help with this project. Louise's guidance and support, particularly during the planning and fieldwork stages of the project, was invaluable, and without Nick's assistance with the data analysis side of the project I would still be number-crunching.

Second, thanks must go to Mike Lim and in particular Dr Nick Rosser for showing remarkable patience and answering all my queries regarding the laser scanner and numerous software packages. Derek Karssenberg and the PCRaster team at Utrecht University also provided the software necessary for this investigation.

Thanks to Professor Mike Kirkby at Leeds University who provided a host of helpful suggestions and an exceptional tour of the catchments. Mike gave me an unparalleled 'crash-course' on driving hire-cars on dry river beds and getting the full deposit back. Louise and Mike also provided the sediment transport and hillslope runoff data used in this study. Thanks must also go to Emma Waterhouse for her assistance in the field and for remaining good-spirited when the conditions were hardly as advertised.

Finally, I would like to thank my parents and grandparents for all their support during this past year and during my first degree. At last, here's what all that fuss was about (but don't feel like you have to read all of it!).

Abstract

Geomorphology is essentially the study of rough surfaces; perfectly smooth, natural surfaces are extremely rare on Earth. There is no single property that can defined as 'surface roughness'; it can be characterised in a variety of ways. Therefore the selection of any roughness measure should be made in consideration of its proposed use. Recent developments in laser scanning technology have removed many of the constraints of analysing surface roughness at the hillslope scale and in natural environments. Such advances have increased the availability of topographic data so that a re-examination of common methods of characterising surface roughness is in order.

This investigation compares the utility of numerous roughness measures for representing particular surface features relevant to less-measurable hydrological processes operating on soil surfaces in two contrasting semi-arid catchments. Roughness oriented in the down-slope direction is related to depressional storage, whereas that element of roughness identified from cross-slope transects represents the convergence of flow-paths as a result of microtopography. Measures that identified a specific feature of rough surfaces perform well; however, the large range of soil surface features and processes exhibited at the hillslope scale limits the ability of general roughness measures (such as the standard deviation of elevations) to represent specific hydrological processes. The division of a semi-arid hillslope into 'Morphological Runoff Zones' provides a suitable background knowledge of the nature of the soil surfaces through which subsequent fine-scale roughness measures can be considered.

Spatially variable processes acting on the soil surface and the nature of the soil surface are interdependent. In semi-arid environments where Hortonian overland flow is dominant, the microtopography of natural soil surfaces is partly determined by the balance between the erosive force of raindrop impact and shear stress caused by overland flow concentrations. Microtopography combines with larger-scale topographic roughness to determine the upslope area of any point of a hillslope. The distribution of areas of water retention and detention with respect to flow concentrations and flow depths also influences the downslope transport of runoff and sediment. Depression storage preferentially occurs in flow concentrations. These are the first areas of the surface where the depression storage capacity will be satisfied.

Knowledge of the spatial configuration of roughness elements and connectivity of responsive areas to the main channel network is important for understanding runoff generation. Measures of surface roughness can also be used to identify units of particular hydrological response and determine their distribution across a hillslope. Placed in the context of large-scale topographic variation of the hillslopes, this reveals suitable criteria for generalising from one hillslope to another.

Contents

Figures

Tables

Chapter 1 Introduction

1.1 Background

The sensitivity of semi-arid environments to geomorphological change means that understanding runoff response and soil erosion is particularly important. However, the processes contributing to the spatially non-uniform generation of runoff and soil erosion in these environments remain relatively poorly understood at the hillslope scale (Fitzjohn *et al.*, 1998). The prediction of runoff production and soil erosion is necessary to assess flood risks and plan flood mitigation works (Martínez-Mena *et al.*, 1998); and with the intense nature of storm events in semi-arid areas (Bull *et al.*, 1999), combined with the torrential nature of floods and their devastating economic and social impacts (Hooke & Mant, 2000), this issue is especially crucial.

The spatially variable processes acting on the soil surface and the soil surface itself are interdependent. Concepts such as 'morphological runoff zones' (MRZs) (Bracken & Kirkby, 2005) have been developed to analyse this relationship at the hillslope scale. An understanding of the processes acting at this scale is essential for the development of effective management techniques for limiting erosion and soil degradation in semi-arid environments (Bergkamp, 1998).

Geomorphology is essentially the study of rough surfaces; perfectly smooth, natural surfaces are extremely rare on Earth. The roughness of soil surfaces is a property that is either ignored or given an extremely basic treatment in hydrological models. However, soil surface roughness affects hydrologic and erosion processes in many ways. It has been shown to influence storage of water on the soil surface, rate of infiltration through the surface, and soil erosion. Therefore, surface roughness deserves consideration in models of hydrologic and erosion processes.

However, surface roughness also affects flowpaths of subsequent runoff, the organisation of drainage patterns and the connectivity of the landscape. These processes are significant at a larger scale than that considered in models applicable to small plots. At present, we understand little about the processes operating at the hillslope scale; specifically to what extent studies conducted at the plot scale may simply be extrapolated, and what thresholds are crossed in doing so? A greater understanding of

surface roughness may play a large role in determining those thresholds and work towards bridging the gap between plot-scale models and large-scale landscape models which operate at a coarser resolution, often using remotely sensed data.

Surface roughness is a vague concept, and as such, it can be made precise in many ways (compare Mosteller & Tukey, 1977). Mark (1975: p.165) suggests that "all aspects of surface form can be considered to reflect surface roughness": therefore all measures of surface form are in some way representative of the 'roughness' of the surface. Geomorphometry is the branch of geomorphology which attempts to quantitatively describe form of the land surface (Chorley *et al.*, 1957); the study of soil surface roughness is suited to what Evans (1972: p.18) labels a '*general geomorphometric approach*': "the measurement and analysis of those characteristics of landforms which are applicable to any continuous rough surface".

Recent technological advances have decreased the time and effort required for the collection and processing of topographic data; this has brought renewed momentum to the science of geomorphometry. Several different measurements of surface roughness taken from profiles have been used to predict depression storage and outflow at the plot scale (e.g. Onstad, 1984) with varying degrees of success (Kamphorst *et al.*, 2000). Additionally, several studies have begun to examine the relationship between surface roughness and the hydraulics of overland flow and subsequent soil erosion (Gilley & Finkner, 1991; Takken & Govers, 2000; Helming *et al.*, 1998; Gómez & Nearing, 2005).

Recent flume studies conducted on a soil surface with a greater area (~2 m across slope and 4 m downslope; Helming *et al.*, 1998; Gómez & Nearing, 2005) have produced controversial results, contradicting earlier studies by suggesting that increasing roughness may increase erosion rates. These results prompted Gómez & Nearing (2005: p.253) to suggest that "...commonly held perceptions of the impact of soil surface roughness on runoff and erosion may not be entirely correct". These studies are rarely undertaken on natural soil surfaces and are usually restricted to plot scale measurements (~1 m ×1 m).

Plot scale investigations cannot take account of the 'spatial mosaic' of roughness elements and connectivity of responsive areas to the main channel (Fitzjohn *et al.*, 1998). These factors can now be assessed more accurately through the development of new techniques such as terrestrial laser scanning and GIS treatments of DEMs. Additionally, these techniques can potentially be applied to acquire data on surface roughness, depression storage and flow route-ways at wider scales than traditionally available.

Different linkages between erosion processes and surface morphology operate at different landscape scales. Therefore, an analysis of surface roughness from plot to hillslope scale may contribute to an increased understanding of this notion of scale dependency in hillslope hydrology (Bergkamp, 1998), allowing analysis of the effect of emergent properties such as the formation of rill and gully networks.

1.2 Aims & Objectives

The overall aim of this project is to assess the influence of soil surface roughness upon runoff generation, depression storage, overland flow hydraulics and soil erosion and to scale up these results from the plot to the hillslope scale.

The following specific objectives may be identified:

1. To assess the accuracy and applicability of several surface roughness measurements used to predict depression storage and runoff.
2. To determine how plot-scale outflow and depression storage vary between 'Morphological Runoff Zones' (MRZs) in different soil-types by simulating flow routeways using plot-scale DEMs.
3. To examine the relationships between surface morphology, infiltration and soil erosion on the hillslope by combining these plot scale results with measurements of infiltration, sediment transport and flow depth taken in different MRZs.
4. To examine briefly how the conversion of natural soil surfaces to ploughed fields influences these processes.
5. To combine these results at the hillslope scale using a larger-scale DEM displaying the spatial configuration of MRZs and land-uses to assess the degree of connectivity on a variety of hillslopes.

These will be achieved by obtaining plot-scale elevation data from a laser scanner and calculating depression storage capacity from the resulting DEMs. Each plot will be located in different MRZs (and on any land converted to ploughed fields) on three hillslopes in south-east Spain which demonstrate contrasting responses to rainfall. The semi-arid environment of south-east Spain supports only sparse vegetation cover on these hillslopes, therefore the interdependency between soil surface morphology and the processes acting upon the surface is particularly apparent. This site was chosen as it offers an extensive opportunity for research into surface roughness on natural surfaces. Infiltration measurements were taken on each plot, and these will be combined with sediment transport and hillslope runoff data obtained as part of an ongoing project. These results will then be combined with a hillslope-scan upon which the arrangement of MRZs and land-uses will be displayed.

1.3 Thesis Structure

Chapter 2 provides an overview of the ways in which soil surface morphology affects runoff generation, overland flow and sediment transport in semi-arid environments. In addition, this chapter provides a critique of several methods of characterising surface roughness commonly applied in present literature (section 2.6). Chapter 3 then details the field sites and methodology of this study. The results of this investigation are divided between two chapters. Chapter 4 examines the variation of several methods of characterising surface roughness between each surface considered, while chapter 5 deals with how this surface roughness affects the hydrological properties of the surfaces (surface water storage, runoff routing, infiltration and sediment transport).

Chapter 6 combines the results of the previous two chapters, suggesting how measures of surface roughness can be practically applied to enhance our understanding of runoff generation and sediment transport at the hillslope scale. Finally, research conclusions are presented in chapter 7.

Chapter 2 Surface Roughness in Semi-Arid Environments

2.1 Introduction

This chapter reviews the ways in which soil surface morphology affects runoff generation, overland flow and soil erosion in semi-arid environments and the ways in which variations in surface topography have been characterised by roughness indices. The characteristics of surface roughness and the factors affecting it are discussed in section 2.2. Section 2.3 describes the relationships between surface roughness and runoff generation, overland flow hydraulics and soil erosion, while section 2.4 briefly considers the influence of surface roughness on landscape connectivity. The scale dependency of surface roughness is examined in section 2.5, while section 2.6 provides a critique of the various ways in which surface roughness has been quantified and used to predict surface properties, particularly maximum depressional storage. Section 2.7 summarises how knowledge of the influences of surface roughness on runoff generation and soil erosion may be incorporated into process-based, spatially-distributed erosion prediction models. Finally, conclusions and research gaps are presented in section 2.8.

2.2 Factors Affecting Surface Roughness in Semi-Arid Environments

Essentially, 'roughness' refers to the irregular shape of the surface of the Earth; measures of surface roughness consider surface topographic variations. Such measures often define roughness as some function of the variance of the residual distances of points from a planar trend surface fitted through them (Campbell & Honsaker, 1982). However there is no single property that can defined as 'surface roughness'; it can be characterised in a variety ways, and so a number of different methods of measuring surface roughness exist. These are discussed in section 2.6.

Surface roughness is a fundamental parameter in all areas of process geomorphology (Lane, 2005). Microtopography has been shown to influence surface depression storage (Onstad, 1984), infiltration and its variability (Fox *et al.* 1998a), evaporation (Allmaras *et al.*, 1977), solar radiation reflection (Allmaras *et al.*, 1972), overland flow hydraulics

(Moore & Larson, 1979; Gilley & Finkner, 1991; Takken & Govers, 2000), soil erosion and sediment transport (Cogo *et al.*, 1983; Helming *et al.*, 1998; Gómez & Nearing, 2005) and water routing (Darboux *et al.*, 2002). However, little work has been directed at quantifying these roughness effects.

The soil surface acts as the interface between the erosive forces of rainfall and runoff and the eroding soil itself. Throughout a rainfall event the morphology of the soil surface is continuously adjusting in response to these surface processes, and likewise, surface processes are influenced by surface topography. Therefore, soil development reflects runoff patterns through the process of erosion (or deposition) and the distribution of soil moisture (Kuhn & Yair, 2004; Solé-Benet *et al.*, 1997). As a result the soil surface bears the 'footprint' of the action of spatially varying processes (Huang & Bradford, 1993).

While analysis of soil microtopography may reveal the physical processes responsible for its development, this strong interrelationship between surface processes and microtopography is somewhat tempered by the presence of a vegetation cover through its interaction with the underlying soil (Kirkby, 2001). Consequently, much of the current literature examining the nature of soil surface roughness considers tilled areas of temperate environments. This has led to a paucity of studies on soil surfaces that are not routinely subjected to direct anthropogenic disturbance. Many of the principles and methods surrounding the study of surface roughness are equally applicable to other areas of exposed soil surfaces, irrespective of geographical location. Semi-arid and arid environments demonstrate large areas of exposed soil surfaces due to the limited extent of vegetation cover. Therefore, the interdependency between soil surface morphology and the processes acting upon the surface is particularly apparent in such areas, offering an extensive opportunity for research into surface roughness on natural surfaces. Despite this opportunity, studies of surface roughness in semi-arid areas (such as that of Bergkamp, 1998) remain extremely rare.

Cremers *et al.* (1996) suggest that surface roughness is mainly influenced by soil texture, vegetation, land-use practices and rainfall and flow concentrations. These operate at a variety of spatial scales and are now considered in turn.

2.2.1 Soil Texture

Soil texture directly affects surface roughness at extremely fine scales through the particle-size distribution of the soil surface (including the presence of any surface rock fragments; Van Wesemael *et al.*, 1996). However, soil texture also indirectly influences surface roughness through surface crust development. Soils with a high amount of silt are both extremely erodible and crustable, thereby decreasing surface roughness and encouraging runoff (Bull *et al.*, 2003). Le Bissonnais (1996) identifies four mechanisms for the breakdown of aggregates: slaking (the compression of air trapped within an aggregate), differential swelling, raindrop impact and physico-chemical dispersion due to osmotic stress. Therefore, soil texture and chemistry also influence surface roughness through determining the erodibility of the soil surface. This will interact with the location of slope-area thresholds as, for instance, patterns of rill development are strongly influenced by properties such as consistency, shrink-swell capacity and dispersibility, which reflect clay mineralogy, clay content and chemistry, and the concentration and chemistry of pore water (Gerits *et al.*, 1987).

2.2.2 Vegetation

While the presence of vegetation on the soil surface dramatically increases the surface roughness, it is often ignored in roughness calculations. Indeed, Solé-Benet *et al.* (1997) identify the problematic distinction between 'permanent' roughness elements (elements of the soil surface itself) and 'mobile' elements (namely plant stems, leaves and plant residue), suggesting that although these mobile elements influence rainfall processes (and to some extent, runoff processes), they add a disproportionate amount of noise to roughness calculations.

However, surface vegetation also affects the processes acting on the soil surface through the formation of mounds and steps. A shrub, for instance, will cause increased sedimentation upslope and increased flow concentration around it (Bergkamp, 1998). More permanent vegetation roughness elements (such as lichens) also contribute to surface roughness (Solé-Benet *et al.*, 1997).

2.2.3 Land-Use Practices

Bull *et al.* (2003) found that land-use and runoff production are strongly related in semi-arid environments. Areas of mattoral scrub often have smooth, compacted surfaces and

experience high runoff, whereas in agricultural areas, tillage operations can induce dramatic increases in surface roughness and subsequent depression storage, having significant implications for soil and water conservation (Onstad, 1984). The effect of tillage on roughness depends on many factors such as the number of passes of the tillage tool, clay content and soil water content. Furrows exactly parallel to contours have a greater depression storage than other orientations (where water is able to flow along furrows as concentrated flow) (Kirkby *et al.*, 2002). This property is reflected in the traditional use of contour ploughing as a conservation technique.

Moore & Larson (1979) found that surface depression storage increased 3.5 times by ploughing, although this effect was soon lost through breakdown of the soil surface by raindrop impact, and should therefore be seen as a dynamic process (Onstad, 1984). Abandoned agricultural land soon loses its characteristic surface roughness at a rate dependent upon aggregate stability (Zobeck & Onstad, 1987). Bull *et al.* (2003) suggest that it takes approximately 1-2 years to erode the roughness derived from ploughing (Figure 2.1). After this time preferential flow pathways begin to emerge as channelisation takes place and gullies potentially form, increasing surface roughness by channelling overland flow (Bull *et al.*, 2003).

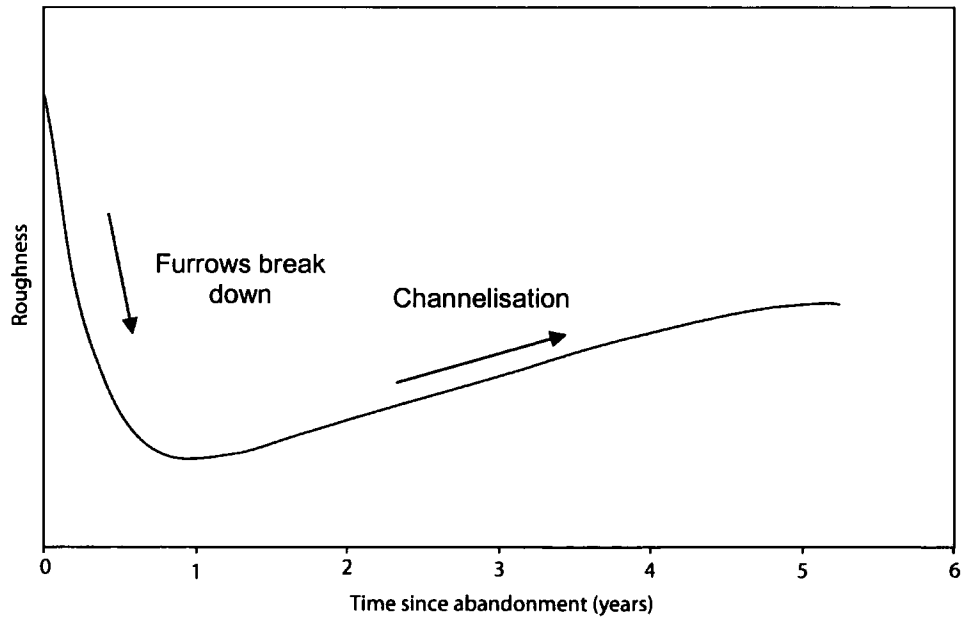

Figure 2.1. Theoretical variations in surface roughness with land abandonment (adapted from Bull *et al.*, 2003). The curve follows $h = h_0[\exp(-t/t_1) + 1 - \exp(-t/t_2)]$ where h is roughness, t_1 is the time for plough roughness to disappear (1-2 years) and t_2 is the time for recovery of natural vegetation and surface channelling to develop (10-100 yrs).

Lasanta *et al.* (2000) showed that abandoned agricultural land demonstrates a particularly rapid runoff response to rainfall with high peak flows and runoff coefficients. This is particularly relevant to semi-arid environments, many of which have experienced large-scale land abandonment in the twentieth century, with migration to urban centres. For example, the agrarian policy of the EU has encouraged the set-aside of cultivated lands (Lasanta *et al.*, 2000): over one million hectares of land have been abandoned in Spain since 1993 (Errea, 1996).

2.2.4 Morphological Runoff Zones

The microtopography of natural soil surfaces is partly determined by the balance between the erosive force of raindrop impact and shear stress caused by overland flow concentrations. Römkens *et al.* (1990) suggest that variations in soil surface morphologies resulting from rain events can be considered as a consequence of three main factors:

1. aggregate collapse due to raindrop impacts;
2. shear stresses induced by runoff;
3. physico-chemical factors from the soil and its solution.

These changes in soil topography during a storm event may cause an increased or decreased roughness depending on the dominant process occurring on the surface (Huang & Bradford, 1993). Raindrop impact will generally cause a decrease in surface roughness through clod breakdown, soil settling and soil particle detachment and deposition affected by both raindrop kinetic energy and total rainfall amount (Römkens & Wang, 1987; Zobeck & Onstad, 1987); however, erosion by runoff will usually increase roughness through material redistribution and the creation of preferential flowpaths between depressions (Huang & Bradford, 1993; Darboux *et al.*, 2001b). This will vary with topographic position within the landscape (related to the slope-area relationship of Patton & Schumm, 1975).

According to Horton's theory of channel incision, the critical distance from the drainage divide where channels begin to form will vary directly with soil resistance, and inversely with gradient, hydraulic roughness and infiltration capacity (Dunne *et al.*, 1995). Surface runoff discharge is low towards the divide (due to the low contributing

area), allowing the diffusive effects of rainsplash to stabilise the soil surface against the advective processes of wash which tend to incise the soil surface (Smith & Bretherton, 1972). Moving downslope from the drainage divide (increasing the contributing area), the microtopography of the soil surface demonstrates systematic changes as runoff gathers into depressions; these depressions increase in size downslope and as the depressions deepen they capture more flow through the cross-grading of the hillslope surface (Dunne *et al.*, 1995). Surface runoff deepens as a result of this 'micropiracy', eventually resulting in the initiation of incision of the soil surface.

This suggests that where Hortonian overland flow is dominant, microtopography (along with downslope position) plays an important role in channel formation, determining the upslope supply of runoff and sediment at any point on a hillslope. However, microtopography is not temporally static: erosional processes modify the soil surface, creating a feedback loop, which as Favis-Mortlock *et al.* (2000) suggest, functions as a self-organising dynamic system. Microrills and eventually rill systems are emergent outputs of such a system. This interdependent relationship between surface topography and surface processes dictates that the distribution of surface characteristics is highly sensitive to rainfall conditions and will shift with any change in the frequency and duration of runoff-effective rainfall (Kuhn & Yair, 2004).

Bracken & Kirkby (2005) mapped variations in morphological evidence of runoff intensity as a result of the factors discussed above and established 'Morphological Runoff Zones' based on the observed surface features outlined in Table 2.1. Small-scale morphological evidence of splash erosion indicates level 1; in level 2 small areas of wash deposits may also be observed (indicating small amounts of runoff); level 3 is reached when small headcuts are also found (suggesting that flow is able to erode the soil surface and is locally concentrated); in level 4 flow is concentrated further and small rills are also found. Level 5 provides evidence of further flow concentration where gullies are found. These qualitatively-defined zones indicate different combinations of processes operating of the soil surface (Bracken & Kirkby, 2005), and this may be used to suggest varying sediment transport rates.

Level of hillslope erosion	Types of evidence noted in the field	Example
1	Surface crusting **Armouring** **Splash pedestals** Small areas of wash deposits	
2	**Depositional steps** (<10 cm^2) (often behind vegetation) Larger areas of **wash deposits** (<50 cm^2)	
3	Some concentrated flow Erosional steps/**small headcuts**	
4	**Concentrated rills** (~0.1 m^2)	
5	**Gullies** (>1 m deep) with own side slopes	

Table 2.1. Morphological Runoff Zones (from Bracken & Kirkby, 2005). Example photographs from the Upper Nogalte field site.

Therefore, with increasing distance from a topographic divide the spatial arrangement of the soil surface roughness changes. This has implications for surface detention storage, infiltration rates (affecting vertical exchanges: see section 2.3) and flowpath distributions (affecting lateral exchanges and the connectivity of the landscape: see section 2.4). Figure 2.2 from Kirkby *et al.* (2005) demonstrates that MRZs are related to the overland flow length-slope product (*LS*) within the same lithology and land use. Indeed, within each site, $MRZ - \ln LS$ is approximately a site constant, which Bracken & Kirkby (2005) suggest represents the hydrological response of the surface.

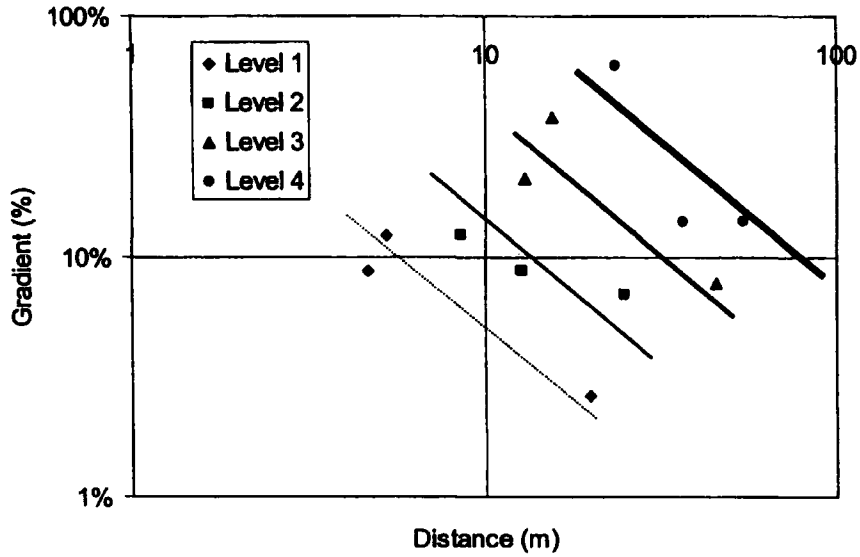

Figure 2.2. The relationship between distance and gradient for different Morphological Runoff Zones (Kirkby *et al.*, 2005).

2.3 Surface Roughness, Runoff Generation and Soil Erosion in Semi-Arid Environments

Soil surface roughness is a dynamic property that controls many transfer processes on and across the soil-atmosphere boundary (Magunda *et al.*, 1997). In particular, soil microtopography exerts a critical influence on the generation and transfer of overland flow and on the resulting sediment transport (Dunne *et al.*, 1995).

Kirkby *et al.* (2002) emphasise the importance of the one-dimensional (vertical) water balance for runoff-generation in semi-arid environments. Precipitation that passes through any vegetation layer and reaches the soil surface may be immediately

infiltrated, may immediately become overland flow, or alternatively may be temporarily stored in a surface depression before taking one of the above pathways (Figure 2.3). Surface roughness plays a dominant role in the partitioning of precipitation through each of these hydrological pathways, and moreover, it further influences the subsequent overland flow routing and soil erosion.

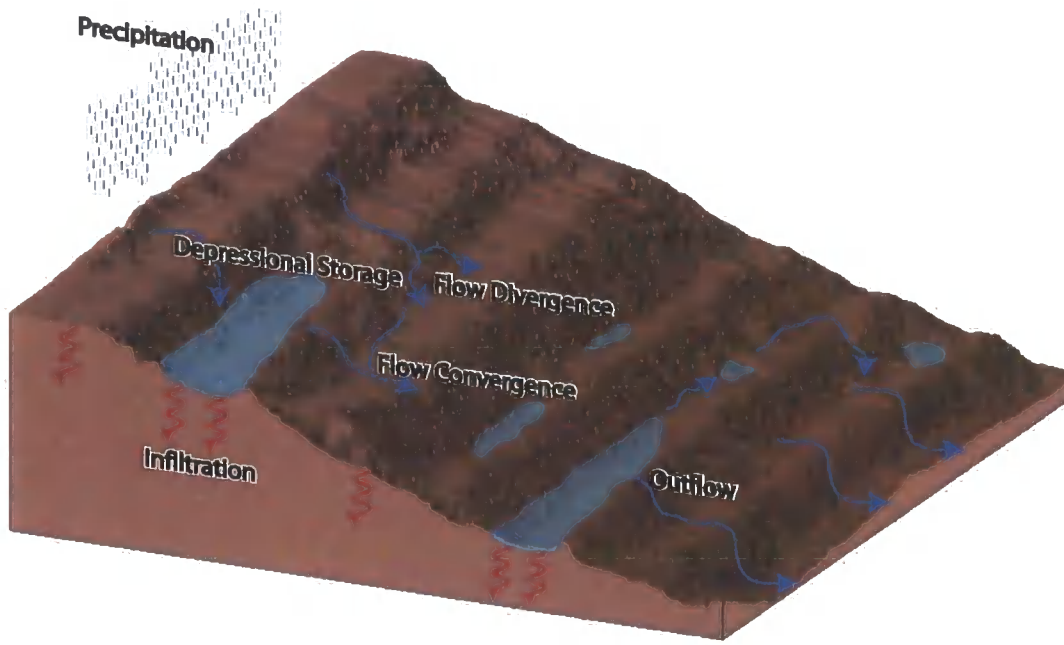

Figure 2.3. Pathways of precipitation falling onto a bare, rough surface. Flow may diverge around roughness elements, thereby concentrating the flow elsewhere.

2.3.1 Surface Depression Storage

Roughness as measured in the downslope direction represents the element of surface roughness that impedes surface runoff, temporarily holding water in depressions on the soil surface (Kirkby, 2001). As with surface roughness, depression storage is highly dependent on the recent history of the soil surface (Moore & Larson, 1979), influenced by rainfall, flow concentrations, land-use, slope, and random surface variations due to the nature of the soil. The detention of water at the soil surface is particularly important where the infiltration rate is slightly lower than the rainfall intensity (Kamphorst *et al.*, 2000) and plays a regulatory role in the generation of surface runoff (Abedini *et al.*, 2005). This situation of 'precipitation excess' is often found in semi-arid environments where high-intensity storms fall upon soils which may exhibit a relatively low infiltration capacity.

Cremers *et al.* (1996) suggest that accurate estimates of such surface depression storage and infiltration are necessary if we are to increase the reliability of models of surface runoff and soil erosion for a particular rainfall event. Currently, models of hydrological processes simply abstract estimates of depression storage and interception values from precipitation amounts with sudden initiation of surface runoff once these abstractions (and initial infiltration) have been met (Onstad, 1984).

However, Hansen (2000) notes that runoff begins before maximum depressional storage (*MDS*) is completely satisfied; therefore, during the filling of surface depressions, precipitation excess is partitioned between surface storage and runoff. A greater understanding of this division of precipitation excess is necessary to model surface runoff generation accurately. Darboux *et al.* (2001a) noted that as these depressions are progressively filled, the soil surface can be divided into two domains: the area contributing to the runoff flux (any depressions have been filled and are 'connected' to the defined runoff boundary) and that area not contributing to the runoff flux (as the precipitation excess remains trapped in partly-filled depressions). The surface area covered with water determines the amount of infiltration of water stored in surface depressions (Hansen, 2000).

When a plot is considered, any generated runoff must travel some distance as overland flow and will experience storage in smaller and larger depressions below the runoff initiation point. The precipitation excess needed to fill all surface depressions is much larger than the *MDS* because of the time taken to fill those depressions towards the top boundary of the area in question and the simultaneous generation of runoff from already 'connected' areas (Hansen, 2000). This brings into question the value of exclusively using plot-scale studies when examining depression storage and surface runoff generation as in the field, run-on from upslope would interact with this process.

2.3.2 Surface Roughness and Infiltration

While the relationship between surface roughness and depression storage is reasonably well studied, the effect of roughness on infiltration has been practically ignored (Govers *et al.*, 2000). Whereas in humid environments the spatial variability of infiltration is mainly attributed to spatial differences in soil moisture, in semi-arid areas this

variability is primarily controlled by rainfall characteristics and surface physical and chemical properties (Martínez-Mena, 1998). Therefore, surface roughness has a large influence on the infiltration rates of soil surfaces in semi-arid environments and offers one explanation of the high variability of infiltration rates at single locations. Such variations in hydraulic conductivity help to explain the spatial and temporal distributions of overland flow and erosional processes which may in turn induce feedback effects on infiltration rates (Heddadj & Gascuel-Odoux, 1999).

Larson (1962) and Moore & Singer (1990) note that soils with greater roughness maintain higher infiltration rates than smooth soils, as the dense crusts that form in depressions of even soils are found over the entire surface of smooth soils. Fox *et al.* (1998a) showed that surface seal characteristics are highly variable over rough surfaces, and that this variability is related to the soil microtopography. Surface roughness reduces surface sealing as it both spreads the impact of rainfall over a greater area and reduces the impact normal to the soil surface. Fox *et al.* (1998a) suggested that although structural crusts eventually form on positive roughness elements (surface mounds) as a result of aggregate breakdown from raindrop impact, surface depressions tend to develop thicker depositional crusts and have lower infiltration rates (Figure 2.4). Similarly, Dunne *et al.* (1991) demonstrated that soil mounds below grass tussocks had higher infiltration capacities than lower-lying areas.

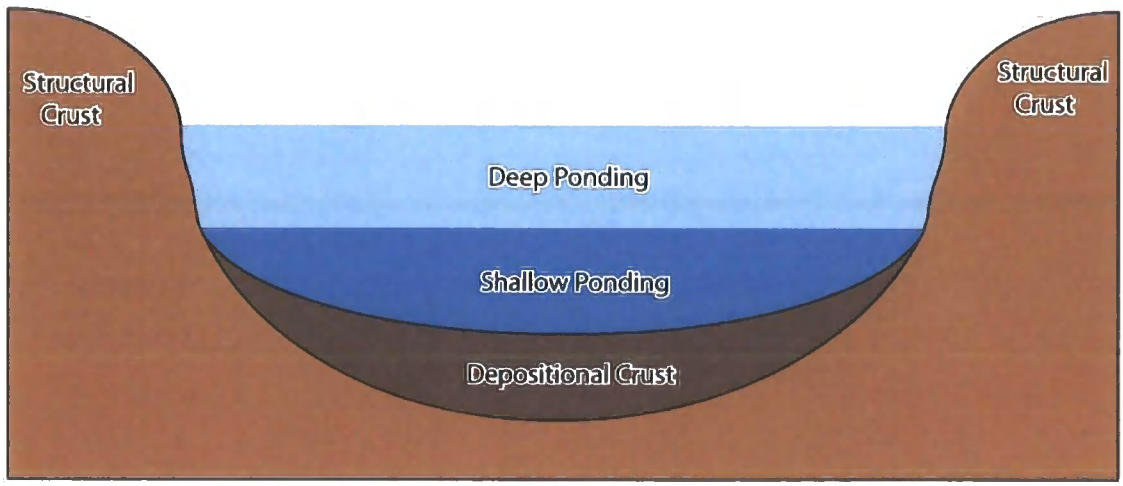

Figure 2.4. Schematic representation of a soil surface depression showing the approximate location of sedimentary (depositional) and structural crusts. Adapted from Fox *et al.* (1998a).

As it is more common for low points to be less permeable than highs, infiltration rates of rough surfaces will increase with runoff depth as surfaces of greater hydraulic conductivity are progressively submerged. Fox *et al.* (1998b) suggest that this effect influences runoff production, measuring a four-fold increase in the infiltration capacity of a silty-loam as the water depth increased from 1.5 mm to 2.5 mm.

Infiltration at any point will continue at the rate permitted by the surface hydraulic conductivity until the local depth supply is exhausted. The water supply at upper parts of the runoff path will run out earlier than those downslope points where water depths are replenished by flows from above (Woolhiser, 2002). This distribution of overland flow is significant at the hillslope scale and is also influenced by surface roughness.

2.3.3 Surface Roughness and Flow Hydraulics

Few studies have addressed the effect of the gradual filling of depressions on overland flow generation, connectivity development and the effect of surface roughness on the overland flow itself (Darboux *et al.*, 2002). Helming *et al.* (1998) note that because of the difficulty of measuring the spatial variation of runoff, little information is currently available on the effect of surface roughness on the routing of runoff, flow concentrations and runoff velocity. Gilley & Finkner (1991) suggest that improved knowledge of this effect is necessary if we are to improve simulation of runoff hydrographs while Takken & Govers (2000) highlight the relevance of this for the calculation of the erosivity and transport capacity of the flow.

Helming *et al.* (1998) suggest that an increase in roughness elements with an amplitude greater than flow depth acts to concentrate surface flow between these areas of greater elevation, which increases the hydraulic radius of surface flow and enhances flow velocity and transport and detachment capacity (with the eventual straightening of flowpaths through clod destruction). This demonstrates the relationship between soil surface roughness and its hydraulic resistance. Abrahams *et al.* (1992) distinguished between 'form roughness' and 'hydraulic roughness'; form roughness has an amplitude greater than flow depth, affects erosion processes, and is the dominant factor on natural hillslopes, whereas hydraulic roughness is effectively the grain roughness. Runoff models operate under the assumption of uniform flow and therefore consider only grain roughness (Helming *et al.*, 1998), however, it should be noted that this distinction

between form and grain roughness is somewhat arbitrary; grain roughness is a type of form drag caused by the interaction of a single particle with the flow.

Through the use of surface roughness measures, the hydraulic behaviour of overland flow can be considered, and therefore we can improve our ability to understand and model upland flow hydraulics (Podmore & Huggins, 1980). However, little research has been directed at relating the hydraulic resistance of a surface to its microtopography.

Plot models only provide input to overland flow. Moore & Larson (1979) note that runoff from a plot must travel some distance as overland flow before encountering an elementary channel. The pathways followed by surface runoff are determined by both topography and macroscale roughness elements of various types (tillage lines, roads, field borders etc.) (Govers *et al.*, 2000). This introduces a considerable time delay during which further modifications to runoff characteristics may occur associated with the connectivity of the landscape. Therefore, plot models should be incorporated into an analysis conducted at larger scales.

2.3.4 Surface Roughness and Soil Erosion

Erosion rates are particularly heterogeneously distributed in semi-arid environments (Cammeraat, 2002). They can be related to the connectivity of the hydrological system which involves several roughness-related thresholds, characteristics of rainfall events, and the influence of humans through land-management practices. Govers *et al.* (2000) note that as surface roughness affects the organisation of drainage patterns, it may have important implications for the spatial distribution of sediment sources and sinks.

Huang & Bradford (1993) suggest that soil erodibility depends not only on the inherent properties of the soil material, but also on the conditions of the surface. Clod size distribution will influence resistance to detachment by raindrop impact; the specific surface area affects the rain energy imparted per unit area, and depressional storage serves as a sediment trap for eroded material (Helming *et al.*, 1998). Additionally, the greater level of hydraulic resistance dissipates the energy of flow, rendering a fraction of the total flow energy unavailable for sediment transport (Abrahams & Parsons, 1991). While these effects are evident during the early stages of the erosion process (i.e. during seal development, before depressions become filled and connected), very few

studies have addressed the influence of surface roughness during the subsequent stages, where flow concentration is present. As a result, the effect of roughness upon soil erosion remains poorly understood for large areas of natural hillslopes (i.e. 'Morphological Runoff Zones' 3-5 in Table 2.1). These areas describe non-permanent channel networks, which Poesen *et al.* (2002) suggest contributes between 50 and 80 % of overall sediment production in semi-arid environments.

A flume study conducted by Helming *et al.* (1998) concluded that 'rough' and 'smooth' surfaces experienced different dynamics and amounts of soil loss. On rough surfaces flow immediately concentrated in pathways between clods and soil losses were 8 times that on the smooth surfaces (due to a high detachment rate by raindrop impact). After several simulated storms, flow also concentrated on the smooth surfaces and soil losses were similar. These results contradict observations usually reported in the literature (Zobeck & Onstad, 1987; Cogo *et al.*, 1983) which suggest that rough surfaces yield less soil loss as ponded water protects the soil surface and entraps a proportion of the entrained sediment. Helming *et al.* (1998) suggest that this disparity is a result of the focus of the previous studies on soil detachment by raindrop impact; their study used a flume of 4 m in length (considerably longer than the plot studies commonly undertaken) which permitted the runoff velocity to increase to a more 'natural velocity' where the transport and detachment capacity of this surface flow was an additional factor. Additionally, the study of Helming *et al.* (1998) included surface roughness elements of greater vertical amplitude than the surface flow (i.e. form roughness) representing a more realistic field situation. Soil erosion on rough surfaces is therefore a complex phenomenon, representing the interplay between changing surface conditions, surface sealing and the erosive power of runoff (Römkens *et al.*, 2001).

Gómez & Nearing (2005) tested the controversial results of Helming *et al.* by conducting a similar study. They also observed higher erosion rates on rougher surfaces; however, they noted that different processes occurred on steeper slopes. Plot measurements of runoff and erosion therefore, do not simulate the entire spectrum of conditions experienced on natural hillslopes and so cannot be extrapolated to quantify hillslope scale processes (Huang *et al.*, 2001).

2.3.5 Hydrologically Similar Surfaces

Areas exhibiting similar depression storage and infiltration characteristics may be grouped together as Hydrologically Similar Surfaces (HYSS) which display a homogeneous hydrological response (Kirkby *et al.*, 2002). They exist independently of topography and have been identified at a variety of scales. HYSS can be used as a basis for scaling up plot and field measures of vertical exchanges while preserving catchment heterogeneity for model inputs (Bull *et al.*, 2003). These vertical exchange processes determining runoff generation are then subject to a number of horizontal landscape processes determining the connectivity of runoff-producing areas to the main channel (Kirkby *et al.*, 2002). The lateral flows (controlled by topographic features, surface gradient, etc.) result from overland flow generation as a result of spatial and temporal variation of the vertical processes, and often feed back into the vertical process domain (Becker & Braun, 1999). Therefore, an analysis of connectivity of runoff processes with regard to surface roughness elements is also necessary to assess runoff generation at larger scales.

2.4 Surface Roughness and Landscape Connectivity

Connectivity is related to the level of connection between runoff-producing areas and channels. Connectivity in the landscape is often related to physically or biologically controlled thresholds; these particularly emphasise the importance of soil moisture (Cameraat, 2002; Fitzjohn *et al.*, 1998). Roughness-related thresholds include such factors as vegetation density and pattern, microtopography, slope gradient, distance to flow concentrations, channel linkage etc. While surface roughness elements determine depression storage in the landscape, it is the connection of overflowing depressions towards the outflow boundary which helps determine the effect of roughness on runoff initiation. The overall effect depends upon the scales of the interacting processes; however, little work has been conducted in quantifying these effects (Darboux *et al.*, 2001b).

Semi-arid surfaces demonstrate extreme spatial variability in runoff-response as a result of a complex interaction of geological, pedological and topographical factors (Fitzjohn *et al.*, 1998; Michaelides & Wainwright, 2002). Superimposed upon this pattern of response is the effect of land management upon runoff generation. Additionally, this

surface runoff-response interacts with the spatial and temporal nature of rainfall events (which are also extremely variable) to determine the catchment response to a particular storm event (Reaney, 2003).

Significant flood source areas consist of HYSS that combine internal characteristics susceptible to rapid runoff generation with good connectivity to the main channel (Kirkby *et al.*, 2002). Disconnection of runoff-producing areas may be caused by long distances with high transmission losses (Bull *et al.*, 2003) or through encountering roughness elements in the landscape that act to impede overland flow such as check dams or terraces. This means that the spatial distribution of infiltration rates and roughness elements (i.e. runoff thresholds) on a hillslope or even in a catchment is a particularly important structural landscape element (Bergkamp, 1998).

Roughness elements measured in the cross-slope direction tend to concentrate flow in depressions (Kirkby, 2001). A greater degree of organisation of the surface generally leads to enhanced connectivity of overland flow; this is related to the distribution of flowpaths (Kirkby *et al.*, 2002). For instance, Lal (1997) demonstrates that rill initiation alters the distribution of flow path lengths (generally resulting in a reduced mean length), increasing connectivity and slope-scale runoff coefficients (the proportion of total precipitation that leaves the slope as runoff). Such concentration of flowpaths lowers the ability of the soil to infiltrate (as soil underneath areas of flow concentration rapidly reaches infiltration capacity) and decreases hydraulic resistance through increasing flow depth, thereby increasing discharge. Baird (1997) emphasises the importance of understanding the microhydraulics of flow over semi-arid slopes as microtopography actively controls such flow concentrations. Therefore the morphology of the soil surface is an important factor when considering the transmission of runoff (Kuhn & Yair, 2004).

The dynamics of runoff-producing areas will, however, vary under changing storm conditions (Kirkby *et al.*, 2002). The landscape-induced flowpath distribution interacts with the temporal distribution of rainfall intensity to determine overall connectivity of the landscape (Reaney, 2003). Therefore, flow travel times derived from a storm event interact with landscape elements such as the distance to the nearest flow concentration, slope gradient and surface roughness to give flow delivery pathways with variable

width, depth and velocity, and determine the strength of connectivity of the landscape (Bracken & Croke, in press). Models which successfully simulate this interaction, however, are unable to simulate the interdependent relationship between generated runoff and the soil surface morphology; they cannot simulate further rill growth or modification in landscape flowpath distributions caused by this generated runoff.

2.5 Roughness and Scale Issues

The variable behaviour and structure of the landscape at different scales is currently at the forefront of contemporary geographical research (Phillips, 2004). Both runoff and erosion processes are highly dependent on scale (Cammeraat, 2002), as is the concept of connectivity (Kirkby *et al.*, 2002). The difficulty of transferring results over a wide range of scales and the independence of processes operating on fundamentally different scales (see Phillips, 2004) dictates that the spatial and temporal scope of any investigation examining the nature of these processes will significantly influence the outcome.

As a result of the spatial mosaic of runoff-producing and runoff-absorbing areas in semi-arid environments (Fitzjohn *et al.*, 1998) runoff is more frequently produced at finer scales than at broader scales (Cammeraat, 2002). This spatial heterogeneity is important when attempting to scale-up measurements from fine scales to broader scales, as the connectivity (or disconnectivity) experienced in the landscape is partly responsible for the non-linear response of the landscape (Cammeraat, 2002). Simple extrapolation overlooks the fundamental idea that runoff-generating processes have specific spatio-temporal domains (Bergkamp, 1998). Indeed, the landscape may be viewed as a network of interlinked dynamic open systems of varying scales (Allen & Star, 1982) consisting of interacting subsystems which simultaneously function as an integrated part of another, higher level system.

Surface roughness can be identified at several scales in the landscape; the overall effect of roughness elements in the landscape depends on the scales of the processes involved (Darboux *et al.*, 2001b). Lane (2005) notes that roughness is effectively a 'residual topography'; the component of topography that must be dealt with implicitly at the chosen scale of enquiry. Many definitions of surface roughness overlook the fact that any notion of surface roughness is essentially scale-dependent. Huang & Bradford

(1993) note that consideration of the spatially correlated and scale-dependent nature of surface topography is of foremost importance in the selection of a roughness measure. Indeed, several of the methods of characterising soil surface roughness examined in section 2.6 are of limited practical use due to their scale dependency (Kamphorst *et al.*, 2000).

Römkens & Wang (1986) divided soil surface roughness into four categories, or layers based upon the spatial extent of the features (Figure 2.5):

1. variations in micro-relief due to individual grains or aggregate sizes (uniform in all directions, 0-2 mm);
2. non-directional, random surface variations due to soil cloddiness (random roughness, 100-200 mm);
3. unidirectional (oriented) systematic differences in elevations such as furrows caused by tillage practices (approximately 100-200 mm deep);
4. higher orders of surface roughness, representing variations at field, basin or landscape level (usually non-directional).

These divisions are clearly arbitrary; which level becomes classified as roughness will depend on the appropriate scale of study. Dietrich & Montgomery (1998) suggest that layers 1 and 2 can be defined as the 'fundamental hillslope'; although roughness elements are present, no organised, persistent convergent areas dissect it. Vegetation and microtopography have an important effect on roughness and runoff at these finer spatial scales (Bergkamp, 1998), as they affect both infiltration rates and the convergence/divergence of runoff. As larger scales are considered (layer 3), land management becomes a key control on the spatial structure of surface roughness and depression storage. The formation of rills and gullies increases surface roughness and runoff by channelling overland flow and so will have a considerable effect at the hillslope scale. Roughness also relates to the catchment morphology at larger scales (layer 4) in terms of the valley shape and network.

Borselli (1999) suggests that every lower order of roughness should be considered as 'random roughness' of the closer higher-order roughness (which may be considered an 'ordered roughness' of that particular scale). This multi-layered influence of surface roughness may, in some part, account for the scale dependency and inherent non-

linearities of runoff coefficients (defined as the proportion of precipitation that becomes runoff).

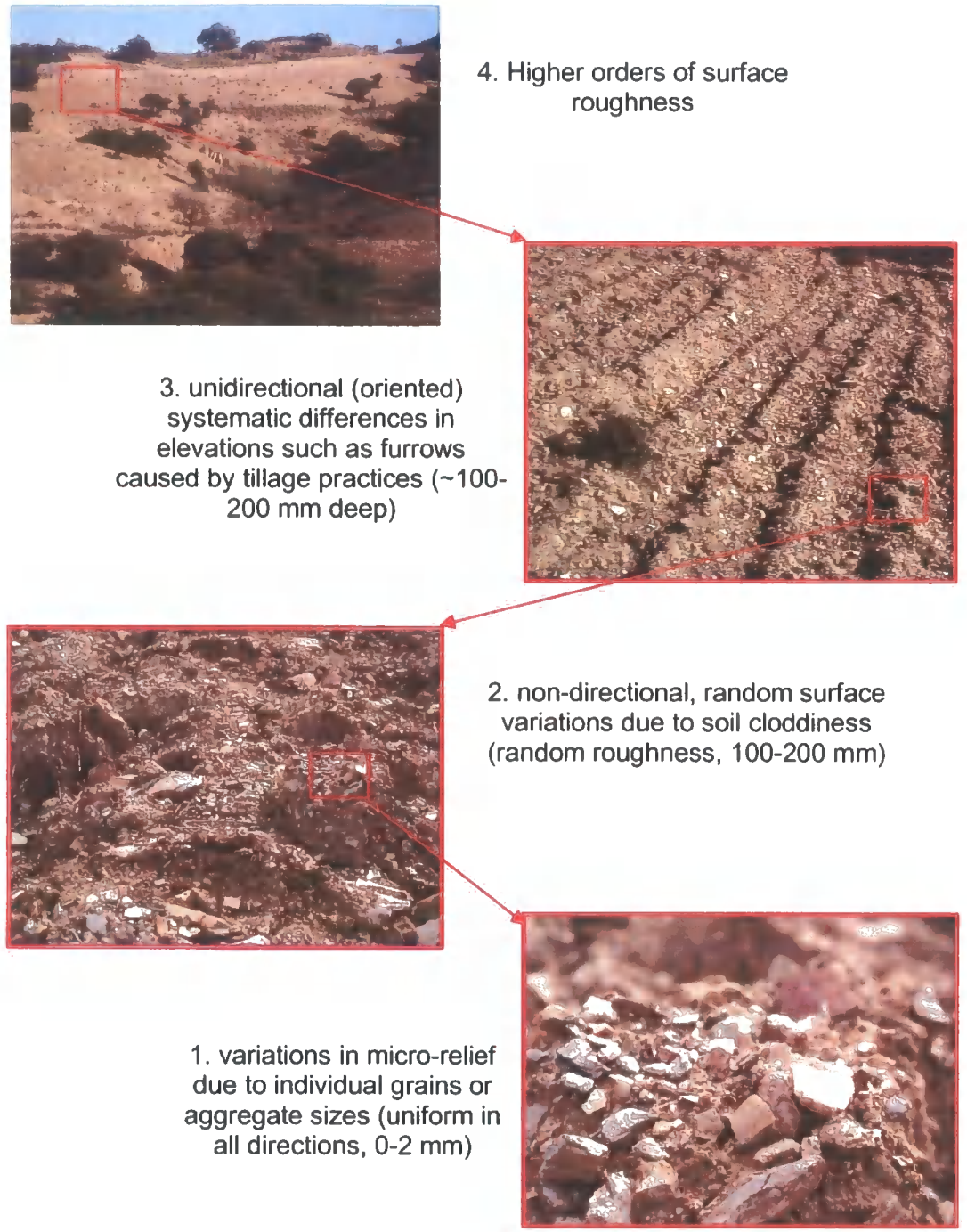

Figure 2.5. The four layers of surface roughness (as identified by Römkens & Wang, 1986) seen at the Upper Nogalte field-site.

Although the interactions between runoff production and erosion rates and surface roughness have been analysed in semi-arid areas, Bergkamp (1998, p.203) suggests that

further progress is limited by 'a lack of synthesis of observations at different scales'. Different linkages between erosion processes and surface morphology operate at different landscape scales. For instance, while most studies of surface roughness have been undertaken at the plot scale (e.g. Darboux & Huang, 2003; Darboux *et al.*, 2002; Kamphorst *et al.*, 2000; Hansen *et al.*, 1999; Helming *et al.*, 1998; Onstad, 1984) at the hillslope scale, new properties need to be taken into account (such as rill formation), yet their characteristics cannot be assessed simply from measurements at the plot scale. Therefore, an analysis of surface roughness of the landscape at various scales may provide important insights into this notion of scale dependency in hillslope hydrology.

Investigations of runoff and erosion at the hillslope scale are particularly relevant for the development of potential management responses (Kirkby & Bracken, in press), yet studies on this scale remain relatively uncommon. While the hillslope scale can be easily related to the smaller plot-scale variations of factors such as runoff thresholds and depression storage capacities (Cammeraat, 2002; Fitzjohn *et al.*, 1998; Kirkby *et al.*, 2002), it also permits a consideration of networks of Hydrologically Similar Surfaces (HYSS; Bull *et al.*, 2003), Morphological Runoff Zones (MRZs; Bracken & Kirkby, 2005) and integration of these concepts with that of connectivity and the continuity of hydrological pathways (and analysis of Hydrological Response Units; Flügel, 1995) at the hillslope and also scaled-up to the catchment scale.

2.6 Representations of Surface Roughness

Surface roughness is a vague concept, and as such, it can be made precise in many ways (compare Mosteller & Tukey, 1977). No single value of 'surface roughness' can be given to entirely describe a surface; instead a large variety of measures have been developed. Each offers a particular representation of a single perspective of surface roughness, rather than encapsulating the entire concept. For example, roughness may be considered as hydraulic resistance in flow equations, characterised by roughness coefficients (such as Manning's n and the Darcy-Weisbach friction factor); or alternatively, as in this study, roughness may be regarded as a property of the interaction between rainfall and runoff and the soil surface.

Surface roughness is often characterised by measuring elevations of the soil surface over areas of about 0.1 to 4.0 m^2 with grid spacings for the elevations typically varying

from 0.01 to 0.10 m (Linden & Van Doren, 1986). A variety of microrelief meters have been used, ranging from hand-held rulers and pin meters to remote sensors, laser scanning techniques and digital photogrammetry. While early techniques involved instruments (rows of pins or chains) that were lowered on the surface itself, techniques not based on contact are preferable in the measurement of the surface elevations to avoid disturbance of the roughness elements.

A wide variety of measures for quantification of soil surface roughness currently exists; these are reviewed in this section and are summarised in Table 2.2. In response to the large number of seemingly random surface roughness elements, statistical procedures are often employed (Huang & Bradford, 1993), most of which are based on the variance of height measurements from transects (RR, MUD, MIF). However, other measures (Tortuosity, LS, LD) are more physically based (Linden & Van Doren, 1986) and take into account the correlation length and spatial configuration of the surface itself.

The selection of a roughness index should be made in consideration of its proposed use. Huang & Bradford (1990a), however, argue that roughness cannot be completely described by a single measure, as it consists of two fundamental components: the variance in elevation measurements, and the correlation length (the distance over which spatial autocorrelation occurs). Representations of surface roughness can only measure one or the other; no measure combines the influence of both properties.

Roughness Measure	*Abbreviation*	*Units*	*Source*
Random Roughness	RR	mm	Allmaras *et al.* (1966)
Limiting Distance	LD	mm	Linden & Van Doren (1986)
Mean Upslope Depression	MUD	mm	Hansen *et al.* (1999)
Microrelief Index & peak Frequency	MIF	-	Römkens & Wang (1986, 1987)
Tortuosity	T_A, T_B, T_S, T_P	-	Boiffin (1984); Auerswald (1992); Saleh (1993); Planchon *et al.* (1998)
3D Tortuosity	3D T_B	-	Helming *et al.* (1992, 1993)
Limiting Slope	LS	-	Linden & Van Doren (1986)
Fractal Dimension	D	-	Bertuzzi *et al.* (1990), Merril (1998), Pardini & Gallart (1998)

Table 2.2. Summary of roughness measures.

As seen in section 2.3.1, information on the maximum depressional storage (MDS) of soil surfaces is necessary to develop reliable models of surface runoff and erosion. However, time-consuming measurement of soil surface microrelief in a densely sampled two-dimensional grid is necessary to produce a digital elevation model (DEM) from which accurate estimations of MDS can be made (Hansen *et al.*, 1999). Because of the difficulty of measuring MDS directly in the field, it is usually estimated using a measure of surface roughness. Several models have been developed to predict MDS from roughness indices and terrain slope (Onstad, 1984; Auerswald, 1992; Linden *et al.*, 1988); these models are also reviewed in this section. However, Onstad (1984) notes that the variable sample area, number and spacing of height readings, and the roughness measure calculated limits the potential use of surface roughness measurements. Because of the spatial dependency of surface roughness, the results are not immediately comparable.

The use of these roughness measures is currently limited to the plot scale, and no attempt has been made to analyse detailed hillslope topography in terms of these surface roughness measures, partly because of the practicalities of undertaking such a task. Additionally, studies have mostly been carried out on agricultural land (focusing on tilled soil surfaces, (e.g. Onstad, 1984; Römkens & Wang, 1986; Brough & Jarrett, 1992), computer-generated surfaces (Darboux *et al.*, 2002), or in flumes (Helming *et al.*, 1998; Gómez & Nearing, 2005). There is a distinct lack of research on surface roughness on the natural soil surfaces which compose the vast majority of real-world surfaces.

2.6.1 Random Roughness

The first roughness index developed was that of Kuipers (1957) and was simply $R = 100 \log s$ where s is the standard deviation of the elevation readings of a grid system. The Random Roughness Index (RRI) of Allmaras *et al.* (1966) is calculated using natural log transformed elevation data with the slope effect and the upper/lower 10 % removed. The RRI is then defined as the product of the standard deviation and overall arithmetic mean of these elevations (Cremers *et al.*, 1996). This provides a widely-used measurement of roughness which can be applied at a variety of scales.

However, it seems that one particularly arbitrary characteristic of the random roughness index is the method of its calculation which raises issues of comparability. Zobeck & Onstad (1987) note that it is sometimes difficult to determine whether all these details of RRI calculation have been carried out in any particular study. Currence & Lovely (1970) argued that log transformation was unnecessary, and several other studies do not mention the removal of the 10 % in each tail or oriented roughness elements (e.g. Hansen *et al.*, 1999). Onstad (1984) even defined random roughness as the standard error among height measurements.

As the RRI describes the random part of roughness (from randomly distributed aggregates), the data are often adjusted to remove any 'ordered' roughness before this calculation is made. These non-random elements (such as furrows) may provide a significant influence on runoff production. Currence & Lovely (1970) note that for studies on the relationships of surface roughness to erosion, MDS, and infiltration, such filtering of 'ordered' roughness elements is inappropriate and may mask some property of the higher-order roughness that produces effective water storage (Borselli, 1999). Therefore, a major limitation for the use of *RRI* is that no standard procedure for calculation has yet been developed, despite its widespread application. In many circumstances, a simple measure of the standard deviation of elevation measurements is more appropriate (Kamphorst *et al.*, 2000; Kuipers, 1957).

Onstad (1984) developed a non-linear model relating random roughness (RR in mm) and slope (*S*, expressed as a percentage) to surface maximum depressional storage (*MDS*, mm) that explained 82 % of the observed variation in 1060 datasets from small, tilled plots:

$$\mathrm{MDS} = 0.112\mathrm{RR} + 0.031\mathrm{RR}^2 - 0.012\mathrm{RR} \cdot S$$

(Equation 2.1)

This relationship suggests that RR has the greatest effect on MDS on gentle slopes. Onstad (1984) also related RR to the rainfall excess required to satisfy the MDS (PR in mm) that explained 79 % of variation:

$$\mathrm{PR} = 0.329\mathrm{RR} + 0.073\mathrm{RR}^2 - 0.018\mathrm{RR} \cdot S$$

(Equation 2.2)

As Figure 2.6 suggests, this predicts that during the filling of surface depressions, only 35 % of precipitation excess is used to satisfy MDS on gentle slopes, and this figure decreases with increasing slope (where roughness also becomes a significant factor).

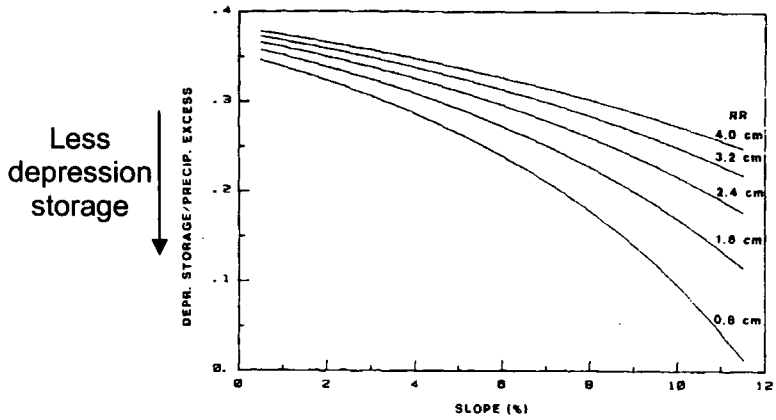

Figure 2.6. Ratio of depressional storage to precipitation excess needed to fill that depressional storage as a function of random roughness (cm) and slope steepness (%). From Onstad (1984).

Gilley & Finkner (1991) used experimental data to derive regression relationships predicting hydraulic resistance (Darcy-Weisbach and Manning hydraulic roughness coefficients) from the Random Roughness Index of Allmaras *et al.* (1966) (taken as a measure of the physical roughness of the flow boundary) and the Reynolds number (which supplied a flow property). The largest hydraulic roughness coefficients usually occurred on those plots with the greatest random roughness. Gilley & Finkner (1991) related the Darcy-Weisbach friction factor f and Manning's n coefficient to random roughness RR and the Reynolds number R_n, by

$$f = \frac{6.30\mathrm{RR}^{1.75}}{R_n^{0.661}}$$

(Equation 2.3)

$$\text{and } n = \frac{0.172\mathrm{RR}^{0.742}}{R_n^{0.282}}.$$

(Equation 2.4)

The random roughness index is not related to a physical surface description, nor is it a process-related parameter necessary for a description of mass and energy exchange processes (Linden & Van Doren, 1986). The measure of variance may be prone to bias if the measurement scale is of a higher magnitude than the smallest scale of variability

in the surface. Additionally, the statistical nature of the RRI limits its ability to describe the actual spatial structure of the surface (such as the mutual location of higher and lower points); a property which is particularly relevant when analysing hydrological processes (Römkens & Wang, 1986). Huang & Bradford (1992) note that surfaces with the same RRI may have different morphologies and therefore different depressional storage characteristics.

2.6.2 Tortuosity

Boiffin (1984) used the term 'tortuosity' to describe a measure of roughness T_B, the ratio of surface profile length L_1 and the length of a straight line formed by its projection L_0:

$$T_B = \frac{L_1}{L_0} > 1.$$

(Equation 2.5)

Several versions of this roughness measure exist, for instance those of Auerswald (1992) T_A, Saleh (1993) T_S and Planchon *et al.* (1998) T_P which are

$$T_A = T_S = \frac{L_1 - L_0}{L_1} = 1 - \frac{1}{T_B} \qquad (1 > T_A \geq 0) \text{ and}$$

(Equation 2.6)

$$T_P = \frac{L_1 - L_0}{L_0} = T_B - 1 \quad > 0.$$

(Equation 2.7)

Helming *et al.* (1992, 1993) also applied T_B to three dimensions (ratio of total surface area to total map area) by summing the surface areas of 3 by 3 mm grid squares. These tortuosity indices are often measured using the 'chain method' which involves laying a chain over the rough ground surface to gain a measure of L_1. However, Skidmore (1997) notes that such measures of tortuosity are problematic when considering values obtained from different sample spacings; this is demonstrated in Figure 2.7. Tortuosity values from different measurement spacings cannot be compared as a chain with smaller links will give a more detailed representation of roughness (with higher tortuosity). This feature of rough surfaces may be considered through the use of fractal-based roughness measures; this is discussed in section 2.6.3.

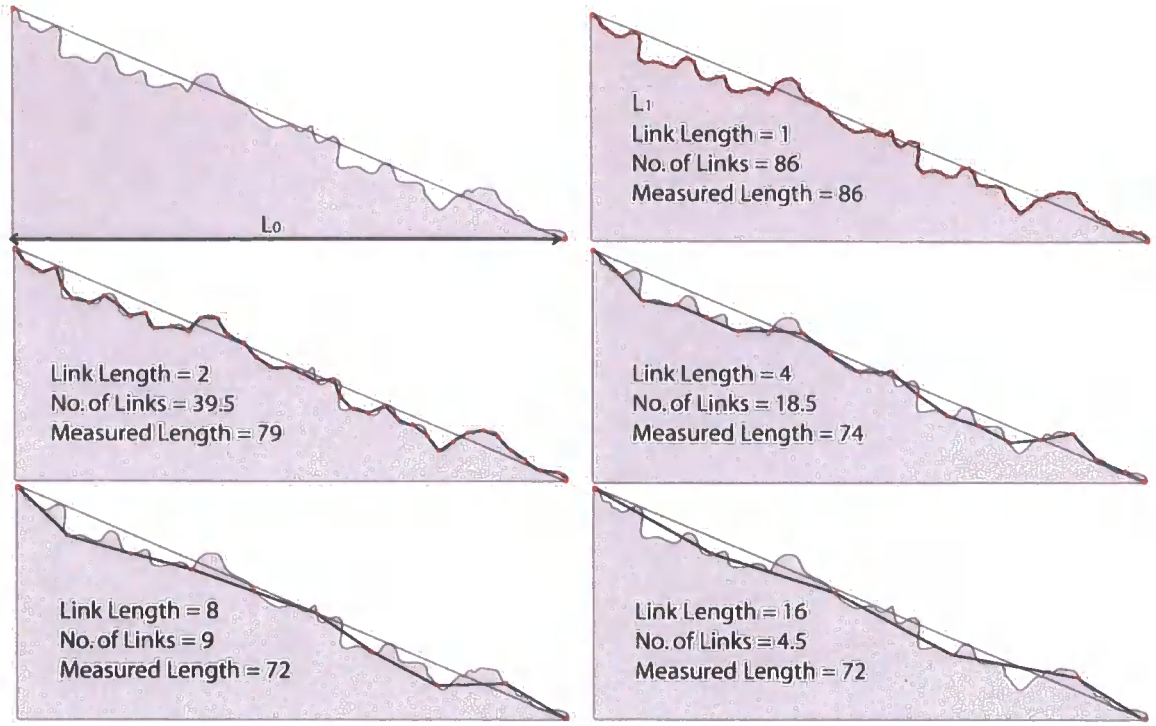

Figure 2.7. Sketch of the principle for calculation of tortuosity and the dependence of this roughness measure on sample spacing.

Morgan *et al.* (1998b) related T_A to MDS (maximum depressional storage, in metres) on 5 DEMs obtained by stereophotogrammetry on laboratory plots with 2 mm grid spacing which explained 93 % of data variation:

$$\mathrm{MDS} = \exp[0.27T_A - 6.66].$$

(Equation 2.8)

Takken & Govers (2000) found that the equations of Gilley & Finkner (1991) described in section 2.6.1 above underpredicted f and overpredicted n, suggesting that the use of random roughness to predict hydraulic roughness is inappropriate. They suggested that any prediction of hydraulic resistance should be made as a function of discharge as surface roughness elements are progressively inundated. Such a model would need to take into account the spatial distribution of flow over the surface as well as the roughness within the flow. Takken & Govers (2000) developed a model relating the Darcy-Weisbach friction factor f to the 'wet tortuosity' perpendicular to flow direction T_w, calculated using the wetted perimeter P, and the surface width, W:

$$T_w = \frac{P}{W-1}.$$

(Equation 2.9)

This 'wet tortuosity' clearly depends upon flow depth and takes into account the gradual inundation of roughness elements with increasing flow depth (however, it does not consider roughness in the flow direction which accounts for depressional storage). Therefore as flow depth gradually increases, the gradual inundation of roughness elements increases T_w and hydraulic resistance, but smaller roughness elements will be simultaneously overtopped, decreasing hydraulic resistance.

However, Kamphorst *et al.* (2000) suggested that the dependency on sample density dictates that tortuosity is inadequate to predict MDS or hydraulic roughness from field data; therefore when attempting to measure surface roughness, the scale of observation must be considered. This may be dealt with through the application of fractal-based roughness measures.

2.6.3 Fractal Characteristics of Soil Surfaces

Pardini & Gallart (1998) suggest that because of the dependency of measured length on the scale of observation demonstrated in Figure 2.7, the measurement of a rough profile represents a classic problem of fractal geometry. The concepts embodied in fractals (Mandelbrot, 1982) offer a mathematical framework for the treatment of complex profiles that display similar patterns or geometric characteristics over a range of scales (Rodríguez-Iturbe & Rinaldo, 1997).

Fractals often display a *self-similarity* whereby an object may be divided into smaller copies of itself; the structure of the whole is contained within each element of the object (Hastings & Sugihara, 1993). Therefore, a self-similar object will not display any characteristic scale; exactly self-similar features have exactly the same form under any magnification, statistically self-similar features are those where, upon magnification the resemblance is not exact, only statistical (Butler *et al.*, 2001). Moreover, Hastings & Sugihara (1993) point out that as the basic building block of a self-similar irregular form is an infinitesimally small copy of itself, such a curve also lacks what we commonly describe as a length. When highly magnified, every small part of the curve will demonstrate a richness of detail equivalent to the whole, and so they do not appear smooth or reduce to the usual building blocks of Euclidean geometry (lines, squares and cubes, etc.).

Rodríguez-Iturbe & Rinaldo (1997) suggest that a self-similar object of special interest for hydrologists and geomorphologists is the Koch curve (Figure 2.8). Here, the middle third of a straight line (called the initiator) is replaced with an equilateral triangle. This results in what is known as the generator, which in this example has length 4/3 if the initiator is unit. This procedure is then repeated on every straight segment of the object and the length of the line becomes $(4/3)^2$. Where this is repeated *ad infinitum*, a curve of infinite length is generated which is not differentiable at any point.

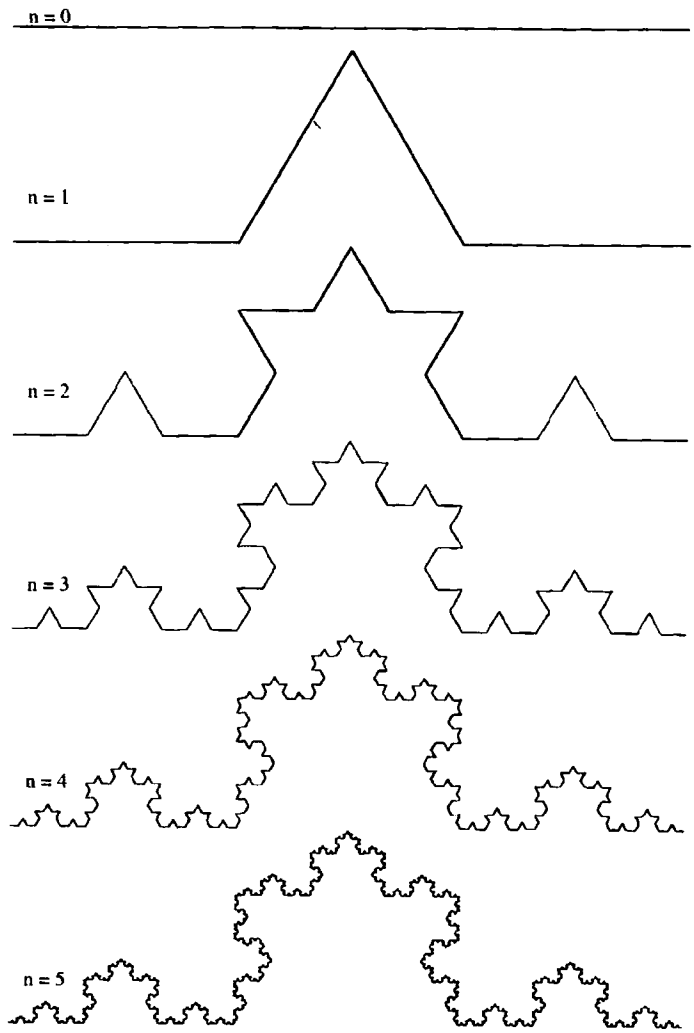

Figure 2.8. From top to bottom: initiator, generator, the next stage in the construction, and high-order approximation for the Koch curve (from Schroeder, 1991).

Examples of fractals in nature are abundant: shapes of coastlines or clouds, graphs of population fluctuations, distributions of intervals between earthquakes, lengths of topographic contours, hillslope profiles, etc. all contain apparently smooth segments which, when magnified, contain a resemblance to the larger object (within a limited range). A magnified section of a slope profile will look the same as the whole (in a

statistical sense) as we cannot say that the magnified section is not actually the whole profile (Figure 2.9). This is why we often need to include objects of a known size (such as a tape measure or a person) in photographs of the earth's surface. As water-worked soil forms would be expected to be aligned to the main flow direction (i.e. downslope) the fractal characteristics of such surfaces are likely to be anisotropic; in this case the surfaces are no longer self-similar, but *self-affine* (the effects of magnification are dependent upon profile direction) (Butler *et al.*, 2001).

The second characteristic of fractals is the fractal dimension; it is through the estimation of this property that a conceptually simple method of calculating surface roughness has been developed as an alternative to the height variance methods which give no regard to scale.

The length of a smooth curve can be approximated by stepping along it N times with a ruler of length r so that the measured length $L(r) = Nr$. As noted in Figure 2.7, the more sinuous the curve becomes, the smaller the ruler necessary to provide an accurate approximation of the length. Therefore, as the step size r tends to zero, the measured lengths will converge to the exact length of the curve:

$$L = \lim_{r \to 0} L(r) = \lim_{r \to 0} Nr$$

(Equation 2.10)

However, while attempting to measure the length of coastlines using this technique, Richardson (1961) found that this limit does not exist. As r tends to 0 the product Nr diverges to infinity because of the infinite number of fine structures contained within the fractal. The product Nr^D does remain finite for a particular exponent $D>1$. For exponents smaller than D, Nr^D tends to infinity, whereas for exponents larger than D, the product goes to 0 (Rodríguez-Iturbe & Rinaldo, 1997). At this critical value of D

$$\lim_{r \to 0} N(r)\, r^D = \text{constant}$$

(Equation 2.11)

where $N(r)$ represents the number of steps on the size of each step. If the surface roughness under consideration is independent of scale over a range of scales then $N(r) \propto r^{-D}$ or $L(r) \propto r^{-D}$. Including a constant of proportionality M gives

$$L = Mr^{1-D}.$$

(Equation 2.12)

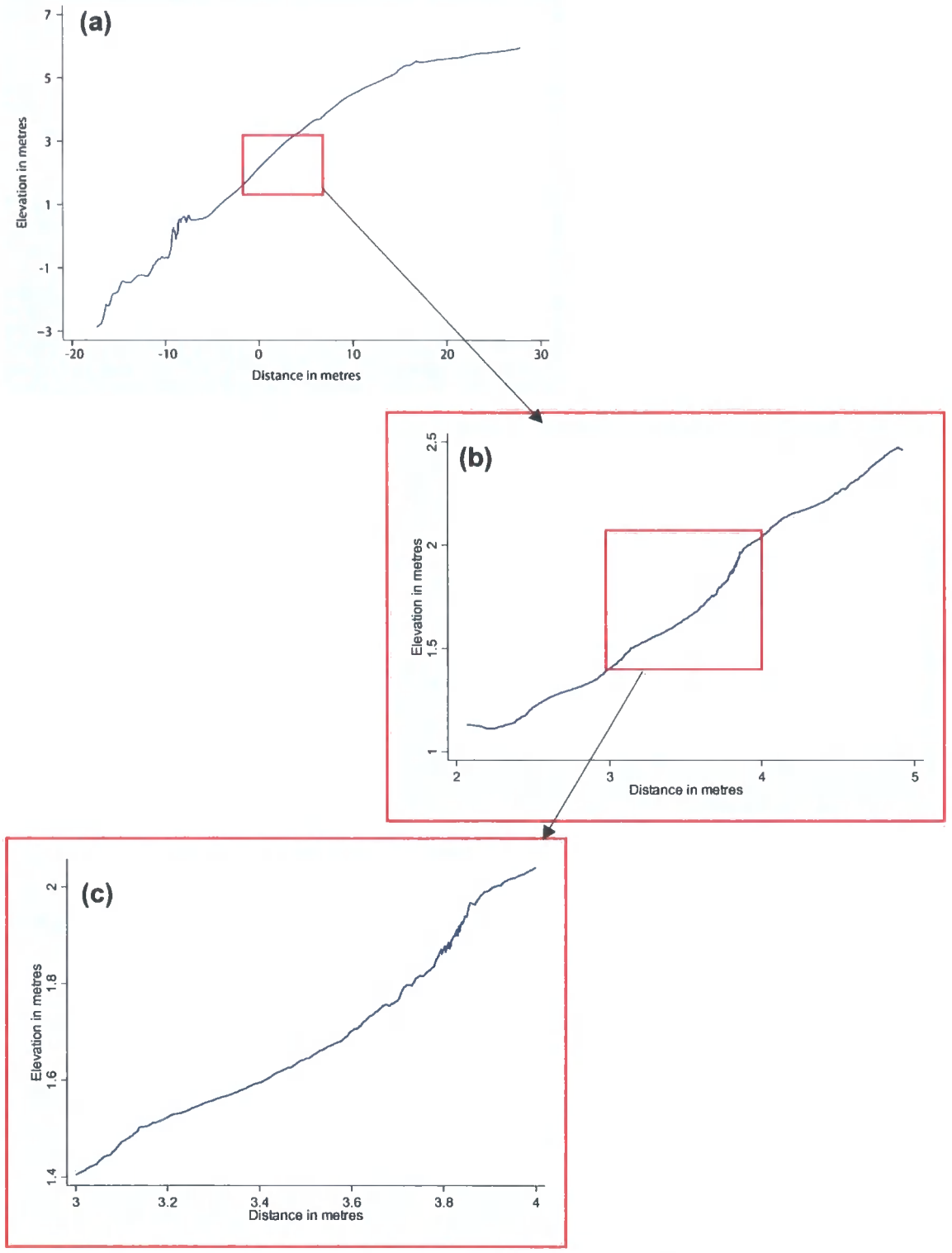

Figure 2.9. Example profile seen at several scales: (a) the whole hillslope profile; (b) a 3 m plot-sized profile within the hillslope; (c) 1 m segment of the profile. Profile (c) is equally as complex as the original (a).

D need not be an integer, but for a fractal curve, it must exceed the topological dimension (which is 1 for profile and 2 for a surface). It is this critical exponent, *D*, that is the most common definition of the fractal dimension. For a smooth curve, equation

2.11 suggests that $D = 1$, and likewise for a smooth surface, the number N or area elements (squares) needed to cover the surface increases with $1/r^2$, therefore $D = 2$.

Transforming equation 2.12 in a logarithmic form produces the linear equation

$$\log L = \log M + (1 - D) \log r \quad \text{(Equation 2.13)}$$

and so the fractal dimension, D, can be indicated by the gradient of the resulting straight line (Pardini & Gallart, 1998). Bertuzzi *et al.* (1990) and Merril (1998) used a similar technique, replacing log L with ln T_B and T_S respectively.

The value of D (which for a profile is bounded by the inequality $1 \leq D < 2$) characterises the roughness of the profile, increasing as the surface becomes more irregular. Dunne *et al.* (1995) found that soil microtopography of natural surfaces is fractal with a dimension that decreases systematically downslope. This was thought to reflect the progressive development of low-frequency roughness ('swaley' microtopography) through wash processes and result in a downslope increase in the size of depressions (forming in broad swales). However, Darboux *et al.* (2002) suggest that surfaces with fractal properties do not display any particular behaviour with respect to depression storage effects on overland flow triggering and so fractal-based roughness measures are represent no improvement over standard measures. Additionally, Kamphorst *et al.* (2000) suggest that fractal indices are merely regression parameters rather than a measure of roughness itself and cannot be used to quantify MDS.

The use of the fractal dimension to characterise surface roughness is advantageous as, unlike tortuosity, it does not require the exact profile length or surface area (which theoretically can never be measured exactly), but only how the measured length or area changes with a changing interval of measure (Pardini & Gallart, 1998). Additionally, the same procedure can be performed on an entire surface area rather than simply a profile taken from the surface.

A fractal index works to the extent there exists a self-similarity in surface roughness across a range of scales (Kamphorst *et al.*, 2000). Many studies have shown that such self-similarity occurs over a limited range of scales (Dunne *et al.*, 1995; Evans, 1972, 2003; Kirkby, 2001); however, Fardin *et al.* (2004) note that D may increase with an

increased sampling window as new scales of variation are encountered. Burrough (1983) showed that a soil surface behaves as a 'pseudo-fractal'; fractal behaviour exists only over a certain range of scales. The various scales of interacting geomorphological processes lead to nested levels of variation with complicated relations between these levels, reflecting the natural heterogeneity of natural landscapes. Bartoli *et al.* (2005) suggest it is possible that the geometric properties of soil surfaces may not be described by a single fractal dimension; instead they may be considered 'multifractal objects'. Therefore it is relevant to consider the scale over which autocorrelation occurs in soil surfaces. This is included within another approach to measuring surface roughness, the use of 'geostatistics'.

2.6.4 Geostatistics

Linden & Van Doren (1986) attempted to develop a measure of surface roughness that was not distributionally dependent. Their limiting elevation distance LD and limiting slope LS measures take into account the strong spatial dependence and non-randomness found at close spacings (but not at wider spacings). These measures are based on the first order variance or mean absolute elevation difference ΔZ_h as a function of lag h.

Linden & Van Doren (1986) performed spatial variance analysis to determine the degree of variance between points at various spacing intervals; this may be expressed in the form of a semivariogram which can be used to assess the scale and magnitude of the spatial variations (Oliver & Webster, 1986). Linden & Van Doren (1986) used linear regression analysis to relate ΔZ_h to lag distance ΔX_h:

$$\frac{1}{\Delta Z_h} = a + b\left(\frac{1}{\Delta X_h}\right)$$

(Equation 2.14)

where a and b are fitted parameters. Figure 2.10 demonstrates the form of this relationship. ΔZ_h rises with increasing lag until it reaches a plateau or 'sill' at a certain lag distance or 'range'. Burrough (1983) suggests that soil surfaces display fractal behaviour until this interval is reached. The 'nugget' is the value of semivariance at zero lag distance and is the measurement error or bias, perhaps 'noise' related to structured spatial variations at a scale below the grid used for sampling (Hypanen, 1996).

The limiting distance roughness measure LD used by Linden & Van Doren (1986) is the reciprocal of the asymptote of the first-order variance (i.e. the sill) and is therefore directly related to the configuration of the surface. As the horizontal spacing ΔX tends to 0, the reciprocal of the first-order variance will approach a and ΔZ will correspondingly tend to $1/a$. Therefore the limiting distance LD is calculated as

$$\mathrm{LD} = \frac{1}{a}.$$

(Equation 2.15)

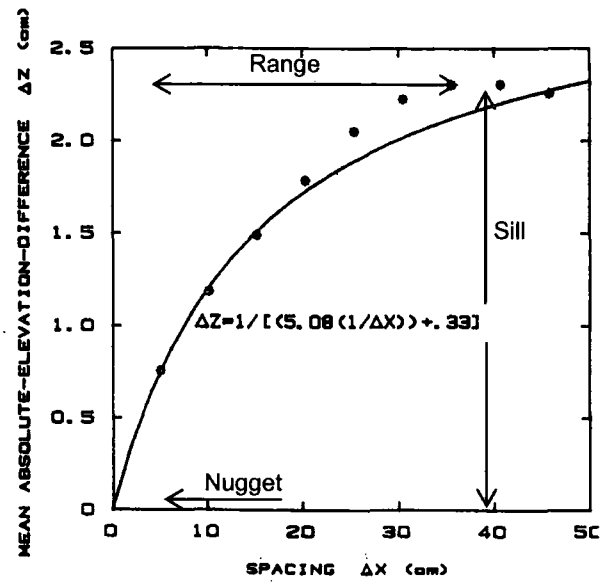

Figure 2.10. A sample data set showing mean absolute elevation difference ΔZ plotted as a function of horizontal spacing distance ΔX. Adapted from Linden & Van Doren (1986). The line represents the equation

$$\frac{1}{\Delta Z_h} = a + b\left(\frac{1}{\Delta X_h}\right).$$

This measure of roughness considers the central tendency in elevation between individual points and is well correlated with RRI (explaining 91% of data variation) (Linden & Van Doren, 1986). The limiting slope LS is defined as

$$\mathrm{LS} = \frac{1}{b}$$

(Equation 2.16)

and is a measure of the slope limit of the surfaces as measurement spacings become very small (Magunda *et al.*, 1997). Linden & Van Doren (1986) noted that LS is related

to soil surface area, and Bertuzzi *et al.* (1990) suggested that it is also related to tortuosity at small intervals.

Linden *et al.* (1988) used a combination of LS and LD to predict MDS with the aim of increasing accuracy through the use of more than one roughness index:

$$\mathrm{MDS} = 0.382\sqrt{\mathrm{LD}\cdot\mathrm{LS}} + 0.017\sqrt{\mathrm{LD}\cdot\mathrm{LS}}\cdot S - 0.077 .$$

(Equation 2.17)

While this takes into account the spatial structure of the soil surface (in a statistical sense), the volume of water in depression storage depends specifically upon the lowest altitude of its perimeter, a characteristic not taken into account in their analysis (Darboux *et al.*, 2001b). Additionally, they note that erosion and sedimentation processes will alter the runoff characteristics of a surface, and these should also be taken into account.

Indeed, although semi-variograms provide a useful measurement of the spatial nature of surface roughness, Hansen *et al.* (1999) suggest that the regressions involved in some calculations neglect important characteristics of the soil surface as reflected in the exact elevation difference between adjacent grid points. Fitting models to experimental variograms is somewhat contentious (Oliver & Webster, 1986). Non-random components of roughness will alter the form of the experimental semi-variogram so that the sill and range are difficult to determine. This will be especially problematic on natural soil surfaces where linear roughness elements are present. Kamphorst *et al.* (2000) even question the physical meaning of the LD and LS parameters, suggesting instead that they are statistical parameters, merely describing the form of the semi-variogram. Other features of a semi-variogram such as the semi-variance at a set separation distance may provide a better indication of the actual form of the soil surface. However, graphs such as Figure 2.10 allow surface variance associated with a given scale to be predicted and thus show information relating to the rate of change of semi-variance (in a geostatistical sense); it is most unlikely that this will reveal anything about the volume of depression storage.

2.6.5 Mean Upslope Depression

The Mean Upslope Depression MUD of Hansen *et al.* (1999) was the first roughness measure developed specifically to predict depressional storage. Unlike the roughness

measures mentioned above, the slope term is integrated into the measure itself; therefore a model to predict MDS requires no additional slope term. MUD is calculated from a transect by choosing a subsegment and defining the most downslope point as the reference point. The mean height difference between this reference point and all other points is then calculated, the subsegment is displaced by one point, and the process is repeated (Hansen *et al.*, 1999) (Figure 2.11). The MUD is the mean value of these calculations.

The nature of the MUD calculation means that several sample size issues need to be addressed, such as the number and length of subsegments used. Such arbitrary decisions may affect the outcome of the calculations. Hansen *et al.* (1999) suggested that longer subsegments are most efficient (suggesting ~30 cm) and that the distance between measured points has no effect on MUD value unless it exceeds some maximum value dependent on roughness and slope. However, the use of arbitrary subsegments produces an extremely complicated measure of roughness, divorced from the actual surface form.

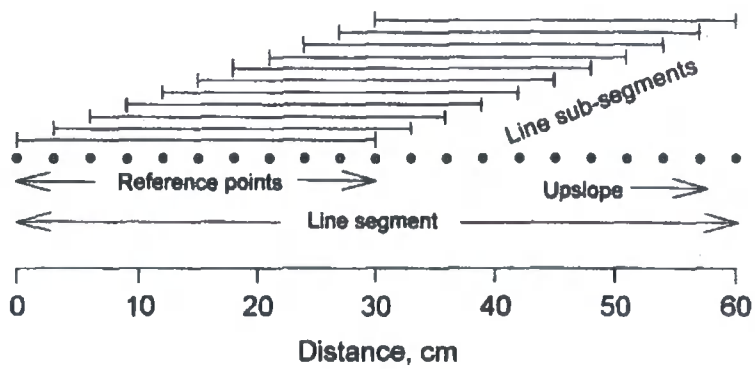

Figure 2.11. A sketch of the principle for calculation of the MUD-index from reference points and sub-segments in a line segment. Exemplified for the up-and-down slope situation. From Hansen *et al.* (1999).

Although roughness elements identified from transects up and down the slope have greater influence on MDS than those oriented across the slope, Hansen *et al.* (1999) found that the highest correlation between MUD and MDS was obtained when calculations are made for both directions:

$$\mathrm{MDS} = 0.224\mathrm{MUD}_u + 2.14\frac{\mathrm{MUD}_u}{\mathrm{MUD}_a}$$

(Equation 2.18)

where MUD_u is measured up and down the slope, MUD_a is measured across slope. Hansen *et al.* (1999) found that this accounted for 86 % of data variation; however high *MDS* values were slightly underestimated. Kamphorst *et al.* (2000) found that this MUD model for predicting MDS on tilled surfaces was the most accurate when compared with other models.

2.6.6 MIF (Microrelief Index and peak Frequency)

Römkens & Wang (1986) developed this roughness index to improve deterministic descriptions of surface microtopography changes during a rainstorm on relatively small interrill areas. It is simply calculated as the product of the microrelief index MI (the area per unit length between a measured surface profile and the regression line of least squares through it) and the peak frequency, F (number of elevation maxima per unit transect length). The result is a simple, dimensionless, non-unique roughness measure that is strongly associated with clod size and frequency (Römkens & Wang, 1987). However, the peak frequency variable is problematic because like tortuosity, it is scale-dependent (a profile described with a smaller sample spacing will exhibit a greater number of peaks). This roughness measure can describe changes in soil surface form, and so has not been applied to the prediction of MDS.

2.7 Modelling Surface Roughness Effects

In order to develop a process-based, spatially-distributed erosion prediction model, we must first understand the relationships between surface morphology and the processes of runoff and soil erosion at different spatial and temporal scales (Huang *et al.*, 2001). Takken *et al.* (2005) identify three potential shortcomings of such a model:

1. process descriptions may be incomplete or incorrect (structural errors);
2. parameterisation may lead to a high degree of uncertainty regarding model inputs (input error); and
3. the spatial implementation of the model (particularly routing methods) may be inadequate.

Although the process of depression storage has been ignored in many hydrological models, EUROSEM (Morgan *et al.*, 1998a) offers an extremely limited treatment whereby a roughness measure based on tortuosity T_A, is used to predict MDS (using equation 2.8 above). This amount is then simply abstracted from precipitation amounts

before runoff is generated. Interrill overland flow is usually modelled as broad shallow sheet flow (the hydraulic radius is simply the flow depth) where the entire surface is fully submerged (Takken & Govers, 2000). Such a condition is rarely met on hillslopes and yet this assumption influences the calculation of hydraulic roughness coefficients used in spatially distributed, deterministic erosion models (such as EUROSEM). Jetten *et al.* (1998) demonstrated that the outcome of these soil erosion models is particularly sensitive to the value of the hydraulic roughness coefficients used.

Lane (2005) suggests that 'surface roughness' is the component of topography that must be parameterised; as the spatial scale under consideration changes, so does the amount of topography that a model must deal with implicitly. Therefore, catchment scale models generally integrate over the details of microtopography (Kirkby *et al.*, 1996). 'Roughness' should be researched at the scale at which either the data or model resolution (whichever is limiting) causes topographic expression to be no longer explicit: there is a direct link to the model and the data. The effective parameterisation of surface roughness is especially difficult considering the vagueness of its definition (section 2.6) and the numerous effects it has on the processes operating on the soil surface (section 2.3).

Jetten *et al.* (1999) note that although total amounts of erosion were often well predicted by soil erosion models, this was not the case for the pattern of the soil erosion. From a management perspective, knowledge of the locations of areas of high runoff and soil erosion risk is particularly valuable. Takken *et al.* (2005) suggest that the spatial implementation of erosion prediction models can be improved by taking into account the effect of roughness on the runoff pattern (section 2.4). Runoff may be directed away from the general slope direction (reducing the effective slope) and so routing algorithms can be used to define where water will be concentrated (and severe erosion is likely to occur). Such an approach emphasises the importance of acquiring topographic data (Takken *et al.*, 2001).

Kirkby (2001) proposes that roughness effects can be effectively incorporated within erosion models while retaining an acceptable level of simplicity by separating surface roughness into two components. This is achieved through the addition of parameters for down-slope roughness (which acts to impede flow, section 2.3.1) and cross-slope

roughness (which concentrates flow, section 2.4). Such an approach may provide a simple framework through which the multifaceted effects of surface roughness on surface processes may be incorporated into process-based, spatially-distributed erosion prediction models.

2.8 Conclusions and Research Gaps

Our knowledge of the effect of soil surface roughness on hydrologic and erosion processes is far from complete (Govers *et al.*, 2000). Surface roughness influences depression storage, infiltration, runoff production, overland flow routing and velocity and soil erosion in many different ways. Few studies have addressed the effect of the filling of depressions on overland flow generation, connectivity development and the effect of surface roughness on the overland flow itself (Darboux *et al.*, 2002). Also, considerable uncertainty exists in the literature on the effect of surface roughness on soil erosion by raindrop impact and, particularly, overland flow. This has considerable consequences for models of runoff and soil erosion; however, these commonly operate under several assumptions that neglect to incorporate the effects of surface roughness. Römkens & Wang (1987) suggest that this largely stems from the complex and seemingly random nature of surface topography and the difficulty of its mathematical description.

Indeed, although several measures have been developed in an attempt to characterise surface roughness, at present the absence of a standardised methodology for characterising surface roughness impedes further developments in this field of study. Few studies have attempted to compare the performance of the various roughness measures (Govers *et al.*, 2000). Kamphorst *et al.* (2000) suggest that the only way to improve our ability to predict depressional storage and overland flow generation is to abandon roughness measures that are applied to transects and to work in three dimensions. Recent technological developments including the use of laser scanners are increasingly allowing the rapid generation of accurate, densely spaced measurements of surface elevation. Such developments may lead the way to substantially improved roughness descriptions and evaluations at the scale below which most runoff and erosion models can explicitly represent topography. With these technological advances set to continue, the acquisition of fine-scale topographic data becomes less time-

consuming, gradually easing the transition of the study of surface roughness from two- into three-dimensions.

Additionally, the increased portability of such instruments means that information may be gathered in the field with relative ease; this may eventually address the issue of the lack of studies on natural soil surfaces. The unprecedented range and accuracy of newly developed laser scanners means that surface roughness at fine-scales may be assessed over larger areas than traditionally achievable, permitting analyses of the relationships between soil surface roughness and both runoff and erosion at the hillslope scale. Results found at this scale are much more appropriate when considering potential management responses to problems caused by runoff and soil erosion.

Many studies concentrate on a single factor influencing surface roughness (such as raindrop impact), neglecting to incorporate the variable importance of other factors (such as flow concentration) in different situations. A study of surface roughness conducted at both plot and hillslope scales may go some way towards improving our understanding of surface roughness and its influence on runoff and erosion processes.

Chapter 3 Field Sites & Methodology

3.1 Introduction

This chapter provides detailed descriptions of the field sites and method used in this study. The study area and the specific locations and characteristics of hillslopes used in this investigation are described in section 3.2. Section 3.3 explains the methods used and is split into several sections. Section 3.3.1 briefly recaps the use of 'Morphological Runoff Zones'; section 3.3.2 deals with the monitoring of sediment transport and hillslope runoff; in section 3.3.3 the use of the minidisk infiltrometer is described; section 3.3.4 describes the terrestrial laser scanner used in the study, explains how scans were conducted in the field and also details how point clouds and surfaces were generated from these scans. Section 3.4 provides a short summary of the methods used and how they relate to the aims previously outlined in section 1.2.

3.2 Fieldwork Location

3.2.1 Catchment Characteristics

The Guadalentín River of south-east Spain is thought to be one of the most torrential rivers in the country (Benito *et al.*, 2002). This investigation considers two typical Mediterranean semi-arid catchments situated within that basin: the Rambla Nogalte catchment, which is on the border of the provinces of Murcia and Almeria, and the Rambla de Torrealvilla catchment, nearby in Murcia (Figure 3.1). This area of Spain is the driest part of the western Mediterranean; Bull *et al.* (2003) report that the catchments receive approximately 300 mm of rain annually. Therefore, Hooke & Mant (2000) suggest that these conditions provide a valuable exemplar of an environment that may become more widespread should global warming predictions prove accurate. These catchments were also chosen because much research has previously been conducted; several Casella 0.2 mm tipping bucket rain gauges with integral loggers have already been installed (Figure 3.1). The two rivers also offer contrasting catchment characteristics, as seen in their different responses to an extreme storm event in September 1997 (Bull *et al.*, 1999).

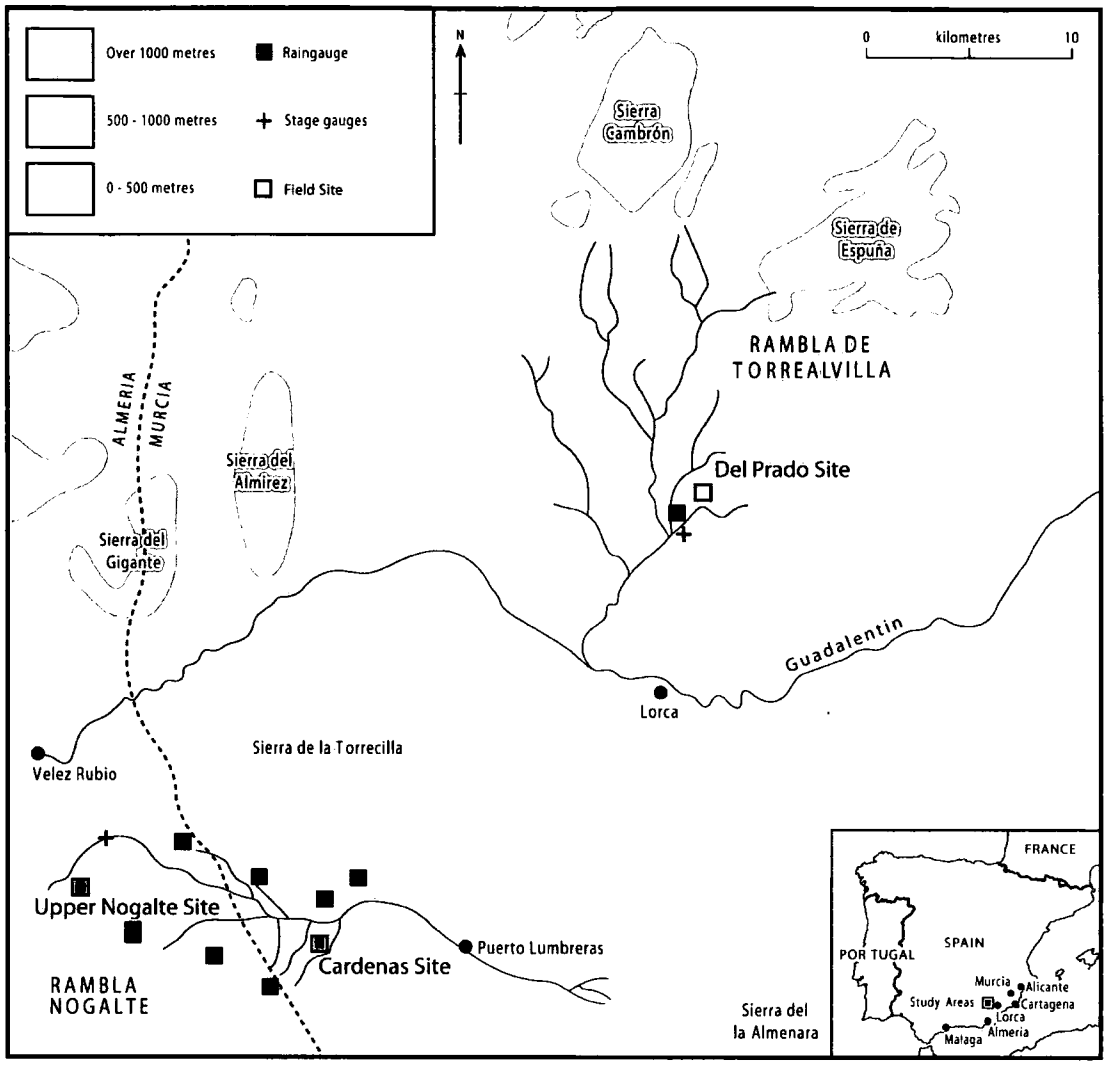

Figure 3.1. The study area in south-east Spain indicating the locations of the Rambla Nogalte and Rambla de Torrealvilla, field sites and rain gauges.

The Rambla Nogalte is a broad gravel bed river draining an area of 171 km^2 which is dominated by schist and other metamorphic rocks. Most of the soils are dominated by thick brownish-red mica schist, but localised outcrops of thin, flaky, blue mica schist are also present (which supports only sparse or no matorral vegetation cover) (Bull *et al.*, 1999). Figure 3.2 shows that natural matorral (composed mainly of anthyllis, grasses, rosemary and thyme) remains on only about a third of the surfaces, as 64.1 % of the convex hillslopes of the Nogalte catchment are used for almond and olive tree cropping (Bull *et al.*, 1999).

These ploughed surfaces provide large areas of bare soil between the almond or olive trees, and therefore provide a much less continuous vegetation cover than the matorral.

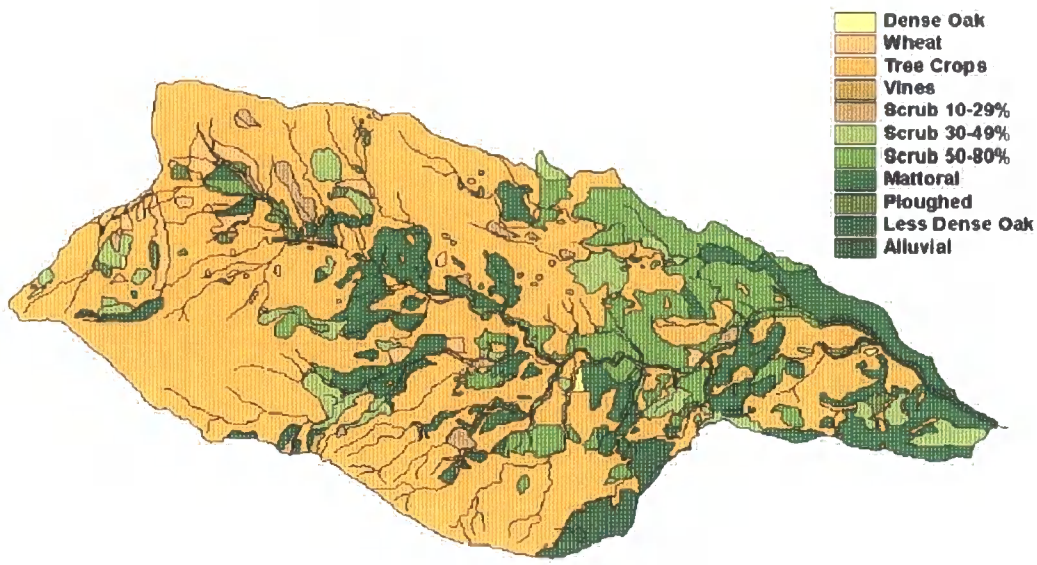

Figure 3.2. Land use within the Rambla Nogalte catchment (from Bull *et al.*, 2003).

The Rambla de Torrealvilla catchment drains an area of 200 km^2 which is dominated by marls. Intensive farming of wheat, water melons and lettuces takes place on the flat pediment surfaces (which are dissected by box-shaped channels). Areas not used for arable farming are left as matorral. Bull *et al.* (1999) report that this catchment generally produces much higher flood peaks from rainfall events than the Rambla Nogalte catchment.

3.2.2. Experimental Locations

Experimental locations were selected on the basis of the size of the hillslopes, their gradient, soil-type, land-use and the availability of suitable vantage points for laser scanning. Additionally, hillslopes with little vegetation cover were selected to maximise soil surface exposure for scanning. The three sites selected represent the entire range of hydrological characteristics found on hillslopes within the catchments, allowing this investigation to be as representative as possible.

The Upper Nogalte hillslope (Figure 3.3) is located in an area of red schist in the Nogalte catchment. This soil is low in clay minerals and high in quartz and feldspar, has a high infiltration capacity and exhibits weak crust development. The vegetation cover consists of thin grasses, thistles and thyme bushes; however, a strip of the hillslope has been recently ploughed. This area of the Nogalte catchment has a relatively high runoff threshold and is thought to be particularly unresponsive to rainfall.

Figure 3.3. Upper Nogalte hillslope located in an area of red schist in the Rambla Nogalte. Note the band across the hillslope which has previously been subject to ploughing.

The Cardenas site (Figure 3.4) is situated in the Cardena sub-catchment, an area of blue schist, believed to be one of the key runoff-producing areas in the Nogalte catchment (Bull *et al.*, 2003). Soil in this area is high in clay minerals and slaty fragments, susceptible to strong crust development, and therefore considered to have a low runoff threshold (Bracken & Kirkby, 2005). The vegetation cover is made up of small bushes of thyme and anthyllis separated by extensive bare areas. The Cardena sub-catchment is characterised by steep gorge-like topography which generates large volumes of runoff compared with the rest of the Nogalte catchment. Land-use of the hillslope is divided; half is used for almond cropping, and the rest has been left to matorral.

Figure 3.4. Cardenas site, situated in an area of blue schist in the Rambla Nogalte. The SE side of the slope (left) supports almond trees whereas the NW side (right) remains untouched.

Finally, the Del Prado site (Figure 3.5) is situated on a bare area of marl in the Rambla de Torrealvilla which is also suspected of producing large amounts of runoff. Bull *et al.* (1999) suggest that runoff thresholds are much lower on the marls of the Torrealvilla than on the schists of the Nogalte. The surface is composed mainly of fines, with evidence of both a structural crust and a lichen crust, and is mostly devoid of vegetation (with occasional grasses and thyme bushes visible) (Bracken & Kirkby, 2005).

Figure 3.5. Del Prado site, situated on a bare area of marl in the Rambla de Torrealvilla.

3.3 Methodology

3.3.1 Morphological Runoff Zones

'Morphological Runoff Zones' (MRZs) use the form of the soil surface to imply spatial differences in runoff and erosion in semi-arid catchments. These are described in more detail in section 2.2.4. Bracken & Kirkby (2005) propose that this hillslope-based approach should be used to provide links with catchment-scale data provided by remote sensing. Field sketches were made to provide an approximation of the MRZs at each site; these were based on morphological evidence of runoff intensity through its impact on sediment movement (Table 2.1). The sketches were used to ensure that a plot scan was conducted in each MRZ and they were combined with hillslope scans to show their location in relation to the overall topography of the hillslopes and to assess the connectivity of each hillslope.

The morphological evidence described earlier is easily identified in the field and provides a simple method of ensuring that a range of surface morphologies are analysed on a hillslope. Additionally, ploughed areas of the hillslopes were scanned to examine briefly how the conversion of these natural soil surfaces to ploughed fields influences hydrologic and erosion processes.

3.3.2 Sediment Transport and Hillslope Runoff

On each hillslope, several monitoring sites were established during previous research (Bracken & Kirkby, 2005) (Table 3.1). These monitor sediment transport (through the use of spray painted lines), weight of transported sediment (with sediment bags) and provide approximations of maximum hillslope runoff (using mini-crest stage recorders). The typical experimental setup is shown in Figure 3.6. These sites use a 'light touch' to gather runoff and sediment transport data in many places on one hillslope. Therefore this methodology is practical when attempting to study processes operating at the hillslope scale and improve understanding of hillslope behaviour, enabling more realistic model development of runoff and erosion at this scale (Bracken & Kirkby, 2005).

Site	*Sprayed Lines*	*Sediment Bags*	*Mini Crest-Stage Recorders*
Upper Nogalte	5	5	2
Cardenas	5	5	2
Del Prado	3	3	1

Table 3.1. Location of sediment transport and hillslope runoff monitoring sites.

Figure 3.6. Typical experimental setup of monitoring stations showing a spray-painted line, sediment bag and mini crest-stage recorder.

The spray painted lines were used to monitor sediment transport (Kirkby & Kirkby, 1974). A 1 m long line (approximately 18 mm in width) was sprayed at each monitoring site and the particle-composition of the line was recorded through size measurements of the sprayed material. During the revisiting of the site, measurements were taken of the downslope travel distance of each moved stone, and the size range each stone falls into. Sediment transport rates and travel distances may then be calculated for each sediment size. This method is simple, effective, cheap and produces much data (Bracken & Kirkby, 2005). However, it

only provides an approximation. Fine sediments often wash away, and particle recovery declines with increasing distance travelled. Kirkby & Kirkby (1974) suggested that this method provides a minimum estimate due to such non-recovery and the burying or turning-over of painted stone faces. Additionally, small movements less than the width of the line are not recorded, and trampling may disturb the sediments on the line. All lines were painted on rangeland surfaces as the lines on ploughed hillslopes were frequently destroyed (Bracken & Kirkby, 2005).

Sediment bags are situated below these sprayed lines to provide weights of the transported sediment to support the sediment budgets. These bags are made from muslin or net and are sewn to ~ 30 cm^2 with an extended lip which is stuck to the ground using resin. The opening is 25 cm wide and the mouth of the bag is kept rigid using a 2 mm diameter wire threaded through the opening, which also helps to keep the bag fixed to the ground surface. The resin used consists of 10 g vinyl acetate-vinyl chloride co-polymer dissolved in a solvent of 50 g acetone and 50 ml iso-butyl ketone (Bracken & Kirkby, 2005). This resin dries to form a smooth lip which directs moving sediment into the bag. The bag is also weighted down with large stones to prevent it from being washed away. During revisiting of the site the bags are removed and replaced and their contents are air dried, sieved and weighed. This technique is both cheap and easy to install, it provides comparable results at different sites and it does not disturb the soil surface. Also, the flexible fabric of the muslin and net bags naturally follows the form of the hillside (Bracken & Kirkby, 2005). However, the bags may fill up between site visits and so can only be used to provide a minimum estimate of sediment weight.

Mini crest-stage recorders were used to provide estimates of maximum depth of flow over the hillslopes. Two of these were installed at each site, one near the top of the slope and another in an area of concentrated flow towards the base of the hillslope. These were constructed from a 35 cm length of 32 mm square wooden poles sharpened at one end and forced into the ground (Bracken & Kirkby, 2005) until approximately 30 cm remained above ground. The pole was then painted with a mixture of food dye and salt and left to dry. It was also covered with a length of drainpipe with a cap on one end and a hole near

the top to let the air escape as the pole becomes inundated (Bracken & Kirkby, 2005). This is a cheap and accurate method which uses materials readily available in the field area. However, it only records maximum flow depth and may present accuracy problems if the dye and salt are removed diagonally (as seen on steep slopes).

3.3.3 Infiltration Measurements

To assess the influence of surface roughness on infiltration parameters it is necessary to make *in situ* infiltration measurements with minimum disturbance of the soil surface. Additionally, the small-scale of some roughness features means that point measurements of infiltration are preferable. Zhang (1997) suggests that hydraulic conductivity is the single most important hydraulic property affecting water flow in soils. However, its measurement can be difficult and time-consuming. The minidisk infiltrometer (Figure 3.7) is well suited to this task. It takes a reading over an area of just 20 mm in diameter, and so is capable of measuring the variability of infiltration rates at a scale appropriate for this investigation. While the minidisk infiltrometer does not disturb the soil surface, a thin layer of wet sand (~3 mm) placed on the soil surface is necessary to ensure a good contact (Figure 3.7). The infiltrometer is filled with water and a rubber stopper is inserted in the top. It is then placed on the sand layer and the volume change is recorded over a period of five minutes.

The minidisk infiltrometer is an acrylic tube with a semi-permeable plastic disk as a base. A small tube installed just above the disk regulates the suction rate. The method is quick and easy, requires no large equipment (such as a rainfall simulator) and very little experimental set-up, and uses only very small amounts of water per test (~100 ml), which is particularly advantageous in a semi-arid environment where supplies of water are limited. It provides comparative data, and can be repeated several times at each site. Li *et al.* (2005) report that steady infiltration rate measured by a minidisk infiltrometer at a tension of 0.5 cm produces results consistent with studies using rainfall simulators. However, a minidisk infiltrometer does not simulate raindrop impact which would allow an analysis of changes in runoff and roughness with aggregate breakdown and surface sealing.

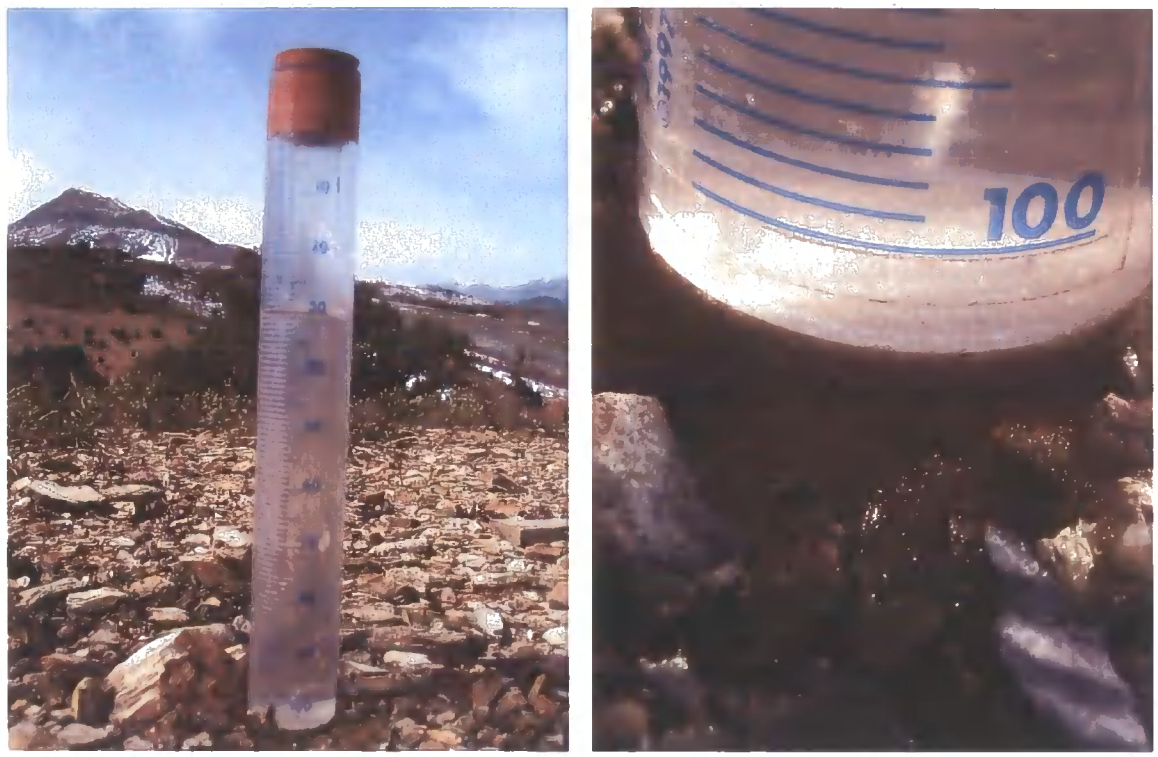

Figure 3.7. The minidisk infiltrometer (left) and the small layer of wet sand needed to ensure a good contact with the soil surface (right)

Using this method, infiltration measurements were taken on transects through the site of each plot scan ensuring that the different elements of surface roughness were all represented at each plot. Soil hydraulic conductivity could then be calculated using the method proposed by Zhang (1997) where the measured cumulative infiltration I is fitted as a function of time t

$$I = C_1 t + C_2 \sqrt{t},$$

(Equation 3.1)

where C_1 and C_2 are fitted parameters. The soil hydraulic conductivity K may then be estimated as

$$K = \frac{C_1}{A}.$$

(Equation 3.2)

A can be calculated from the minidisk radius r_0, the suction at the disk surface h_0 and the van Genuchten parameters for the soil n and α (Zhang, 1997):

$$A = \frac{11.65(n^{0.1} - 1)\exp[2.92(n - 1.9)\alpha h_0]}{(\alpha r_0)^{0.91}} \quad (n \geq 1.9)$$

(Equation 3.3)

or

$$A = \frac{11.65(n^{0.1} - 1)\exp[7.5(n - 1.9)\alpha h_0]}{(\alpha r_0)^{0.91}} \quad (n < 1.9)$$

(Equation 3.4)

The minidisk infiltrometer used in this study has a radius of 1.59 cm and infiltrates water at a suction of 2 cm. The van Genuchten parameters for the 12 texture classes of soil were obtained from Carsel & Parrish (1988).

3.3.4 Terrestrial Laser Scanning

The collection of elevation data for use with surface roughness measurements is problematic; many methods involve laborious field techniques which result in low resolution data. A variety of microrelief meters have been used, ranging from hand-held rulers and pin meters to remote sensors, laser scanning techniques and digital photogrammetry (see Table 3.2). While early techniques involved instruments (rows of pins or chains) that were lowered on the surface itself (Saleh, 1993), techniques not based on contact are preferable in the measurement of the surface elevations to avoid disturbance of the roughness elements. Oelze *et al.* (2003) successfully used acoustic backscatter techniques to measure surface roughness statistics. However, while this proved quick and inexpensive, it could only offer roughness statistics of a surface rather than measurements at the full profile, thereby limiting further data analysis.

This study uses a MDL LaserAce 600 terrestrial laser scanner to obtain elevation data (Figure 3.8). This represents a significant advance in laser scanning technology, offering a new method of field survey in geomorphology (Nagihara *et al.*, 2004). Such terrestrial laser

scanners are capable of rapidly making a large number of elevation and position measurements from which high-density point clouds can be produced. The use of a terrestrial laser scanner removes the need to conduct laborious measurements of elevation data and so reduces the restrictions that this poses. Such time-consuming measurements may disturb the soil surface and may be of a lower resolution than the data obtained using scanning equipment.

Figure 3.8. The MDL LaserAce 600 terrestrial laser scanner used to obtain position and elevation data.

Roughness Measure	Measurement Method	Plot Type	Plot Area	Number of Surfaces	Measurement Spacing	Subject	Study
RR (mm)	Mechanical Pin meter	Tilled field plots	1 × 1 m	16	5 × 5 cm	Effect on rainfall on roughness and runoff	Moore & Larson (1979)
RR (mm)	Pin meter	Tilled field plots	0.9 × 1.5 m	1060	15 × 1.3 cm	Predicting MDS from surface roughness measures	Onstad (1984)
RR (mm)	Mechanical Pin meter	Tilled field plots	1 × 1 m	2	6.4 × 50 mm	Relationship between RR and hydraulic roughness	Gilley & Finkner (1991)
RR (mm)	Laser scanner	Flume (seedbed)	0.65 × 0.65 m	4	2 × 2 mm	Relationship between RR and hydraulic roughness	Takken & Govers (2000)
RR (mm) & Tortuosity (T_B)	Laser scanner	Flume (tilled)	2 × 4 m	6	1.5 × 1.5 mm	Effect of roughness on runoff distribution and soil erosion	Gómez & Nearing (2005)
LD (mm) and LS	Pin meter	Tilled field plots	2 × 2 m and 0.9 × 0.9 m	159	2 × 2 cm or 5 × 5 cm	Predicting MDS from surface roughness measures	Linden & Van Doren (1986)
MUD (mm)	Automated pin meter	Ploughed/ drilled field plots	2.6 × 1.3 m	32	6 × 3 cm	Predicting MDS from surface roughness measures	Hansen *et al.* (1999)
MIF	Automated non-contact surface profile meter	Tilled field plots	1.5 × 1.8 m	33	5 × 20 mm	Effect of tillage on roughness	Römkens & Wang (1986)
MIF	Automated non-contact surface profile meter	Tilled field plots	1.5 × 1.8 m	3	5 × 20 mm	Effect of rainfall on roughness	Römkens & Wang (1987)
Tortuosity (T_A)	Stereo-photogrammetry	Lab plots (seedbed)	0.4 × 0.5 m	5	2 × 2 mm	Predicting MDS from surface roughness measures	Morgan *et al.* (1998)
Specific Surface Area (3D T_B)	Laser microrelief meter	Flume (seedbed)	0.6 × 3.7 m	9	3 × 3 mm	Effect of roughness on runoff distribution and soil erosion	Helming *et al.* (1998)
Various	Terrestrial laser scanner	Natural and ploughed surfaces/hillslopes	3 × 3 m & ~100 ×100 m	16 & 3	~5 × 5 mm & ~ 30 × 30 mm	The influence of surface roughness on runoff generation and soil erosion	This study

Table 3.2. Methods used to generate surface roughness measures

The scanner used in this study is appropriate for data collection in the natural environment as it is portable (in contrast to laser scanners mounted on a rail system; Huang & Bradford, 1990b), is water and dust resistant, can run off a car battery, and is relatively simple to set up in the field. Therefore the scanner can record surfaces in a range of environmental conditions (Nagihara *et al.*, 2004) and so elevation data suitable for roughness measurements may be obtained in the field with greater ease; these surfaces are currently under-represented in surface roughness studies (Table 3.2). Moreover, this method easily generates surfaces, rather than simply extracting several transects of elevation measurements from the surface. This approach lends itself to analysing statistics relating to the entire surface rather than just calculating roughness measures based on several transects (as described in section 2.6). Such three-dimensional analysis may permit the development roughness measures capable of predicting surface processes such as MDS with less uncertainty (Kamphorst, *et al.*, 2005).

The laser scanner emits radiation at wavelengths beyond those of visible light and operates under the assumption that the speed of this laser pulse remains constant. Using this time-of-flight principle, the delay recorded as the signal is returned can be used to calculate the distance to the surface from which the beam was reflected. The scanner then records the three-dimensional coordinates of any solid surfaces from which the laser rays are returned. Lim *et al.* (2005) note that as these coordinates are collected directly, many uncertainties associated with data processing and digital elevation model (DEM) generation are bypassed. While many other laser scanners have a small maximum scan area (often limited to less than 10 m^2; Darboux *et al.*, 2001b), this scanner manipulates the laser emitter using motorised mirrors enabling the scanner to pan around 360° and tilt through a large angle collecting over 250 points per second (Rosser *et al.*, in press).

While this non-contact, time-of-flight distance measurement system is extremely practical, Kersten *et al.* (2004) note that the absence of a calibrated target imposes limitations on the use of such terrestrial laser scanners. As the emitted radiation reflects off the ground surface itself, numerous variables are introduced, meaning that the time taken for the pulse to return is not exclusively a function of distance. Lichti & Harvey

(2002) observe that surface properties such as roughness, wetness and angle of incidence may influence the strength of the return signal. Additionally, Lim *et al.* (2005) note that while the scanner functions using band widths of 750-1500 nm which are beyond those of visible light, they are nevertheless on the periphery of atmospheric wavelengths, and so parts of the radiation may be absorbed into the atmosphere. Therefore, as wet surfaces have a lower reflectance, the signal strength of the reflected beam is degraded.

Despite these problems, Lim *et al.* (2005) reported that the point cloud data produced over the ranges associated with monitoring of cliff faces (i.e. scanning an area in the order of thousands of square metres from a distance of approximately 100 m) was capable of producing accuracies within ±0.06 m. The reported 0.003 m/m divergence of the emitted beam (Lim *et al.*, 2005) suggests that this may be much improved wherever the scanner can be positioned closer to the surface.

3.3.4.1 Data Collection

The terrestrial laser scanner used in this study is able to scan a surface 700 m away to a resolution of 1 cm. A greater resolution may be achieved by placing the apparatus nearer the scanned surfaces, as the minimum angle between two returned rays is 0.01 arc-seconds ($\sim 0.28 \times 10^{-5}$ °). This precision allows both small-scale high-resolution plot scans ($\sim 3 \times 3$ m) and lower-resolution hillslope scans to be made using the same technique.

At each study site a high-resolution plot scan was made for each 'Morphological Runoff Zone' identified in the field. Before data collection, the scanner was calibrated to a range precision of 0.01 m at 200 m. For each scan the laser scanner was located approximately 3 m from the plot itself to stay above the minimum operational range of the scanner. This produced an average point spacing of approximately 5 mm (in practice this ranged from 3.0 mm to 5.8 mm). To reduce any occlusion effects caused by surface features, each plot was scanned from two directions as displayed in Figure 3.9. One scan was made from downslope of the plot while a second scan was made from an angle of 90° to the first. The slope of the hillside meant that a scan from 3 m upslope of the plot offered a poor perspective of the plot, so a scan taken from the side of the plot was

considered preferable (Figure 3.9). Control points were staked out around the plot to allow the separate scans to be merged.

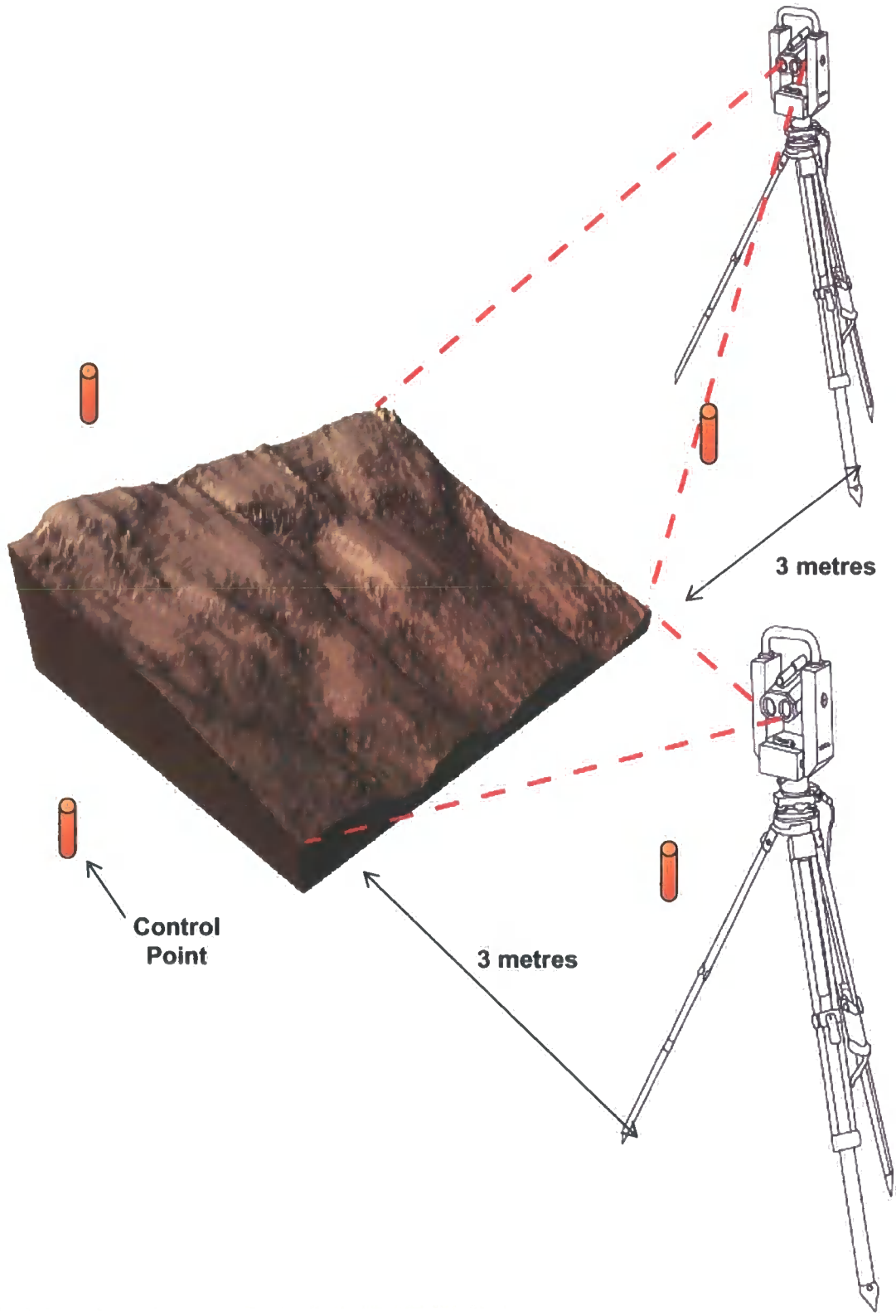

Figure 3.9. Sketch of the experimental setup for the plot scans.

At each site a digital elevation model (DEM) of the entire hillslope was made to capture the hillslope-scale surface roughness of the site. For each hillslope-scan, the scanner was calibrated to a range precision of 0.1 m at 200 m away. No single location offered a field-of-view which encompassed the entire hillslope, so several scans were needed from different vantage points to create a DEM of the hillslope. The co-ordinates of several control points were taken from each scanning point to ensure that the point clouds could be accurately merged.

3.3.4.2 Generation of Point Clouds

While the lack of a thick vegetation cover in semi-arid environments permits the large-scale measurement of the soil surface using this technique, none of the hillslopes used in this investigation were entirely devoid of vegetation. Although Solé-Benet *et al.* (1997) suggest that vegetation elements contribute to surface roughness, they may have a considerable effect on the roughness of the resultant surfaces. With this in mind, the sites of the high-resolution plot scans were chosen away from any shrubs or grasses. Any small shrubs or grasses that were found within the 3 by 3 m plots were removed with clippers before data capture commenced.

However, such an approach is clearly inappropriate at the hillslope scale. Where any large vegetation features (such as almond trees) were present on the hillslopes, these were removed from the resultant point clouds. This was achieved in the Archaeoptics Demon software package, as demonstrated in Figure 3.10. The point clouds were rotated to the perspective where such vegetation features could easily be distinguished from the soil surface (Figure 3.10a). The points representing the vegetation elements could then be highlighted (Figure 3.10b) and deleted from the point cloud (Figure 3.10c) cleanly and efficiently.

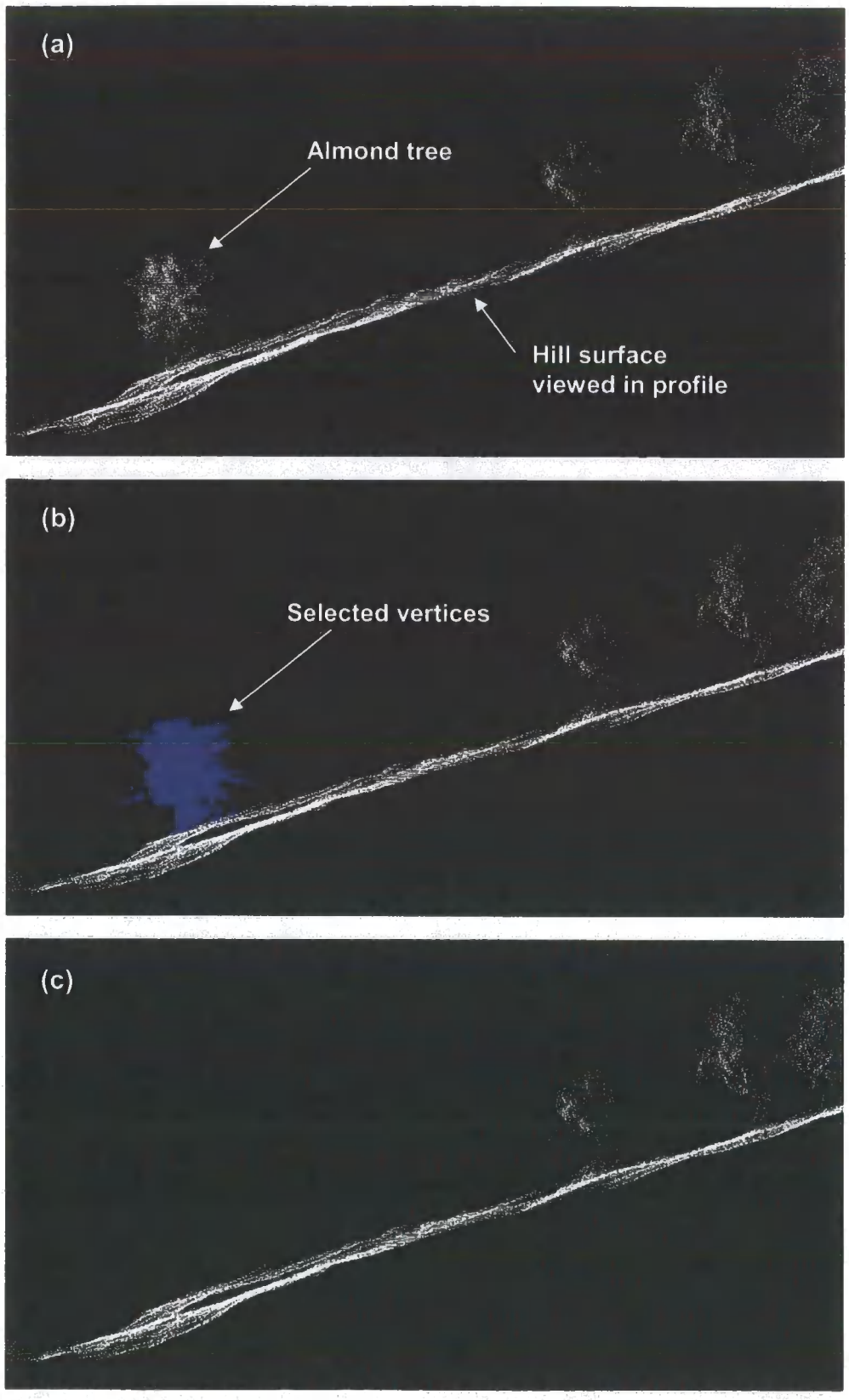

Figure 3.10. Method for removal of trees: (a) point cloud is rotated to an angle where the trees protrude from the soil surface; (b) tree is highlighted; (c) tree is removed from point cloud.

However, several areas of the hillslopes (particularly the matorral area of the Cardenas hillslope) were covered with low-lying shrubs where a thick density of foliage was present near the soil surface. These could not be easily removed from the point clouds. As they are found so close to the soil surface, they were likely to affect the processes acting on the surface. Therefore, such low-lying features remained in the coarser resolution hillslope scans as they would only have a limited influence on the resultant surfaces.

Where such large surface features are found on the hillslope they produce a 'shadow' where they obscure the scanner's view of the surface behind it and so this portion of the surface is unrepresented in the resultant point cloud (Figure 3.11a). Once the feature is removed (as demonstrated in Figure 3.10) the shadow remains (Figure 3.11b). As each slope was scanned from several different perspectives, control points were demarked on the hill surface with wooden stakes to enable the scans to be merged. The limited field of view from each scan position meant that it was not possible to hit each control point from every location and so several control points were spread across the hillslope.

The resultant scans were converged using the Archaeoptics Demon software package. The overlapping scans were first transformed and rotated manually until the control points converged (Figure 3.12). To achieve a better fit between the two surfaces, Archaeoptics Demon uses least-squares. This is achieved by employing a three-dimensional transformation algorithm to determine the optimal vector translation between each point in one scan and the point on the second scan of shortest Euclidean separation (Lim *et al.*, 2005). If the root mean squared (RMS) deviation between the two point clouds is greater than required, the algorithm reiterates and the process is repeated.

Once the scans were merged, a limitation of this technique became clear (Figure 3.11c). As previously noted, the resolution achieved by the laser scanner depends on the distance of a surface from the scanning position and the inclination of the surface relative to this position (as the scanner operates using the angle between returned laser pulses). Typical geomorphological applications of terrestrial laser scanners such as cliff

face monitoring (Lim *et al.*, 2005) involve near-vertical faces. However, the hillslopes scanned in this study displayed a range of slope angles and aspects and so the point cloud density from a single scan is extremely variable across the hillslope. While an attempt was made to conduct multiple hillslope scans from different perspectives at the finest resolution possible (given time limitations in the field), this was insufficient to ensure consistent point spacings for all the hillslopes. Several areas (particularly at the bowl-shaped Cardenas hillslope) exhibit relatively large point spacings where a surface feature has been removed but the resultant shadow remains (Figure 3.11c). This problem may be overcome by conducting more hillslope scans, strategically positioned to ensure as even a point spacing as possible.

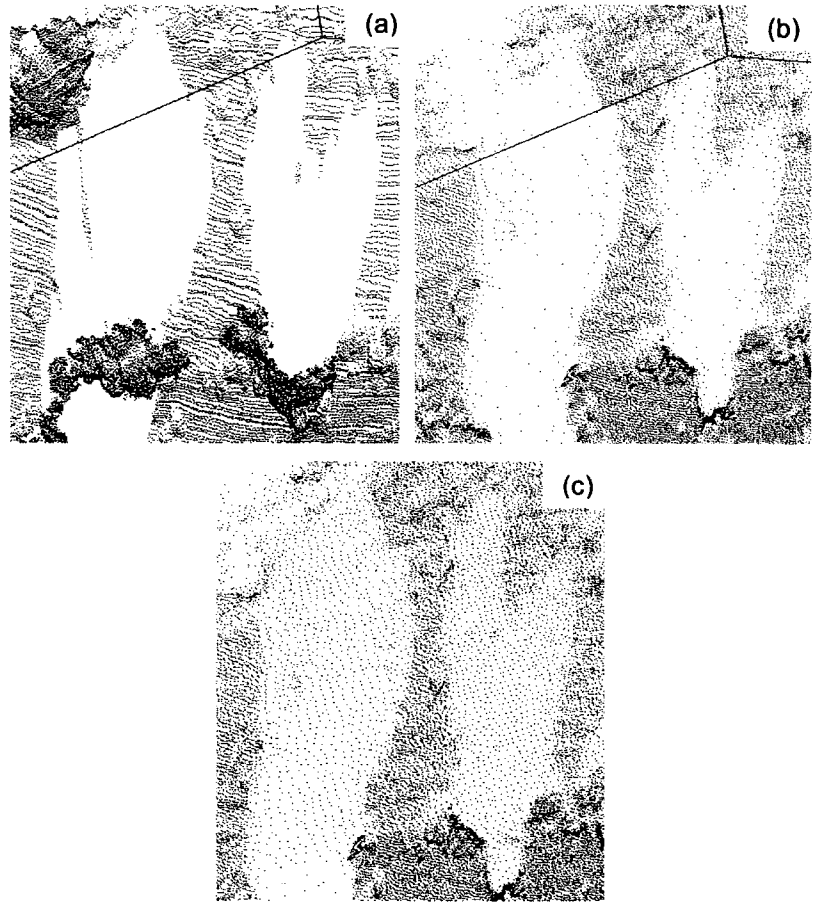

Figure 3.11. The shadow effect of large surface features (particularly trees): (a) feature is present in scan and has cast a 'shadow' on the surface behind; (b) feature has been removed, but the surface behind remains unrepresented in the point cloud; (c) the shadow is filled once several scans are merged, but there remains a contrast in the point resolution.

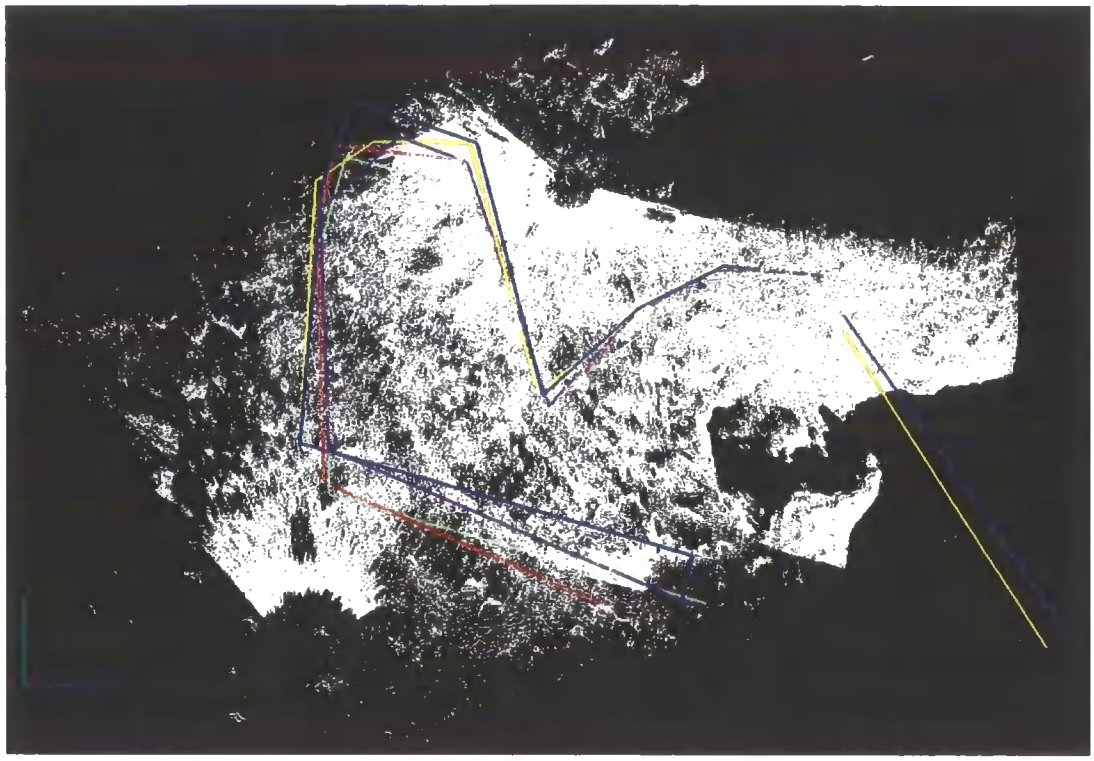

Figure 3.12. The hillslope scans for the Del Prado site, each displaying a polyline linking control points.

This issue was overcome for the plot-scale scans by elevating the scanner on a tripod as high as possible above the plot to be scanned (Figure 3.9). While it was expected that some occlusion effects would arise from small surface features, such an elevated perspective much reduced any such occlusion, and so merging of scans from multiple directions was not always necessary.

3.3.4.2 Generation of Surfaces

Calculation of profile-based measures of surface roughness from these point clouds requires surfaces to be generated. This can also be done with the Archaeoptics Demon software. However, Lim *et al.* (2005) note that surface accuracies, are not the same as point accuracies as the process of meshing the point cloud data introduces error. The resultant surfaces are degraded in areas where the point cloud density is low, but more importantly, the angle from where triangulation is performed influences the resultant surface.

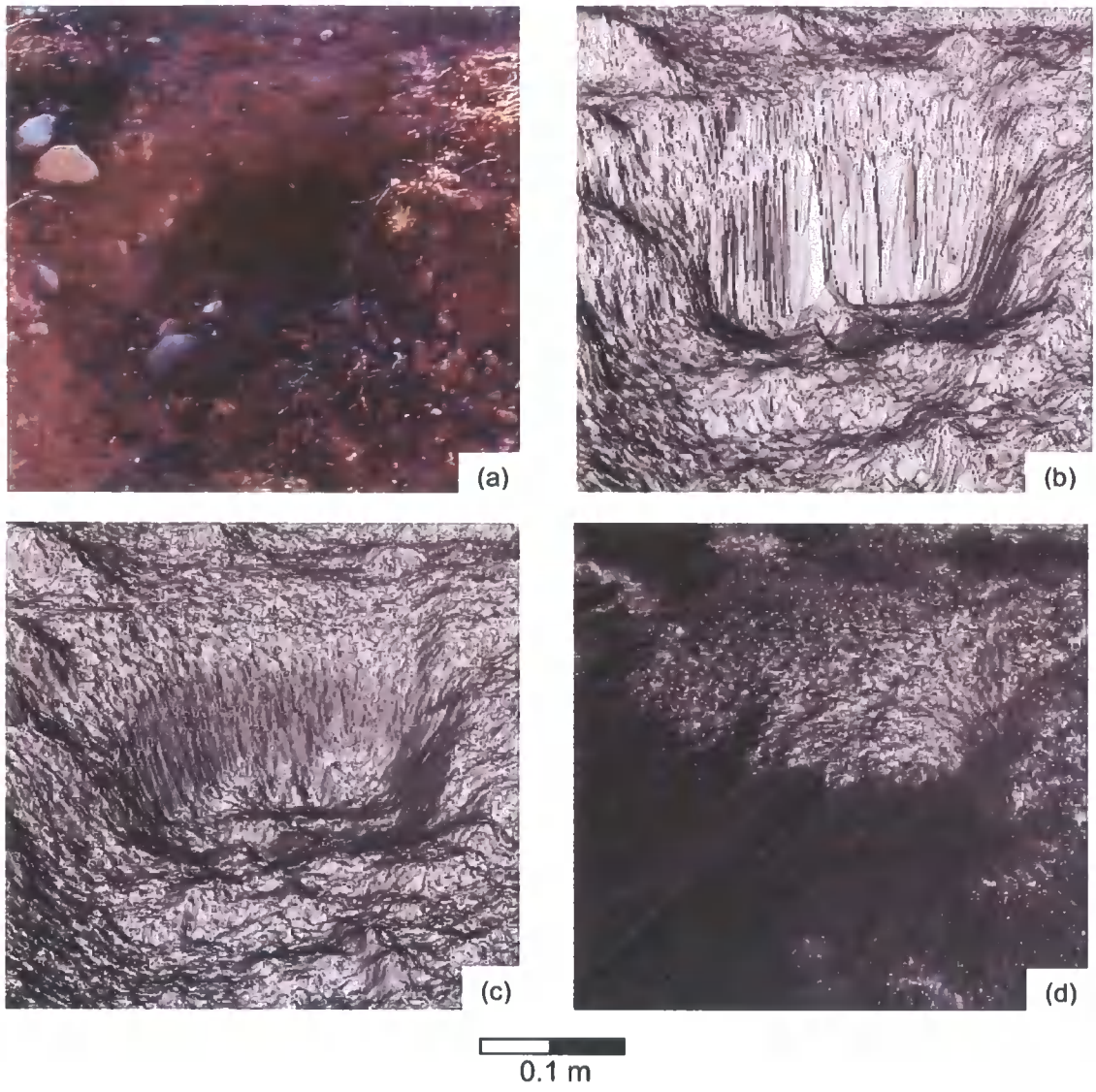

Figure 3.13. The effect of angle of triangulation upon surfaces as demonstrated in MRZ 4 at the Del Prado hillslope: (a) picture of the surface as seen in the field; (b) triangulated from vertically above; (c) triangulated from 45° from vertical; (d) triangulated from the laser scanner position.

Unfortunately, it is difficult to obtain a fixed camera position in the Archaeoptics Demon software package. This is problematic as it is essential that the camera position for triangulation remains identical between each surface. However, the software automatically views each surface from a perspective vertically above the surface generated (resulting in surface (b) of Figure 3.13) and so this perspective can be accurately reproduced. It is then possible to rotate each surface about the x axis while the camera remains in the same position. Figure 3.13c demonstrates the surface

generated as the surface is rotated through 45° around the x axis. Finally, the laser scanner treats the point where it was positioned as origin (0, 0, 0). Therefore it was possible to locate the camera here and triangulate each surface from the perspective of the scanner itself (Figure 3.13d). The actual surface as observed in the field (Figure 3.13a) is best represented by the surface triangulated from 45° to vertical.

To test which angle of triangulation gave the most 'realistic' representation of the original surface (i.e. visually similar to the surface observed in the field), each point cloud was triangulated from these three directions (Figure 3.14). As unrealistic surface representations contain many long triangles, the surface areas of each plot were measured in Demon and the surface tortuosity was calculated as surface area divided by plan surface area. Surfaces with many long triangles will have large surface tortuosity.

Figure 3.15 shows that while the surface triangulated at 45° to vertical has consistently the lowest surface tortuosity, the relationship between all three surfaces is not constant between sites. For instance, the 'vertical' triangulated surface displays higher surface tortuosity than the 'laser position' triangulated surface at MRZ 3. This plot had the steepest general slope angle (at 29° to horizontal). Each plot had a different slope angle in the field, therefore, while these triangulation angles are consistent in absolute space, they are variable relative to the surface of interest.

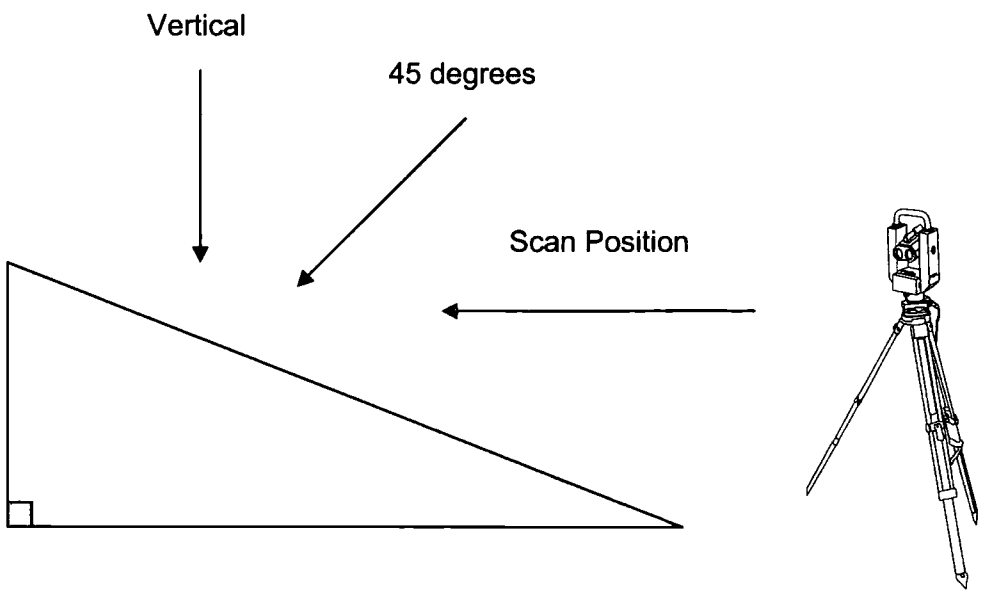

Figure 3.14. Directions of triangulation for each surface.

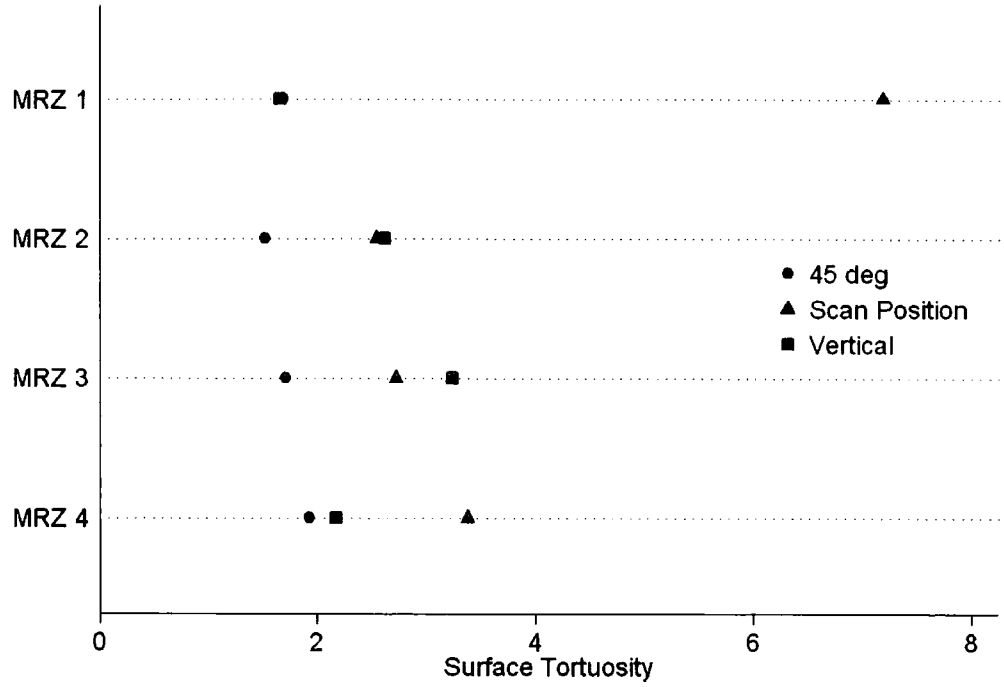

Figure 3.15. The effect of angle of triangulation on surface tortuosity for MRZs 1-4 of the Cardenas hillslope.

Therefore, to remain consistent between plots, each point cloud was triangulated from a direction perpendicular to the general slope as this offers the most realistic representation of the surface. The largest value of surface tortuosity in Figure 3.15 (MRZ 1 from the scan position) is for the angle furthest from perpendicular (as this plot was found near the crest of the hillslope with a slope of only 6°).

However, even this remains an approximation of the surface as seen in the field. Ideally, a stereonet would be produced for each surface. This could identify the mean direction that each surface faces; this direction would then be considered as the optimum camera position for triangulation. However, the surface needs to be generated before the stereonet can be produced, so the optimum camera position must be eventually reached by iteration. While most plots contained no especially large surface features, this procedure would be particularly valuable where large gullies are found (and therefore steep gully walls). In this case triangulation from a perspective perpendicular to the general slope is unfavourable, as much of the detail from the almost vertical gully walls is lost. These surfaces were split into two sections (each containing a gully wall) and each half was rotated 45° cross-slope in opposite

directions before triangulation. Each half was then rotated back and combined together. This procedure is thought to provide the best approximation to the angle that would be exposed as a result of the stereonet iteration process.

3.4 Summary

Recent developments in laser scanning technology have removed many of the constraints of analysing surface roughness at the hillslope scale and in natural environments. Such advances have increased the availability of topographic data. A re-examination of methods of characterising surface roughness is thus in order. This new technology was combined with more traditional methods to achieve the objectives outlined in Chapter 1 (Figure 3.16).

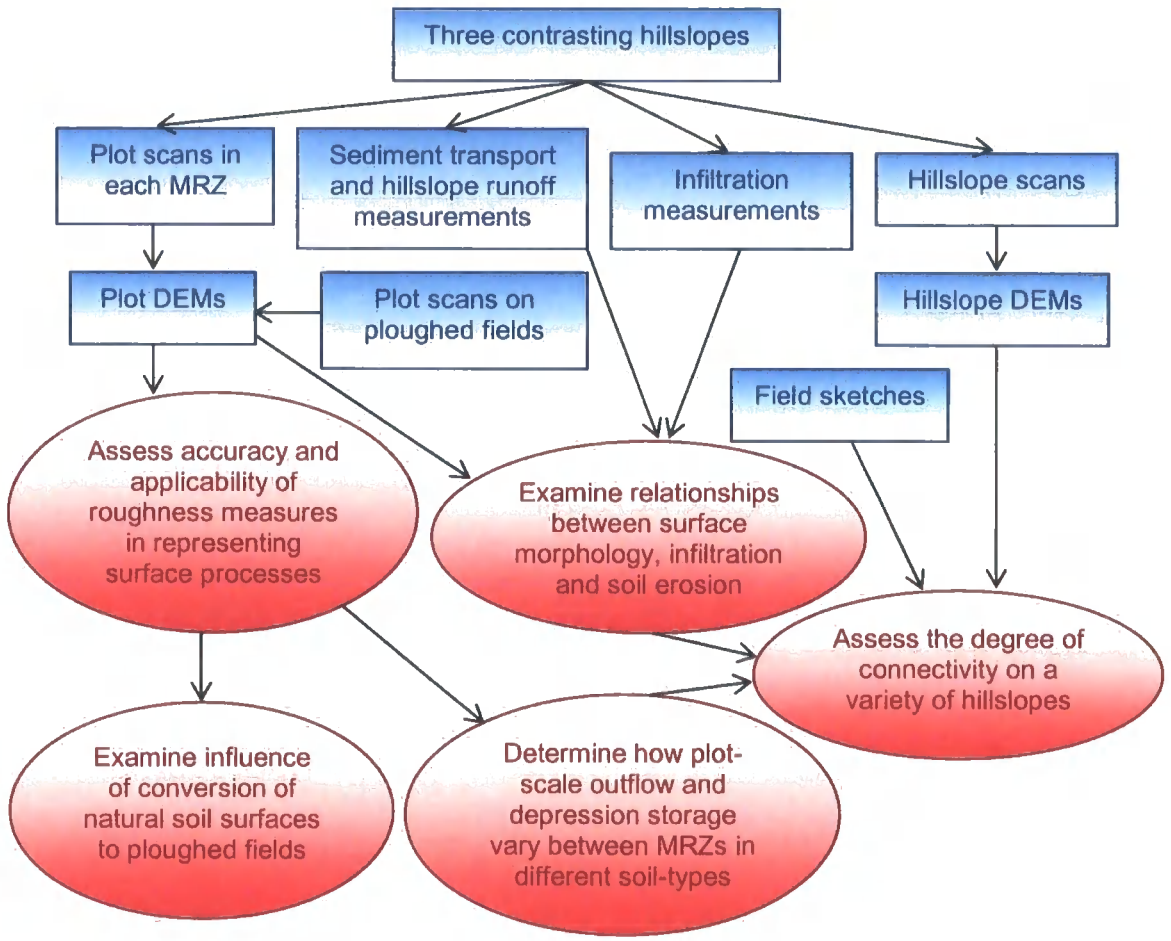

Figure 3.16. The relationships between the field methods and aims of this study (outlined in full above).

Plot-scale scans taken in different Morphological Runoff Zones can provide a quick method of relating different roughness measures to soil surface hydrological processes. These results were combined with cheap and simple methods of measuring sediment transport, runoff and infiltration across a hillslope to permit analysis of their relationships and how these change both within and between hillslopes. Additionally, the large-scale surface roughness obtained from hillslope scans were combined with field sketches and the plot-scale results to assess the connectivity of the three contrasting hillslopes featured in this study.

Chapter 4 Surface Characterisation

4.1 Introduction

This chapter uses several methods to examine the variation surface roughness between the scanned plots and hillslope surfaces. Section 4.2 offers a brief overview of the plot surfaces generated by the terrestrial laser scanner. The variation of profile-based roughness measures between each plot is assessed in section 4.3, while section 4.4 reviews several surface statistics generated directly from the point clouds themselves which act as three-dimensional roughness measures. Section 4.5 provides an analysis of the surface morphology at each plot. Section 4.6 looks at how both the profile-based and surface-based roughness measures perform when applied at the hillslope scale.

4.2 Plot Surfaces

Each morphological runoff zone (MRZ) was clearly identifiable in the field, although no part of the Cardenas hillslope was classified as MRZ 5 (see Table 2.1 for details of each MRZ). Areas of ploughing were evident at both the Upper Nogalte and Cardenas hillslopes. Therefore, in all, sixteen plot scans were undertaken. The tripod upon which the terrestrial laser scanner was positioned permitted each surface to be scanned from a considerable height above the surface. This led to a reduction in occlusion effects which proved less problematic than expected on plots with small surface features.

However, large gaps appeared due to occlusion effects on the two plots classified as MRZ 5, as the gully head and walls obscured the view of the gully bottom. To compensate for this, both MRZ 5 plots were scanned from two directions (as depicted in Figure 3.9). The two scans (each with an average point spacing of just 5 mm) were then carefully merged so that the 'shadow' areas could be filled in.

Each scan was then triangulated from a direction perpendicular to the general slope (as described in section 3.3.4.2). Figure 4.1 shows how the surface features associated with each MRZ can be easily recognised from the surface generated using this technique. Figure 4.1a shows a plot representing MRZ 1, taken from the crest of a hillslope; small areas of wash deposits can be seen in Figure 4.1b (MRZ 2); Figure 4.1c also displays minor areas of flow concentration (MRZ 3), further exaggerated in Figure 4.1d where three rills are clearly visible (MRZ 4). A large gully can be seen in Figure 4.1e (MRZ

5), while Figure 4.1f clearly depicts a ploughed area. Elevation range and average slope data for each plot are given in Table 4.1.

Site	*Plot*	*Elevation Range (m)*	*Slope (°)*
Upper Nogalte	MRZ 1	0.52	2
	MRZ 2	1.09	20
	MRZ 3	0.81	18
	MRZ 4	1.70	20
	MRZ 5	2.07	24
	Ploughed	0.96	18
Cardenas	MRZ 1	0.47	7
	MRZ 2	1.31	23
	MRZ 3	1.71	32
	MRZ 4	1.50	29
	Ploughed	1.83	26
Del Prado	MRZ 1	0.30	7
	MRZ 2	0.30	6
	MRZ 3	0.60	12
	MRZ 4	0.85	18
	MRZ 5	1.80	29

Table 4.1. Elevation range (m) and average slope (°) for each plot.

The definition of an MRZ remains a subjective procedure. The following sections attempt to link these divisions of hillslopes with quantitative measures of surface roughness.

4.3 Profile-Based Roughness Measures

Calculation of many of the roughness measures discussed in section 2.6 requires that transect data be extracted from the surfaces. Cross-sections were taken at intervals of approximately 15 cm over each of the 9 m^2 plots, both downslope and cross-slope. This allowed both components of roughness (as identified by Kirkby (2001)) to be included in the analysis. It should be noted, however, that this approach assumes knowledge of the flow direction and any deviation from the chosen perpendicular directions may result in a confused distinction between the two. While many formal procedures leading to significance levels are problematic when applied to spatially autocorrelated data (such as the profile- or area- based elevation measures analysed in this study), a graphical exploratory approach is sufficient to show patterns between surfaces. The analysis presented in the following chapters is therefore dominated by such a graphical approach.

Figure 4.1. Example surfaces for each plot type.

4.3.1 Random Roughness

As section 2.6.1 suggests, the calculation of random roughness is a somewhat confusing issue, with little consensus in the literature. As strictly 'random' roughness does not occur on natural surfaces, this section follows Kamphorst (2000) by measuring random roughness by the standard deviation of height measurements.

In this study, both the standard deviation sd and interquartile range iqr of elevation measures were calculated for each profile. Additionally, each profile was then linearly detrended (the linear slope trend removed) and standard deviations and interquartile ranges were calculated for the detrended profiles. Figure 4.2 shows the relationships between these measures: each point represents one transect. Many of the 'detrended' standard deviation values are lower than the original sd values, whereas some points are hardly changed by this detrending. This accounts for the differential effect of slope (some profiles were across near-flat surfaces, therefore detrending altered very little). This pattern can also be observed with iqr and 'detrended' iqr.

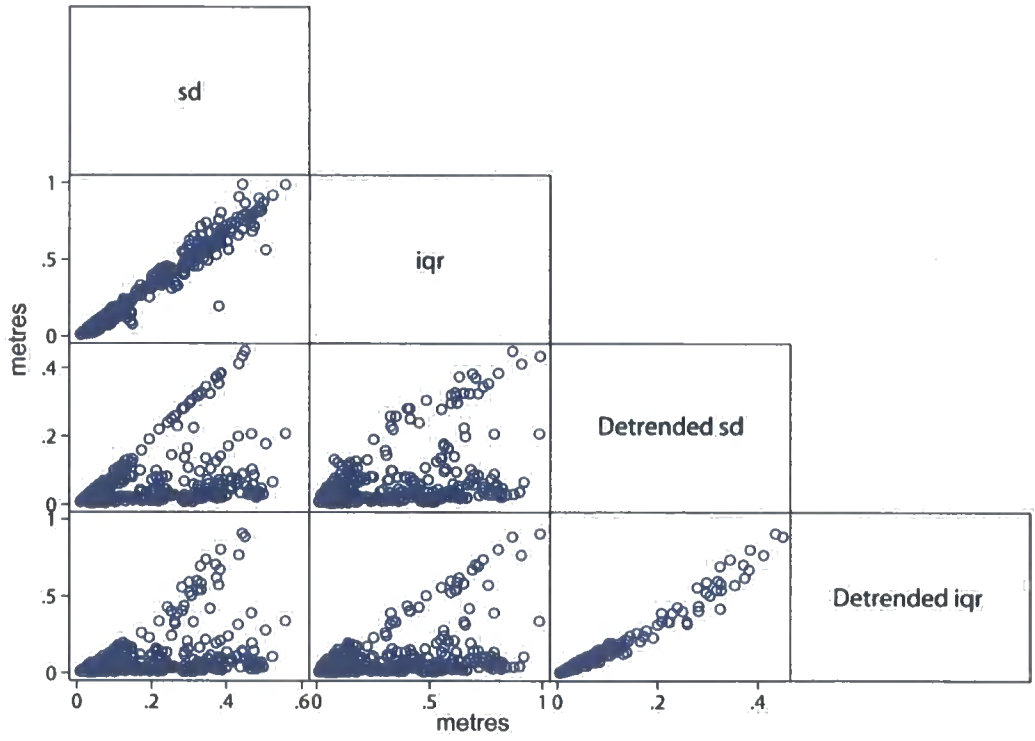

Figure 4.2. The relationships between the standard deviation (sd, in metres) and interquartile ranges (iqr, in metres) of the elevation data for each profile, and the detrended versions of both values.

The cell displaying the scatter plot of sd against iqr demonstrates near linearity. Figure 4.3 displays the linear relationship between sd and iqr in detail, superimposed over the relation expected by normal (Gaussian) distributions. The plotted points do not deviate much from this line, although two outliers (both from adjacent profiles at the crest of the Upper Nogalte hillslope) can be identified. The majority of points in Figure 4.3 plot slightly above the line expected by Gaussian distributions. Shape measures such as skewness and kurtosis are useful for quantifying such deviations from a Gaussian distribution. Figure 4.4 shows the spread of these measures around what would be expected from a Gaussian distribution (a skewness of 0 and kurtosis of 3).

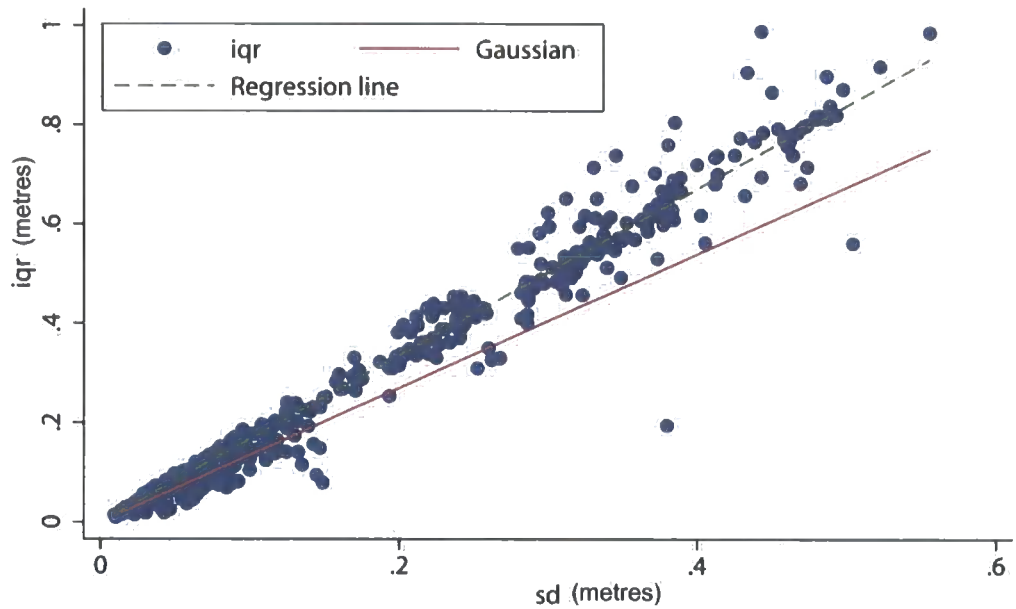

Figure 4.3. The relationship between standard deviation and interquartile range. The solid red line represents the relation expected with normal (Gaussian) distributions.

Figure 4.4 shows that the distributions are approximately symmetrical around a skewness of 0 (although there appears to be a slight dominance of small positive skewness). Skewness and kurtosis are not independent of each other and so the points describe a parabola shape around a skewness of 0. This makes it more difficult to identify patterns and to fit distributions to the data. Hosking (1992) proposes that L-moments have better properties as measures of distributional shape, as they provide an easier way of matching a data-set to a parent distribution. Figure 4.5 shows the

relationship between L-skewness and L-kurtosis, with the expected location of a Gaussian distribution located at the intersection of the two grey lines (as in Figure 4.4).

Both Figure 4.4 and 4.5 show that the majority of distributions have a kurtosis lower than that expected from a Gaussian distribution. A lower kurtosis value suggests that less extreme values are contained in the data; this could be expected of such geomorphological data as the natural tendency of surface processes is to erode extreme peaks and fill-in deep pits. Therefore, such a deviation from a Gaussian distribution could be typical of microtopographic data. While the data remain close to demonstrating a normal distribution, before examining the variation of roughness measures between surfaces, it is important to note that the elevation data generally have a slightly higher skewness and lower kurtosis than would be expected from a normal distribution.

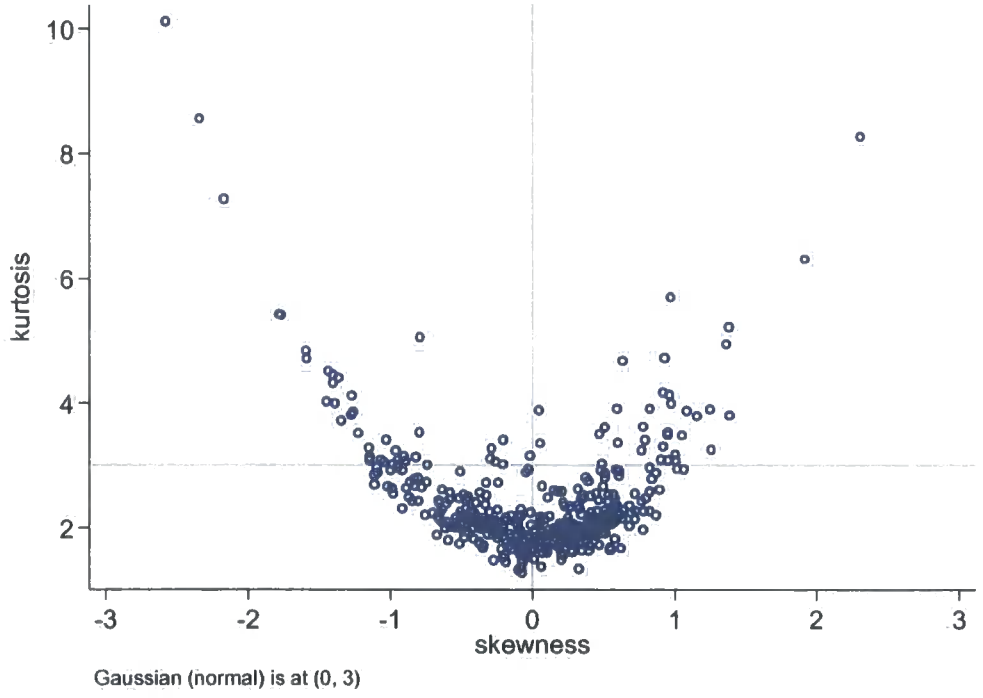

Figure 4.4. The relationship between skewness and kurtosis of profile data. The grey lines represent the values expected with normal (Gaussian) distributions (skewness 0 and kurtosis 3).

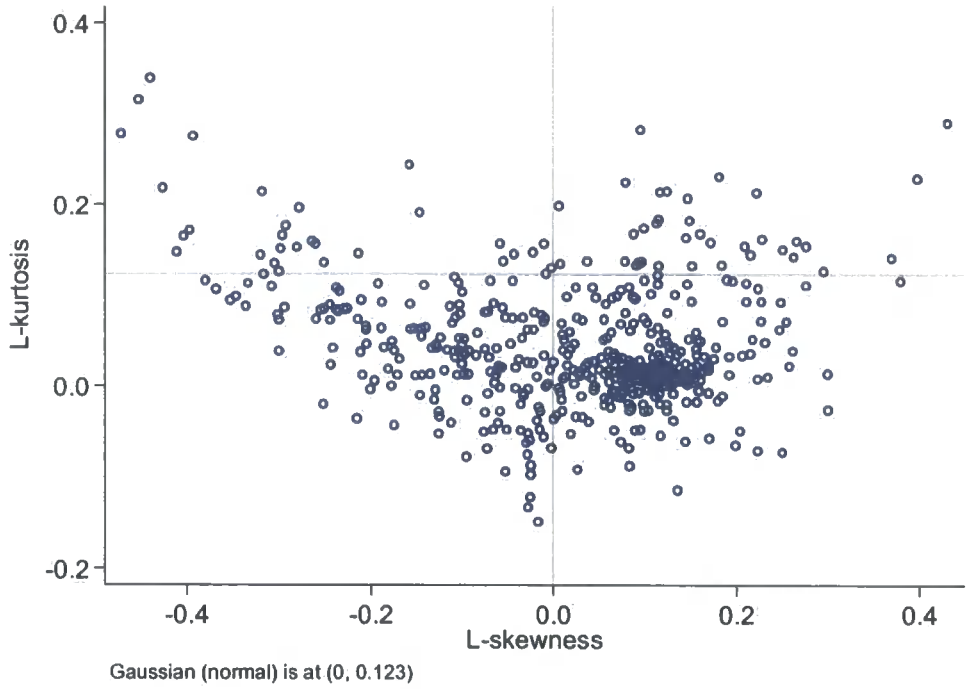

Figure 4.5. The relationship between L-skewness and L-kurtosis of profile data. The grey lines represent the values expected with normal (Gaussian) distributions (L-skewness 0 and L-kurtosis 0.123).

When detrended sd against detrended iqr is examined, the result is almost the same. However, the slight curvature of the line deserves further examination. Figure 4.6 shows that for the detrended versions of sd and iqr, although the points remain close to the Gaussian trendline, a quadratic regression is more suitable than linear. Despite this minor variation, it appears that the dataset is reasonably well represented by Gaussian distributions.

Figure 4.7 shows profile elevation standard deviations for each surface as a box plot: the boxes represent the interquartile range of the standard deviations at each surface. Figure 4.7a displays how the elevation standard deviations of the profiles are spread within each plot, and how they compare between plots and sites. In most cases, there is a large spread of values within each plot. The higher values of sd of each plot are dictated by the slope of the plot itself, while the lower limit will most likely be determined by profiles taken in the cross-slope direction (which will display less variation in elevation). To make this pattern clearer, the profile data are split into their components.

Figure 4.7b displays sd for profiles running downslope and Figure 4.7c for profiles running cross-slope. Figure 4.7d displays the 'detrended' standard deviation of all the profiles combined. These values are also displayed in Table 4.2.

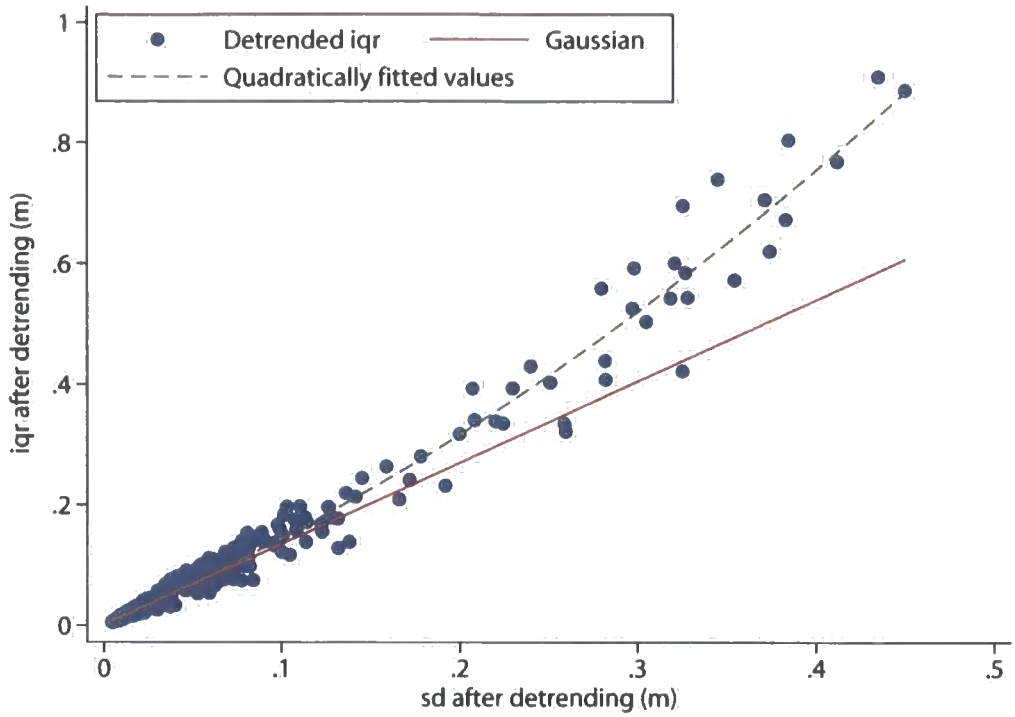

Figure 4.6. The relationship between detrended standard deviation (m) and detrended interquartile range (m). The solid red line represents the relation expected with normal (Gaussian) distributions.

While there is a general pattern of increasing sd moving downslope from MRZ 1 to MRZ 5 in Figure 4.7b (particularly for the Del Prado site), this is slightly confused as the general slope of the plot remains the dominant influence (further emphasising the important distinction between roughness and topography). The pattern is more evident when only the cross-slope profiles are taken into account (Figure 4.7c), with the gullied plots (MRZ 5) understandably displaying the largest standard deviations of elevation measurements. This pattern is repeated with all the linearly detrended profiles (Figure 4.7d). The detrended ploughed profiles demonstrate standard deviations comparable to those for the plots which experience no incision by surface runoff (MRZ 1-2). Overall, the Cardenas values are slightly higher, with Del Prado generally displaying the lowest values.

Site	Plot	Mean Downslope sd (m)	Mean Cross-slope sd (m)	Mean Detrended sd (m)
Upper Nogalte	MRZ 1	0.039	0.054	0.013
	MRZ 2	0.294	0.035	0.012
	MRZ 3	0.206	0.046	0.030
	MRZ 4	0.317	0.104	0.056
	MRZ 5	0.365	0.332	0.208
	Ploughed	0.246	0.023	0.021
Cardenas	MRZ 1	0.069	0.065	0.025
	MRZ 2	0.326	0.080	0.020
	MRZ 3	0.474	0.065	0.026
	MRZ 4	0.351	0.089	0.067
	Ploughed	0.359	0.077	0.020
Del Prado	MRZ 1	0.048	0.034	0.010
	MRZ 2	0.064	0.013	0.011
	MRZ 3	0.135	0.036	0.021
	MRZ 4	0.208	0.109	0.057
	MRZ 5	0.427	0.278	0.173

Table 4.2. Mean standard deviations of elevation measurements of both orthogonal components and the 'detrended' profiles for each plot.

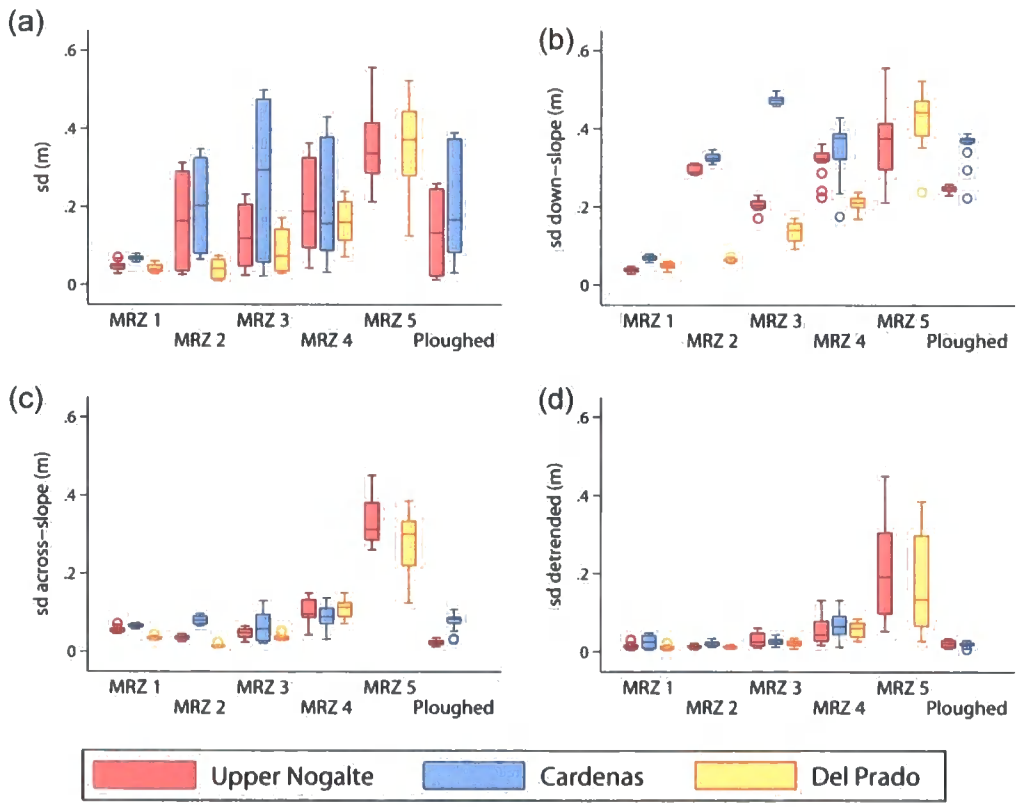

Figure 4.7. Standard deviations of elevation measurements for each plot and site: (a) sd using all profiles; (b) for downslope profiles only; (c) for cross-slope profiles only; (d) sd 'detrended' for all profiles.

4.3.2 Profile Tortuosity

The tortuosity of each profile (as defined by Boiffin, 1984) was calculated both downslope and cross-slope. The results in Table 4.3 show both mean and standard deviation of tortuosity for each plot, measured down-slope and cross-slope.

Site	*Plot*	*Mean Downslope Tortuosity*	*Sd of Downslope Tortuosity*	*Mean Cross-slope Tortuosity*	*Sd of Cross-Slope Tortuosity*
Upper Nogalte	MRZ 1	1.063	0.017	1.079	0.043
	MRZ 2	1.185	0.030	1.199	0.085
	MRZ 3	1.172	0.052	1.144	0.063
	MRZ 4	1.191	0.063	1.154	0.145
	MRZ 5	2.559	1.492	3.364	1.840
	Ploughed	1.362	0.060	1.272	0.224
Cardenas	MRZ 1	1.088	0.043	1.092	0.024
	MRZ 2	1.282	0.084	1.155	0.080
	MRZ 3	1.482	0.133	1.197	0.155
	MRZ 4	1.486	0.283	1.925	0.494
	Ploughed	1.308	0.039	1.281	0.182
Del Prado	MRZ 1	1.056	0.026	1.056	0.035
	MRZ 2	1.108	0.050	1.116	0.073
	MRZ 3	1.180	0.060	1.134	0.070
	MRZ 4	1.530	0.396	1.691	0.582
	MRZ 5	3.235	2.059	3.550	1.090

Table 4.3. Means and standard deviations of tortuosity for each plot down-slope and cross-slope.

As mean downslope tortuosity correlates well with mean cross-slope tortuosity (with a Pearson correlation of 0.97), Figure 4.8 displays the spread of all the tortuosity values for each plot (with all tortuosity values log transformed for clarity). Tortuosity increases downslope from the drainage divide, with a substantial increase to MRZ 5. This increase is more marked for cross-slope tortuosity (as would be expected with channel incision). The ploughed plots demonstrated tortuosity similar to MRZ 3 (i.e. similar to natural slopes before incision of rills). The Cardenas site has the highest mean tortuosity for each natural plot and also the highest spread of values.

As this measure of tortuosity combines the effects of general slope and microtopography, Table 4.4 presents the results of tortuosity measurements applied to detrended profiles. Although values decreased slightly, the variation between each plot and site is similar to that seen in Figure 4.8.

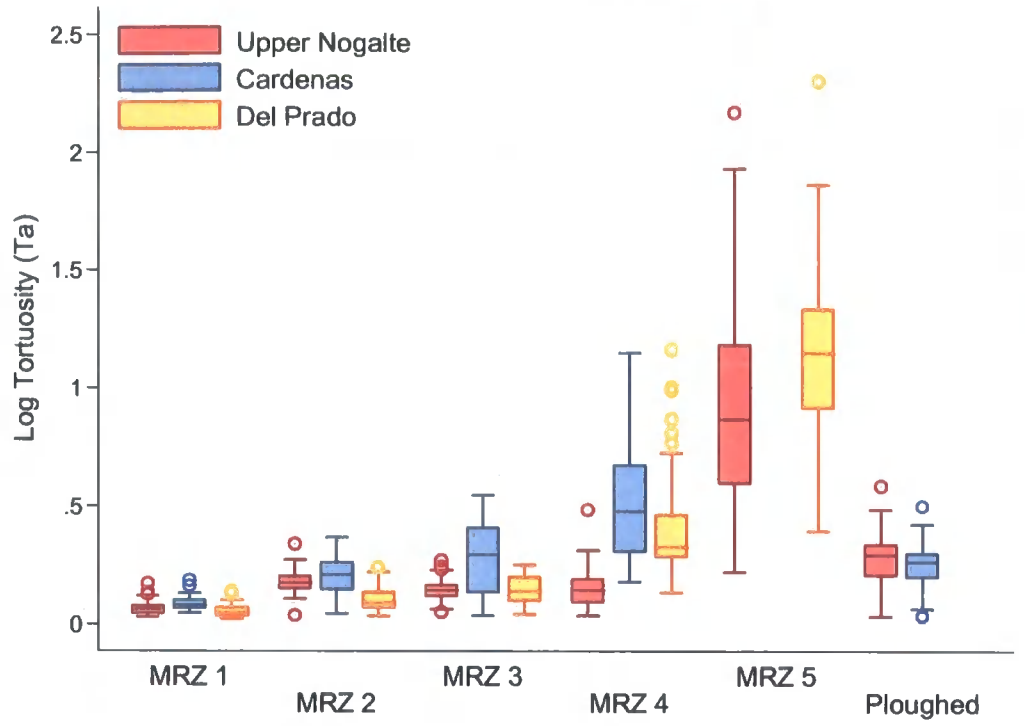

Figure 4.8. The variation of (log) tortuosity T_A in both directions for each plot and site.

Site	*Plot*	*Mean Downslope Tortuosity*	*Sd of Downslope Tortuosity*	*Mean Cross-slope Tortuosity*	*Sd of Cross-Slope Tortuosity*
Upper Nogalte	MRZ 1	1.062	0.017	1.077	0.043
	MRZ 2	1.126	0.030	1.198	0.085
	MRZ 3	1.137	0.052	1.144	0.063
	MRZ 4	1.130	0.063	1.146	0.145
	MRZ 5	2.325	1.492	3.360	1.840
	Ploughed	1.305	0.060	1.272	0.224
Cardenas	MRZ 1	1.083	0.043	1.090	0.024
	MRZ 2	1.197	0.084	1.150	0.080
	MRZ 3	1.285	0.133	1.192	0.155
	MRZ 4	1.351	0.283	1.924	0.494
	Ploughed	1.199	0.039	1.275	0.182
Del Prado	MRZ 1	1.055	0.026	1.055	0.035
	MRZ 2	1.104	0.050	1.116	0.073
	MRZ 3	1.161	0.060	1.134	0.070
	MRZ 4	1.480	0.396	1.687	0.582
	MRZ 5	2.714	2.059	3.530	1.090

Table 4.4. Means and standards deviation of detrended tortuosity down-slope and cross-slope.

4.3.3 Geostatistics

Experimental semi-variograms derived from the soil surfaces did not always conform to the theory described in section 2.6.4 upon which the calculation of the 'limiting distance' and 'limiting slope' roughness measures is based. This echoes the findings of Kamphorst *et al.* (2000), who suggested that the non-random component of roughness found in field situations alters the form of the semi-variogram. Although in some cases the semi-variance was seen to rise with increasing lag before reaching an identifiable 'sill', these represented only a subset of all the profiles examined in this study. As the non-random component of surface roughness is particularly important for the study of soil surface hydrological processes, it was concluded that the roughness measures as proposed by Linden & Van Doren (1986) were inappropriate for this project. For a more detailed discussion of fitting semi-variograms to soil properties, see McBratney & Webster (1986).

Despite this, several properties of the semi-variograms deserve further examination. The minimum and maximum lag-spacings for which semi-variance was calculated were 0.02 m and 1.5 m respectively. The example semi-variograms displayed in Figure 4.9a-c display three common forms produced from the soil surfaces. A well defined sill can be seen for some cross-slope transects on plots found near the drainage divide (Figure 4.9a), suggesting that random roughness dominates these profiles. Semi-variograms of downslope profiles and some cross-slope profiles were of the form of Figure 4.9b. This pattern most likely represents the effect of general slope on some plots, but such an explanation is insufficient to account for all occurrences of the pattern. Semi-variograms in the form of Figure 4.9c were produced by cross-slope transects of plots further downslope, where deep surface incision is present. The shape of the curve represents the periodic elevation fluctuations associated with regularly spaced surface incisions.

Several of these example forms could be found in each plot, so such general explanation can only partially account for the variation observed. Bearing in mind the variability in the forms of each of these curves, the root of the semi-variance (in metres) at two arbitrarily chosen points, 0.5 m and 1.0 m was calculated for each profile. Means are displayed in Table 4.5. The advantage of these measures is that they have a physical interpretation given their dimensions and units (m) (Cox, personal communication 2005).

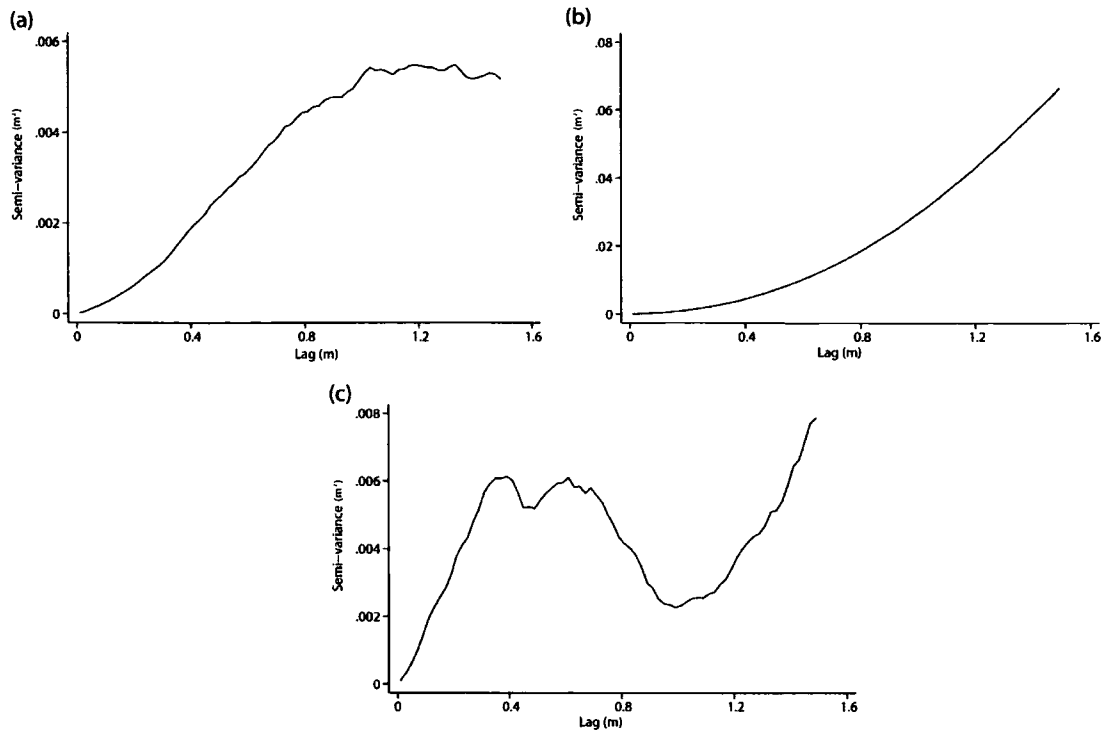

Figure 4.9. Experimental semi-variograms from natural soil surfaces: (a) well-defined sill (as seen for the cross-slope transects at upslope locations); (b) gradually increasing semi-variance with lag (as seen for the majority of downslope-oriented transects and some cross-slope transects); (c) 'hole-effect' semi-variogram (common for cross-slope oriented transects of deeply incised surfaces).

Figures 4.10 and 4.11 demonstrate how these vary between each plot and site (for the combined directions). Figure 4.10 shows a gradual increase in the root of the semi-variance at 0.5 m lag with distance downslope (with the ploughed sites displaying relatively low values). Certainly, the order of each site within each plot-type remains consistent: Cardenas boasts the highest values, followed by Upper Nogalte and Del Prado. Such a consistent relationship may reflect fundamental differences in the soil surface morphometry between these sites (such as lateral extent of roughness elements), irrespective of hillslope location.

Site	*Plot*	*Downslope root of S-V at 0.5 m (m)*	*Downslope root of S-V at 1 m (m)*	*Cross-slope root of S-V at 0.5 m (m)*	*Cross-slope root of S-V at 1 m (m)*
Upper Nogalte	MRZ 1	0.016	0.030	0.022	0.041
	MRZ 2	0.117	0.235	0.018	0.029
	MRZ 3	0.093	0.183	0.043	0.062
	MRZ 4	0.125	0.236	0.078	0.118
	MRZ 5	0.230	0.371	0.271	0.385
	Ploughed	0.107	0.218	0.014	0.020
Cardenas	MRZ 1	0.034	0.068	0.036	0.060
	MRZ 2	0.142	0.277	0.035	0.067
	MRZ 3	0.200	0.406	0.035	0.059
	MRZ 4	0.182	0.340	0.097	0.081
	Ploughed	0.159	0.318	0.040	0.069
Del Prado	MRZ 1	0.024	0.043	0.015	0.027
	MRZ 2	0.032	0.057	0.012	0.013
	MRZ 3	0.064	0.125	0.029	0.040
	MRZ 4	0.117	0.229	0.068	0.094
	MRZ 5	0.251	0.449	0.275	0.390

Table 4.5. The root of the semi-variance (in metres) at 0.5 m and 1.0 m lag spacings for each plot and site (separated into orthogonal components).

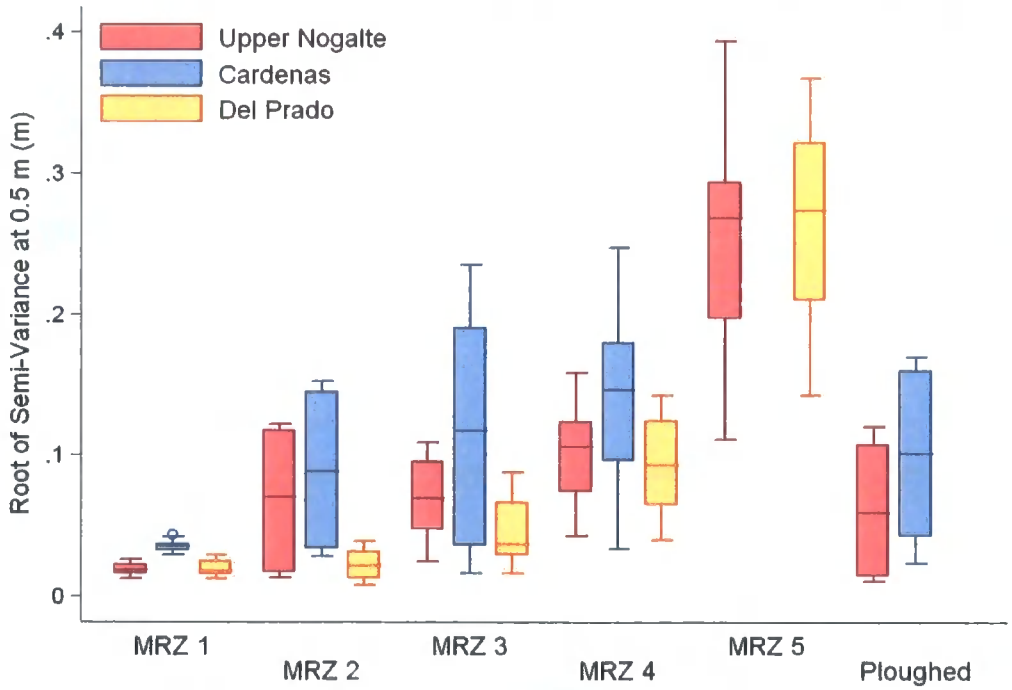

Figure 4.10. The variation of the root of semi-variance at 0.5 m lag spacing (m) for each plot and site (both directions combined).

With the exception of MRZ 5, this relationship is maintained in Figure 4.11 which shows the variation in the root of semi-variance at 1 m lag spacing. The increase downslope is not as obvious for this lag, which is most likely a result of semi-variograms in the form of Figure 4.9c. Also, in general the roots of semi-variance are slightly higher than in Figure 4.10, as a result of the greater separation distance.

Figure 4.12 displays the contributions of each of the orthogonal components of roughness to the square-root of semi-variance at 0.5 m lag spacing. It is clear that the down-slope value increases more steadily with distance downslope than the cross-slope component. Figure 4.13 shows the relationship between the root of the semi-variance at 0.5 m and 1 m. Most points are clustered around the line where the 0.5 m lag semi-variance is half that at 1 m. As semi-variances increase, so does the deviation from this line. Generally, more points are above this line, indicating that with a doubling of the lag, the root of the semi-variance less than doubles. These mostly represent transects taken from MRZ 5 plots where steep gully walls influence the results.

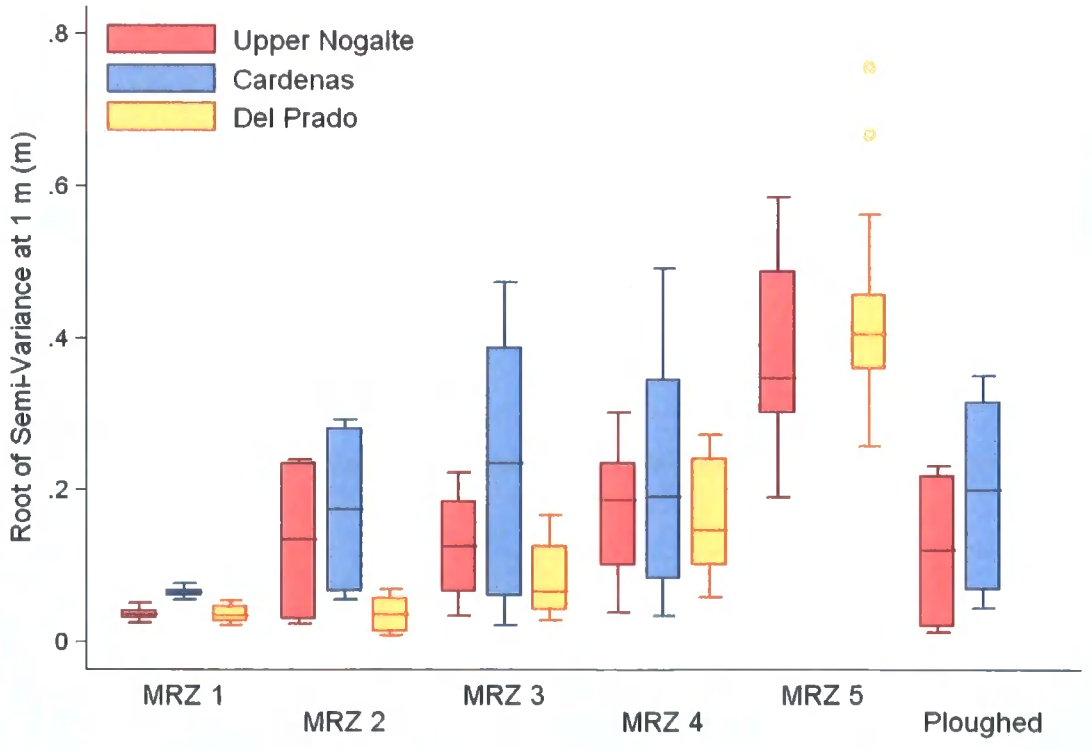

Figure 4.11. The variation of the root of semi-variance at 1 m lag spacing (m) for each plot and site (both directions combined).

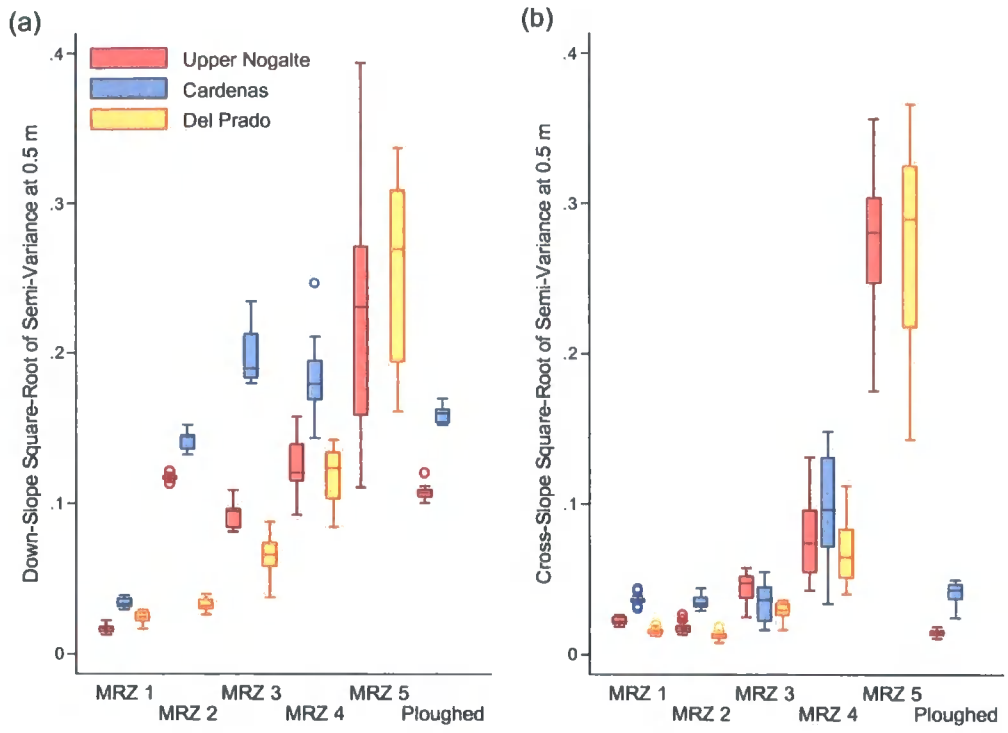

Figure 4.12. The variation of the root of semi-variance at 0.5 m lag spacing (m) for: (a) the down-slope profiles; and (b) the cross-slope profiles, for each plot and site.

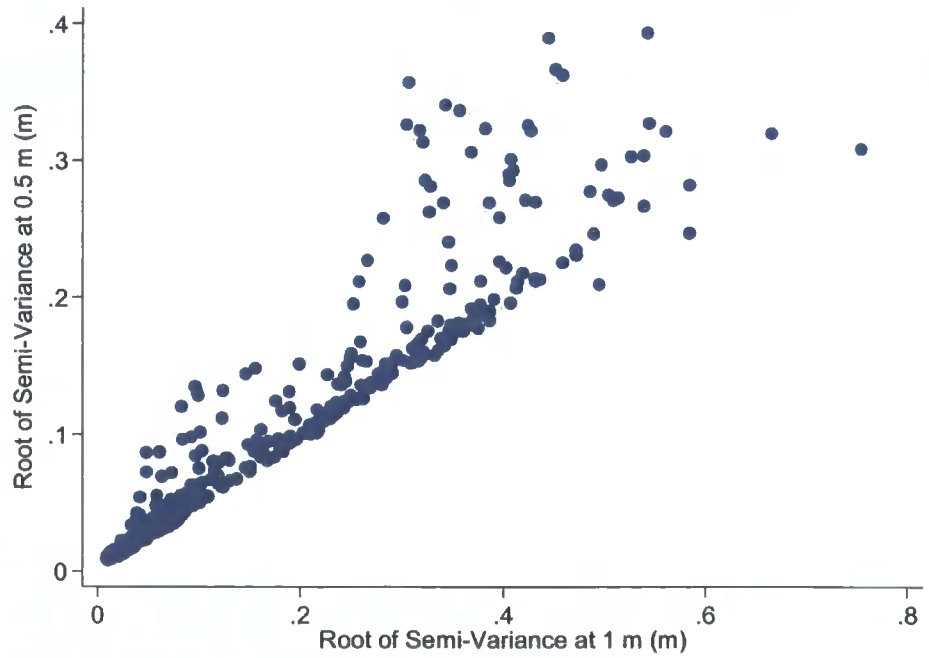

Figure 4.13. The relationship between root of semi-variance at 0.5 m and 1 m (m).

4.3.4 Pit Density

In addition to the roughness measures evaluated above, the density of pits on each transect was calculated. However, it is first necessary to define a pit from the perspective of a profile. For a transect with sequence of heights z_i, $i = 1, \ldots, n$ measured at horizontal coordinates u_i, $i = 1, \ldots, n$, each depression will have within it a point lower than its neighbours. However, as measurement is to a finite precision, several points may tie for a local minimum of z. To overcome this, one inequality is chosen arbitrarily, so that point i is declared a pit if $z_i < z_{i-1}$ and $z_i \leq z_{i+1}$. As a depression is bounded by two peaks, neither the beginning ($i = 1$) nor the end ($i = n$) is regarded as a pit. Using this principle, the number of pits on each profile can be identified and counted. Table 4.6 displays the average pit counts and pit densities for each plot (again separated into downslope and cross-slope components).

Site	*Plot*	*Pit Count Downslope*	*Pit Density Downslope (m^{-1})*	*Pit Count Cross-Slope*	*Pit Density Cross-Slope (m^{-1})*
Upper Nogalte	MRZ 1	142	44	108	33
	MRZ 2	109	34	158	50
	MRZ 3	117	41	154	47
	MRZ 4	135	40	143	43
	MRZ 5	206	68	126	41
	Ploughed	151	52	172	57
Cardenas	MRZ 1	114	46	106	33
	MRZ 2	84	28	107	36
	MRZ 3	54	19	80	27
	MRZ 4	129	47	223	70
	Ploughed	95	34	124	45
Del Prado	MRZ 1	128	45	116	35
	MRZ 2	139	52	133	40
	MRZ 3	142	54	135	43
	MRZ 4	203	83	255	75
	MRZ 5	203	88	131	45

Table 4.6. Mean pit counts and pit densities (m^{-1}) for each plot, separated into both down-slope and cross-slope components.

The most noticeable difference between the down and cross-slope components is that the cross-slope transects reveal a larger range of pit densities. Nevertheless, both the cross-slope and downslope components of roughness exhibit a similar pattern of pit density between the plots. Figure 4.14 shows this pattern for the combined dataset (with pit density log-transformed). The Cardenas site generally has the lowest pit density of

the three hillslopes, despite having the greatest 'roughness' as defined by each of the previous three profile measures. Conversely, the Del Prado site (which has previously been seen as the least rough surface) has the highest pit density. No increase in pit density is observed moving downslope from MRZ 1 to MRZ 3 (except for a slight increase in the Del Prado values). Downslope from MRZ 3, a noticeable increase in pit density occurs to MRZ 4. Therefore, the incision of rills causes an increase in the number of pits observed on the plot transects. This increase was evident for both components of roughness.

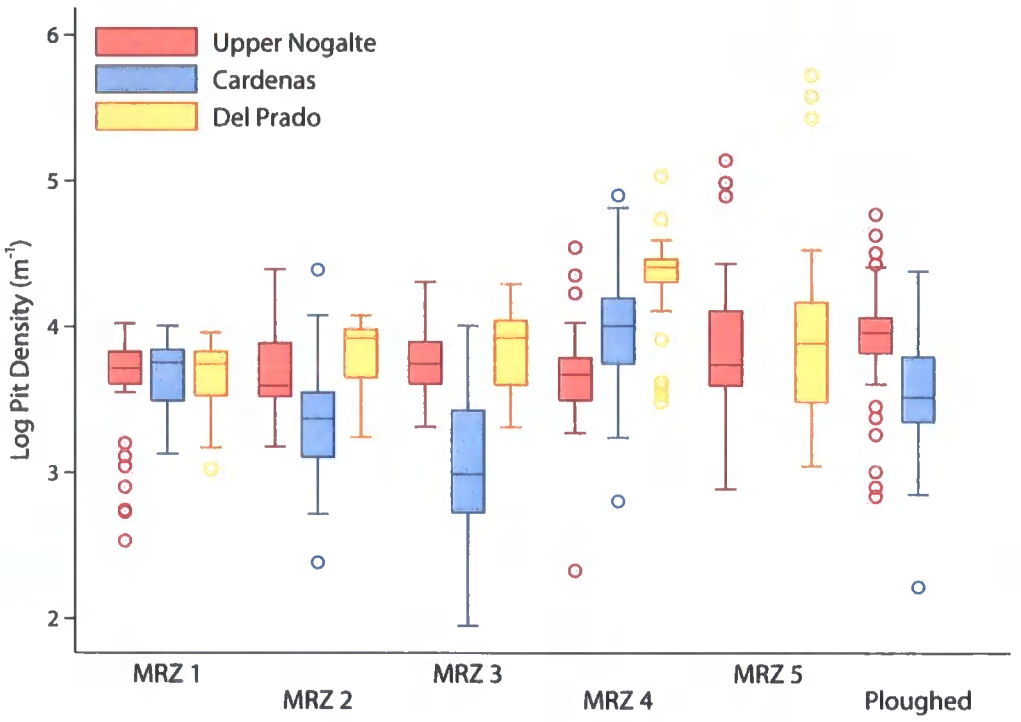

Figure 4.14. The variation of the log of pit density (m^{-1}) in both directions for each plot and site.

Given the different response of surface runoff to pits identified in the downslope direction (ponding) and pits recognized from cross-slope transects (flow concentration), Figure 4.15 shows which orthogonal component of roughness is more effective at forming pits at each plot. Figure 4.15 shows the pit density in the downslope direction minus the pit density in the cross-slope direction. At the Del Prado site, more pits were evident in the downslope direction at each plot (this also shows a general downslope increase). Pits become more frequent in the cross-slope direction at Upper Nogalte and

Cardenas as flow concentration and channel incision began (MRZs 2-4). The ploughed plots also displayed higher pit density cross-slope (i.e. along the plough furrows), but it should be noted that this property takes no consideration of the size of the pits encountered. Finally, MRZ 5 demonstrated many more pits in the downslope direction.

Despite these observed trends, the differences in pit densities between plots and sites are not particularly striking. Moreover, what may be identified as a pit on a profile may not form a pit on the surface. This point reflects the inherent limitations of using profile measures of surface roughness. Therefore, the following section considers how properties of entire surfaces can provide a representation of surface roughness.

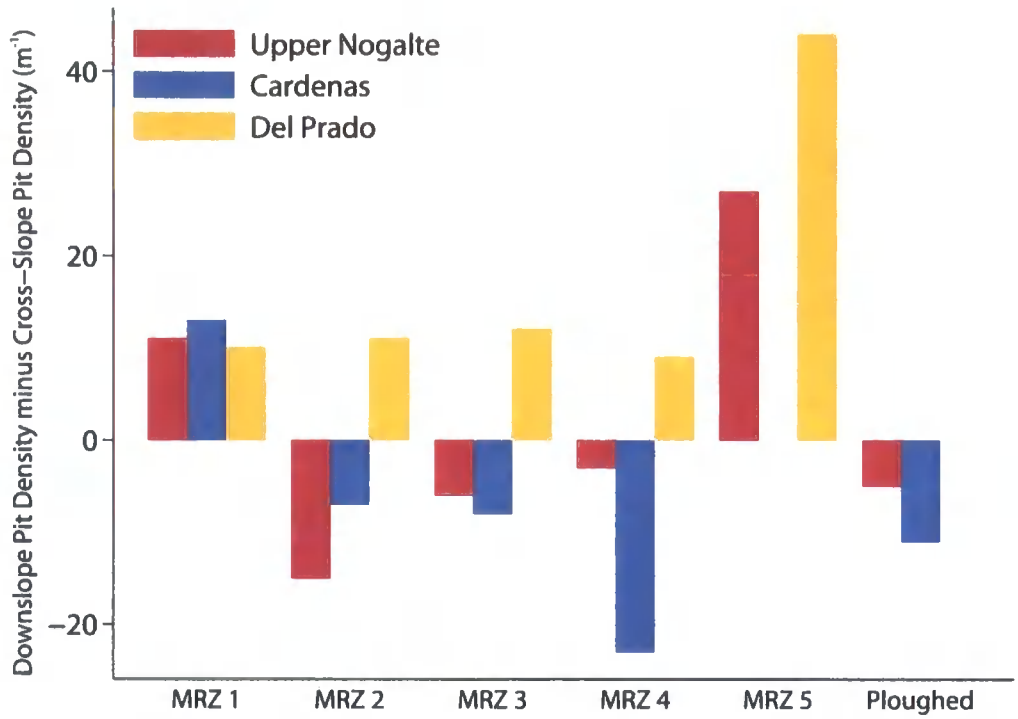

Figure 4.15. The relative importance of the downslope and cross-slope transects pit densities for each plot and site.

4.4 Surface Statistics

Kamphorst *et al.* (2005) argue that predicting maximum depressional storage from roughness indices derived from profiles is subject to a great deal of uncertainty. This is necessarily the case, as reducing any surface to a series of profiles will neglect certain elements of the surface that determine depression storage. One advantage of the use of a

terrestrial laser scanner to provide surface elevations is that several software packages permit the direct analysis of the resultant point cloud data. Such an analysis provides an intermediate step between those roughness measures based on profiles and the surface hydrological analysis. Moreover, this sidesteps the surface triangulation issues discussed in section 3.3.4.2.

4.4.1 Spread of Elevations

Dealing with point cloud data directly, the standard deviations of elevation of the entire plot could be calculated. This produces a single measure for each surface (unlike the results from multiple profiles displayed as box plots above). The standard deviations are reported in Table 4.7 and graphed in Figure 4.16.

Site	*Plot*	*Sd (m)*	*Detrend Sd (m)*
Upper Nogalte	MRZ 1	0.060	0.076
	MRZ 2	0.260	0.034
	MRZ 3	0.191	0.054
	MRZ 4	0.302	0.119
	MRZ 5	0.418	0.314
	Ploughed	0.222	0.035
Cardenas	MRZ 1	0.091	0.150
	MRZ 2	0.290	0.076
	MRZ 3	0.431	0.055
	MRZ 4	0.360	0.089
	Ploughed	0.337	0.075
Del Prado	MRZ 1	0.057	0.046
	MRZ 2	0.061	0.015
	MRZ 3	0.134	0.043
	MRZ 4	0.203	0.110
	MRZ 5	0.417	0.268

Table 4.7. Surface elevation standard deviation for each plot. 'Detrend' standard deviation refers to the surface with the general slope removed.

Figure 4.16 shows that in general the Cardenas site displays a greater spread of elevations for each plot, while the Del Prado site has the lowest standard deviations for each plot. However, Figure 4.17 demonstrates that these standard deviations are dominated by the general slope of the plots. To provide surface statistics of this type which isolate the effect of soil microtopography, it is more useful to 'detrend' the surface first by removing the general slope. This was achieved by rotating each surface

individually in the DEMON software package. The detrended values of the surface standard deviations are given in Table 4.7, while the variation between each plot is shown in Figure 4.18.

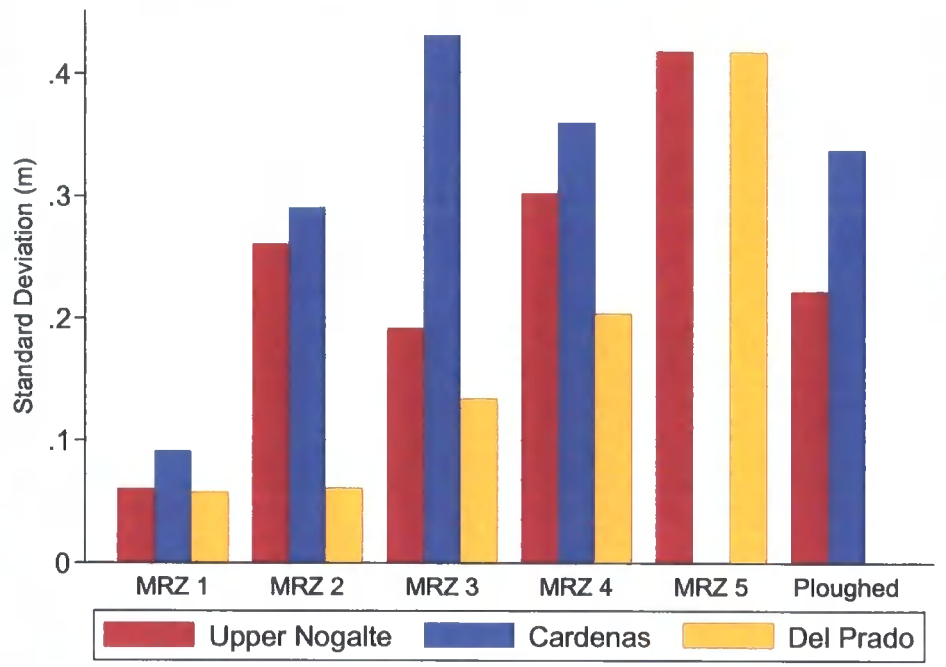

Figure 4.16. Surface standard deviation of elevations for each plot and site.

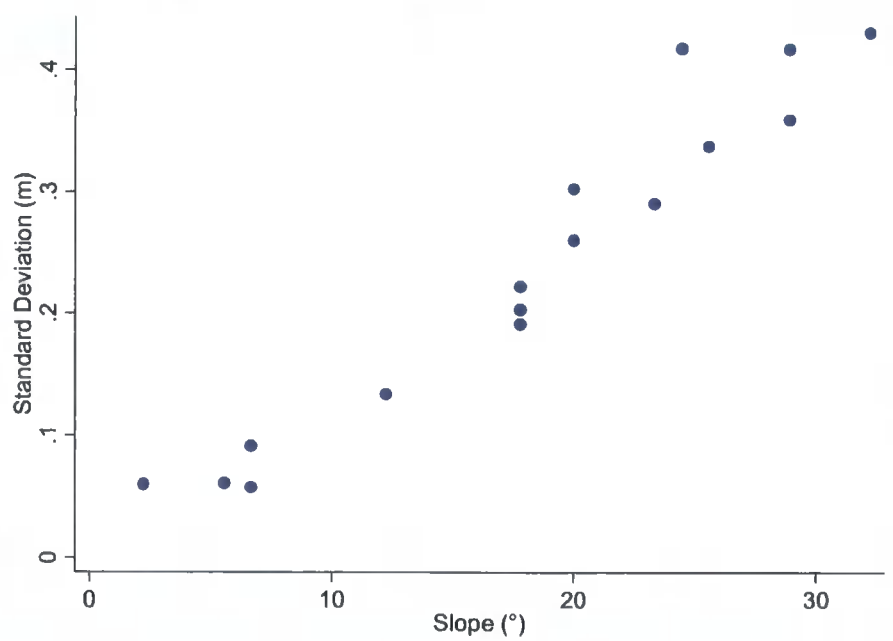

Figure 4.17. The relationship between the standard deviation (m) of the elevation measures of each plot and the general plot slope (°).

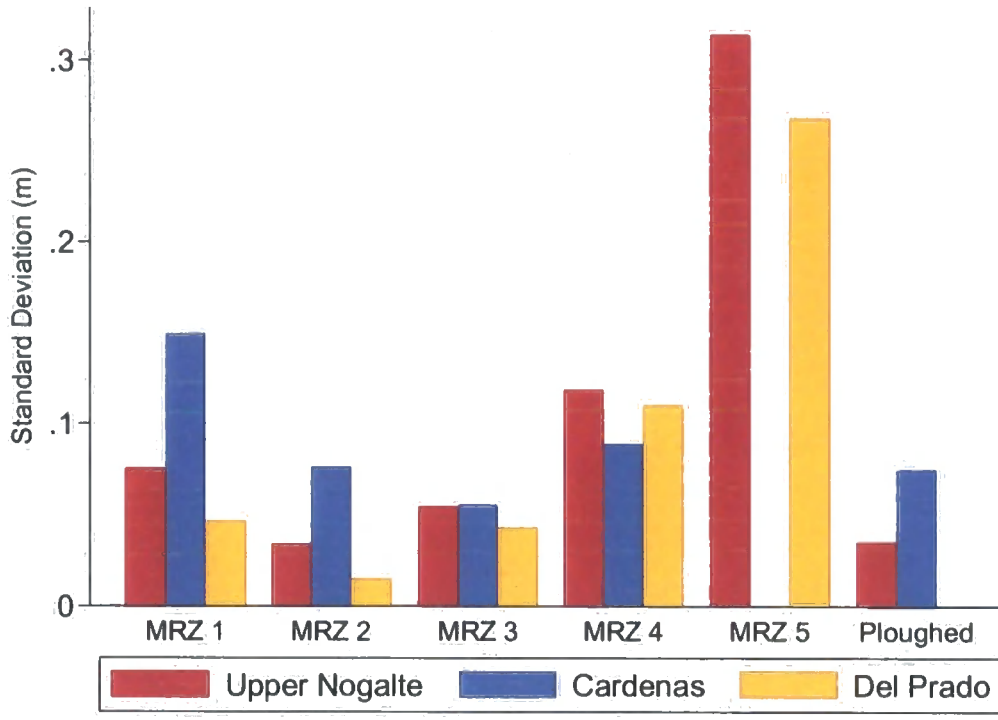

Figure 4.18. 'Detrended' standard deviation of elevations (m) for each plot and site.

A comparison of Figure 4.16 and Figure 4.18 above reveals several important points. The standard deviations are generally much smaller in Figure 4.18 as the general slope has been removed and so there is a smaller range of elevations under consideration. Figure 4.18 shows a decrease in the standard deviations of elevations downslope from MRZ 1 to MRZ 2, which perhaps represents deposition of sediment, before incision begins, after which the detrended standard deviation increases downslope to MRZ 5. The relative values of the different sites have not changed. Cardenas still generally shows the greatest spread of values and Del Prado the smallest (although this no longer holds true for MRZ 4). The sd of the ploughed plots has decreased substantially. The standard deviations of both 'detrended' ploughed plots are similar to the values found at MRZ 2.

4.4.2 Nearest Neighbour Statistics

While the spread of elevation measurements is important when considering water storage on a surface, the relationship between each elevation point and its neighbour is equally interesting. A family of statistics are available in the 'Surfer' surface mapping

system (Golden Software), called '*Nearest Neighbour*' (NN) statistics, which consider this relationship. The nearest neighbour of a data point is calculated simply on the basis of separation distance, whereby the point with the smallest separation distance from another point is considered its nearest neighbour. Table 4.8 below gives the values for the mean NN (mean absolute value of elevation differences between neighbours), the 5% Trim mean NN (with the upper and lower 5 % removed), and the standard deviation of the absolute NN values. While the average spacing of points for each plot scan will also influence these results, this was reasonably constant (± 1 mm) and was not significantly related to the NN measures.

Figure 4.19 reveals that each of the NN statistics increases with distance downslope. Notably, the two MRZ 5 plots have considerably larger values than the other plots (Figure 4.19d); this is most likely because of the data points comprising the gully walls, where the elevation differences between neighbouring points will be higher. The strong positive skewness for these plots supports this claim (results not presented). The ploughed plots have values similar to those displayed by MRZ 4 (Figs. 4.19a and b) or MRZ 3 (Fig 4.19c). No consistent pattern between the three sites can be identified.

Site	*Plot*	*Mean NN (mm)*	*5% Trim Mean NN (mm)*	*Sd NN (mm)*
Upper Nogalte	MRZ 1	1.759	1.515	2.101
	MRZ 2	2.583	2.342	2.341
	MRZ 3	2.296	2.100	2.009
	MRZ 4	3.082	2.665	3.950
	MRZ 5	14.845	8.429	37.764
	Ploughed	3.395	3.046	3.238
Cardenas	MRZ 1	1.731	1.558	1.643
	MRZ 2	1.884	1.700	1.802
	MRZ 3	2.503	2.249	2.418
	MRZ 4	4.017	3.442	4.544
	Ploughed	3.389	3.062	3.133
Del Prado	MRZ 1	1.613	1.447	1.549
	MRZ 2	2.106	1.825	2.282
	MRZ 3	2.381	2.128	2.290
	MRZ 4	3.574	2.820	5.490
	MRZ 5	19.035	12.129	42.982

Table 4.8. Mean of Nearest Neighbour (mm), 5% trim mean of Nearest Neighbour (mm) and standard deviation of Nearest Neighbour (mm) elevation differences.

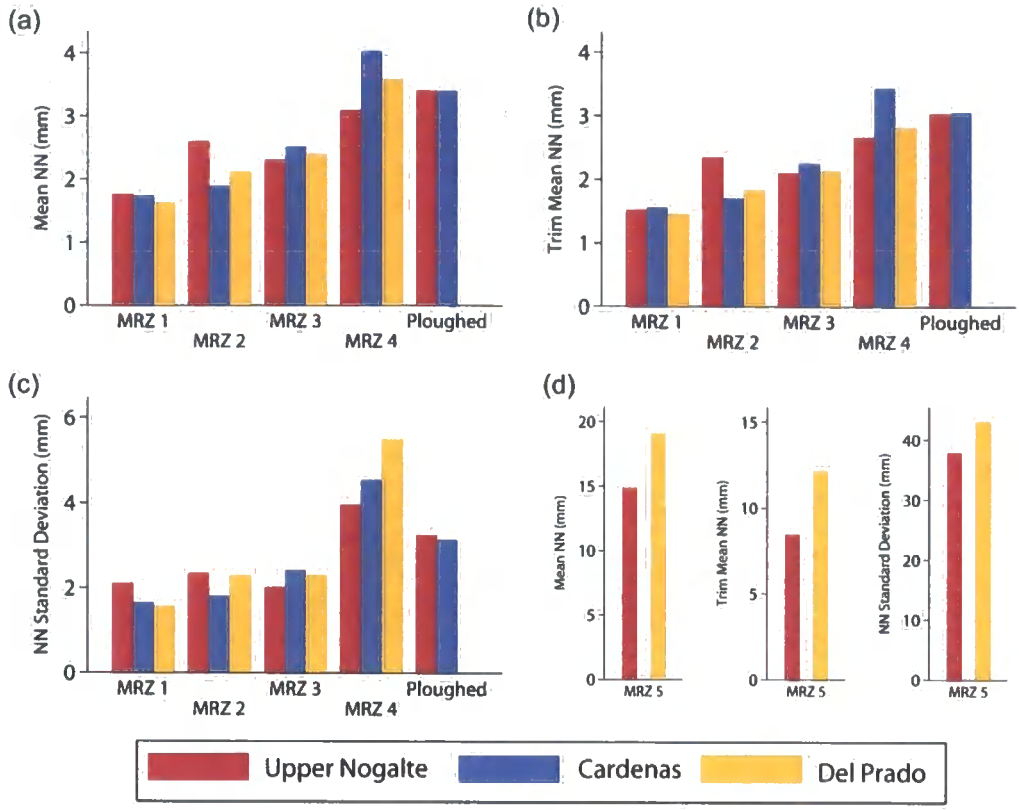

Figure 4.19. Nearest Neighbour statistics for each plot and site: (a) mean of Nearest Neighbour (mm); (b) 5% trim mean of Nearest Neighbour (mm); (c) standard deviation of Nearest Neighbour (mm) elevation differences; and (d) each measure for MRZ 5.

Once again the process was repeated using a detrended surface to isolate the separate influences of general slope and microtopography. The nature of these surface statistics meant that such detrending only decreased the NN values slightly, so NN statistics are not as dominated by general slope as the measures of spread analysed in section 4.4.1 (compare Figure 4.20 with Figure 4.17).

4.4.3 Surface Tortuosity

The 'Surfer' surface mapping system (Golden Software) was able to create a grid of the point cloud data using ordinary kriging techniques. Once a grid of the surface is created, both the surface area and planar area of the plots may be extracted. With this information, the concept of tortuosity (discussed in section 2.6.2) can be brought into three dimensions (Helming *et al.*, 1992, 1993). Using grid cell sizes of 5 mm × 5 mm, the 'surface tortuosity' was calculated as total measured area divided by planar area.

Table 4.9 summarises surface tortuosity for each plot; this is also illustrated in Figure 4.21.

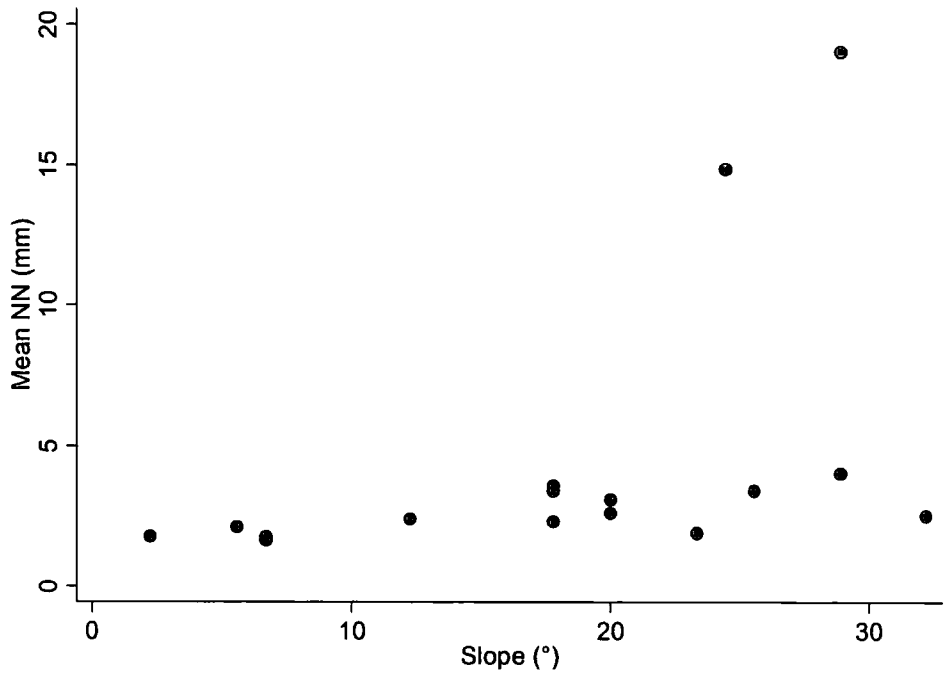

Figure 4.20. The relationship between mean of Nearest Neighbour differences (mm) and plot slope (°).

Site	*Plot*	*Surface Tortuosity*
Upper Nogalte	MRZ 1	1.073
	MRZ 2	1.149
	MRZ 3	1.130
	MRZ 4	1.190
	MRZ 5	1.787
	Ploughed	1.249
Cardenas	MRZ 1	1.075
	MRZ 2	1.183
	MRZ 3	1.264
	MRZ 4	1.414
	Ploughed	1.201
Del Prado	MRZ 1	1.043
	MRZ 2	1.086
	MRZ 3	1.140
	MRZ 4	1.376
	MRZ 5	1.974

Table 4.9. Surface tortuosity for each plot.

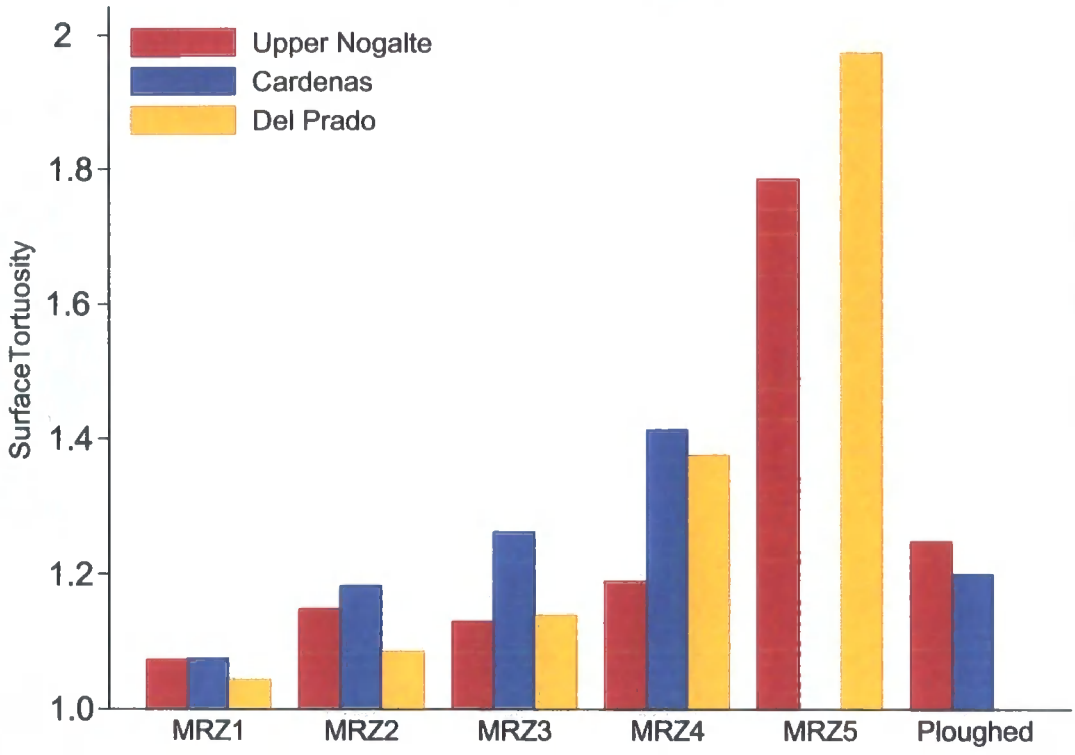

Figure 4.21. Surface tortuosity for each plot and site.

As expected surface tortuosity increases downslope as incisions are made into the soil surface by flowing water. The Cardenas values are highest at all natural slopes, whereas the Del Prado values are lowest until incision begins, whereafter they gradually become the highest. Surface tortuosity was also calculated for the detrended plot surfaces, but the difference between these values and those given above was only very slight in each case.

4.4.4 Fractal Dimension of Surfaces

Grids of each plot were created using different grid cell sizes ranging from 5 mm × 5 mm to 2.56 m × 2.56 m. Figure 4.22 displays example wireframes of the Upper Nogalte MRZ 1 plot, ranging from 20 mm × 20 mm (Figure 4.22a) to 640 mm × 640 mm (Figure 4.22f).

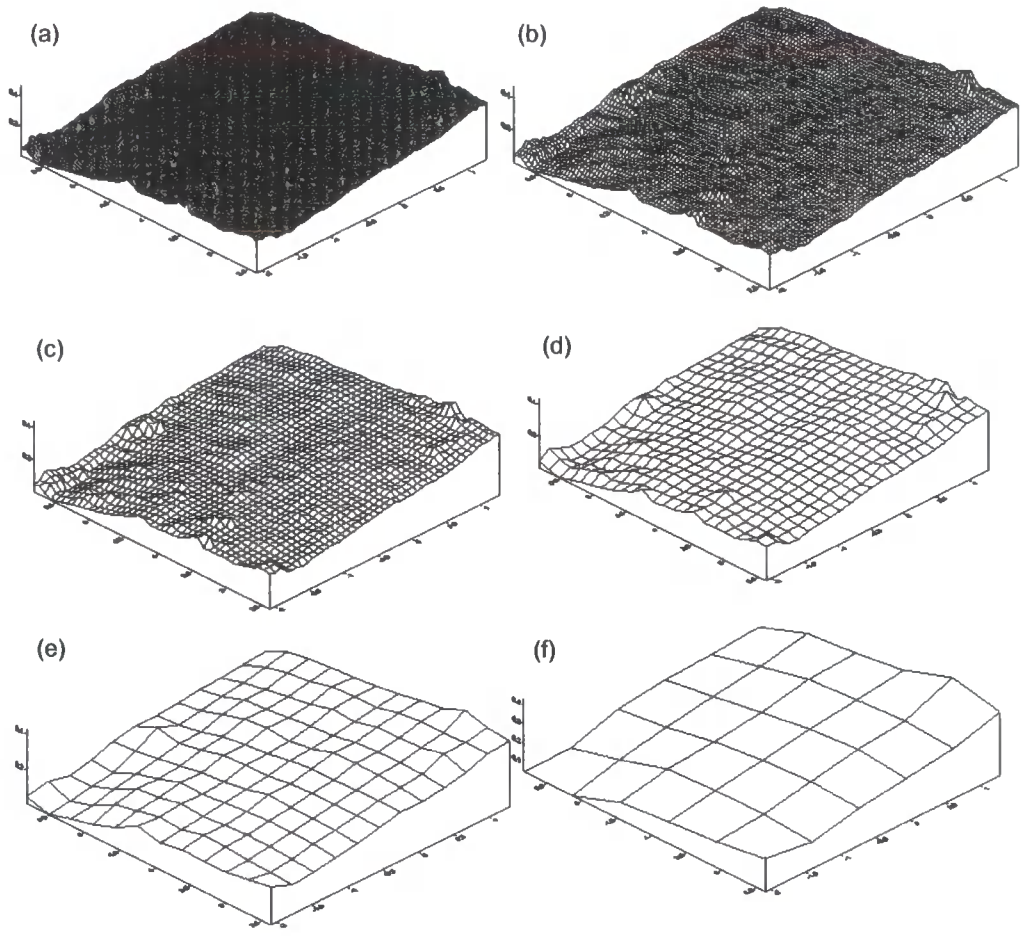

Figure 4.22. Grids of Upper Nogalte MRZ 1 with increasing grid spacing: (a) 20 × 20 mm grid; (b) 40 × 40 mm; (c) 80 × 80 mm; (d) 160 × 160 mm; (e) 320 × 320 mm; and (f) 640 × 640 mm.

Through gradually increasing the grid spacings and calculating the area of the plot for each grid spacing, the fractal dimension of the surfaces could be calculated, using the principle discussed in section 2.6.3, only applied to whole surfaces. Figure 4.23 demonstrates how excess area (measured area minus planar area) changes with grid spacing for each plot at the Upper Nogalte site. The decline of excess area with grid cell size is well described by a power function.

In all cases, an initial rapid decrease in area with increasing grid spacing is evident. However, this decrease is larger for some plots (e.g. MRZs 2 and 5), than in others. As the point separation increases from 5 mm to 200 mm, the rapid decrease in surface area comes about as a result of the effective smoothing of surface microtopography. The area of each plot experiences this decrease as all plots have some elevation variation at this

scale, whatever the hillslope location. Further decreases in area beyond 0.5 m separation, for instance, involve the eradication of larger features from the plots, such as rills and gullies. Indeed, the MRZ 5 plot area in Figure 4.23 continues to decrease beyond 2 m grid spacing, which reflects large features at this location. This shows one advantage of using plot areas of 3 m by 3 m, as larger features such as gullies can be taken into account.

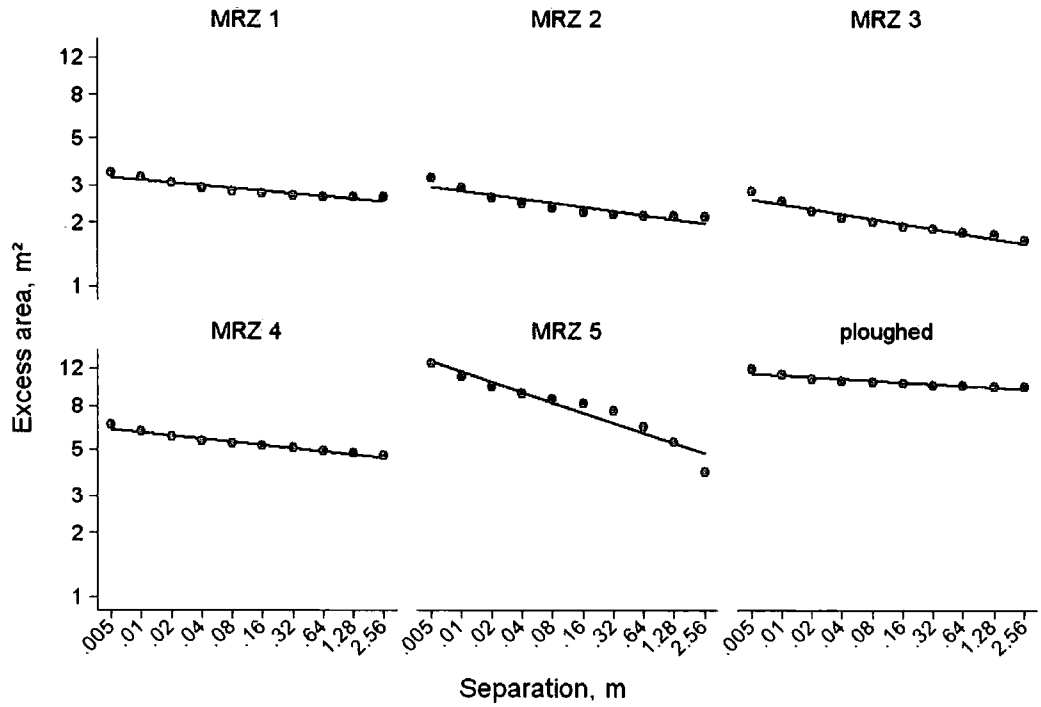

Figure 4.23. The decline of excess area (m^2) with increasing grid size (or separation, in m) for the Upper Nogalte plots.

The estimates of the fractal dimension *D* for each plot are related to the gradient of these curves in log-log space (as was discussed in more detail in section 2.6.3). The surface fractal dimensions for each plot can be found in Table 4.10; these are displayed in Figure 4.24.

A fairly consistent pattern has emerged: a general increase in *D* occurs from MRZ 1 downslope through to MRZ 5, but in all cases, the fractal dimension is not much greater than 2.0. The Cardenas site seems to generally have the highest *D* on natural surfaces (except for MRZ 4). Ploughed surfaces at the Upper Nogalte site have a higher fractal

dimension than natural surfaces (excluding MRZ 5), but at Cardenas, this is not the case.

Site	*Plot*	*Surface Fractal Dimension*
Upper Nogalte	MRZ 1	2.0108
	MRZ 2	2.0140
	MRZ 3	2.0146
	MRZ 4	2.0190
	MRZ 5	2.0724
	Ploughed	2.0274
Cardenas	MRZ 1	2.0105
	MRZ 2	2.0174
	MRZ 3	2.0194
	MRZ 4	2.0425
	Ploughed	2.0185
Del Prado	MRZ 1	2.0064
	MRZ 2	2.0122
	MRZ 3	2.0181
	MRZ 4	2.0439
	MRZ 5	2.0852

Table 4.10. Surface fractal dimensions of each plot.

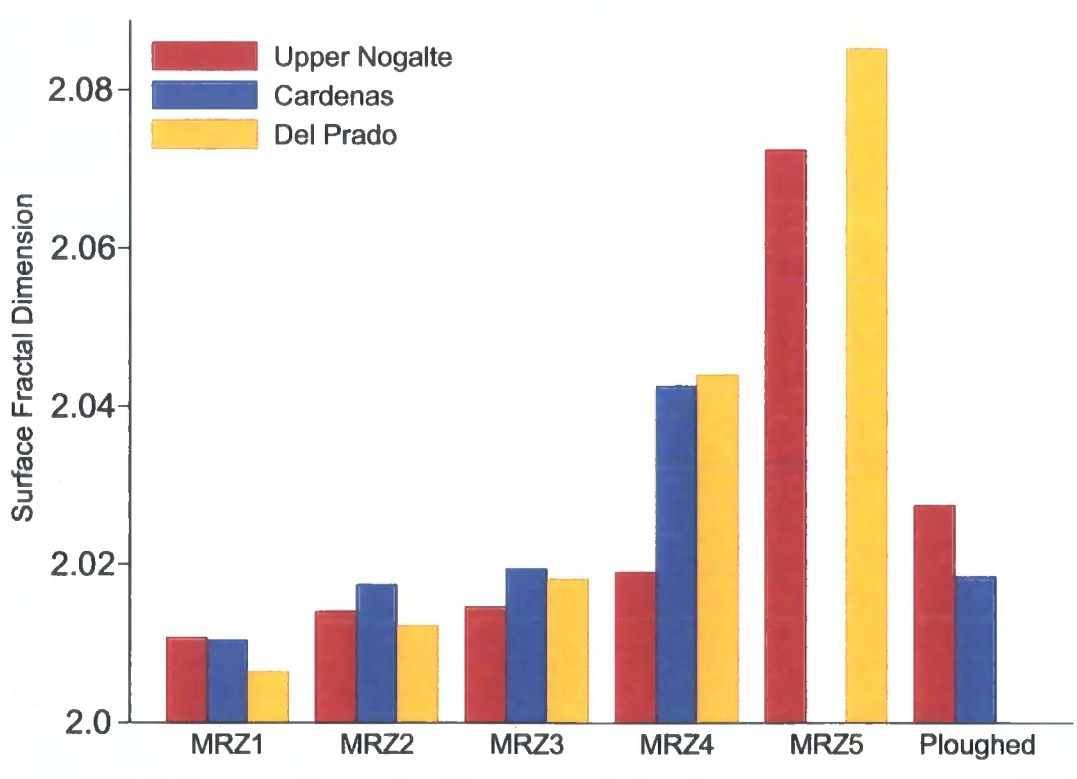

Figure 4.24. Surface fractal dimensions for each plot and site.

4.5 Surface Topographic Features

The point clouds of each surface were also imported into the ENVI image visualisation software (Research Systems, Inc.). Rasters of the point cloud data were created at 10 mm resolution from which information such as slope angle and slope convexities from different perspectives could be extracted. The distribution of slope angles within each plot is presented in section 4.5.1. Additionally, section 4.5.2 compares the terrain of each plot as ENVI was also able to classify pixels of the surfaces into morphometric features. Due to edge effects experienced (with slope angles of 90 degrees recorded at the plot boundaries) the plot boundaries were not included in this analysis to exclude artefacts.

4.5.1 Distribution of Slope Angles

Thus far, only a single value of slope has been assigned to each plot. However, as seen in Figure 4.25, each plot contains a range of slope angles. The standard deviations of the slope angles (in degrees) calculated for each surface are found in Table 4.11 and the variation of this value between plots can be seen in Figure 4.26.

Figure 4.26 shows relatively little variation between sites compared with that between plots. There is a steady increase in the standard deviation of slope angle moving downslope from MRZ 1 to MRZ 5. This is perhaps a reflection of the progressively larger surface features visible on the soil surface increasing local slope angles.

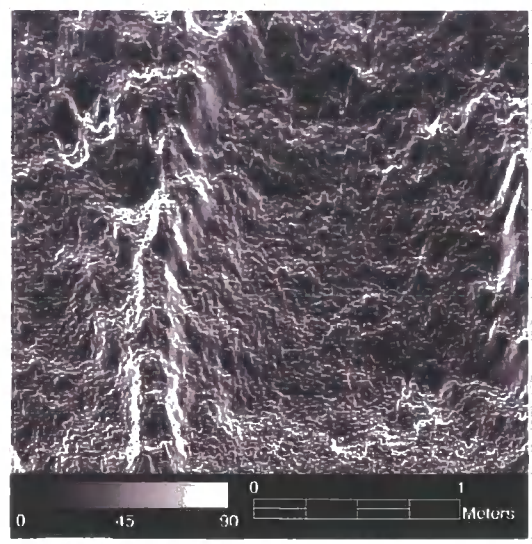

Figure 4.25. Distribution of slope angle across the Upper Nogalte MRZ 3 plot. The linear feature observable the left of the image is a small flow concentration.

Site	*Plot*	*Standard Deviation of Slope Angles (°)*
Upper Nogalte	MRZ 1	8.13
	MRZ 2	11.31
	MRZ 3	10.83
	MRZ 4	10.76
	MRZ 5	16.81
	Ploughed	15.57
Cardenas	MRZ 1	8.38
	MRZ 2	11.69
	MRZ 3	11.52
	MRZ 4	16.12
	Ploughed	13.41
Del Prado	MRZ 1	7.42
	MRZ 2	10.48
	MRZ 3	11.94
	MRZ 4	16.15
	MRZ 5	18.44

Table 4.11. The standard deviations of the slope angles of each plot.

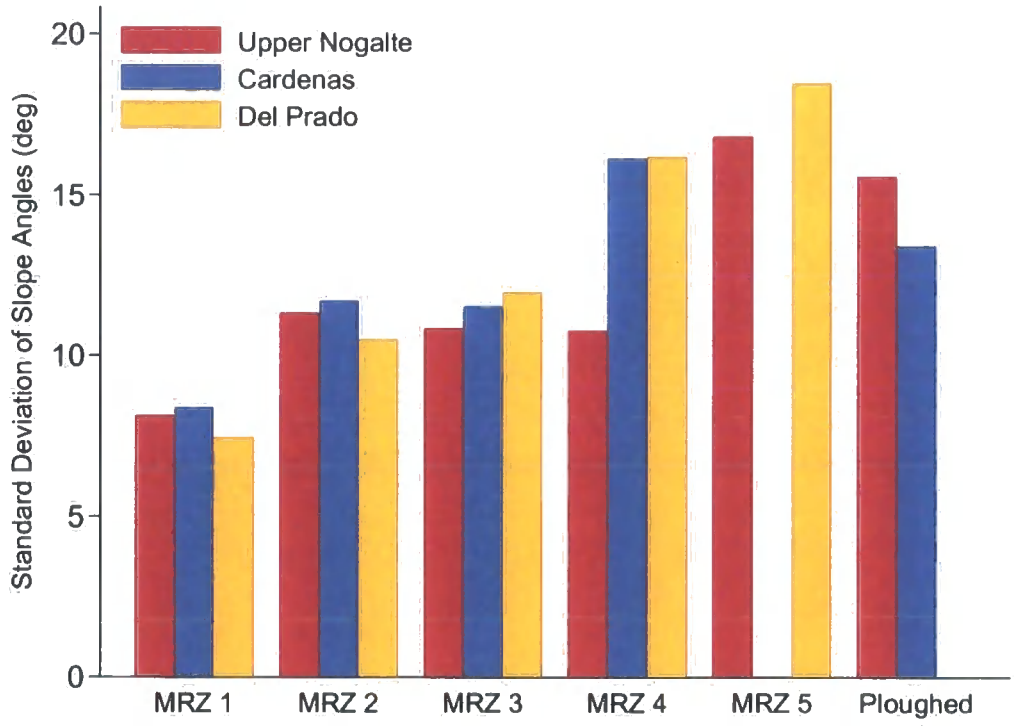

Figure 4.26. Standard deviations of the slope angles for each plot and site.

4.5.2 Morphometric Features

Although the slope of the plot surfaces has already been dealt with, the convexity (or concavity) of the surfaces under investigation deserves some attention, as these second-order differentials of the surface are also geomorphologically significant (Evans, 1972, 2003; Wood, 1996). These rates of change of slope can be used to characterise the terrain of each plot. Wood (1996) suggests that the most commonly used set of morphometric characteristics is the subdivision of each point on a surface into peak, pit, channel, ridge, pass or plane. Each of these six features can be unambiguously defined by the local rate of change of slope of three orthogonal components. These definitions are given in Table 4.12 above.

The above classification produces point-based categories (pits, passes and peaks), line-based categories (channels and ridges) and an area-based category (planes). Wood (1996) notes that when using this classification to identify surface features, the continuity of line-based channels and ridges is preserved over the point-based categories. Figure 4.27a displays the division of a plot into morphometric features for the Cardenas MRZ 4 plot. Figure 4.27b however, demonstrates how the identification of surface features is dependent upon the scale under consideration. A similar pattern is observed with the slope angles discussed earlier.

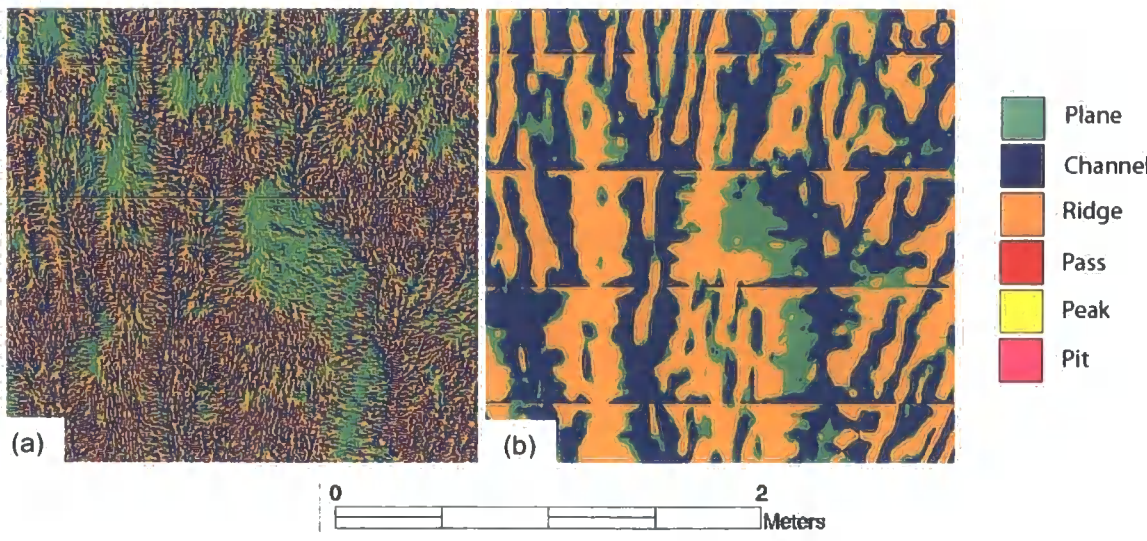

Figure 4.27 Morphometric features of the *Cardenas* MRZ 4 plot: (a) kernel size of 3; (b) kernel size of 25.

Feature	*Description*	*Derivative Expression*	*Diagram*
Plane	Points do not lie on any surface convexity or concavity	$\frac{\partial^2 z}{\partial x^2} = 0$, $\frac{\partial^2 z}{\partial y^2} = 0$	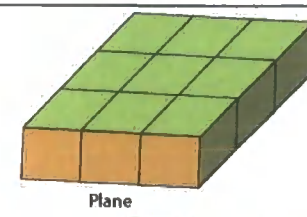 Plane
Channel	Point lies in a local concavity that is orthogonal to a line with no convexity or concavity	$\frac{\partial^2 z}{\partial x^2} < 0$, $\frac{\partial^2 z}{\partial y^2} = 0$	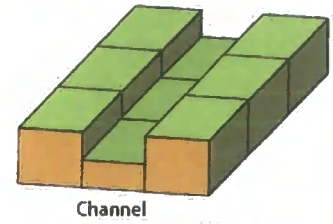 Channel
Ridge	Point lies in a local convexity that is orthogonal to a line with no convexity or concavity	$\frac{\partial^2 z}{\partial x^2} > 0$, $\frac{\partial^2 z}{\partial y^2} = 0$	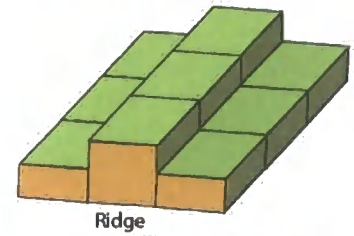 Ridge
Pass	Point lies in a local convexity that is orthogonal to a local concavity	$\frac{\partial^2 z}{\partial x^2} > 0$, $\frac{\partial^2 z}{\partial y^2} < 0$	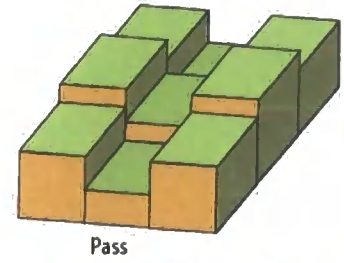 Pass
Peak	Point lies on a local convexity in all directions	$\frac{\partial^2 z}{\partial x^2} > 0$, $\frac{\partial^2 z}{\partial y^2} > 0$	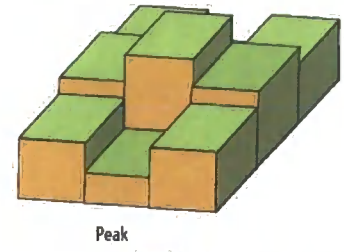 Peak
Pit	Point lies on a local concavity in all directions	$\frac{\partial^2 z}{\partial x^2} < 0$, $\frac{\partial^2 z}{\partial y^2} < 0$	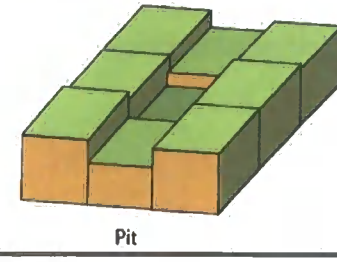 Pit

Table 4.12. The six categories of morphometric feature, illustrated by the relationship between a central DEM cell and its eight neighbours and defined by second derivatives. Descriptions adapted from Wood (1996).

For a robust analysis of each surface, the changing arrangement of these categories with increasing kernel size should be considered. However, for the purposes of this investigation, a comparison of all plots using the standard kernel size of 3 was considered sufficient, as this will identify surface morphometric features at the fine scale. Table 4.13 displays the percentage of each plot area covered by each surface feature.

Figure 4.28 illustrates how the percentage of each surface classified as a pit varies with each plot. For each MRZ, Del Prado has the highest pit area, but even the maximum area does not rise above 0.05% of the total plot area (because continuous linear features are preferentially preserved). There is a general decrease in percentage pit with distance downslope from the drainage divide. The percentage areas of the peak and pass features display a similar pattern.

Site	*Plot*	*Plane*	*Channel*	*Ridge*	*Pass*	*Peak*	*Pit*
Upper Nogalte	MRZ 1	40.31	29.56	29.92	0.14	0.03	0.03
	MRZ 2	33.07	33.63	33.25	0.03	0.01	0.01
	MRZ 3	33.37	33.33	33.25	0.04	0.01	0.01
	MRZ 4	31.27	34.27	34.43	0.02	0.01	0.01
	MRZ 5	39.24	30.23	30.53	0	0	0
	Ploughed	35.29	32.19	32.44	0.05	0.01	0.01
Cardenas	MRZ 1	35.48	31.85	32.53	0.09	0.02	0.02
	MRZ 2	36.68	31.81	31.48	0.02	0	0.01
	MRZ 3	39.23	31.14	29.62	0	0	0
	MRZ 4	40.14	29.8	30.05	0	0	0
	Ploughed	50.03	24.88	25.07	0.01	0	0
Del Prado	MRZ 1	40.54	29.3	29.86	0.2	0.05	0.05
	MRZ 2	33.01	33.12	33.63	0.16	0.04	0.04
	MRZ 3	35.45	32.4	32.03	0.07	0.02	0.02
	MRZ 4	24.58	37.76	37.58	0.05	0.01	0.02
	MRZ 5	48.42	25.98	25.59	0	0	0

Table 4.13. Surface morphometric features of each plot (given as % of total plot area).

The percentage area classified as a channel is also particularly interesting. Figure 4.29 shows how it increases with distance downslope to either MRZ 3 or 4. This represents the incision of the surface by overland flow. This percentage decreases with distance further downslope, but this is most likely a result of the increasing channel width and the shortcomings of the morphometric feature identification when limited to fine scales

(see Figure 4.27a and b). The ploughed plots contain a lower percentage area classified as a channel than most of the natural surfaces.

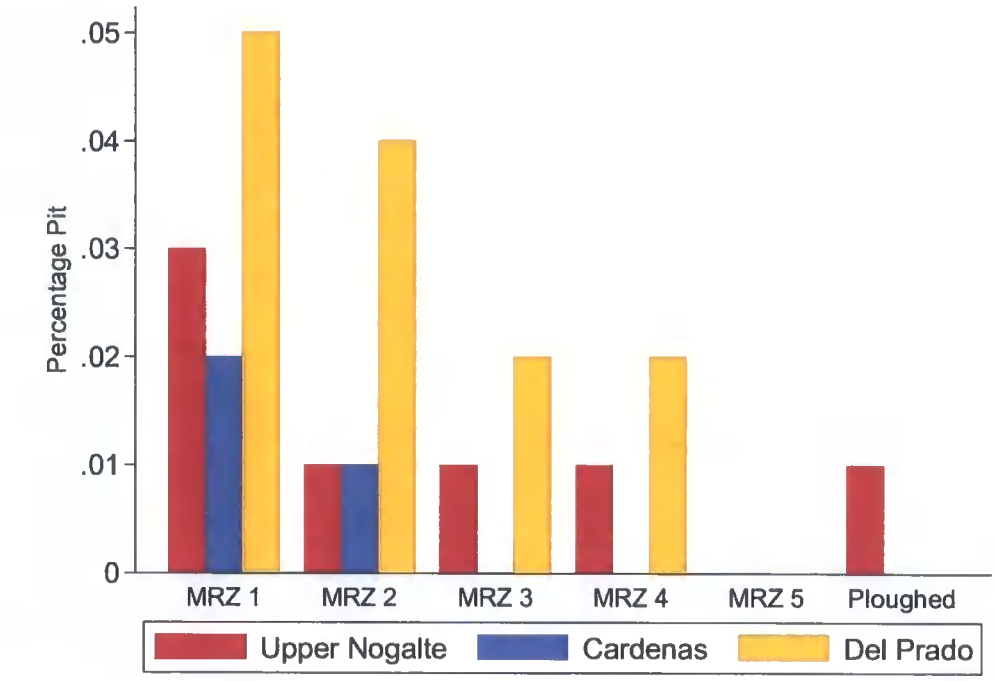

Figure 4.28. Percentage of total plot area classified as a pit for each plot and site.

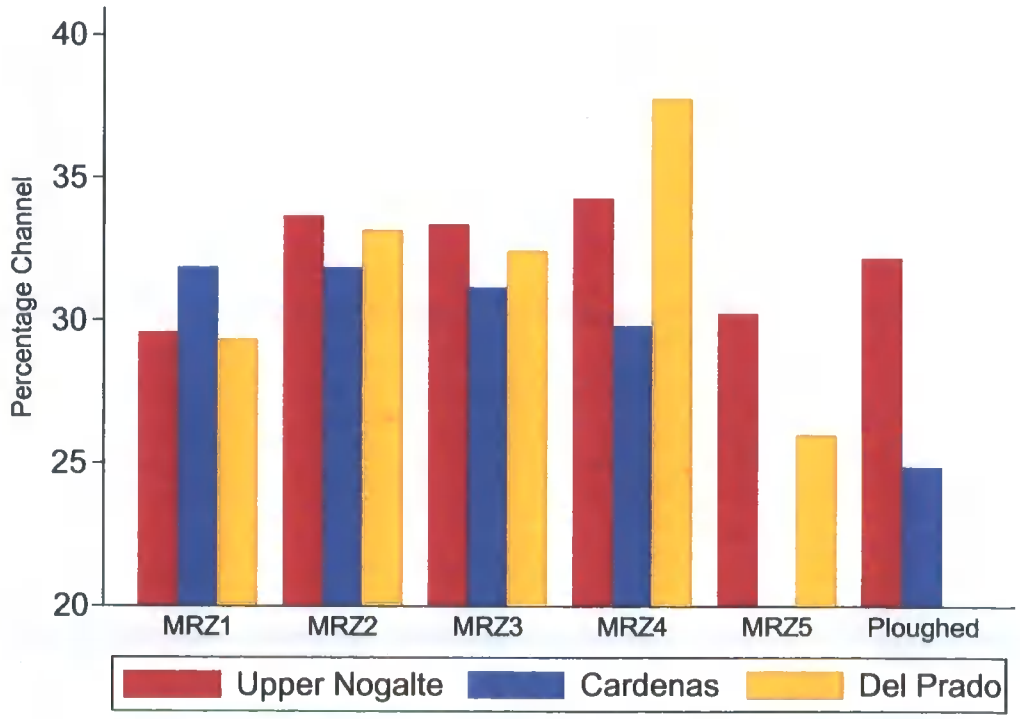

Figure 4.29. Percentage of total plot area classified as a channel for each plot and site.

4.6 Hillslope-Scale Surfaces

Laser scanning each hillslope with an even distribution of points proved difficult within the timeframe of this project (see section 3.3.4.2). At several areas, particularly on the Cardenas hillslope, the point resolution is lower than desired. Figures 4.30, 4.31 and 4.32 display plan views of each hillslope, with contours at every metre. Each figure was produced through ENVI image visualisation software using cell sizes of 50 mm × 50 mm. Section 4.6.1 examines how the profile roughness measures perform at the hillslope scale, while section 4.6.2 deals with the surface measures discussed earlier in this chapter.

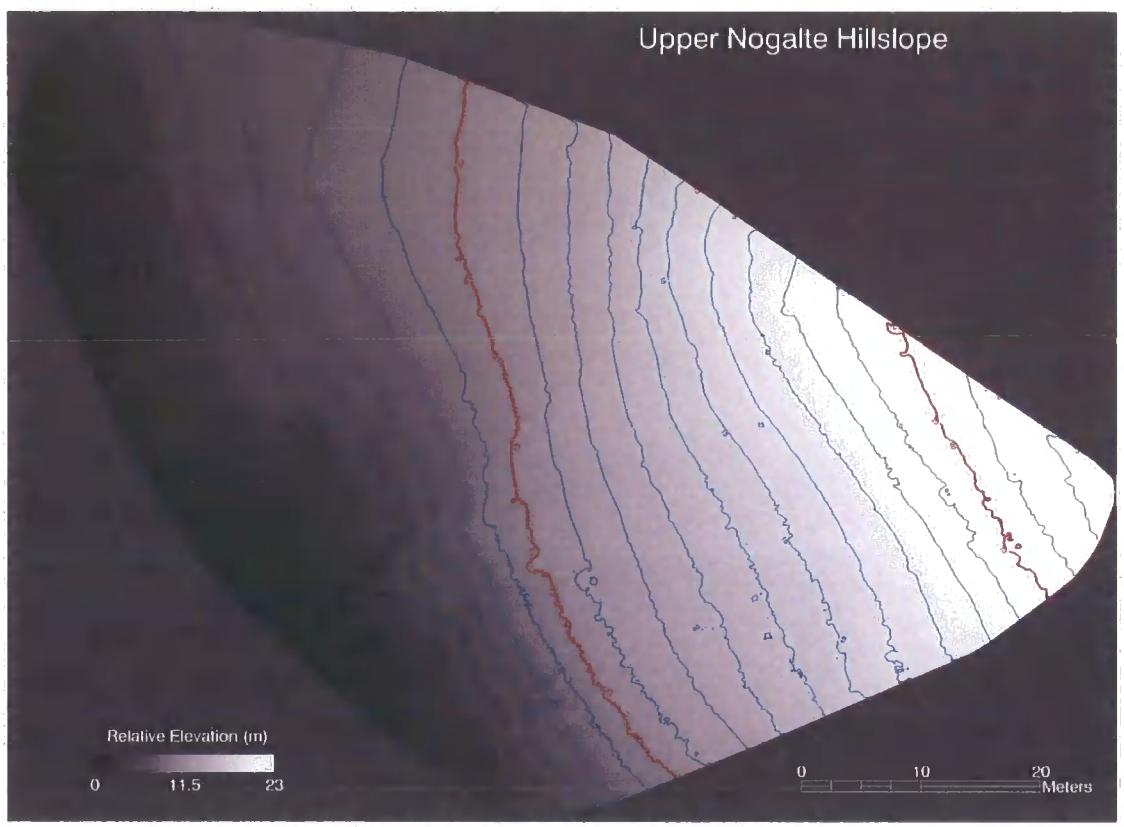

Figure 4.30. Plan view of the Upper Nogalte hillslope.

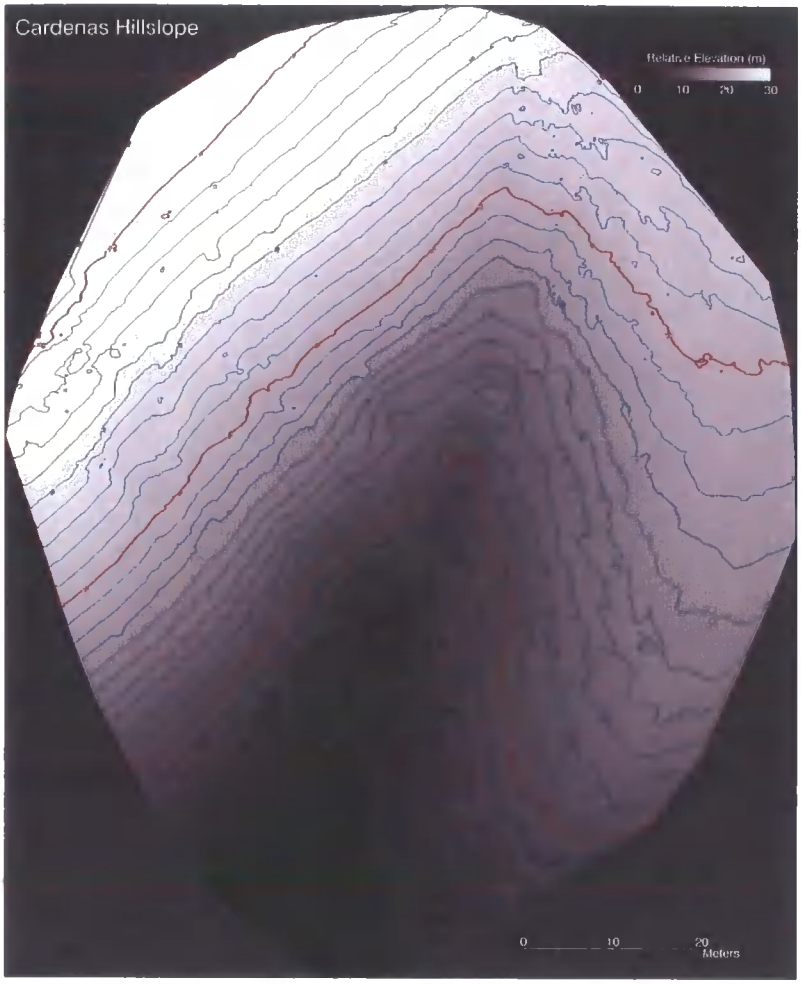

Figure 4.31. Plan view of the bowl-shaped Cardenas hillslope.

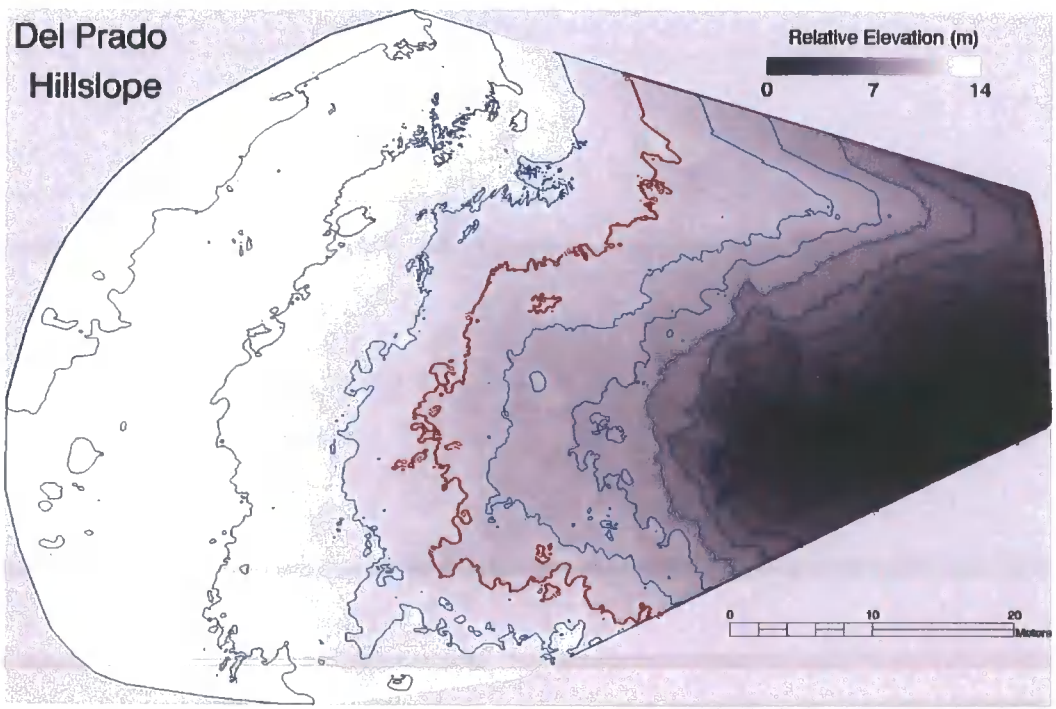

Figure 4.32. Plan view of the Del Prado hillslope.

4.6.1 Hillslope Profile Measures

As each hillslope is composed of multiple slope components, a simple linear detrending of the profiles to remove general slope is not appropriate. The results of various profile-based roughness elements that were calculated at the hillslope scale are displayed in Table 4.14 and Figure 4.33. The measures of spread and tortuosity are sensitive to general slope at this scale. The Cardenas site has the steepest slopes, and has the greatest values of downslope roughness, as calculated through these measures. Similarly, the Upper Nogalte site showed the greatest values in the cross-slope component (as the bowl-shaped Cardenas slope had a lower range of elevations in this direction) (Figure 4.33).

The pit density measures possibly represent a better reflection of hillslope microtopography and surface conditions. The Del Prado has much higher pit densities in both directions than the other two slopes (but this may simply reflect slightly higher point resolution at this site). Cardenas has a greater pit density than Upper Nogalte in the cross-slope direction, but the values in the downslope-direction are similar.

Hillslope	*Upper Nogalte*	*Cardenas*	*Del Prado*
Mean down-slope sd (m)	2.369	7.131	1.359
Mean cross-slope sd (m)	4.513	3.202	2.132
Mean down-slope iqr (m)	3.969	14.300	2.320
Mean cross-slope iqr (m)	7.792	4.442	3.305
Mean down-slope tortuosity (T_A)	1.618	1.352	1.123
Mean cross-slope tortuosity (T_A)	1.325	2.557	1.088
Mean pit density down-slope (m^{-1})	2.644	2.604	19.586
Mean pit density cross-slope (m^{-1})	3.330	6.058	26.689

Table 4.14. Profile-based roughness measures calculated for each hillslope.

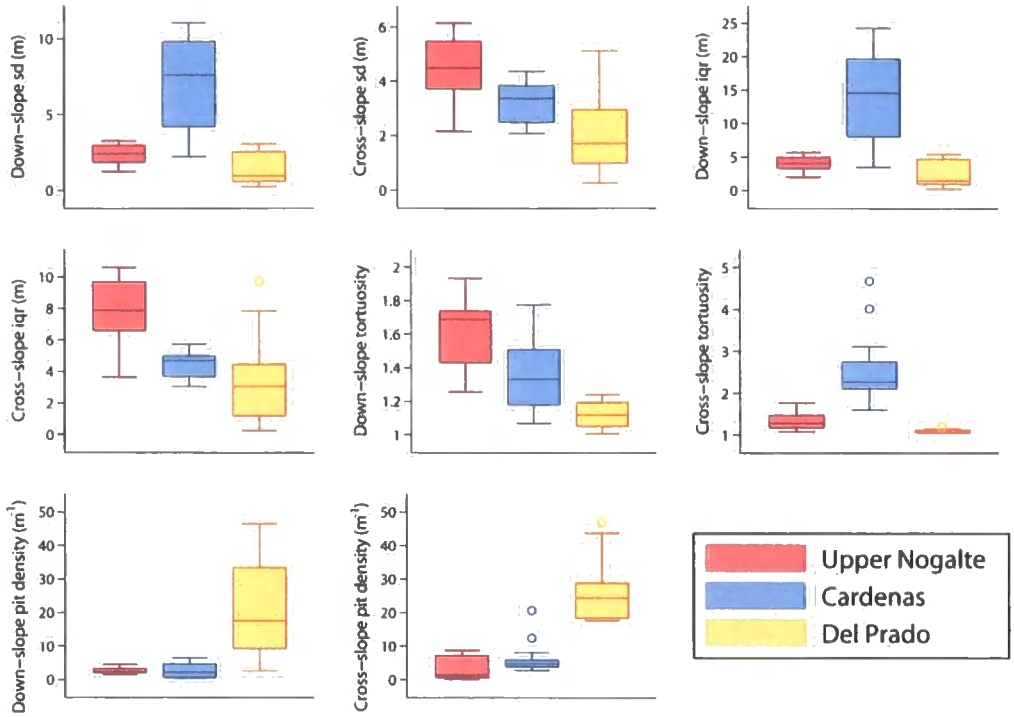

Figure 4.33. Profile-based roughness measures calculated for each hillslope.

4.6.2 Hillslope Surface Measures

Table 4.15 summarises each of the surface measurements (previously described for the plot scale), at the hillslope scale for each site; this is also represented in Figure 4.34. From this it is clear that Cardenas had the largest spread of elevation measurements, followed by Upper Nogalte and Del Prado. The mean nearest neighbour statistics show that Upper Nogalte has a much larger mean elevation difference between neighbouring points than the other sites. These values are generally larger than that displayed at the plot scale because of the larger separation distance between points. Indeed, because of the regions of the hillslopes with larger separation distances between points, the 5% trim mean NN statistic is more reliable. The larger standard deviation of NN differences at Upper Nogalte and Cardenas is a good reflection of this feature of the hillslope point clouds.

Del Prado displays the highest surface tortuosity of the three hillslopes, but this measure of the hillslopes was lower than at the plot scale. This is possibly a result of the irregular shape of the hillslope when viewed from above which means that surface tortuosity calculations will be subject to error. The SURFER grids must form a rectangular shape,

and so were larger than the hillslope surface, producing a flat area around the edges of the hillslope. Such a flat surface will influence the results, underestimating each of the surface measures. For this reason, the distribution of surface morphometric features at this scale has also been discarded as a disproportionate percentage of the surfaces was identified as a plane. As the hill surfaces were not detrended, the surface fractal dimension was also not calculated. The Del Prado hillslope also exhibits the highest standard deviation of slope angles.

Hillslope	*Upper Nogalte*	*Cardenas*	*Del Prado*
Elevation Range (m)	22.639	31.154	17.268
Standard Deviation (m)	4.555	7.286	2.605
Mean NN (mm)	22.537	13.559	12.852
Trim Mean NN (mm)	19.034	9.418	11.144
NN Standard Deviation (mm)	25.770	26.609	14.312
Fractal Dimension	2.002	2.000	2.010
Slope Standard Deviation (deg)	10.292	10.671	15.174

Table 4.15. Surface-based roughness measures calculated for each hillslope.

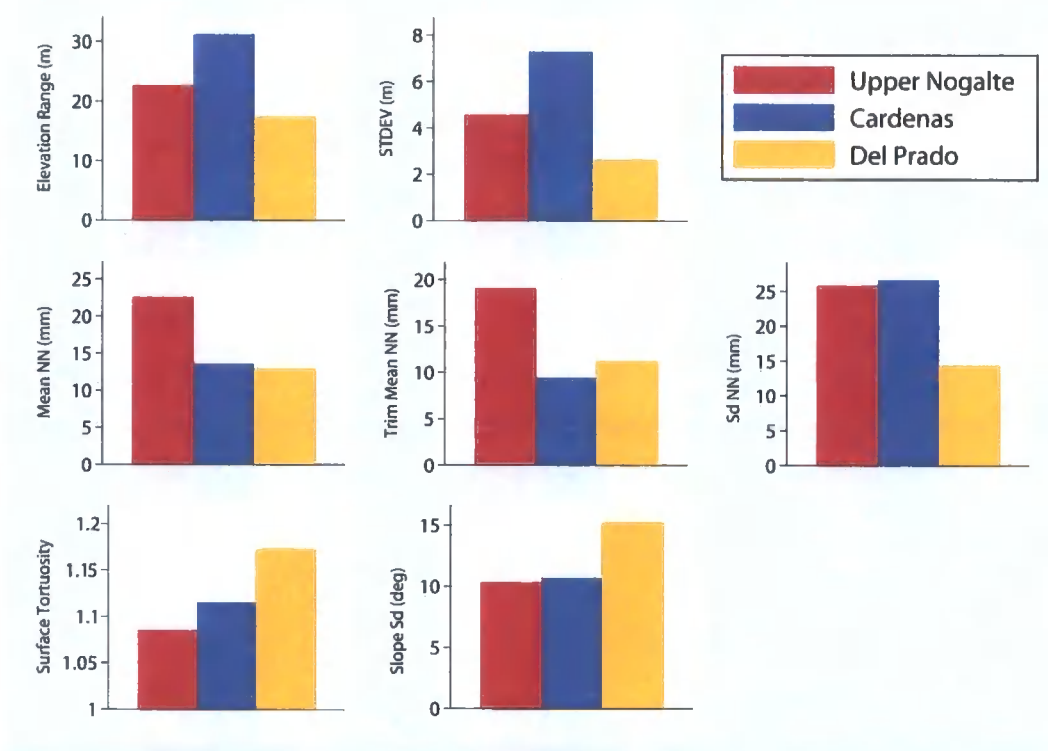

Figure 4.32. Surface-based roughness measures calculated for each hillslope.

4.7 Conclusion

This chapter applied a wide range of measures of surface roughness to soil surfaces both at the plot and hillslope scale. Each measure represents a different aspect of the surface under consideration, and so each varies uniquely between plot-type and site. Several measures (particularly the root of semi-variance at 0.5 m, surface fractal dimension and surface tortuosity) vary considerably and consistently between each plot-type. Other measures of surface roughness may be related to the hydrological characteristics of these surfaces. A measure of roughness may capture the morphological signal of a particular surface processes. To determine which measures reflect which process, it is first necessary to examine the variation of surface hydrological features between each plot and site. This is the subject of chapter 5.

Chapter 5 Hydrological Analysis

5.1 Introduction

While chapter 4 discussed the physical form of the surfaces generated by the terrestrial laser scanner, how this spatial variation in roughness elements affects hydrological processes was not considered. This chapter presents a hydrological analysis of each plot and hillslope. The calculation of depression storage is discussed in section 5.2, while section 5.3 examines the flow patterns of each plot. Section 5.4 looks at how the contributing area varies within and between each plot. The results of the minidisk infiltration tests are presented in section 5.5 and the findings of hillslope runoff and sediment transport monitoring sites are discussed in section 5.6. Finally, section 5.7 investigates how each of these aspects of catchment analysis performs when applied to the hillslope-scale surfaces.

5.2 Maximum Depression Storage

The maximum depression storage MDS of each plot was calculated using the PCRaster GIS software (Van Deursen & Wesseling, 1992), which created raster-based DEMs. However, the rough nature of the surfaces studied, combined with the non-vertical viewpoint of the laser scanner, meant that when the surfaces were viewed from above, increments between consecutive data points were irregular. In some cases, the interval between points was greater than 5 mm. As PCRaster requires regular square cells, when converting the point clouds into a PCRaster map at 5 mm resolution, a number of grid cells contained missing values. This had the effect of interfering with the simulated flow routing. Additionally, the missing values present within the surface generated extra 'pit cells' on the surface (Figure 5.1), thereby influencing the calculation of depression storage.

The hydrological features of a surface are dependent upon the DEM spatial resolution (Abedini *et al.*, in press). Each plot in Figure 5.1 demonstrates a considerable decrease in the pit area from between 15 and 27 % at 0.005 m resolution to a much more stable value beyond 0.02 m cell size. Finer grid resolutions are defining extremely minor surface irregularities as pits which, upon inspection, seemed unlikely to contribute significant depressional storage capacity. Based on this and the identification of missing values upon viewing the PCRaster maps, a cell size of 0.025 m × 0.025 m was selected

as the minimum cell size where all values contained within the surfaces were present. This study provides a comparative analysis of several surfaces; as the resolution remains approximately constant between surfaces, this reduces the problem of the scale dependency of hydrological characteristics. It should be noted, however, that effects of scale dependency, attributable due to the differing surface variability between plots, will remain.

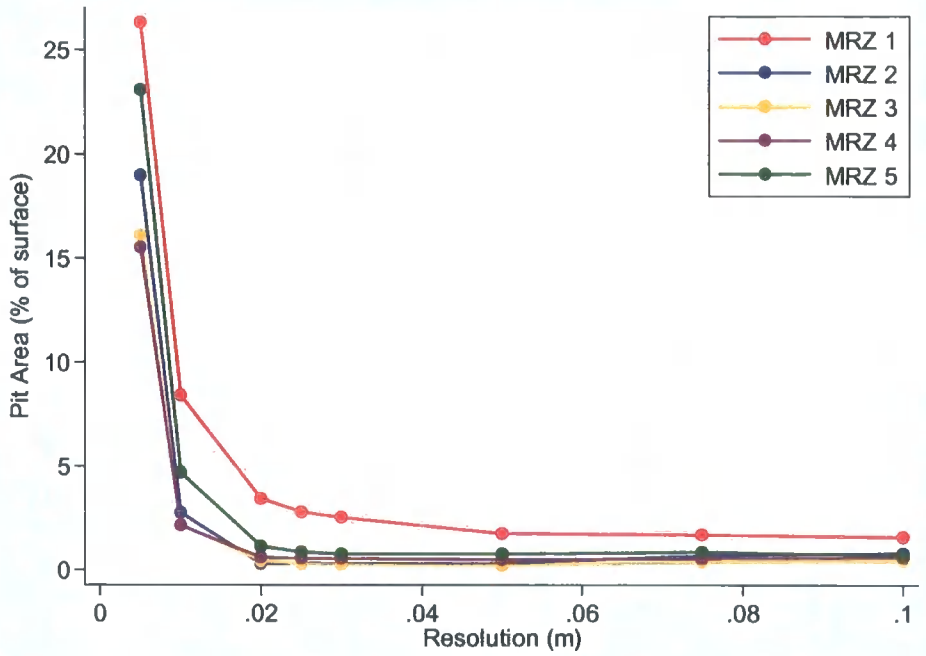

Figure 5.1. The effect of decreasing the resolution of the PCRaster maps on the percentage of the plot area identified as a 'pit cell' for each MRZ at the Upper Nogalte hillslope.

It should be noted, however, that the gullied nature of MRZ 5 at both the Upper Nogalte and Del Prado sites meant that, despite the combination of two scans from different directions, an area in the bottom of the gully was not scanned to sufficient resolution, and a gap is evident in the PCRaster maps of these plots.

The area of the plot surfaces containing 'pit cells' (graphed in Figure 4.28 and Figure 5.1) cannot be directly equated with depression storage, as this says nothing about the size of the pits involved in water storage. A 'pit cell' is defined simply as a cell which has an elevation lower than each of its eight neighbouring cells. Depressions encompass much more than simply the lowest point in the locality. Figure 5.2 explains some useful terms when considering depression storage.

Each depression contains both a pit cell and an outflow cell. Water draining the pit catchment collects in the depression, building up until the local water surface reaches outflow level. After this point (assuming zero infiltration) any further water added into the depression will be matched by an identical amount of water leaving the depression through the outflow cell. Therefore, the core volume now represents MDS. PCRaster was able to fill all the depressions found on a map until they reach this 'pour point', and re-calculate the elevation of the surface (including the stored water) (Figure 5.3). Through subtracting the original surface map from this new map, the MDS of the surface can be estimated. Additionally, a map is created displaying the spatial distribution of these depressions within each plot surface (Figure 5.4).

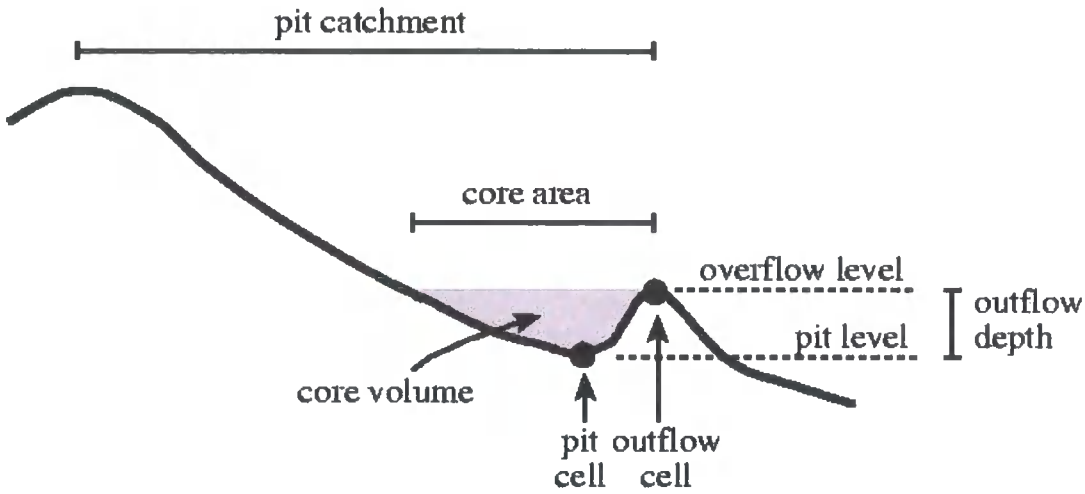

Figure 5.2. Definition of important terms used for the calculation of surface depression storage (from Van Deursen & Wesseling, 1992).

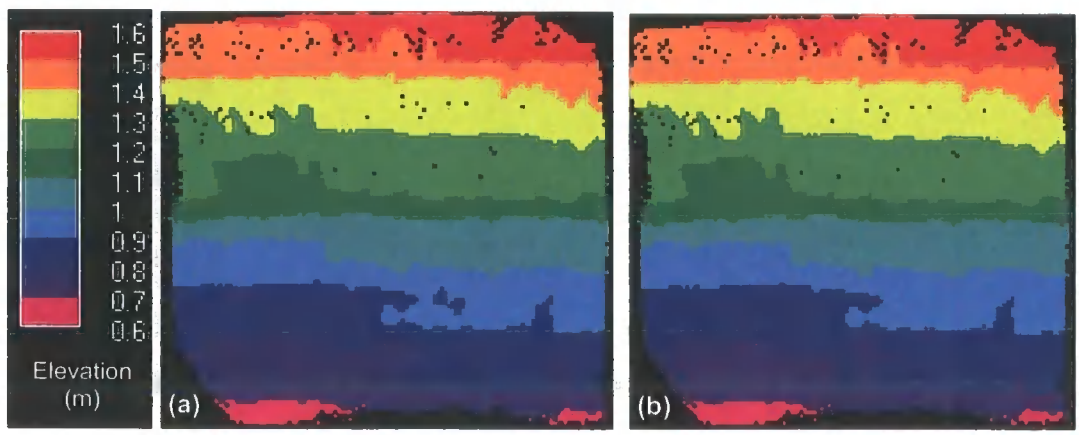

Figure 5.3. PCRaster maps of the Upper Nogalte Ploughed plot: (a) original topography; (b) all depressions have been filled to outflow point. Key is elevation (in metres). Plot is approximately 3 m × 3 m.

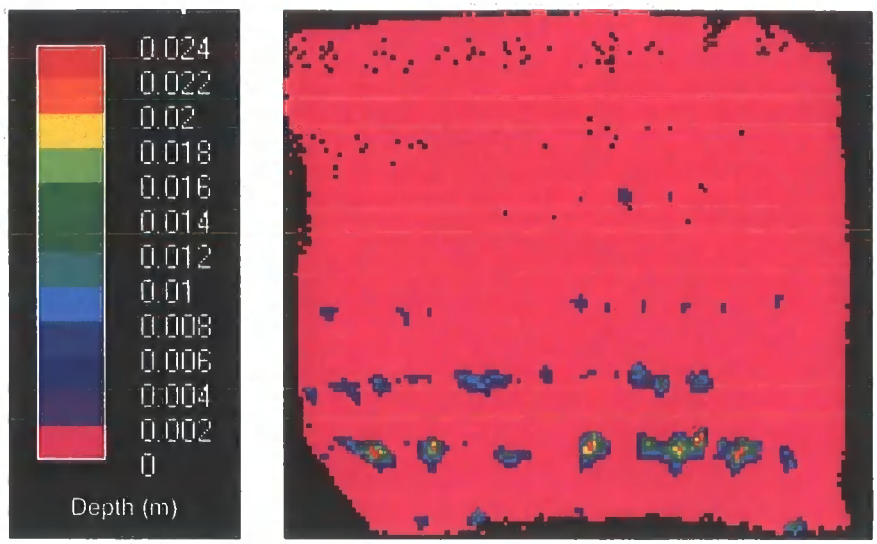

Figure 5.4. PCRaster map of depression storage for the Upper Nogalte Ploughed plot. Key is water depth (in metres); plot is approximately 3 m × 3 m.

The MDS values calculated using this technique possibly represent a slight underestimate as open boundaries allowed water to drain freely off the edge of the surface. However, given the reasonably large area under study (~9 m^2 for all plots) compared with the area of those watersheds touching the open boundaries, this would have only a small effect on the results. Additionally, the relatively large cell size necessary for the creation of these maps (25 mm × 25 mm) will tend to underestimate the total number of depressions found on the surface, and therefore MDS. Nevertheless, this cell size remains considerably smaller than that used in other studies of depression storage (Kamphorst *et al.*, 2000). The MDS estimates from each plot surface can be found in Table 5.1 and are displayed in Figure 5.5.

For each MRZ, the MDS at the Del Prado site (in the Torrealvilla catchment) was the highest. The Upper Nogalte and Cardenas sites have very similar MDS for each plot, which was no more than 30 % of the Del Prado value. MRZ 1 generally records a high value of MDS which decreases to either MRZ 2 or 3, after which there is a steady rise in MDS with distance downslope. The effect of ploughing at the Upper Nogalte site significantly increased the MDS of the surface, but this was not the case at the Cardenas site, where negligible MDS is recorded (as is also the case for the MRZ 2 of both Upper Nogalte and Cardenas).

Site	*Plot*	*MDS (mm)*	*Flat Surface MDS (mm)*
Upper Nogalte	MRZ 1	0.0703	0.0537
	MRZ 2	0.0002	0.5012
	MRZ 3	0.0042	0.1961
	MRZ 4	0.0241	0.1609
	MRZ 5	0.0556	0.0446
	Ploughed	0.3459	1.8731
Cardenas	MRZ 1	0.0623	0.0057
	MRZ 2	0.0010	0.2953
	MRZ 3	0.0158	0.7883
	MRZ 4	0.0186	5.6914
	Ploughed	0.0006	0.2276
Del Prado	MRZ 1	0.2061	0.2302
	MRZ 2	0.1641	0.5803
	MRZ 3	0.0503	0.5234
	MRZ 4	0.1856	1.2441
	MRZ 5	0.5436	0.1245

Table 5.1. Maximum Depression Storage values (mm) for each plot surface, and for each plot with general slope removed.

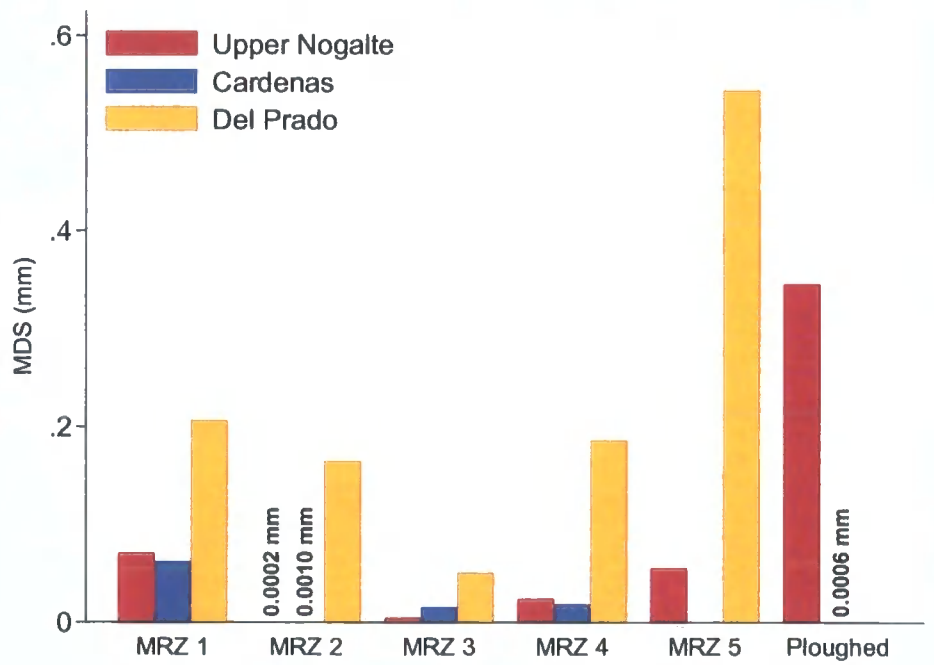

Figure 5.5. Maximum depression storage (in mm) for each plot and site.

The size of the depressions contributing to the MDS on each surface reveals whether the plot contains one or two large depressions, or many shallow depressions. Figure 5.6 shows how the volume of water stored (in mm^3) changes with water depth (in mm) for each plot and site. Although straight lines have been fitted to each plot (for consistency), it should be noted that some plots display non-linear trends.

Whereas each Upper Nogalte and Del Prado plot demonstrated an inverse relationship between depth of water and volume of water stored at that depth, the plots from the Cardenas hillslope (excluding MRZs 1 and 3) demonstrate an increasing dominance of water stored in large depressions. These were the same surfaces that held relatively little water as depressional storage. Del Prado MRZ 5 (and to some extent MRZ 2) however, showed a wide distribution of depths at which water was stored. Figure 5.5 shows that this plot had the highest MDS of all the plots investigated.

The estimates of MDS above are considerably lower than values observed in the literature (which can reach 13 mm). One reason for this is that the topography of the surfaces is made up of two distinct roughness elements: the microtopography of the soil surface on one hand, and the larger-scale roughness of the general slope on the other. Although this combination determines the actual depression storage in the field (given in Table 5.1 above), most studies calculating MDS first remove the general slope. When considering the total dataset, no relationship between MDS and general slope can be seen (Figure 5.7).

An analysis of how MDS changes with general slope within each plot type would be much more useful. Such an analysis enables the microtopographic contribution to depression storage to be kept reasonably constant, and the effect of slope on MDS to be isolated. However, the data gathered from this study are insufficient to provide a detailed analysis of this effect, as each 'morphological runoff zone' is only represented by three (or even two) plots in areas exhibiting differing hydrological response. Figure 5.8 displays the outcome of such an analysis on this extremely limited dataset.

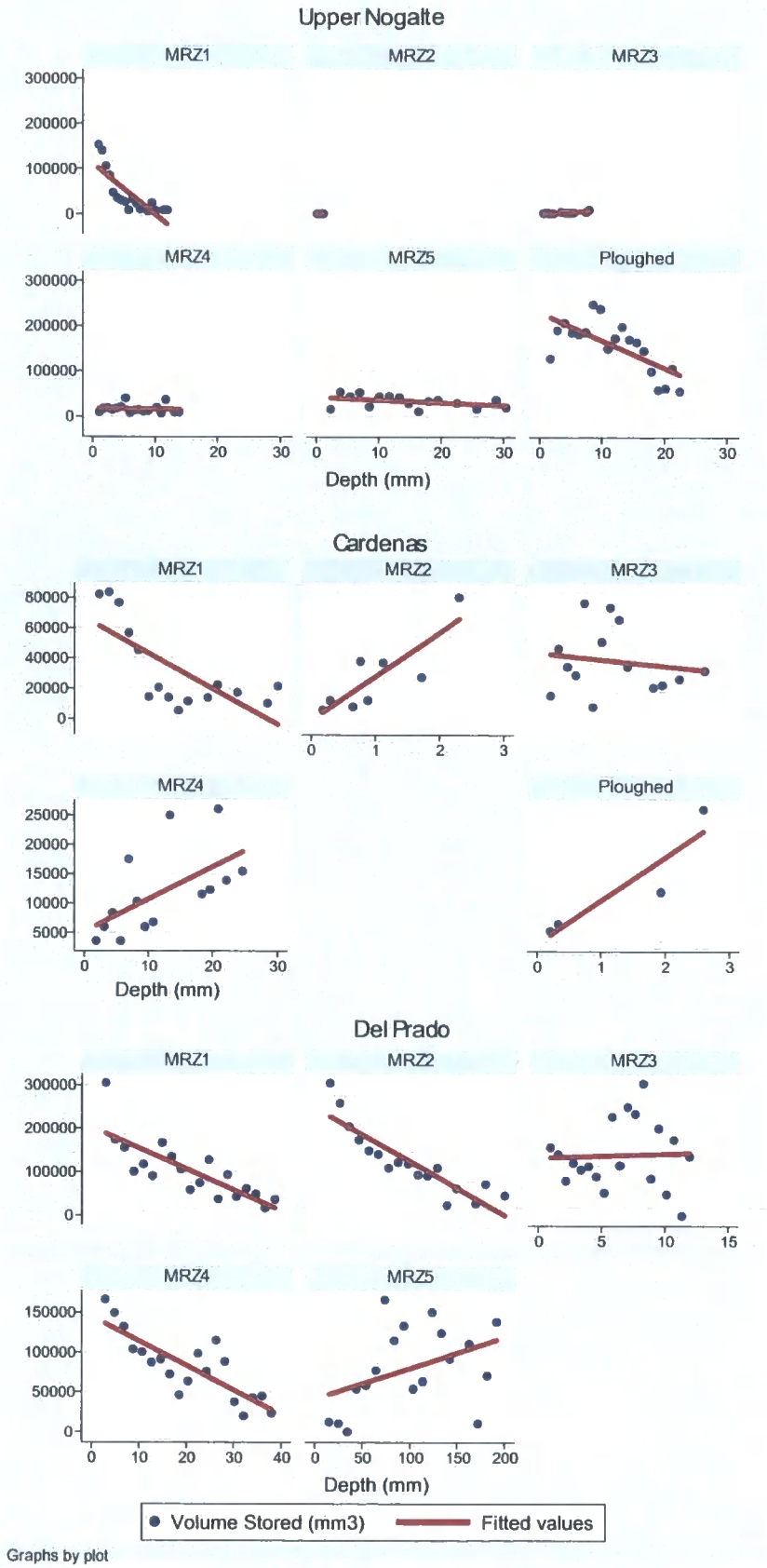

Figure 5.6. The relationship between volume of water stored (mm^3) and depth of water (mm) for each plot and site.

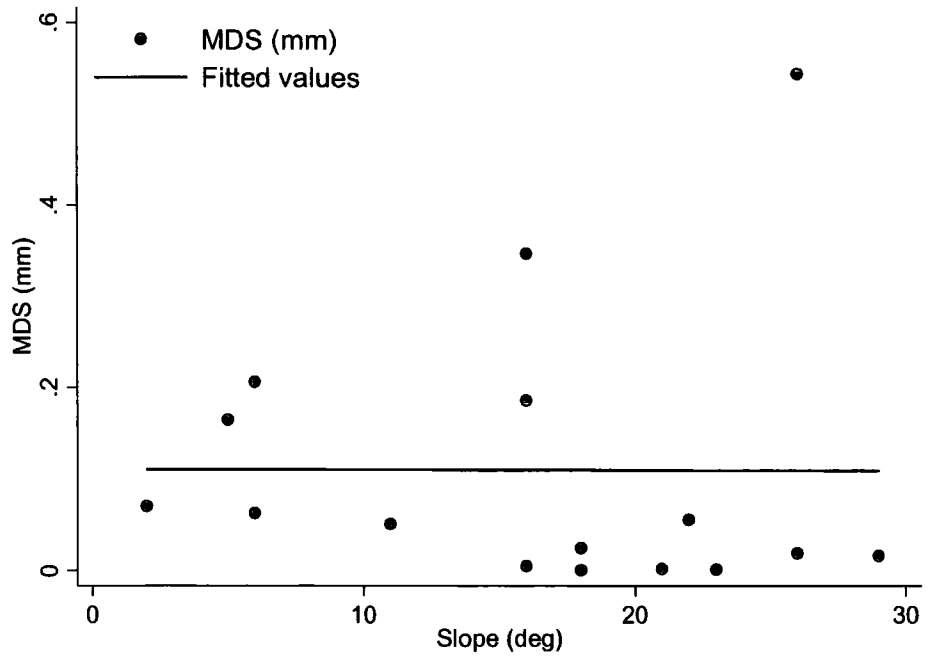

Figure 5.7. The relationship between MDS (in mm) and general slope (degrees) for the entire dataset.

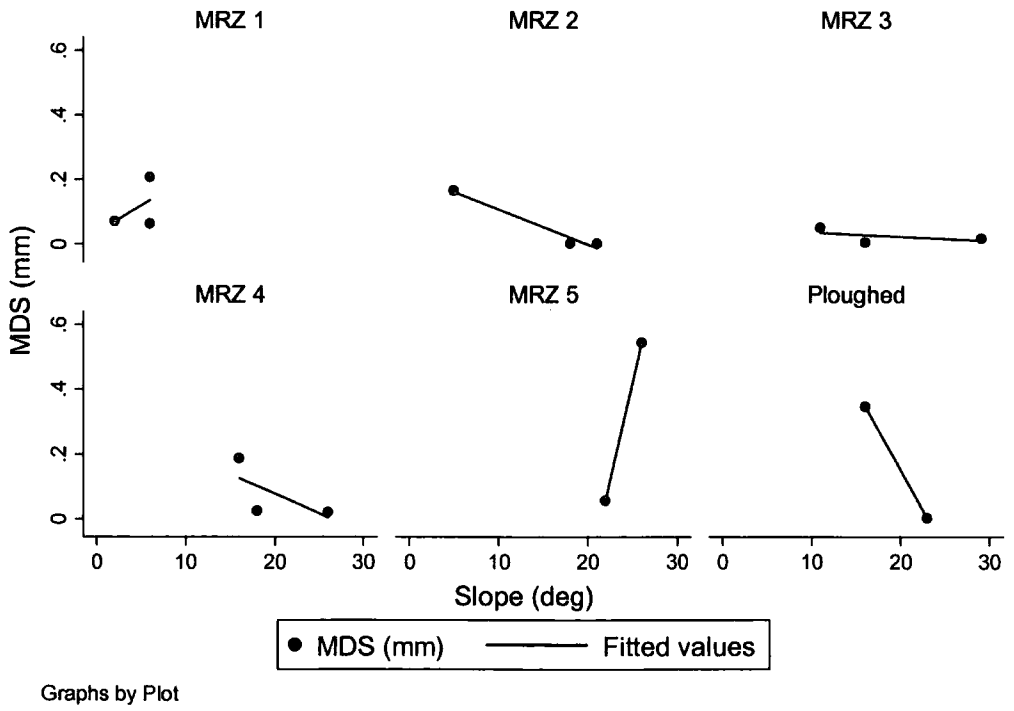

Figure 5.8. The relationships between MDS (mm) and general slope (degrees) for each plot type.

Although MRZ 1 displays a slight increase of MDS with slope, the maximum slope found in this category is only 6°. MRZs 2-4 all demonstrate a decrease of MDS with general slope. Only two plots are represented in both the MRZ 5 and Ploughed categories, and both show a strong variation in estimated MDS between these two points, with MRZ 5 sharply increasing with slope, and Ploughed MDS sharply decreasing with slope.

To provide MDS estimates comparable to those found in the literature, the general slope of each plot was removed using the Archaeoptics DEMON software package. PCRaster maps were then created for each flattened plot. Such detrending is, however, extremely contentious when calculating depression storage. Figure 5.9 displays the MDS estimates thus obtained for each surface.

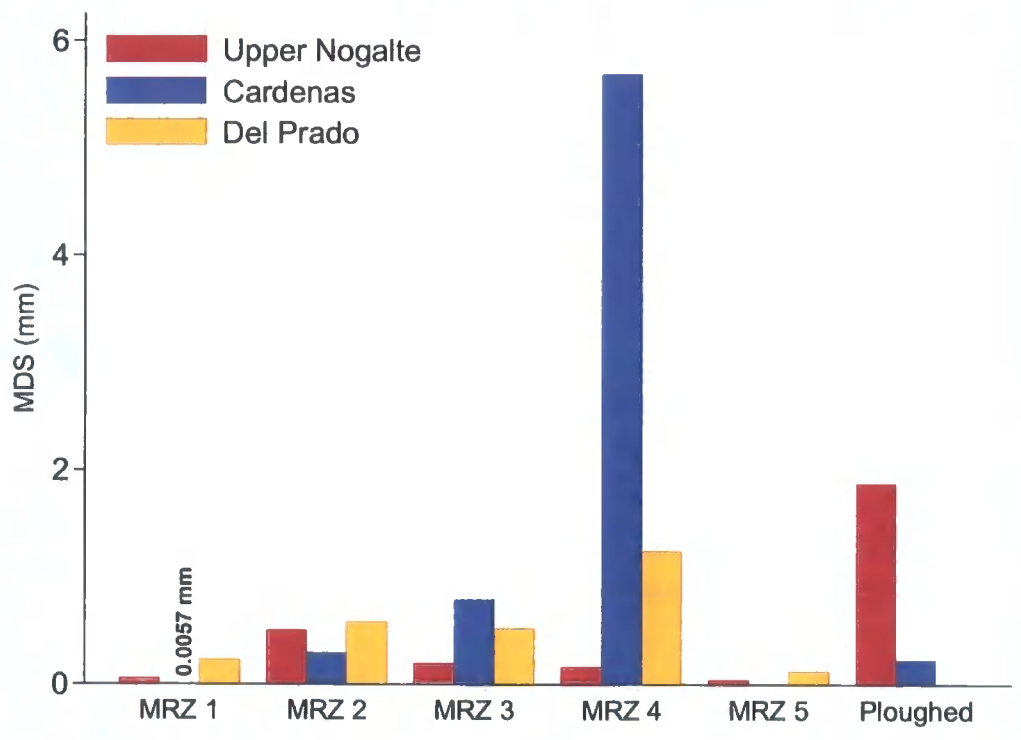

Figure 5.9. Maximum depression storage (in mm) for each plot after the general slope was removed.

The Cardenas site demonstrates a gradual increase in MDS due to microtopography with increasing distance downslope; the ploughed plot here still experiences a relatively

low depth of MDS (approximately equivalent to that seen at MRZ 2). The downslope pattern to MRZ 4 is repeated for the Del Prado site (albeit with a minor fluctuation around MRZ 2), while MDS at Upper Nogalte increases to a maximum at MRZ 2 (formerly a negligible depth) and decreases downslope. The ploughed plot at this site still holds a much greater depth of surface water than the undisturbed plots.

While some plots have seen an increase in MDS as a result of the removal of the general slope, others have seen a slight decrease in MDS. Figure 5.10 shows the difference in MDS that has occurred as a result of removing the general slope.

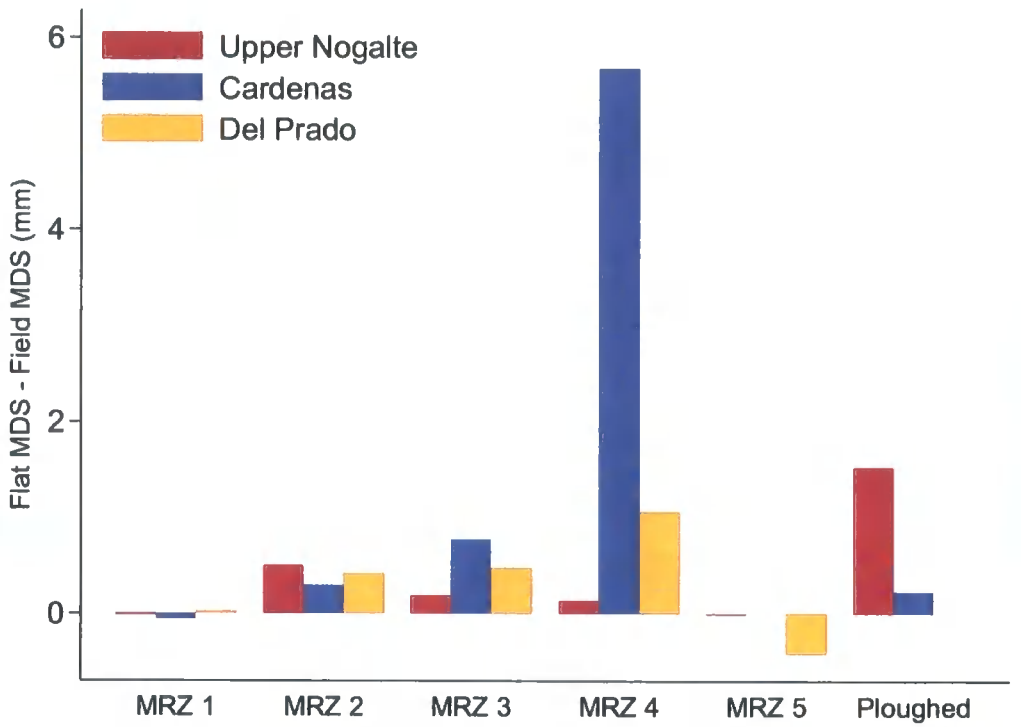

Figure 5.10. The effect of removing the general plot slope on MDS (in mm). Positive values represent an increase in MDS with detrending of elevation measurements.

The first point of interest here is that MRZs 1 and 5 have experienced a decrease in MDS as a result of removing the general slope for each plot. Notably, these two MRZs were the only plot categories to display a positive relationship between MDS and slope in Figure 5.8. The second significant detail of Figure 5.10 is that MRZ 4 of the Cardenas site (Figure 5.11a) has experienced a remarkable increase in MDS. In order to explain this increase, it is necessary to analyse the original surface of Cardenas MRZ 4

(Figure 5.11b) and the location of the depressions contributing to the detrended value of MDS (Figure 5.11c).

Figure 5.11 clearly demonstrates that the high values of MDS for this plot are a result of water being ponded in rills after the general slope has been removed. Such depression storage is unlikely to occur in the field and brings into question the conventional practice of removing the general slope from plots before the calculation of MDS.

Each surface will respond individually to the method of surface rotation and depression calculation. Depressions observed after the slope has been removed, do not necessarily act as depressions in the field. In the case of the Cardenas MRZ 4 plot, they form as a result of downslope profile convexities.

Figure 5.12 displays a downslope profile taken from this surface, and demonstrates the effect of removing the general slope of MDS. The effect was particularly noticeable for this plot, as distinct cross-slope roughness elements are present, concentrating flow into rills, and providing a high 'rim' for the depression to fill to. Therefore, standard methods of calculating depression storage do not necessarily accurately represent natural conditions. Rotation of surfaces is an unacceptable technique for the measurement of MDS on natural surfaces.

5.3 Flow Directions

PCRaster also enables the flow direction for each cell to be calculated and mapped. As the point cloud data of each plot contain microtopographic detail, it is possible to compare the influence of surface roughness on the flow patterns at each MRZ. A map of flow directions for each plot from the Upper Nogalte hillslope is displayed in Figure 5.13. Each map represents a 2 m × 2 m section of the plot (allowing the flow lines to be seen more clearly) and each cell could drain into any one of its eight neighbouring cells.

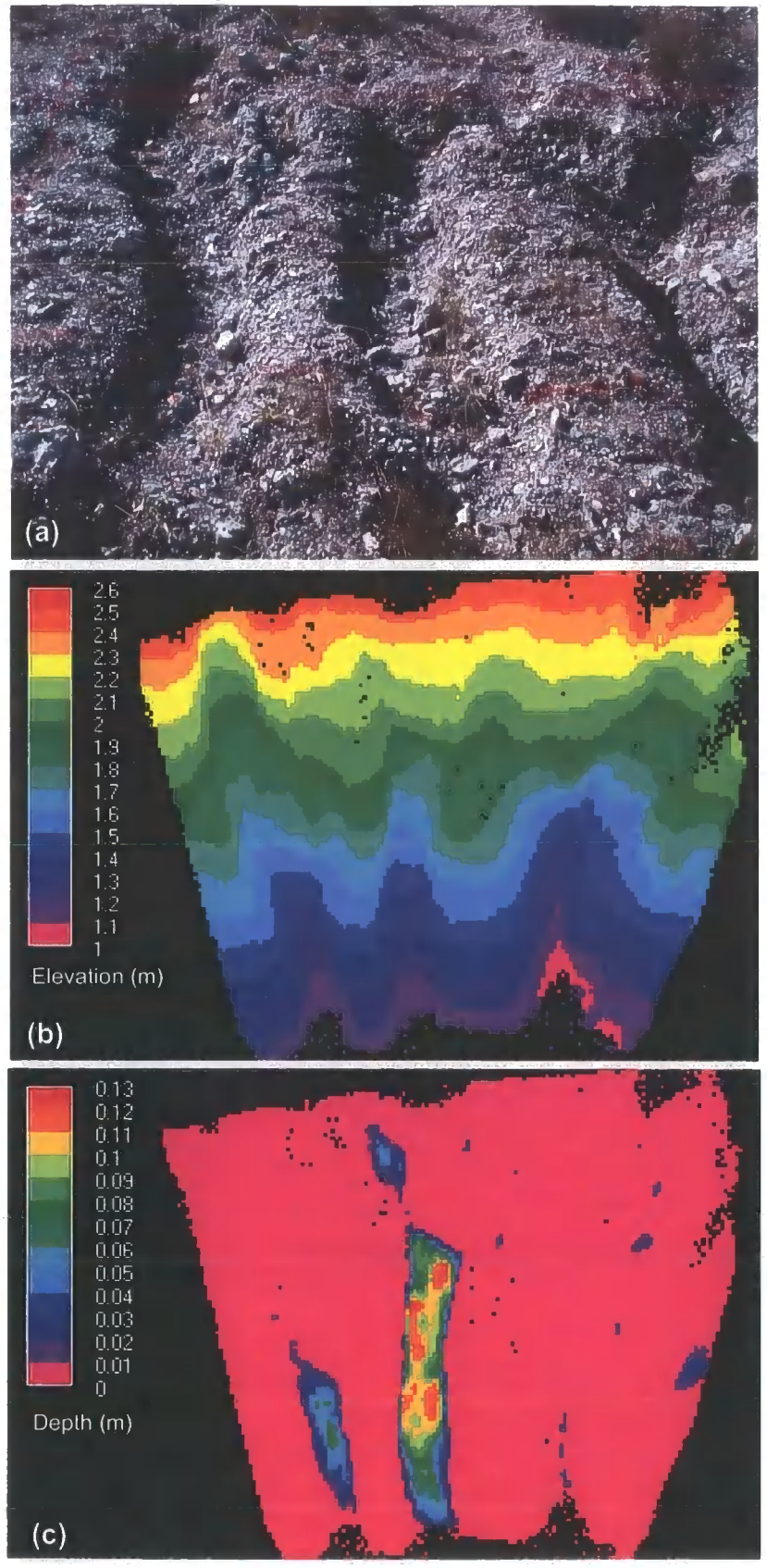

Figure 5.11. The location of the depressions for the detrended Cardenas MRZ 4 plot (a) with respect to the original surface: (b) the original surface (key is elevation in metres); (c) location of depressions on the detrended surface (key is depth in metres).

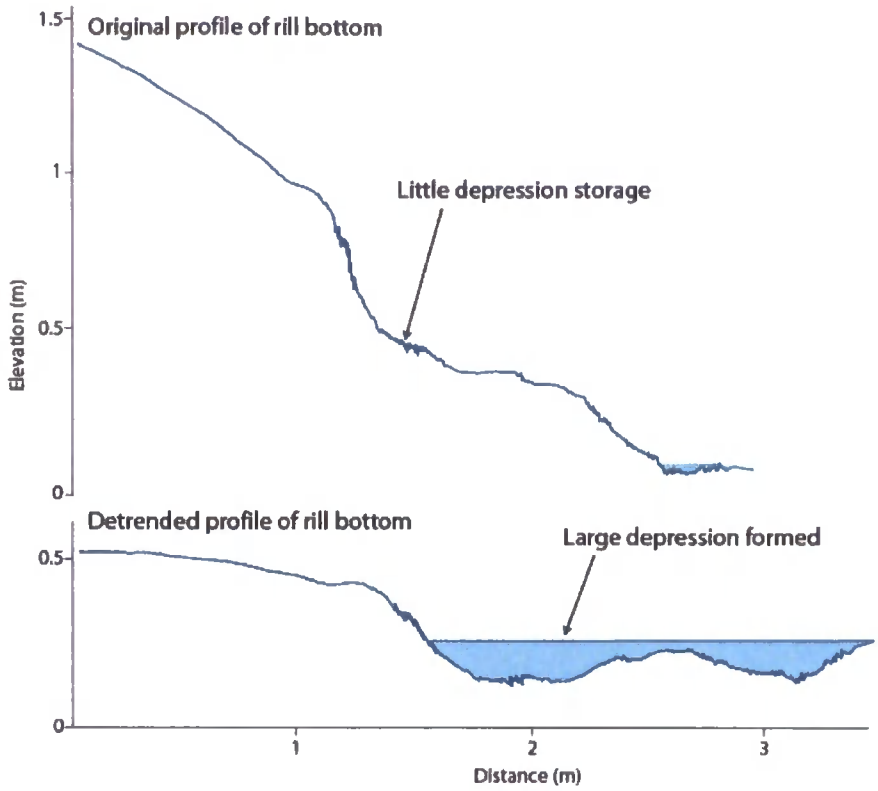

Figure 5.12. The creation of artificial depressions through removing general slope. Transect taken along a rill bottom on the Cardenas MRZ 4 plot displayed in Figure 5.11.

Moving from the map of MRZ 1 to MRZ 5, a greater proportion of the cells drain against the general slope; flowing across slope into flow concentrations. Figure 5.13a (MRZ 1) shows pits (small squares) littered across the map, each of which has a separate contributing area which may be either small or reasonably large. Figure 5.13b (MRZ 2) reveals that the slope component dominates this plot. Some flow divergence around microtopographic obstacles is detectable. Figure 5.13c (MRZ 3) exhibits a greater level of flow concentration into a incipient rill running through the centre of the image. It is difficult to identify the rill running through Figure 5.13d (MRZ 4), but towards the top of the map, a large area flows into a reasonably wide channel, within which small areas of pits exist. The variable point density experienced at the gullied sites manifests itself as a gap in the map of Figure 5.13e (MRZ 5). This area represents the gully bottom; most of the upslope cells direct water towards this point. Finally, ploughing furrows are obvious in Figure 5.13f with a line of pits visible across the map in the furrow bottoms (see Figure 5.4).

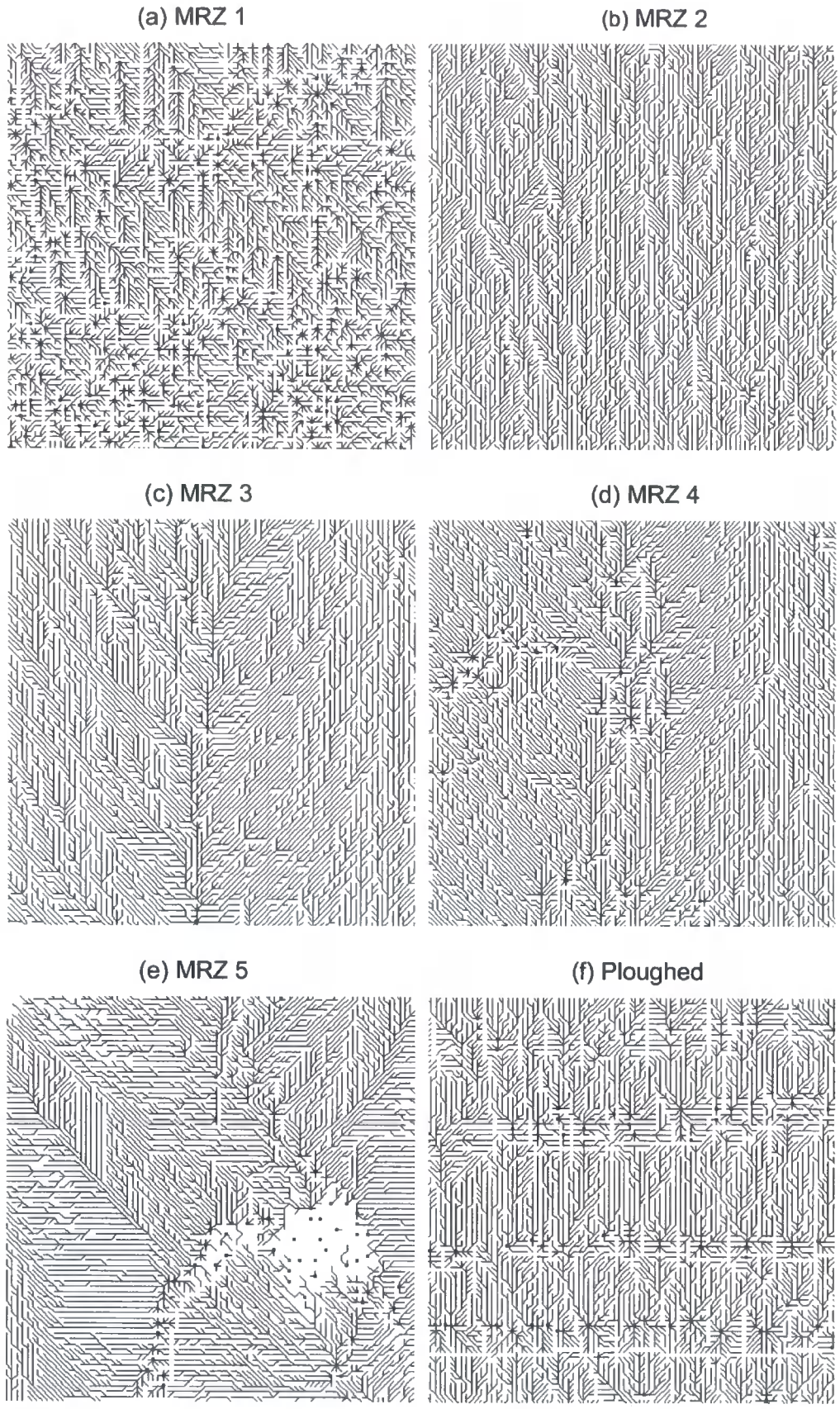

Figure 5.13. Flow direction maps for each plot of the Upper Nogalte hillslope. Each map represents a 2 m × 2 m section of the plot.

From these maps, the percentages of each plot displaying each flow direction could be assessed and compared. Each cell possesses one of nine possible flow directions; these can be represented as numbers 1-9 in the manner of a standard keyboard (Figure 5.14). A cell labelled '5' represents a cell which has a lower elevation than each of the eight surrounding cells (defined as a pit).

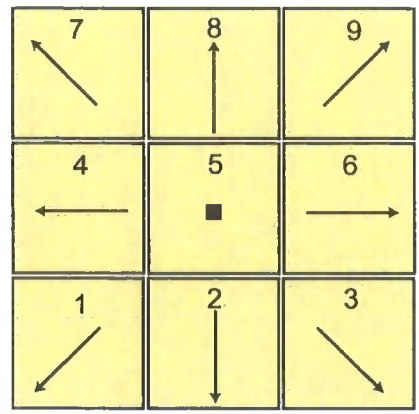

Figure 5.14. The numerical identifiers of the possible flow directions of each cell.

Figure 5.15 displays the variation of the percentages of flow directions for each surface in the form of a tableplot (Cox, 2004). It is clear that each MRZ 1 plot exhibits a more even spread across the flow directions. As each of these plots was located at the drainage divides of the hillslopes, they experienced the lowest general slope. Each of the remaining plots are heavily dominated by the downslope flow directions (1-3) as would be expected. The flow directions perpendicular to the general slope (4 and 6) are generally more important as channelisation occurs through MRZs 3-5.

These flow directions for each plot are also useful for comparing the percentage of each surface which is covered by a 'pit' (*%pit*). Figure 5.16 shows that in all cases, the Del Prado site boasts the highest percentage of pits. MRZ 1 displays the highest values of *%pit* for each hillslope. At the Rambla Nogalte sites (Upper Nogalte and Cardenas) MRZ 2 has the lowest *%pit*, while for Del Prado there is a high percentage of pits at this plot-type. Beyond MRZ 2 the percentage of each surface designated as a pit increases downslope in a regular fashion. The two ploughed plots show contrasting features. From observation, the furrows at Upper Nogalte appeared larger and fresher, whereas at the Cardenas site they were much less prominent and possibly a few years old; this is reflected in the *%pit* measurements below and also in the MDS results (Figure 5.5).

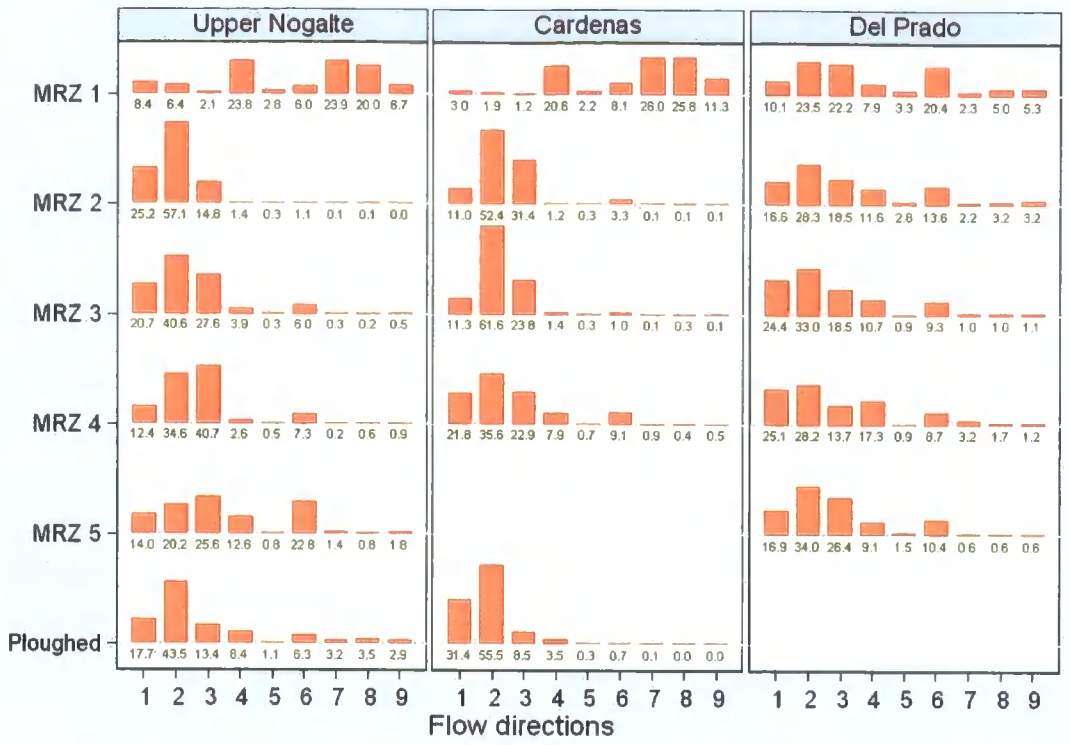

Figure 5.15. Variation of the percentages of flow directions for each plot.

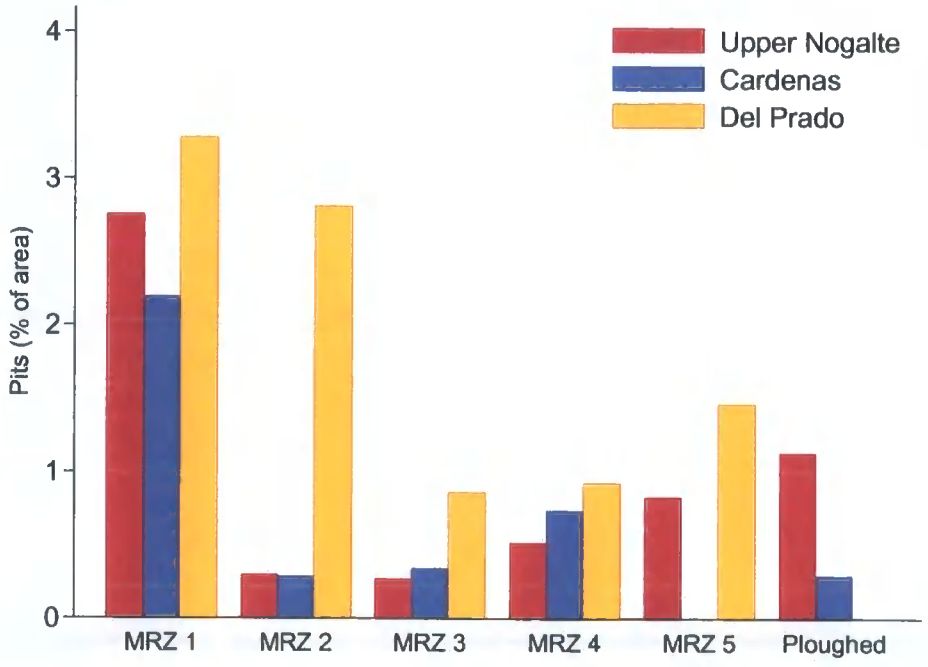

Figure 5.16. Percentage of each surface covered by a 'pit' *(%pit)* for each plot and site.

Figure 5.17 examines the relationship between the percentage of each surface over which water runs in a downslope direction (directions 1-3) and the general plot slope for each MRZ. The fitted line reflects a fairly strong relationship (R^2 = 0.524), but other factors influence this. The MRZ 5 surfaces tend to have fewer cells directing water in a downslope direction than expected from the linear regression, whereas MRZ 2 and ploughed plots have more downslope-draining cells than would be predicted from this relationship.

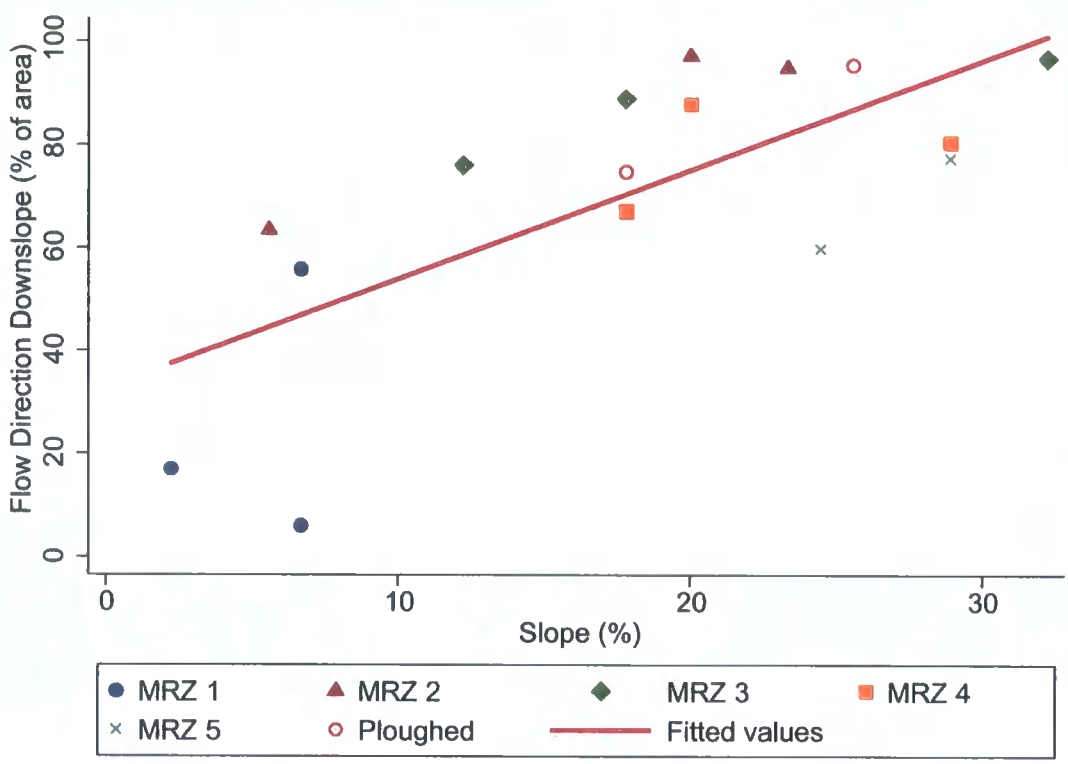

Figure 5.18. The relationship between general plot slope (%) and the percentage of the plot area that directs overland flow in a downslope direction (1-3 of Figure 5.14) for each plot-type.

As the slope of the plots has been shown to influence the flow direction, Figures 5.19a-f display the flow directions for each of the plots of the Upper Nogalte site with the general slope removed. The flow routing in these maps is simply a result of the microtopography of the surfaces. In comparison with the maps of Figure 5.13, these plots display a wider range of flow directions.

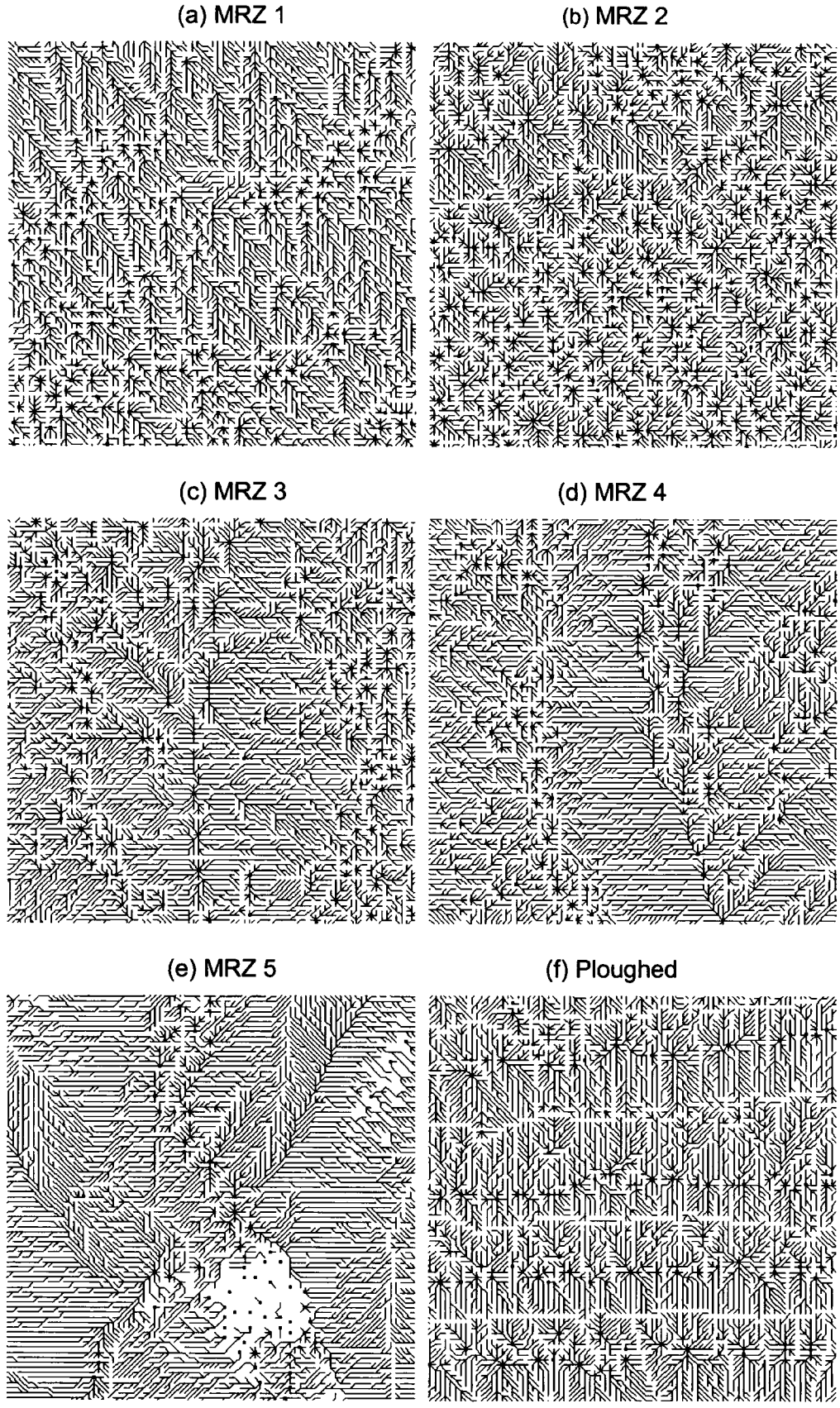

Figure 5.19. Flat flow direction maps for each plot of the Upper Nogalte hillslope. The general slope has been removed from the plots. Each map represents a 2 m × 2 m section of the plot.

Also, pit cells are more numerous and can be seen as linear features running from the top to the bottom of the maps in Figures 5.19c and d. These represent flow concentrations in the cross-slope direction. The small catchment areas of the individual furrows can be identified in Figure 5.19f where rows of pit cells run across the plot, representing the furrow bottoms.

Figure 5.20 displays the variation of the percentages of flow directions for each of these detrended plots. The downslope and upslope flow directions (2 and 8) along with the pit cells (5) have been removed for clarity. Moving downslope from MRZ 1 to MRZ 5 the contribution of the cross-slope flow directions increases steadily, demonstrating the gradual incision of channels directing flow across the slope. As these features are removed through ploughing, the ploughed plots show lower percentages of flow in the cross-slope direction.

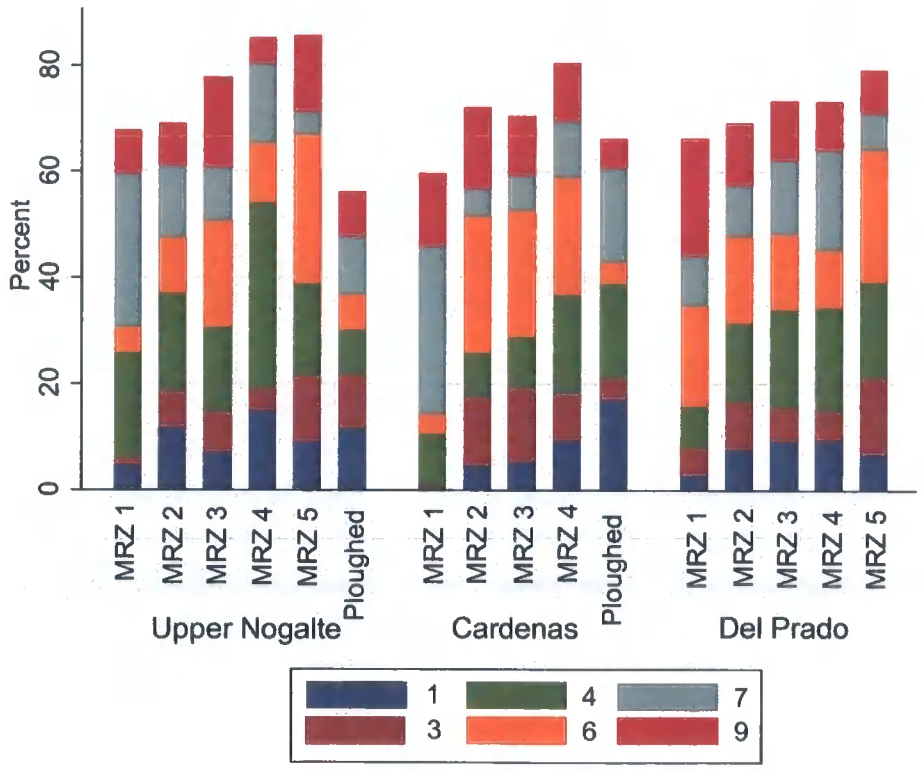

Figure 5.20. Variation of the percentages of flow directions for each flat plot.

The percentage of the plots containing pits increased with the removal of the general slope. However, this increase in was uneven across each plot, confirming the generation

of artificial pits as a result of rotating the plot surfaces to remove the general slope trend (as discussed in section 5.2).

5.4 Upslope Contributing Area & Runoff Routing

Figure 5.20 suggests that the surface roughness characteristics of each MRZ concentrate overland flow to different degrees. Therefore comparison of such flow concentration is essential to assess the connectivity of hillslopes. Maps displaying the upslope area of each cell were produced for each plot. All depressions were first filled to prevent interference with the upslope areas: a practical necessity to allow the routing algorithm to work. While each plot is only a small part of the upslope area of the hillslope (the plot boundaries were not chosen on the basis of any catchment drainage divides), such maps provide an appreciation of the degree of flow concentration experienced within each plot which can be related to the connectivity of the hillslopes (although more specifically, this relates to the connectivity once all surface depressions have been filled).

As the upslope contributing area increases, the area of each map exhibiting that upslope area decreases. Therefore, many cells will drain a small area, while only a few cells will drain larger areas (however, edge effects will artificially lower the amount of larger drainage areas – this effect will be similar for each plot). This is demonstrated in Figure 5.21 for each plot of the Upper Nogalte site. Both the upslope area and map area are expressed as a percentage of the total map area, while the upslope area has also been log-transformed. Points are taken at the midpoint of a regular increase in upslope area. These results will also be extremely sensitive to the type of flow routing algorithm used: only a basic 'd8' algorithm has been applied here.

A high percentage of the cells of MRZ 1 drain a very small proportion of the map. The curve on Figure 5.21 is very steep, indicating that few cells on the map drain larger areas. MRZ 4 contains the cell which drains the largest area of all the plots, which can be seen on the graph above as the line extends furthest to the right. The pattern identified in Figure 5.21 above becomes clearer when both variables are log transformed.

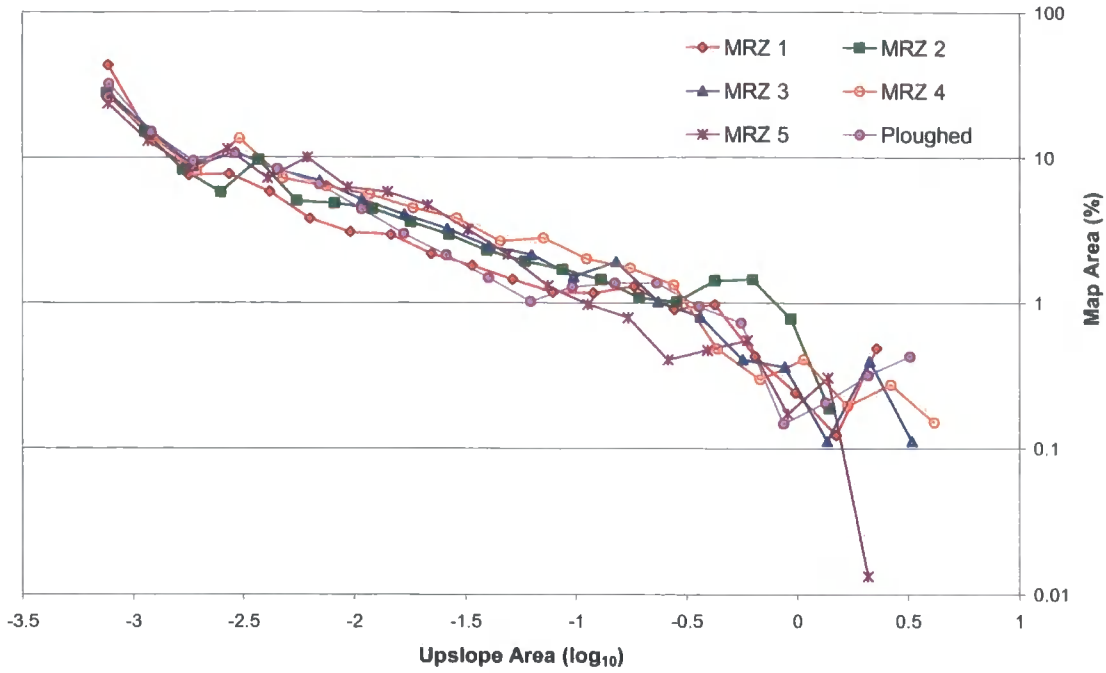

Figure 5.21. The relationship between upslope contributing area (as a log-transformed percentage of total map area) and the area of each map exhibiting that upslope area (expressed as a percentage of total map area) for each plot at the Upper Nogalte site.

Figure 5.22a-c demonstrate that each surface follows a linear relationship between these two variables. Each line falls close to passing through the origin. In this case, a line passing through the origin represents the condition whereby 1 % of the map area has an upslope contributing area of 1 % of the map area. In general, the lower each line is towards the right-hand side of the graphs, the less concentrated flow through the plot becomes. Also, the further each line stretches towards the right-hand side of the graph, the greater the percentage of the plot that drains through one single cell.

To understand these patterns, they should be analysed in conjunction with the spatial distribution of cells within each plot. Figure 5.23 displays maps of upslope contributing area for each plot.

Figure 5.23a shows that at the Upper Nogalte site, few cells on the MRZ 5 plot drain a large percentage of the plot. This may be associated with the difficulties experienced achieving a sufficiently high resolution at the gully bottoms (resulting in the black areas of Figure 5.24), or alternatively may arise as a result of the wide gully bottom dividing the plot drainage between many cells. MRZ 1 shows a similar pattern. Although MRZ 2

has a relatively large percentage of cells draining about 6 % of the plot area, no single cell drains more than 14 % of the plot, as Figure 5.24 shows that many parallel flow lines run down the plot. The MRZ 3 and 4 and plots behave similarly; each has a reasonably large percentage of cells draining large plot areas at each increment, and each has a few cells which drain a large percentage of the plot area (36-37 % of the plots) as all flow is directed into two microtopographic convergences . The furrows of the ploughed plot effectively channel flow over the lowest point in the crest of the furrow (as the depressions have been filled). This acts to concentrate flow in several areas and so this plot behaves similarly to MRZs 3 and 4 (Figure 5.23a), but as all surface depressions have been artificially filled this represents a situation rarely seen in reality.

Compared with Figure 5.23a, the Cardenas plots (in Figure 5.23b) demonstrate slightly shallower lines which do not extend as far to the right of the plot space. Therefore, in general, flow concentration may be taking place to a lesser degree. The differential behaviour of each plot type is also less pronounced. MRZs 2-3 have a greater proportion of cells draining larger areas than both MRZ 1 and the ploughed plot, as flow concentration is more pronounced (Figure 5.24). MRZ 4 shows the dominance of a small number of rills: while the line extends far to the right of the graph (with a maximum upslope area of 28 % of the plot), less cells drain 1-10 % of the plot in comparison to the other surfaces.

At the Del Prado site (Figure 5.23c), moving downslope from MRZ 2-4, greater maximum flow concentration occurs and in general, a higher percentage of cells drain 1-10 % of each plot. However, this does not occur to the same degree as seen at the other sites. The MRZ 5 plot behaves in the same manner as at the Upper Nogalte plot, potentially for the same reasons. Also, the maximum flow concentration at this site is found at MRZ 1 where one particular cell of the plot has a large upslope contributing area (Figure 5.24).

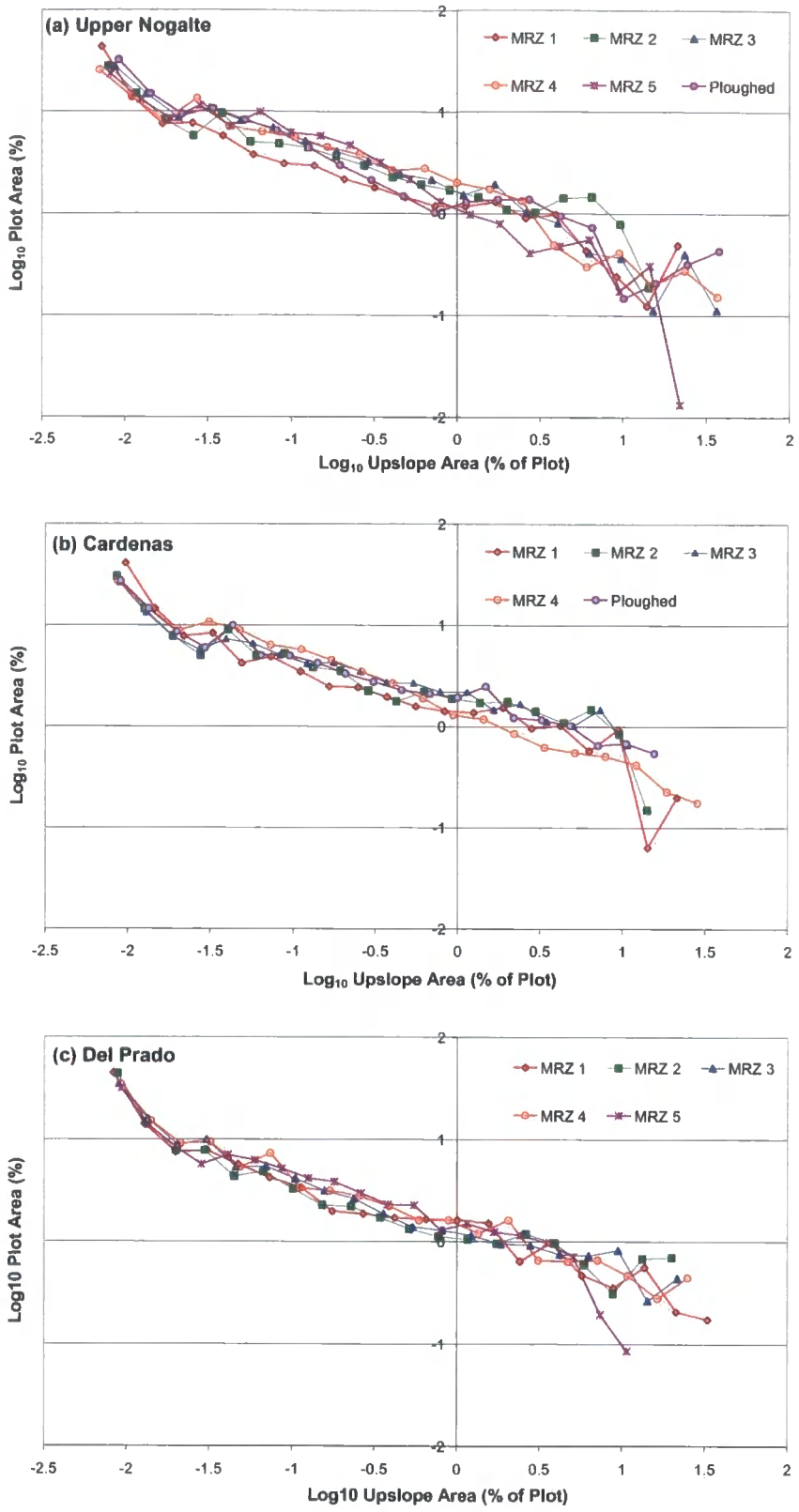

Figure 5.23. The relationships between upslope contributing area and the area of each map exhibiting that upslope area (both expressed as log-transformed percentages of total map area) for each plot at: (a) the Upper Nogalte site; (b) the Cardenas site; and (c) the Del Prado site.

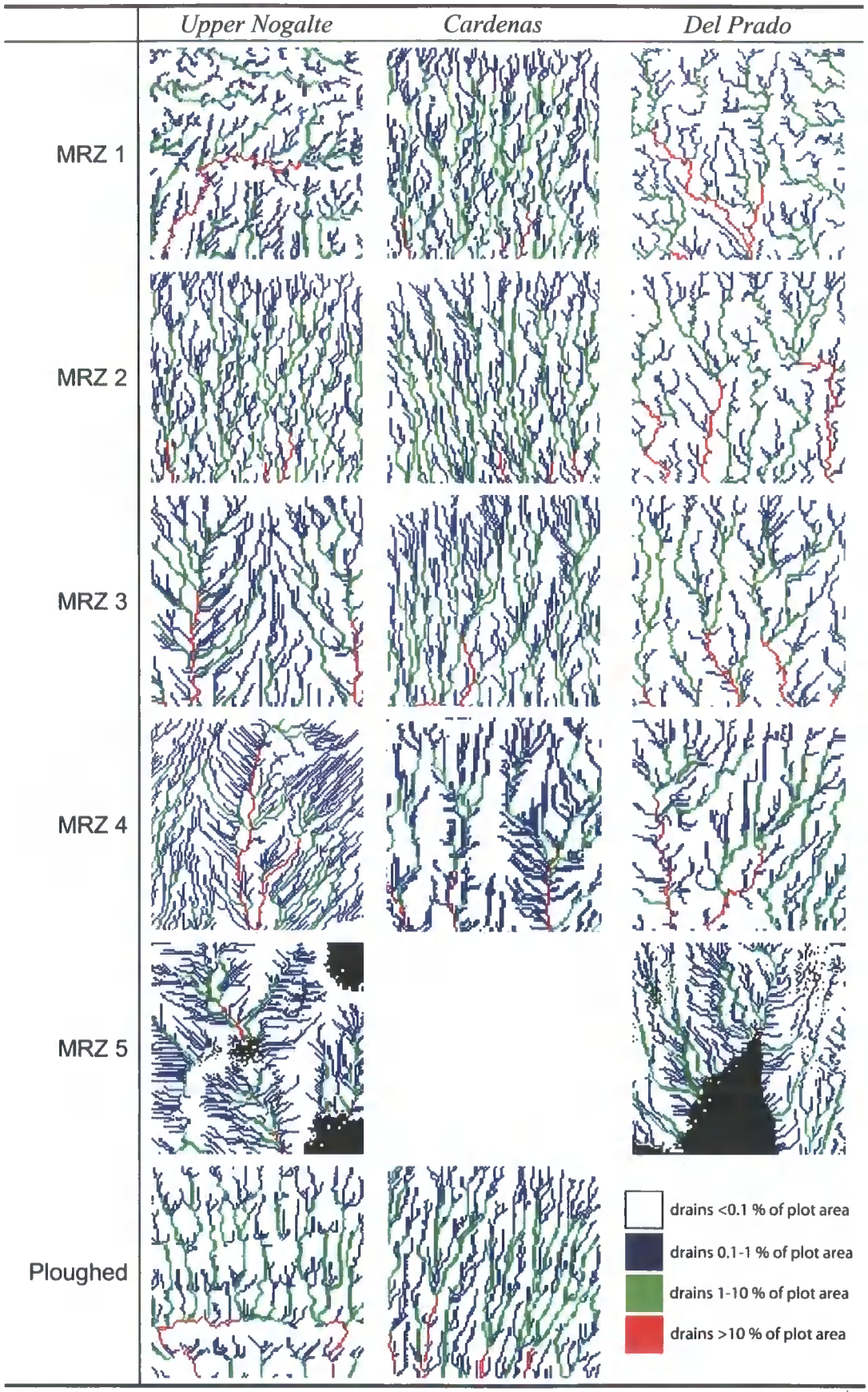

Figure 5.24. Spatial distribution of flow concentrations for each plot.

From Figures 5.23 and 5.24 it is clear that certain properties of the relationship between upslope contributing area and the area of each plot exhibiting that upslope area are useful in the analysis of flow concentration and hence, connectivity of landscapes. Table 5.2 displays values of both the maximum upslope contributing area experienced by any cell in each map (as a percentage of total map area) and the percentage of each map area with an upslope contributing area of greater than 1 % of the total map area. These values are displayed graphically in Figure 5.25 and 5.26.

Site	*Plot*	*Maximum upslope area (% of plot)*	*Percentage of plot area draining >1 % of plot*
Upper Nogalte	MRZ 1	21.2	5.6
	MRZ 2	14.3	7.3
	MRZ 3	36.4	6.6
	MRZ 4	36.8	4.8
	MRZ 5	21.9	3.7
	Ploughed	37.7	6.8
Cardenas	MRZ 1	21.3	6.6
	MRZ 2	14.1	8.4
	MRZ 3	10.7	9.5
	MRZ 4	28.3	4.5
	Ploughed	15.6	7.7
Del Prado	MRZ 1	32.8	6.5
	MRZ 2	19.9	6.4
	MRZ 3	21.6	6.0
	MRZ 4	24.8	5.9
	MRZ 5	10.7	5.8

Table 5.2. Maximum upslope contributing area experienced by any cell in each map (as a percentage of total map area) and the percentage of each map area with an upslope contributing area of greater than 1 % of the total map area, for each plot.

From Figure 5.25 it is clear that each MRZ 1 plot has a relatively large maximum contributing area, which decreases to MRZ 2 as parallel flow dominated. This maximum upslope area then increases as surface incision occurs and flow is concentrated in rills. At the ploughed plots, a big difference exists between the Upper Nogalte and Cardenas sites. As the furrows are generally larger at Upper Nogalte the ridges appear to exhibit one area that is relatively lower than the remainder of the ridge. The flow overtops at this micro-col and so these few cells drain a large area of the plot. The lower and more dissected ridges at Cardenas meant that flow overtops them at several areas of the plot. The MRZ 5 results again are disturbed by point density problems. In general, the Del Prado site has a larger maximum upslope area towards the

top of the hillslope, but the Upper Nogalte plots have much larger maximum upslope areas at each other plot.

Figure 5.26. shows that the percentage of the plot cells draining > 1 % of the total plot area increases downslope to MRZ 3. Beyond this point, as only a few cells drain very large areas, this value decreases. The ploughed plots show a relatively large percentage of cells draining greater than 1 % of the plots. Between sites, the Cardenas hillslope displays the highest values at most plots.

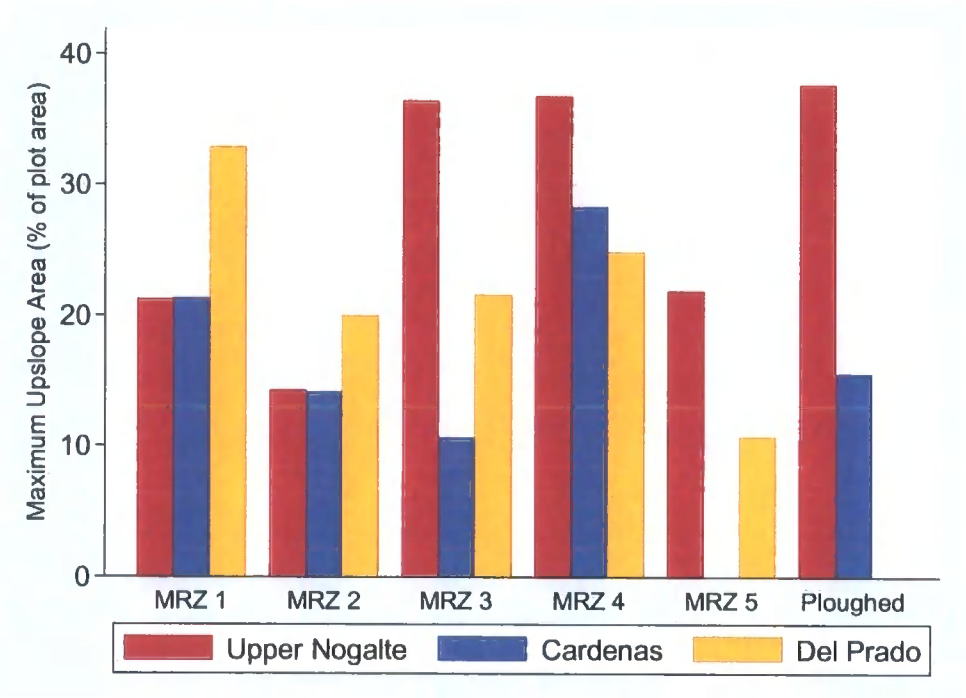

Figure 5.25. Maximum upslope contributing area experienced by any cell at each plot (as a percentage of total map area).

The results presented so far represent the plot surface in the condition where depression storage capacity is filled (i.e. MDS is achieved). Otherwise water will flow into depressions and fail to drain out. The upslope contributing areas experienced by a surface will then generally decrease. The difference between the two conditions indicates how the hydrological connectivity of the surface changes with the filling of surface depressions. Figures 5.27 and 5.28 display the increase in the properties calculated above as a result of depressions being filled to capacity. The results are also found in Table 5.3.

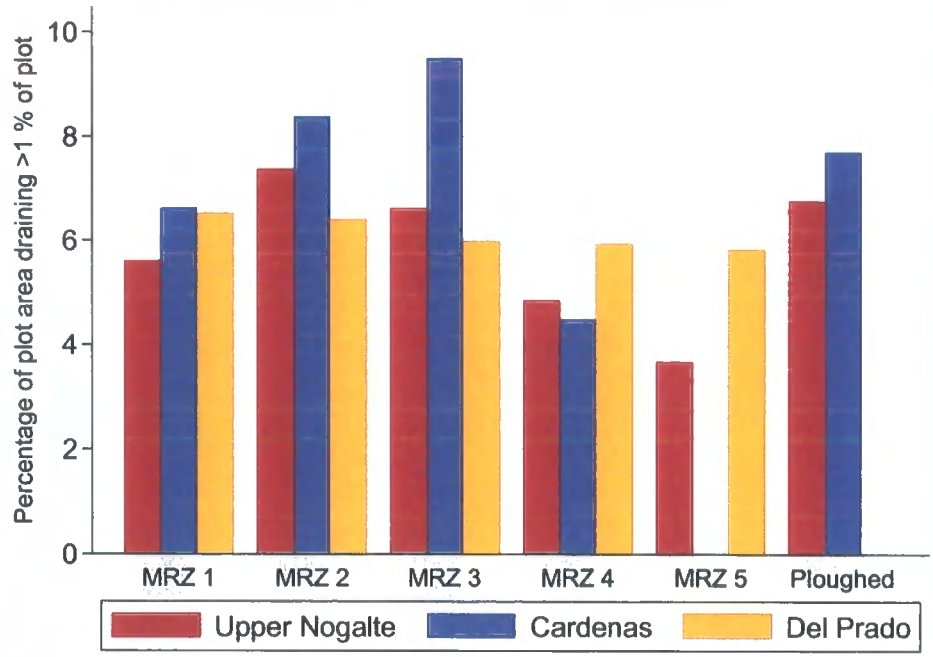

Figure 5.26. Percentage of each map area with an upslope contributing area of greater than 1 % of the total map area for each plot.

Site	*Plot*	*Increase in maximum upslope area (% of plot)*	*Increase in percentage of plot area draining >1 % of plot*
Upper Nogalte	MRZ 1	18.2	4.7
	MRZ 2	0.0	0.1
	MRZ 3	16.9	0.6
	MRZ 4	29.2	0.2
	MRZ 5	11.8	0.5
	Ploughed	32.5	4.9
Cardenas	MRZ 1	18.3	5.2
	MRZ 2	4.8	-1.0
	MRZ 3	1.5	0.0
	MRZ 4	5.4	-0.2
	Ploughed	-0.1	-1.8
Del Prado	MRZ 1	31.7	6.4
	MRZ 2	17.5	6.0
	MRZ 3	12.3	2.4
	MRZ 4	18.2	2.4
	MRZ 5	3.1	1.9

Table 5.3. Increase in maximum upslope contributing area experienced by any cell in each map (as a percentage of total map area) and the percentage of each map area with an upslope contributing area of greater than 1 % of the total map area as a result of depression filling, for each plot.

Figure 5.27 demonstrates that, as expected, the maximum upslope area (%) of each plot increases as depressions are filled. This is noticeable at the MRZ 1 plots and is generally more exaggerated at the Upper Nogalte site than elsewhere. Whereas the Upper Nogalte ploughed plot generally has low maximum upslope contributing area (5 %) due to flow into depressions caused by regular furrows, once these depressions are filled this value increases to nearly 38 %. While this increase is partly related to MDS of each surface (as seen by the low increase of the Cardenas plots), location of these depressions in relation to areas of flow concentration also influence this increase because enough surface runoff will encounter the depressions on any particular surface for MDS to be achieved in any one rain event. Such juxtaposition of MDS and overland flow pathways is an important feature of soil surfaces that is rarely considered. This is discussed further in section 6.3.

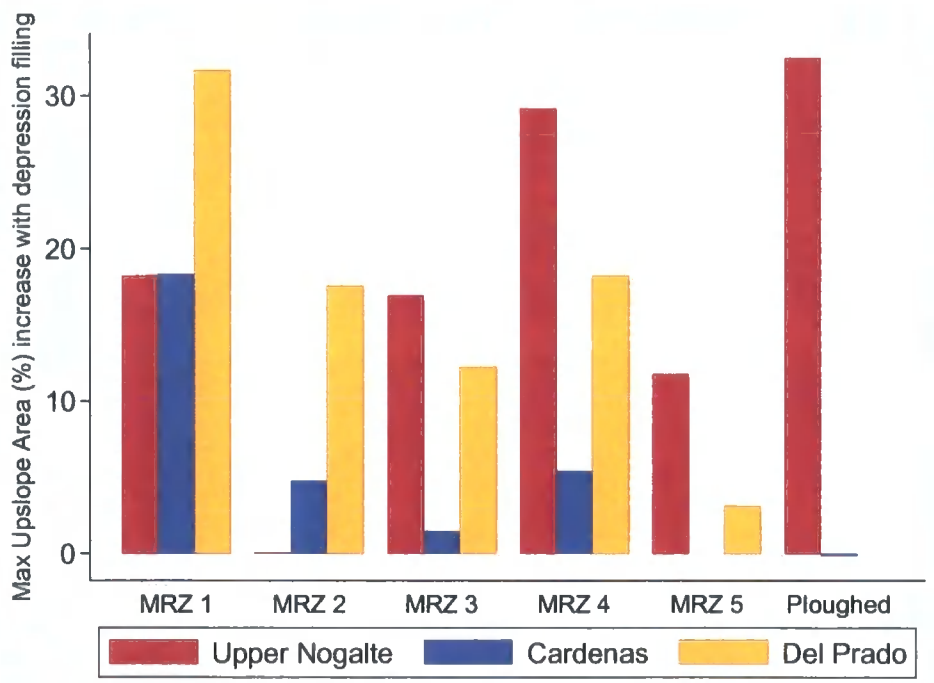

Figure 5.27 Increase in maximum upslope contributing area (%) with depression filling for each plot.

Figure 5.28 demonstrates the effect of filling surface depressions on the percentage of each plot draining greater than 1 % of the total plot area. In general, the observed increase becomes less noticeable with distance downslope; the Del Prado site

experiences the largest increases as a result of the filling of depressions. The pattern resembles that seen in Figure 5.27, however there is one noticeable difference. For many of the Cardenas plots, the filling of depressions has decreased the percentage of each plot draining greater than 1 % of the total plot area. The largest decrease was seen at the ploughed plot. Here, when depressions were empty, water could flow into furrows and be channelled down the furrow bottom, before reaching a depression at some point on this route. As the depressions were filled, the water was directed over the furrow and continued flowing downslope as several separated areas of parallel surface flow. This unexpected result reflects the complicated interactions between surface microtopography and the routing of runoff during rainstorms.

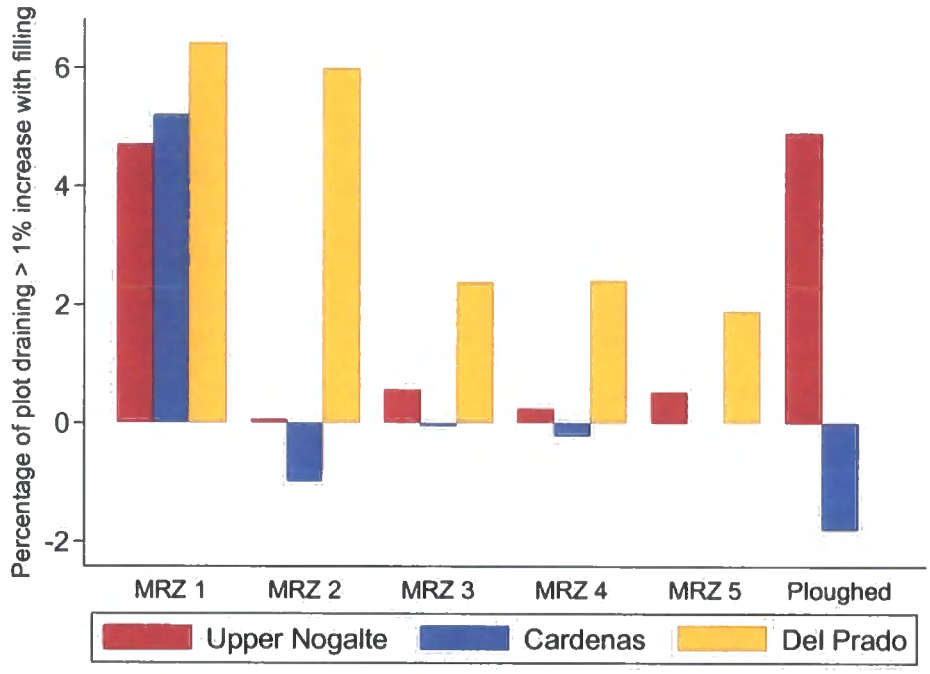

Figure 5.28. Increase in the percentage of map area with an upslope contributing area of greater than 1 % of the total map area with depression filling, for each plot.

5.5 Minidisk Infiltration Measurements

This section deals with variations in infiltration as a result of microtopography. Four infiltration tests were undertaken in each plot, attempting to encompass a broad range of microtopographic features in each. Section 5.5.1 describes the general pattern of the infiltration curves found at each site, while section 5.5.2 compares the results of these

infiltration tests averaged over each plot. Finally, the variability seen within each plot as a result of microtopography is examined in section 5.5.3.

5.5.1 Infiltration Curves

For the majority of infiltration tests, the cumulative depth infiltrated increased with time in the manner displayed in Figure 5.29.

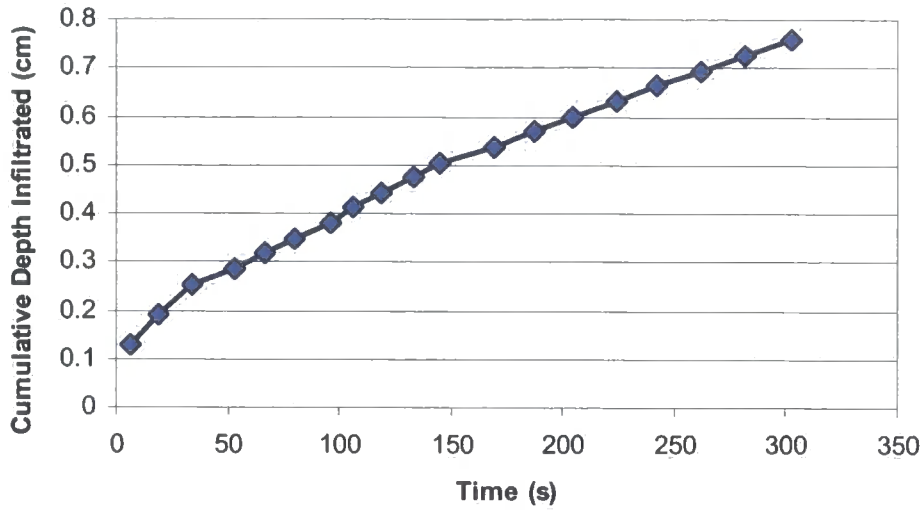

Figure 5.29. The increase in cumulative depth infiltrated (I in cm) with time observed for the majority of infiltration tests. The dataset above is from *Upper Nogalte* MRZ 1.

As the form of the relationship is expected to be $I = c_1 t + c_2 \sqrt{t}$ (equation 3.1), it is more useful to plot cumulative depth infiltrated (I) against the square root of time (x in the Figure below), forcing the curve through the origin (Figure 5.30).

The relationship seen in Figure 5.30 below represents $I = 0.0004t + 0.037t^{0.5}$. The unsaturated hydraulic conductivity k is directly calculated from c_2. Figure 5.31 shows how both the declining term and the constant term of this equation change with time to give the infiltration rate as seen for the majority of tests. The declining term is initially the dominant influence, but the effect of the constant term becomes more significant after the first thirty seconds when the total infiltration rate becomes reasonably constant.

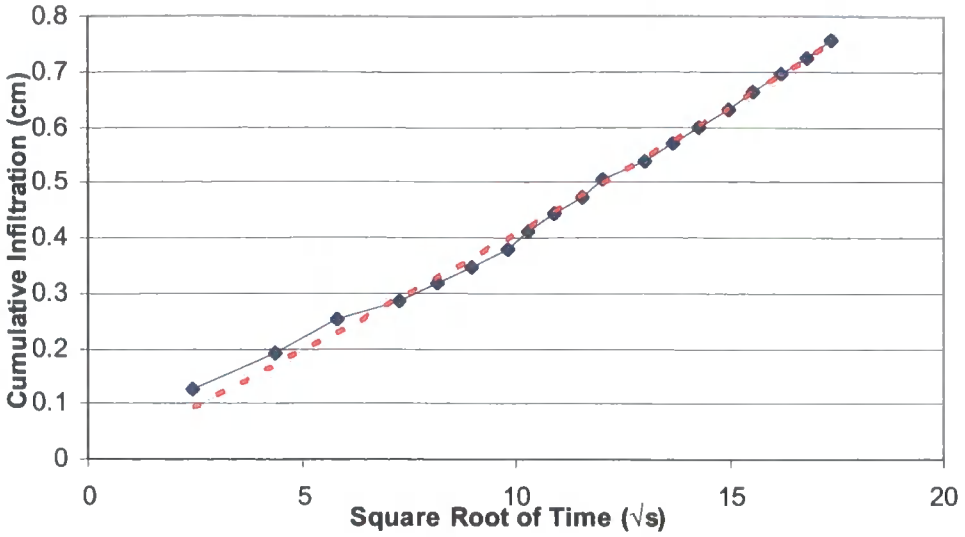

Figure 5.30. The relationship between cumulative depth infiltrated (cm) with the square root of time, as observed for the majority of infiltration tests. The dataset above is from Upper Nogalte MRZ 1.

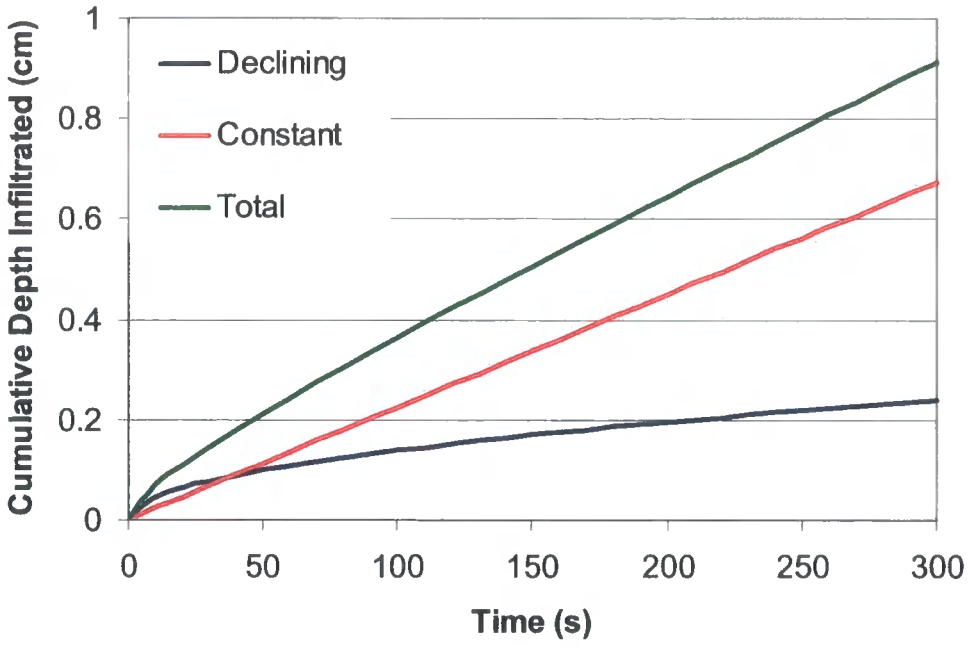

Figure 5.31. Contribution of both the constant term and the declining term of the equation $I = C_1 t + C_2 \sqrt{t}$ to the infiltration rate, as seen at the majority of sites. The curves are taken from the regression equation of the relationship seen at Upper Nogalte MRZ 1.

However, some infiltration tests did not follow this pattern. Figure 5.32 shows one example from the Cardenas ploughed plot. Unlike the majority of tests (Figure 5.29), the curve in Figure 5.32 shows a sharper initial increase in cumulative depth infiltrated. Figure 5.33 shows how the relationship between cumulative depth infiltrated and the square root of time appears for these tests.

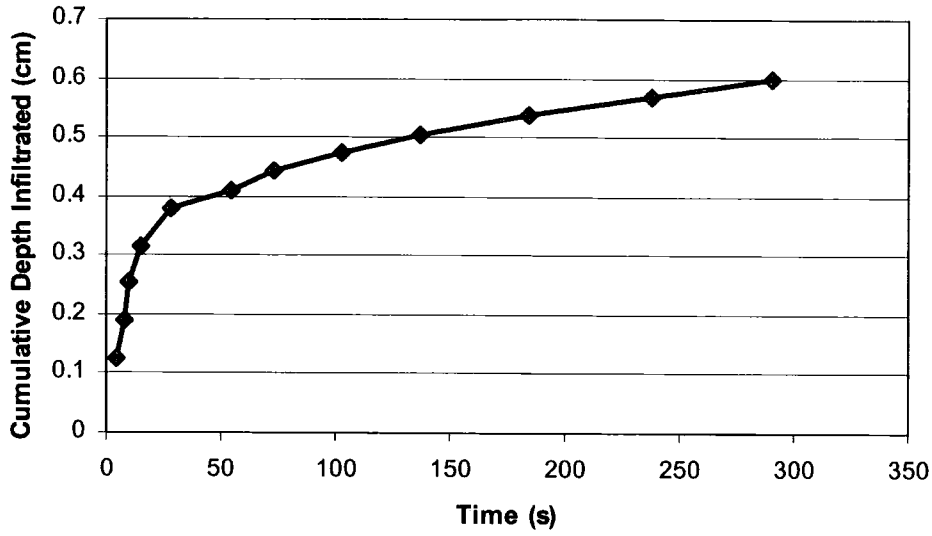

Figure 5.32. Increase in cumulative depth infiltrated (I in cm) with time observed for a subset of infiltration tests. The dataset above is from the Cardenas ploughed plot.

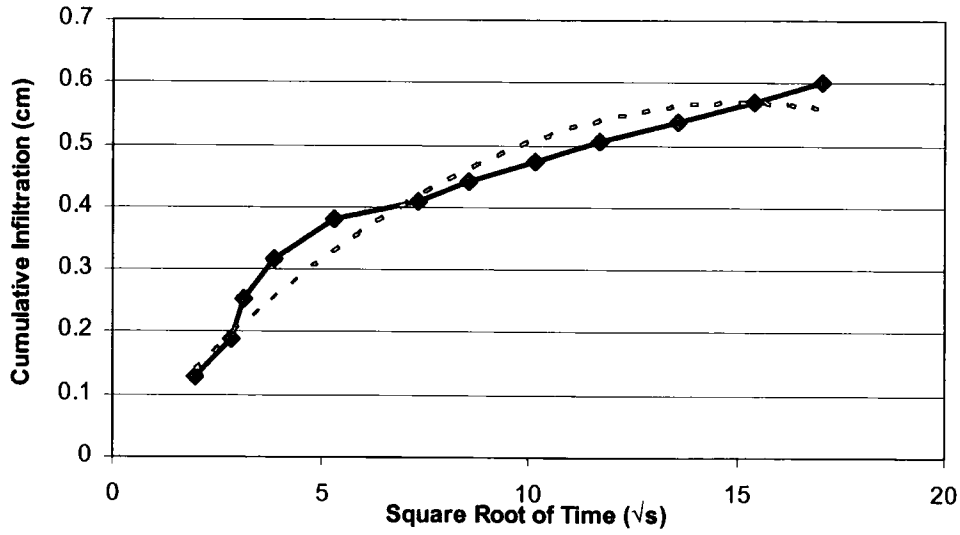

Figure 5.33. The relationship between cumulative depth infiltrated (cm) with the square root of time, as observed for some infiltration tests. The dataset above is from the Cardenas ploughed plot.

The rapid infiltration at the start of these infiltration tests has raised problems, as the dominance of the declining term has caused the constant term to become negative. This can be seen more clearly in Figure 5.34 (compare with Figure 5.31).

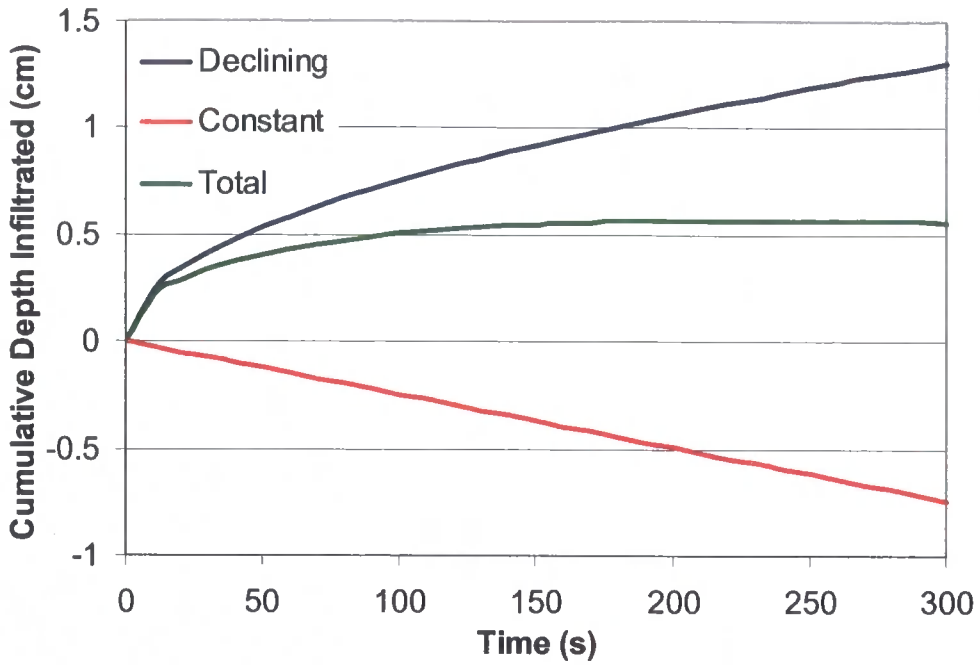

Figure 5.34. Contribution of the constant term and the declining term of the equation $I = C_1 t + C_2 \sqrt{t}$ to the infiltration rate, as seen for some infiltration tests. The curves are taken from the regression equation of the relationship seen at the Cardenas ploughed plot.

As a consequence of this, the estimated unsaturated hydraulic conductivity k is negative in some cases. Obviously the rapid initial infiltration is the cause of this. One hypothesis may be to blame the wet sand layer placed beneath the minidisk infiltrometer to ensure a good contact with the surface. However, this was reasonably constant between all tests and so could not have led to such measurements. An alternative hypothesis involves the nature of the soil surface. Perhaps shrink-swelling behaviour of clay aggregates is responsible as micro-fissures may have been present at some sites, allowing initial high infiltration rates, followed by a decrease in this rate as the clay aggregates swell and close up the flow pathways. Therefore, the total depth infiltrated should be considered alongside the unsaturated hydraulic conductivity and compared between each test.

5.5.2 Variation of Infiltration between Plots

Table 5.4 displays the mean and standard deviation of unsaturated hydraulic conductivity k, and the total depth infiltrated (in cm) during the 5 minute infiltration tests for each plot.

		Mean		*Standard Deviation*	
Site	*Plot*	*k* ($\times 10^4$ cm s^{-1})	*Total Depth (cm)*	*K* ($\times 10^4$ cm s^{-1})	*Total Depth (cm)*
Upper Nogalte	MRZ 1	1.772	0.821	1.310	0.100
	MRZ 2	7.206	1.641	1.688	0.502
	MRZ 3	2.674	1.294	4.903	0.488
	MRZ 4	1.656	1.326	1.537	0.412
	MRZ 5	3.831	1.547	1.884	0.432
	Ploughed	-0.945	0.623	2.200	0.208
Cardenas	MRZ 1	0.114	0.765	1.320	0.290
	MRZ 2	1.662	1.018	1.510	0.250
	MRZ 3	1.203	1.010	1.548	0.129
	MRZ 4	-2.802	0.726	1.227	0.106
	Ploughed	-2.590	0.750	1.431	0.119
Del Prado	MRZ 1	2.453	1.823	1.995	0.848
	MRZ 2	1.229	1.199	1.334	0.279
	MRZ 3	1.913	1.878	5.054	0.943
	MRZ 4	1.148	0.781	2.234	0.181
	MRZ 5	2.785	1.484	2.261	1.249

Table 5.4. Means and standard deviations (based on four tests) of unsaturated hydraulic conductivity (k, in $\times 10^4$ cm s^{-1}) and total depth infiltrated (in cm) for each plot.

Figure 5.35 demonstrates that the average value of k is negative for only three sites. Both ploughed plots fall into this category. Unsaturated hydraulic conductivity generally increases from MRZ 1 to MRZ 2 and then decreases for each site moving downslope from MRZ 2 to 4. Generally, values of k are lowest for the Cardenas site which may reflect the higher clay concentration in the soil.

While k is important for determining how infiltration rate changes within a rainstorm, the total amount infiltrated within 5 minutes also provides some interesting comparisons between and within plots. Figure 5.36 shows that the largest ranges in total amount infiltrated seem to be found at Del Prado. Again, Cardenas tended to have the lowest overall amount, and in many cases the lowest range of values. Like k, this value generally increases to MRZ 2 before decreasing with further distance downslope. The

total amount infiltrated at the ploughed plots was significantly lower than at most other plots.

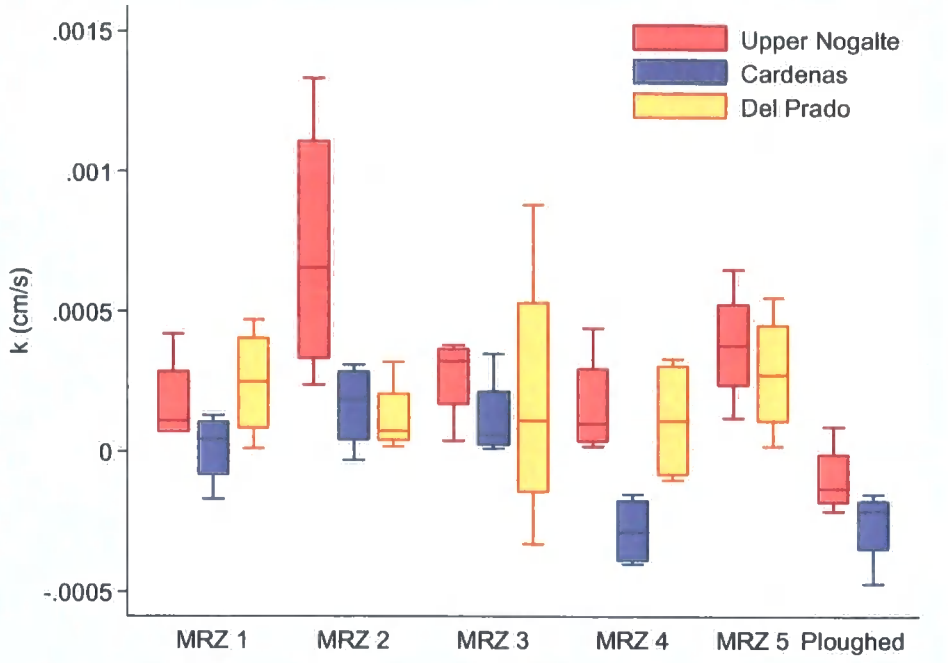

Figure 5.35. The variation of unsaturated hydraulic conductivity (k, in cm s^{-1}) between each plot and site.

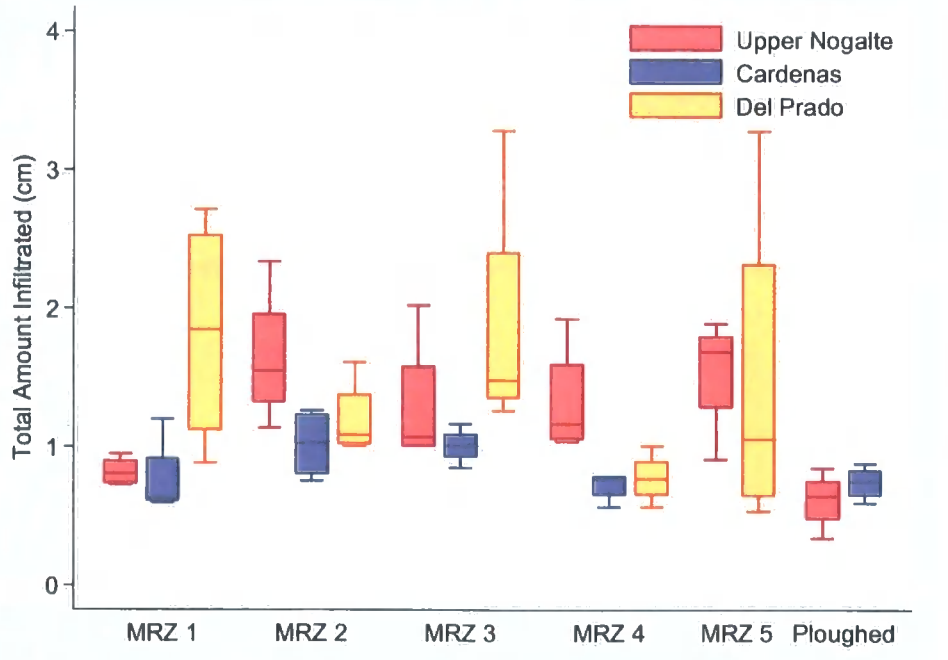

Figure 5.36. The variation of total amount infiltrated (cm) between each plot and site.

Figure 5.37 demonstrates that the variation in total amount infiltrated has a poor relationship with the general slope of the plots. Therefore, some other factor must influence the infiltration rates observed. The following section examines the effect of microtopography of the soil surface on infiltration rates.

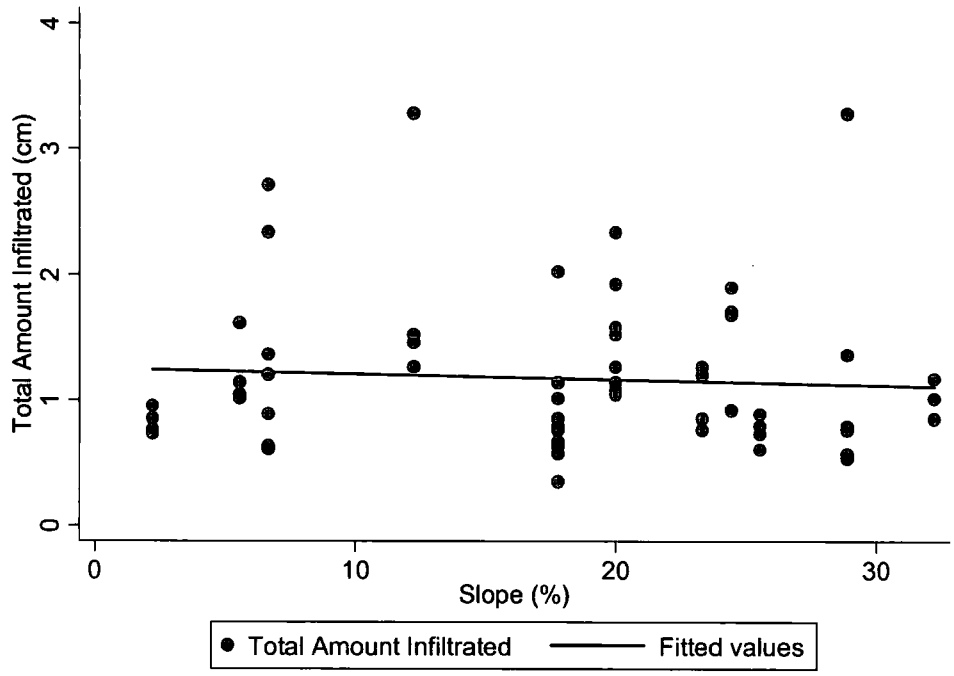

Figure 5.37. The relationship between total amount infiltrated (cm) and general plot slope (%). The markers stack in vertical rows as four tests were undertaken at each plot.

5.5.3 Variation of Infiltration within Plots

This leads to the question of how infiltration varies within the plots. Although only four infiltration tests were carried out on each plot, these tests strategically sampled various roughness elements of the soil surface (Figures 5.39-5.43).

Figure 5.38 displays how the standard deviation of total amount infiltrated varies between and within sites. Cardenas tends to have the lowest standard deviations, while Del Prado has the highest. Although it is well documented that differential crusting causes large differences in infiltration parameters between furrow top and bottom (Figure 2.4), the ploughed plots demonstrated a relatively small standard deviation of total amount infiltrated.

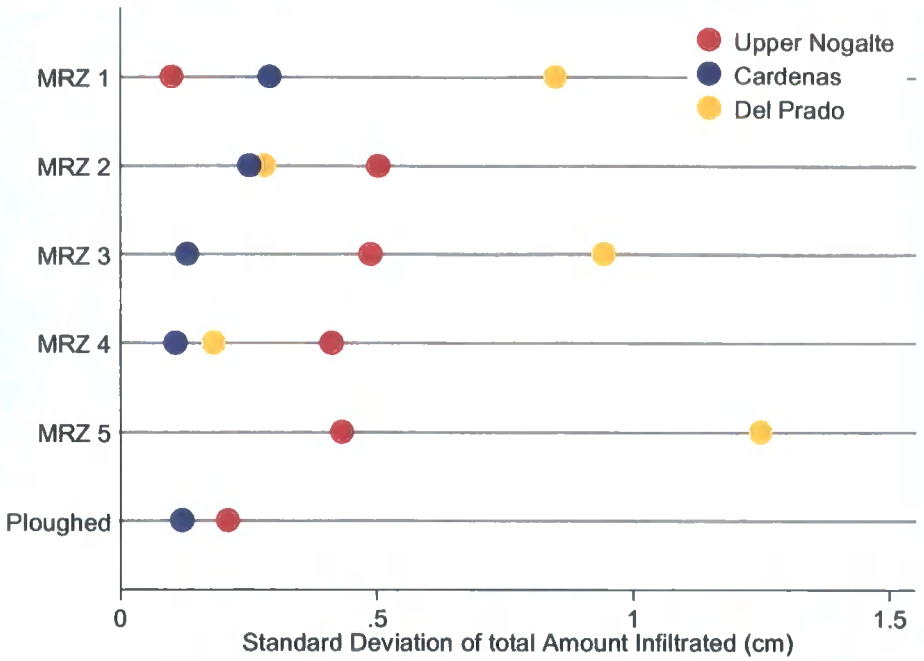

Figure 5.38. The variation of the standard deviation of the total amount infiltrated (in cm) between each plot and site.

No distinct roughness elements could be identified at MRZ 1. The tests on MRZ 2 were sub-divided into those carried out on what was identified as a small 'wash deposit' and those on a surface away from such a deposit. Figure 5.39 shows how both *k* and total amount infiltrated are influenced by these roughness elements. In all cases the total amount infiltrated by the wash deposits is lower than on the remainder of the surface. This is likely to be a result of the higher concentration of fines found on these small deposits. Both on and off the deposit Upper Nogalte exhibits the greatest *k* and total amount infiltrated, followed by Del Prado with Cardenas generally displaying the lowest values.

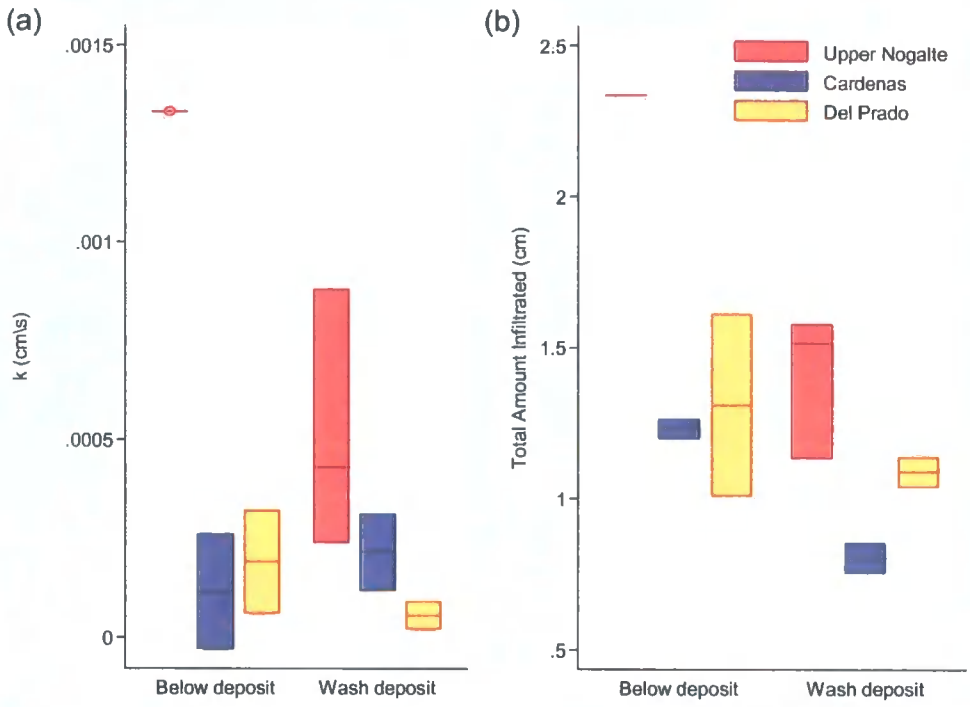

Figure 5.39. The variation of (a) unsaturated hydraulic conductivity, *k* and (b) total amount infiltrated within the MRZ 2 plots.

Infiltration tests carried out on MRZ 3 plots were subdivided into those in a flow concentration as identified in the field, and those on surfaces away from any such flow concentrations (Figure 5.40). With only four measurements in total at each plot, it is difficult to produce any meaningful conclusions. In general, *k* is higher in flow concentrations, with Del Prado experiencing the greatest range of values. Again Cardenas has relatively low total amounts infiltrated for both elements of the microtopography. Both Del Prado and Cardenas show a lower total amount infiltrated out of flow concentrations than in flow concentrations, but Upper Nogalte experiences the reverse trend.

Infiltration tests on the plots demonstrating evidence of rill incision were also divided into two categories: in rill bottoms and on the surface above the rills. Figure 5.41a shows that there is not much difference in the unsaturated hydraulic conductivity between these categories. However, once again, the Cardenas site displayed lower (even negative) values than the other sites. Figure 5.41b shows that Cardenas and Del Prado infiltrated similar amounts over the five minute tests in both microtopographic categories. At Upper Nogalte there is a large difference between these categories; values

from the rill bottom are lower than those from tests undertaken out of the rill. This was the same pattern observed for the Upper Nogalte at MRZ3 with flow concentrations (Figure 5.40b). It seems that any flow concentration decreases the relatively high infiltration rate observed at the Upper Nogalte hillslope.

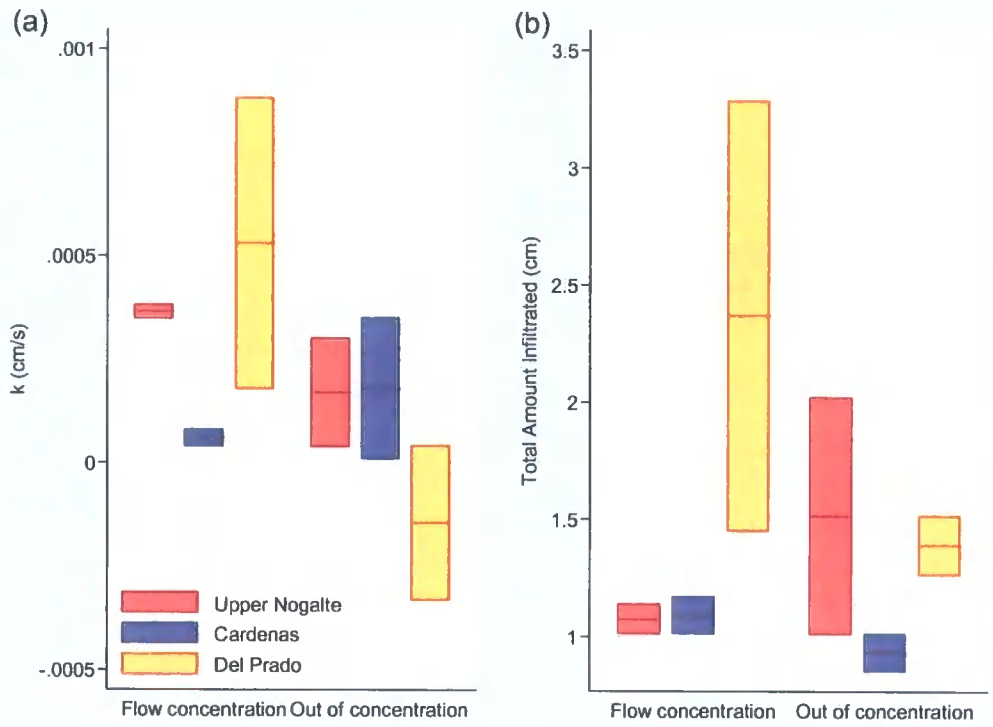

Figure 5.40 The variation of (a) unsaturated hydraulic conductivity, *k* and (b) total amount infiltrated within the MRZ 3 plots.

The MRZ 5 plots were also divided into two categories of infiltration tests: those in gully bottoms, and those on the soil surface away from the gully features. Figure 5.42a shows that the unsaturated hydraulic conductivity was much higher in the gully bottom than on the surrounding soil surfaces. However, when the total amount infiltrated is considered (Figure 5.42b), no obvious pattern can be seen.

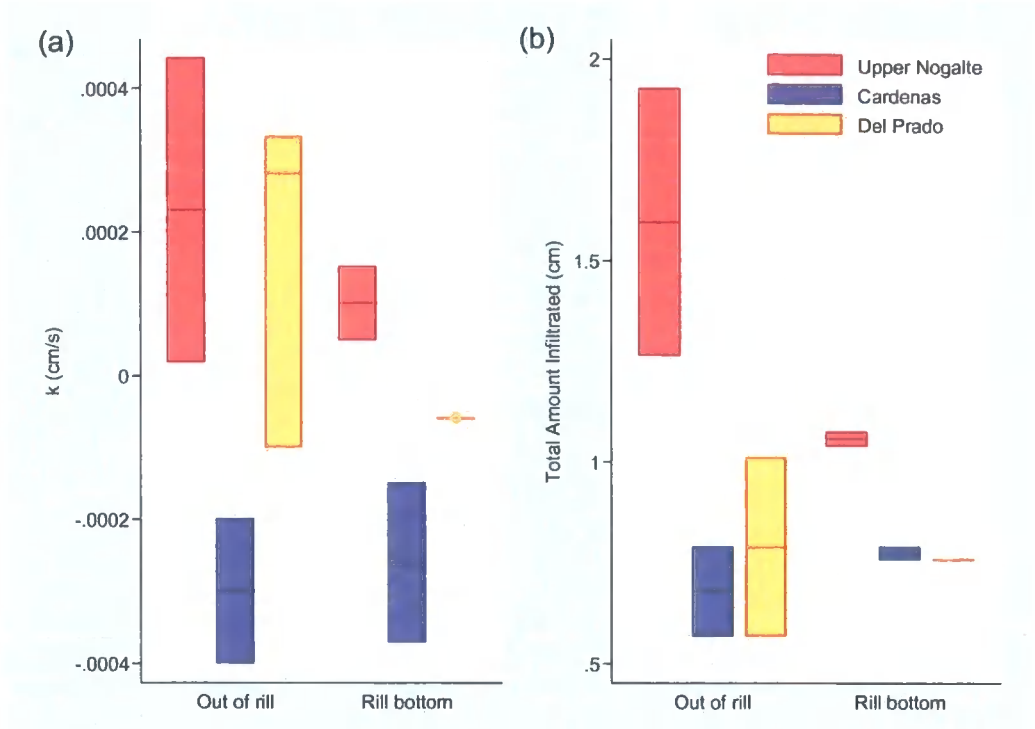

Figure 5.41. The variation of (a) unsaturated hydraulic conductivity, *k* and (b) total amount infiltrated within the MRZ 4 plots.

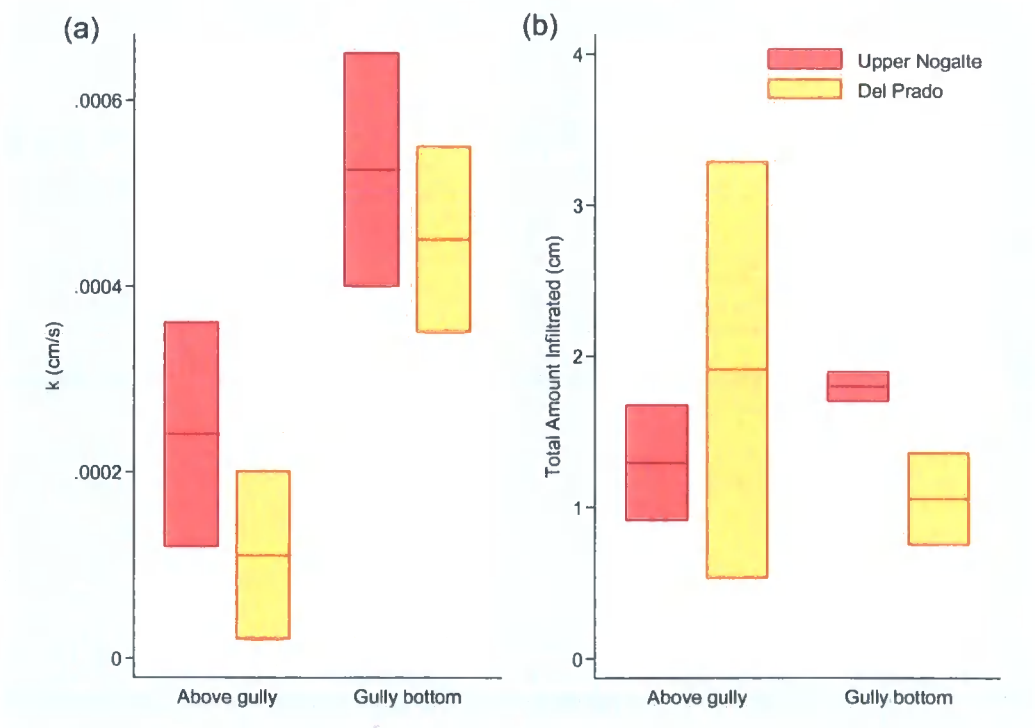

Figure 5.42. The variation of (a) unsaturated hydraulic conductivity, *k* and (b) total amount infiltrated within the MRZ 5 plots.

Finally, Figure 5.43 displays how the results of the infiltration tests vary within the two ploughed plots investigated. Tests were undertaken at both the bottom and top of plough furrows. The Cardenas hillslope did not show a great difference in infiltration between these two categories. This suggests that the plough furrows at Cardenas are not as effective at holding water as those at the Upper Nogalte hillslope. The persistence of spray painted lines used to monitor sediment transport suggests that, unlike at the Upper Nogalte site the ploughing at Cardenas is several seasons old. In general, the furrow bottom infiltration results represent a lower infiltration rate than those taken at the top of the furrow. This supports the claim that thicker depositional crusts form in furrow bottoms (section 2.3.2).

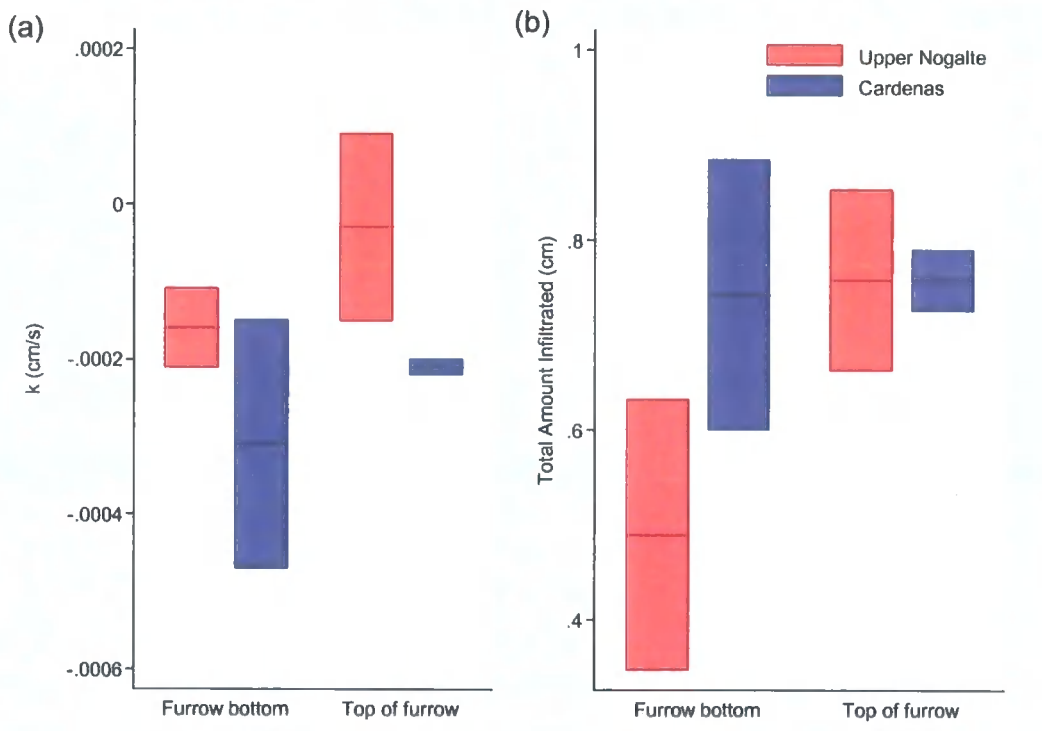

Figure 5.43. The variation of (a) unsaturated hydraulic conductivity, *k* and (b) total amount infiltrated within the ploughed plots.

5.6 Sediment Transport and Hillslope Runoff

Data on sediment transport and hillslope runoff from spray-painted lines, sediment bags and mini-crest stage recorders were collected for MRZ 2, MRZ 3 and MRZ 4 at each hillslope. Sediment transport and runoff were too low to measure at MRZ 1 and too high to measure at MRZ 5 (where bags and lines are simply washed away). The line and

bag sediment measurements and the maximum runoff depths recorded between May and September 2002 are displayed in Table 5.5 along with a summary of the location of each sediment transport monitoring site.

Site	*Plot*	*Position*	*Distance from divide (m)*	*Line sediment (cm^3m^{-1})*	*Bag sediment (g)*	*Runoff Depth (cm)*
Upper Nogalte	MRZ 2	Close to divide	10	89	6.57	
	MRZ 3	Below terrace	40	145	20.92	3
	MRZ 3	Mid slope	70	47	4.75	
	MRZ 3	Concavity side slope	90	366	16.85	
	MRZ 4	Base of slope, in concavity, above rill head	138	337	2.27	5
Cardenas	MRZ 2	Close to divide	7	693	5.71	
	MRZ 2	Upperslope	15	571	24.04	
	MRZ 3	Mid slope	25	878	15.86	12
	MRZ 3	Under bush	28	349	13.64	
	MRZ 4	Base of slope	34	853	761.33	8
Del Prado	MRZ 2	Near divide	4	823	1.60	
	MRZ 3	Middle of slope	8	2311	5.14	
	MRZ 4	Base of hillslope concavity	13	1170	1690.75	10

Table 5.5. Line and bag sediment transport measurements and maximum runoff depths recorded on each hillslope between May and November 2002. Monitoring was undertaken during previous research (Bracken & Kirkby, 2005).

The data displayed in Table 5.5 are reported in greater detail in Bracken & Kirkby (2005). A single storm event was believed to be responsible for the majority of sediment transport. This storm event produced 83.0 mm of rainfall in the Rambla Nogalte (on 30th June 2002), and was responsible for a maximum of 5 cm of runoff and 366 cm^3m^{-1} of sediment transport at the Upper Nogalte hillslope; and a depth of runoff of 12 cm resulting in 878 cm^3m^{-1} of sediment transport at the Cardenas site. This same storm reached the Rambla de Torrealvilla on 1st July 2002 where 53.4 mm of rainfall was recorded. This produced a maximum runoff depth of 10 cm at the Del Prado site (although 26 cm was recorded elsewhere in the catchment) with 2311 cm^3m^{-1} of sediment transport (Bracken & Kirkby, 2005).

Sediment transport generally increased downslope from MRZ 2 to MRZ 4 (Figure 5.44) although the maximum sediment transport was recorded at MRZ 3. The Del Prado

hillslope experienced the greatest sediment transport at each plot, followed by Cardenas and finally Upper Nogalte. From Table 5.5, it is clear that there is a lot of variation in sediment transport for each MRZ. For example, the Cardenas MRZ 2 site reports sediment transport values from two lines, one of which was immediately below a bush. This value is less than half of the sediment transport recorded elsewhere at the site, and presumably reflects the spatial pattern of sediment transport within the plot that eventually leads to the formation of the small wash deposits visible on the surface. This same variation is found for the Upper Nogalte MRZ 3 plot where a line sprayed in a concavity recorded significantly higher sediment transport than found elsewhere on the plot.

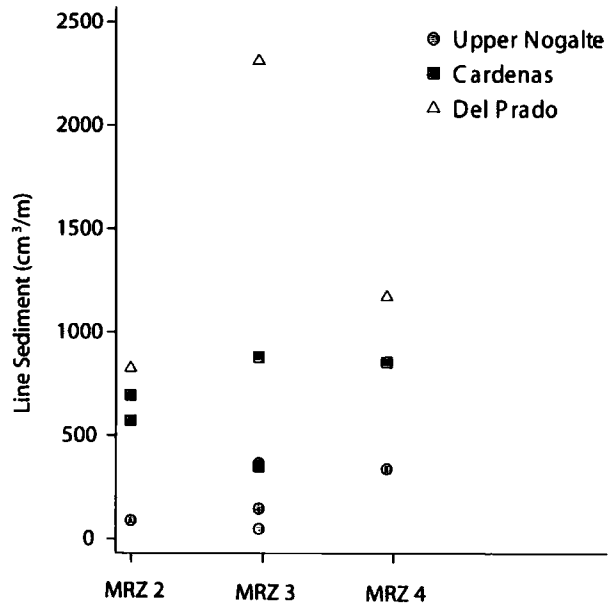

Figure 5.44. Sediment transport rates (cm^3m^{-1}) from spray-painted lines for each plot and site.

The weight of sediment trapped in each bag is displayed in Figure 5.45. The Cardenas and Del Prado sites demonstrate a steady increase in trapped weight with distance downslope from the divide. The Upper Nogalte MRZ 4 sediment bag trapped little sediment in comparison with other sites. The differences in values recorded within each plot follow approximately the same pattern as that of the sediment transport rates.

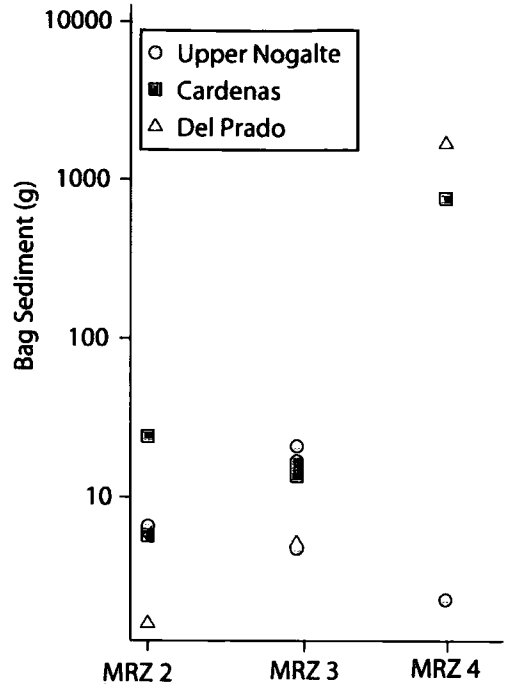

Figure 5.45. Weight of sediment trapped in bags (g) for each sediment transport and hillslope runoff monitoring site.

The graphical analysis of sediment size data in Figure 5.46 depends on four ideas (Cox, personal communication 2005). First, particle size is often easier to work with as logarithm of particle size, as exemplified by the use of phi or psi scales in sedimentology.

Second, cumulative distribution curves can be useful as, in this case the relatively small number of sediment classes means that anomalies in individual samples would be more prominent on histograms: it is easy to be distracted by such details, which may be no more than quirks in the original data, possibly even particular clasts that happened to be included in the sample. Thus the mild smoothing provided by cumulation can be welcome (Cox, 2004).

Third, it is almost inevitable that most cumulative curves have some kind of sigmoid or S-shape, as all start at probability 0 and end at probability 1 (or 100%). Convergence near the extremes makes the graph noisier, so that it may be difficult to see structure in the tails of the distribution. In addition, simultaneous comparison of several irregular curves can be a considerable mental challenge. A remedy is to plot cumulative

probability on a scale in which the tails are relatively stretched out and the middle is relatively compressed. For simplicity the transformed scale should do similar things in each tail and thus be a so-called folded transformation (Mosteller and Tukey 1977). Two possibilities are the inverse normal scale and the logit scale. In practice the results are very similar and the logit (= ln p/(1 - p)) is used here arbitrarily.

Fourth, a side-effect of such transformations is that cumulative probabilities of 0 and 1 are unplottable, as logit 0 and logit 1 are indeterminate, as is always true for an inverse normal scale. This is solved in practice by plotting the midpoint cumulative probability for each class.

Therefore, Figure 5.46 shows the contribution of each particle-size class to the cumulative percent of total weight transported (plotted using a logit scale at the midpoints of cumulative probability). Sediment trapped in bags from the Upper Nogalte site is predominantly composed of larger grains when compared with the other sites. The sediment trapped at the Del Prado site, however, is more dominated by finer particles. Although there is considerable variation within the MRZs, the sediment traps nearer the drainage divide contained a larger proportion of coarser particles than those further downslope. This may represent the cumulative influence of preferential transport of finer particles from a greater upslope area (although the trap at Del Prado MRZ 4 contained particles relatively coarse for that hillslope).

Only five values of maximum runoff depth have been recorded (Table 5.5). These demonstrate variations both within and between hillslopes. It is clear that the assumption of an increasing water depth with distance downslope is inconsistent with the data (as seen for the Cardenas hillslope). The Upper Nogalte slope generated much less runoff from the 30th of June storm than the other slopes. Both sediment transport and weight of trapped sediment increased with the recorded maximum runoff depth (Figure 5.47), therefore the distribution of runoff depth across a hillslope is obviously an important consideration when considering soil erosion.

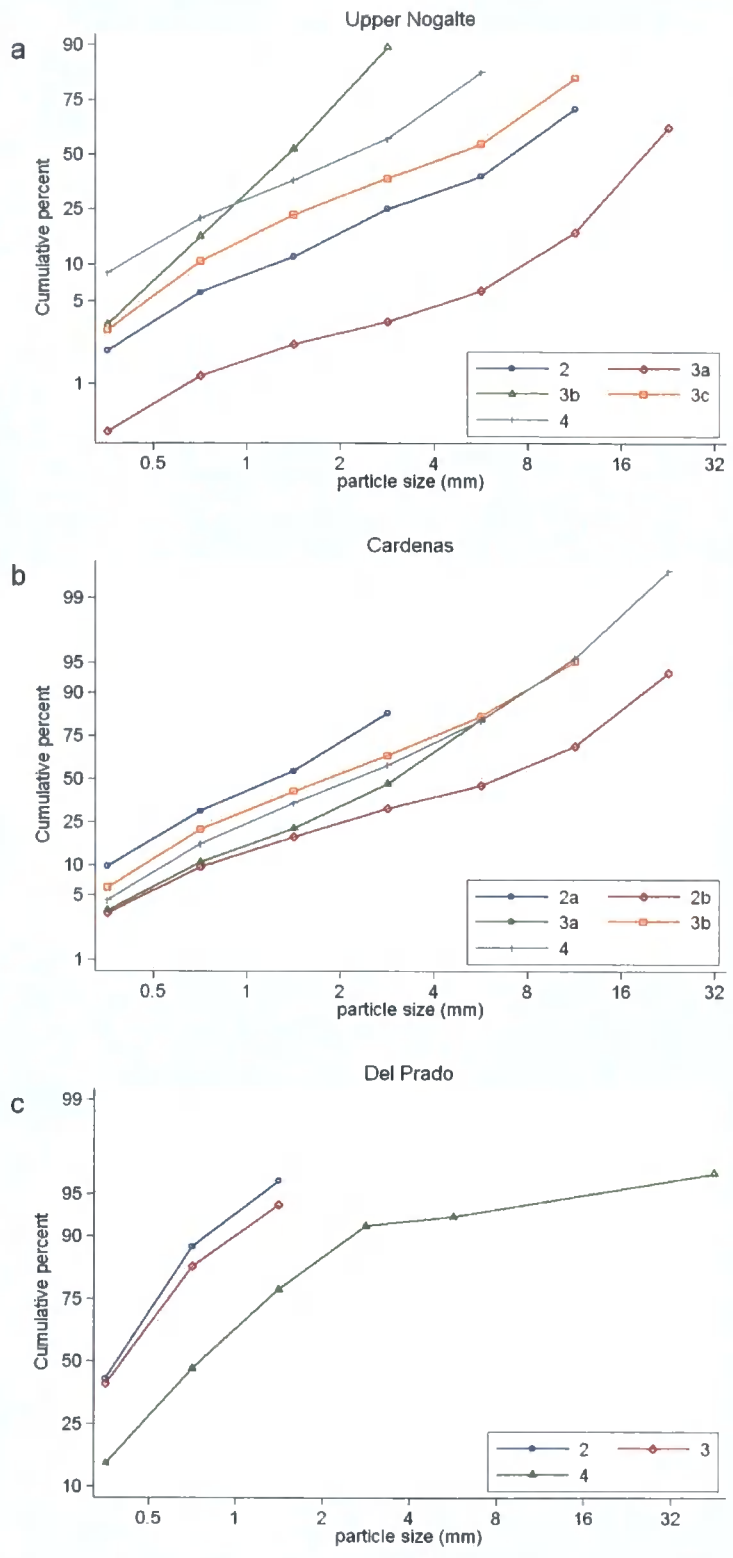

Figure 5.46. Relative contributions of grain sizes to the total weight of sediment trapped by bags (cumulative percent on a logit scale) for each plot for: (a) the Upper Nogalte hillslope; (b) Cardenas; (c) Del Prado. Legend represents MRZ number. Data from Bracken & Kirkby (2005).

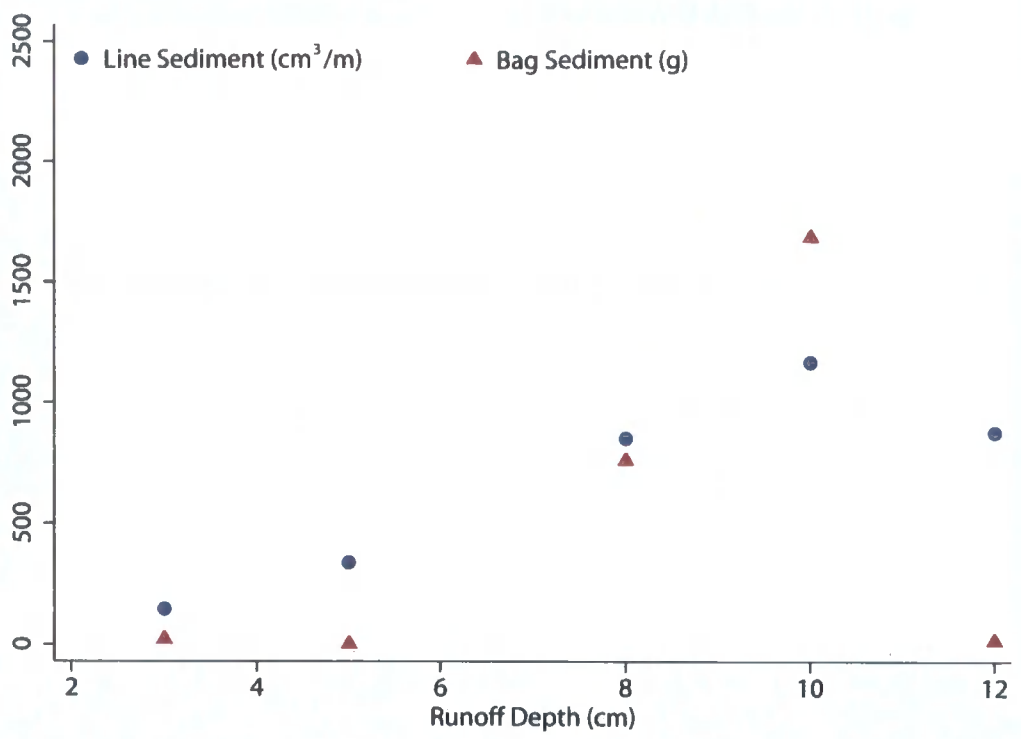

Figure 5.47. The relationship between runoff depth and both sediment transport off spray-painted lines (cm^3m^{-1}) and weight of sediment trapped in bags (g).

5.7 Hillslope-Scale Hydrological Analysis

As each hillslope is composed of multiple slope components and aspects, no attempt was made to rotate the hillslopes to remove the general slope. The general slope of each hillslope is a fundamental property of surface roughness when viewed at the hillslope scale; therefore it is of interest in this final section.

To import the elevation data into PCRaster (with data points in each grid square) a cell size of 0.25 m by 0.25 m was selected. This choice was particularly problematic as a result of areas of the hillslopes with a poor point resolution (as discussed in section 3.3.4.2). At the Upper Nogalte hillslope this had a minor effect near the drainage divide and where several large bushes had been removed from the point clouds (Figure 5.48a). However, at the bowl-shaped Cardenas site a large gap was found in the centre of the map (Figure 5.48b). As this interfered with hydrological analysis, this hillslope was imported again into PCRaster at a 1 m resolution (Figure 5.48c). Table 5.6 displays several summary statistics for each hillslope (each of which has been explained in more detail earlier in this chapter).

	Upper Nogalte	*Cardenas*	*Del Prado*	*Cardenas (1 m Res)*
MDS (mm)	0.169	0.289	1.805	0.917
Maximum upslope area (%)	14.022	2.869	46.298	47.989
Percentage of hillslope area draining >1 % of slope	2.663	0.326	3.285	8.271
Increase in maximum upslope area with filling of depressions (%)	7.496	1.051	40.263	5.004
Increase in percentage of hillslope area draining >1 % of slope with filling of depressions	0.996	0.212	2.713	-0.3102

Table 5.6. Summary statistics of the hydrological analysis of the three hillslopes (analysed at 250 mm × 250 mm resolution). The Cardenas site was repeated with a cell size of 1 m by 1 m.

The Upper Nogalte hillslope demonstrates a more linear drainage pattern than seen at the other sites. The bowl-shaped Cardenas hillslope concentrates all flow into the central concavity before flowing out of the hillslope. The Del Prado map (Figure 5.48d) shows that much of the hillslope is drained by two areas (where gullies were located).

Once again, the relationships between upslope contributing area and percentage of the hillslope area exhibiting that upslope area followed a linear trend in log-log space (Figure 5.49). Both the maximum upslope contributing area (%) and the percentage of hillslope area draining > 1 % of the slope values were largest for the 1 m resolution Cardenas raster, followed by Del Prado, Upper Nogalte, and finally, the original Cardenas raster demonstrated the lowest values (Figure 5.50 a and c).

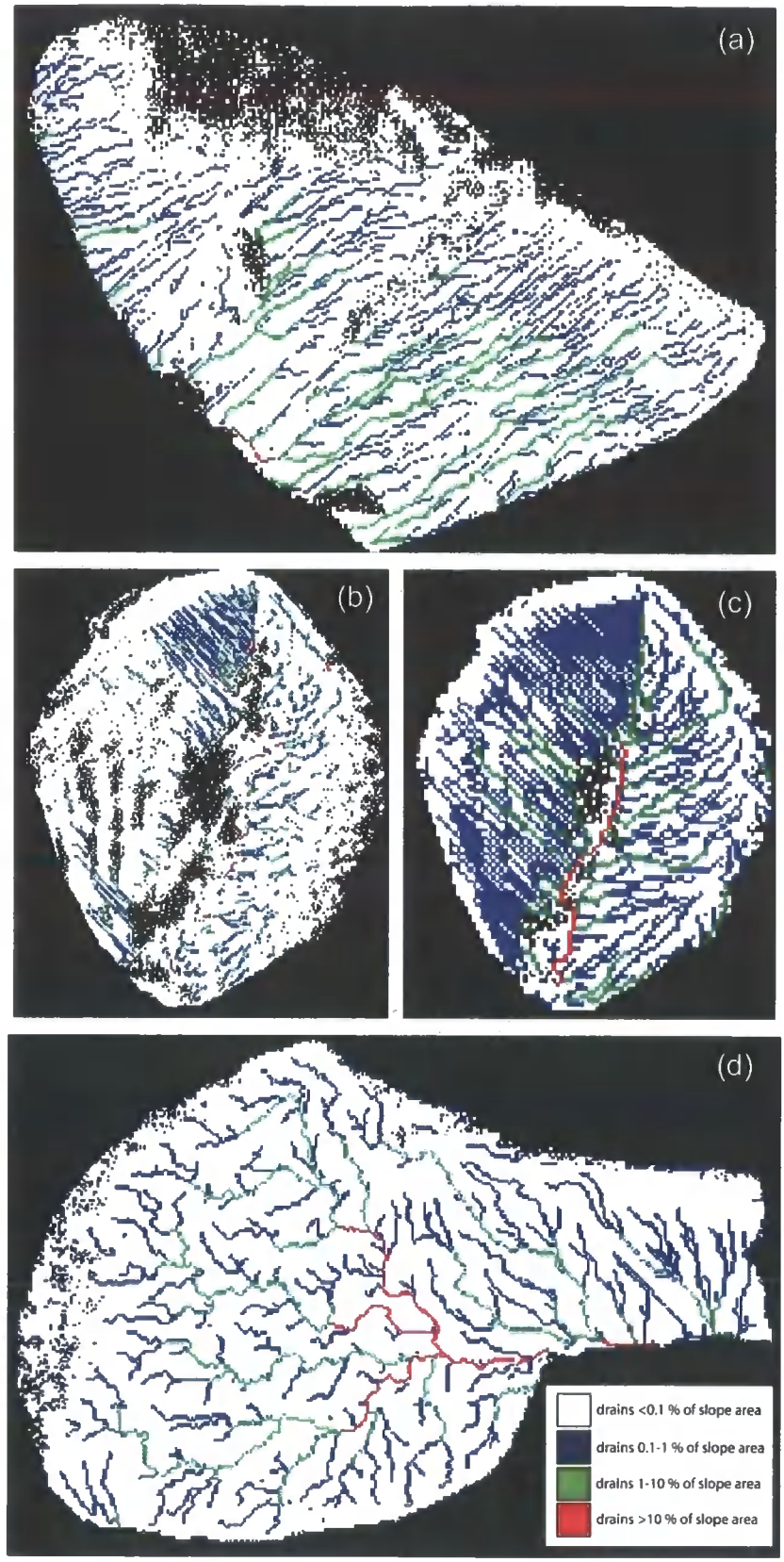

Figure 5.48. Spatial distribution of flow concentrations for each hillslope at 0.25 m resolution: (a) Upper Nogalte; (b) Cardenas; (c) Cardenas (at 1 m resolution); (d) Del Prado.

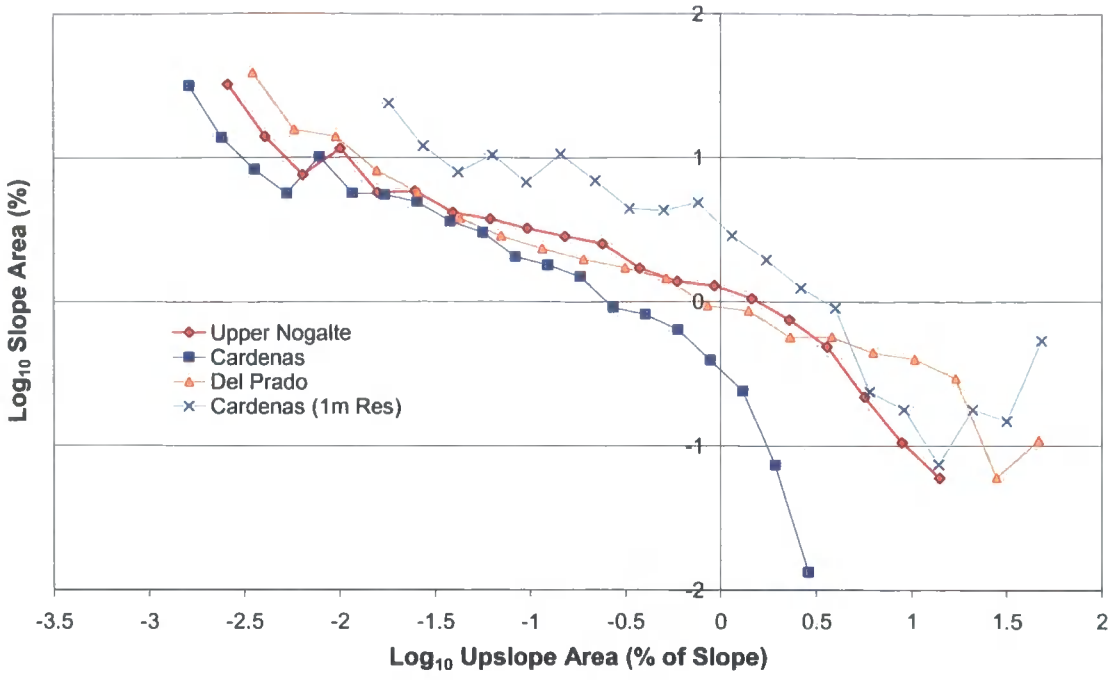

Figure 5.49. The relationships between upslope contributing area and the area of each map exhibiting that upslope area (both expressed as log-transformed percentages of total map area) for each hillslope.

The results displayed in Figure 5.50 show the degree to which each of the upslope area values were a result of the assumption of MDS conditions. The maximum upslope area percentages were much smaller when surface depressions remained available to capture overland flow. Indeed, the maximum Del Prado upslope area increased from just 6 % of the slope to 46 % of the hillslope upon attainment of MDS. The Cardenas 1 m resolution raster was less sensitive to depression storage effects. In general the percentage of hillslope area draining >1 % of the slope was also less sensitive to depression storage. The 1 m resolution Cardenas raster value decreased with the removal of depressions.

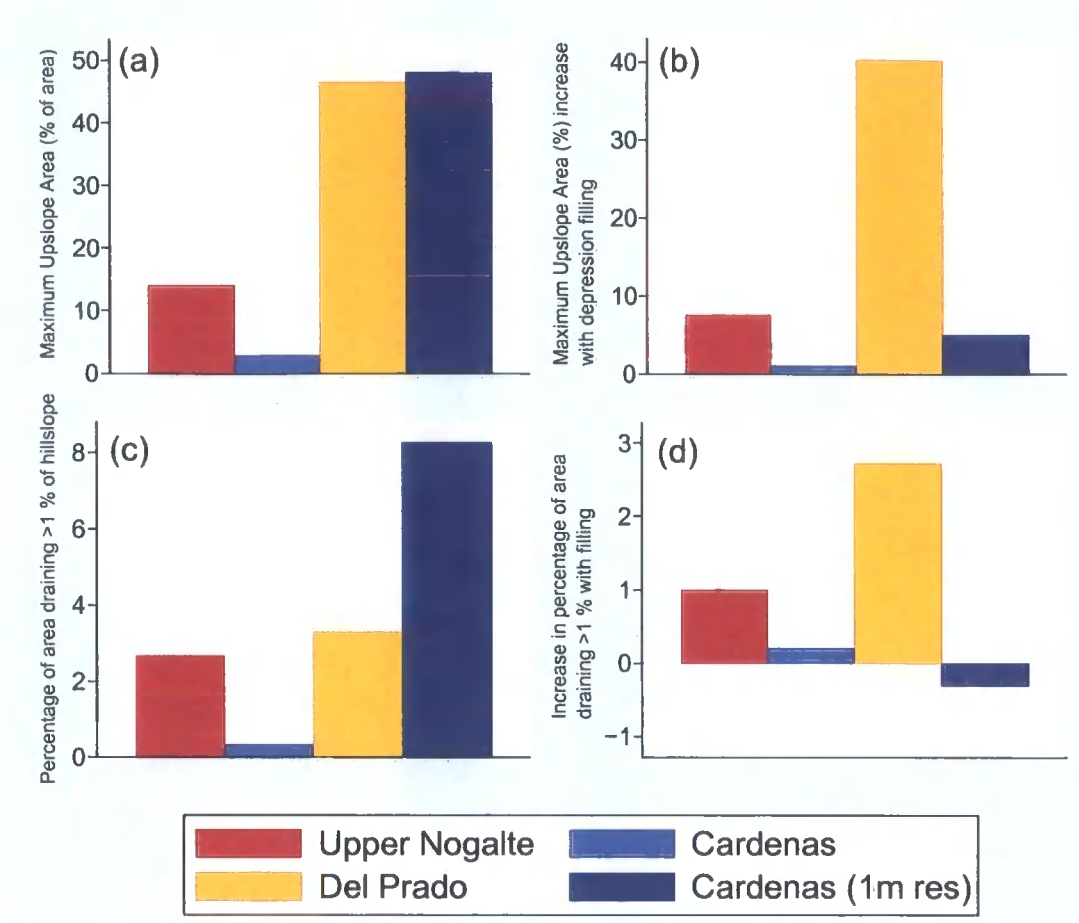

Figure 5.50. Variation of upslope contributing area between hillslopes: (a) Maximum upslope area (as a percentage of total area); (b) absolute increase in this value with filling of depressions; (c) percentage of hillslope area draining >1 % of the slope; (d) absolute increase in this value as a result of filling depressions.

Finally, Figure 5.51 shows the variation of MDS between the hillslopes. Upper Nogalte recorded the lowest maximum depression storage, followed by Cardenas, with Del Prado therefore storing the largest depth of water on the soil surface. The 1 m resolution Cardenas hillslope (with fewer missing values compared to its 25 cm resolution counterpart; Figure 5.48) recorded a larger MDS than the original Cardenas hillslope despite this larger grid-size. These values of MDS are slightly higher than would be expected from the plot scale results. Figure 5.52 shows that the presence of particularly deep surface depressions (up to 1 m deep for the Del Prado site) as a result of hillslope-scale concavities could be one explanation for this increase in MDS with scale. Therefore, it seems that surface depression storage, like roughness, occurs at many scales in the landscape. This suggestion is discussed further in the following chapter.

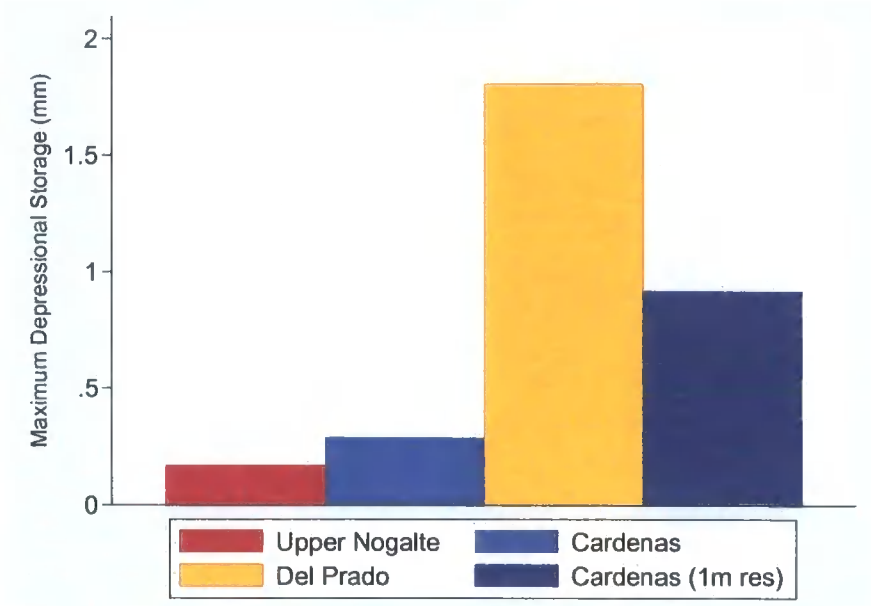

Figure 5.51. Maximum Depressional Storage (mm) for each hillslope.

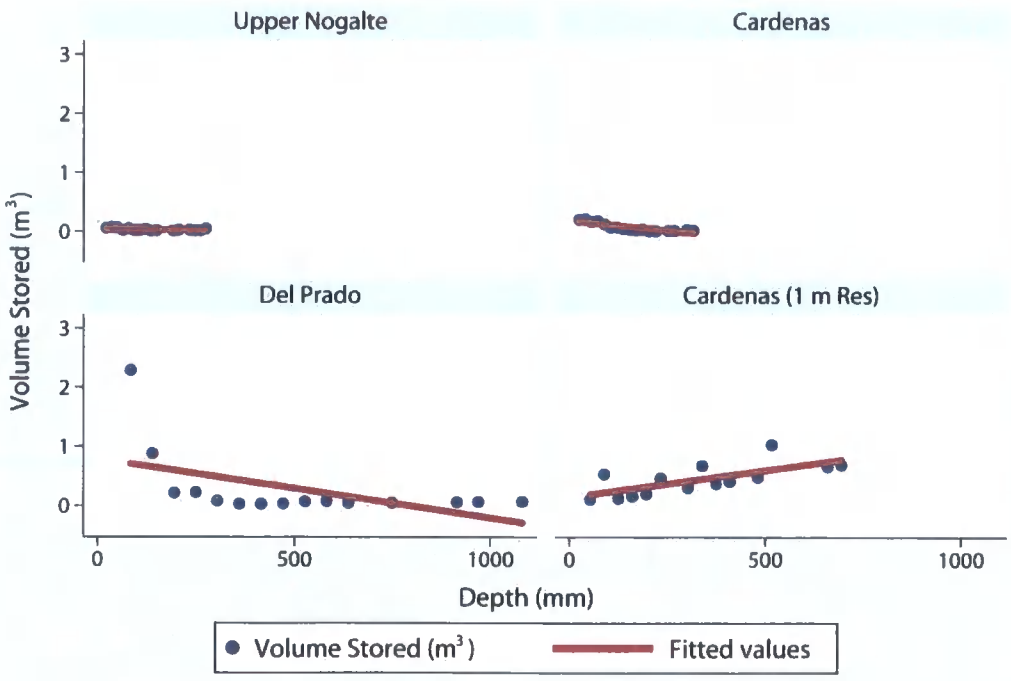

Figure 5.52. Relationship between volume of water stored (m^3) and depth of water (mm) for each hillslope.

5.8 Conclusion

The fine-scale hydrological characteristics of natural soil surfaces can be analysed using high-resolution scans obtained in the field. In particular, this chapter has focused on the dual effects of microtopography and general slope (i.e. surface roughness at two distinct scales) on MDS, flow directions and flow concentration. Such analyses provide us with an appreciation of the gradual downslope organisation of surface runoff into flow concentrations and rills on natural soil surfaces. Moreover, this chapter considered how infiltration properties of the soil varied between individual elements of roughness within each plot. The results presented in this chapter, considered alongside the variation of several aspects of surface roughness between surfaces (presented in chapter 4) provide an indication of how surface roughness influences these processes.

The variation of sediment transport and hillslope runoff across each hillslope demonstrates how surface processes vary at the hillslope-scale in relation to the upslope contributing area (determined by both upslope area and microtopography). Surface flow directions and concentration has also been considered at this scale; these can be considered in conjunction with hillslope surface roughness measures (discussed in section 4.6). Chapter 6 now provides this necessary synthesis of results presented in the previous two chapters.

Chapter 6 Discussion

6.1 Introduction

As the overall aim of this investigation is to assess the influence of soil surface roughness upon hydrological processes, one purpose of this chapter is to combine the results from the preceding two chapters. Figure 6.1 provides a brief summary of how measures of surface roughness can be used to enhance our understanding of runoff generation and sediment transport at the hillslope scale.

Surface roughness can be described in a variety of ways. Chapter 4 applied a variety of methods of characterising soil surface form and examined how results varied between plots and hillslopes. One application of such a variety of 'roughness measures' is to provide a more detailed terrain analysis. Chapter 5 then investigated the small-scale hydrological processes operating at each plot, focusing on the influence of surface roughness on depression storage, runoff routing and infiltration. Section 6.2 attempts to use observations of surface form as indicators of these less-measurable parameters (Le Bissonnais *et al.*, 2005). Identification of these aspects of surface roughness that influence these hydrological processes at the plot scale would improve our understanding of the relevant attributes of surface roughness to parameterise in the modelling of hillslope hydrological processes.

The classification of soil surfaces into Morphological Runoff Zones (MRZs) used throughout this investigation provided a rapid method of identifying the processes acting on the soil surface through a qualitative visual analysis of soil surface features. This system was used to sample the range of surface features found at each hillslope. Although this classification of an entire hillslope surface into just six 'plot-types' is rather crude, it permits a hillslope-scale analysis of hydrological processes. However, these 'plot-types' are distributed over the hillslopes in a manner that will determine the hydrological response to any particular rainfall event. In addition, the large-scale hillslope surface form (examined in section 4.6) will influence the distribution of these plot-types through hillslope-scale surface processes (examined in section 5.7).

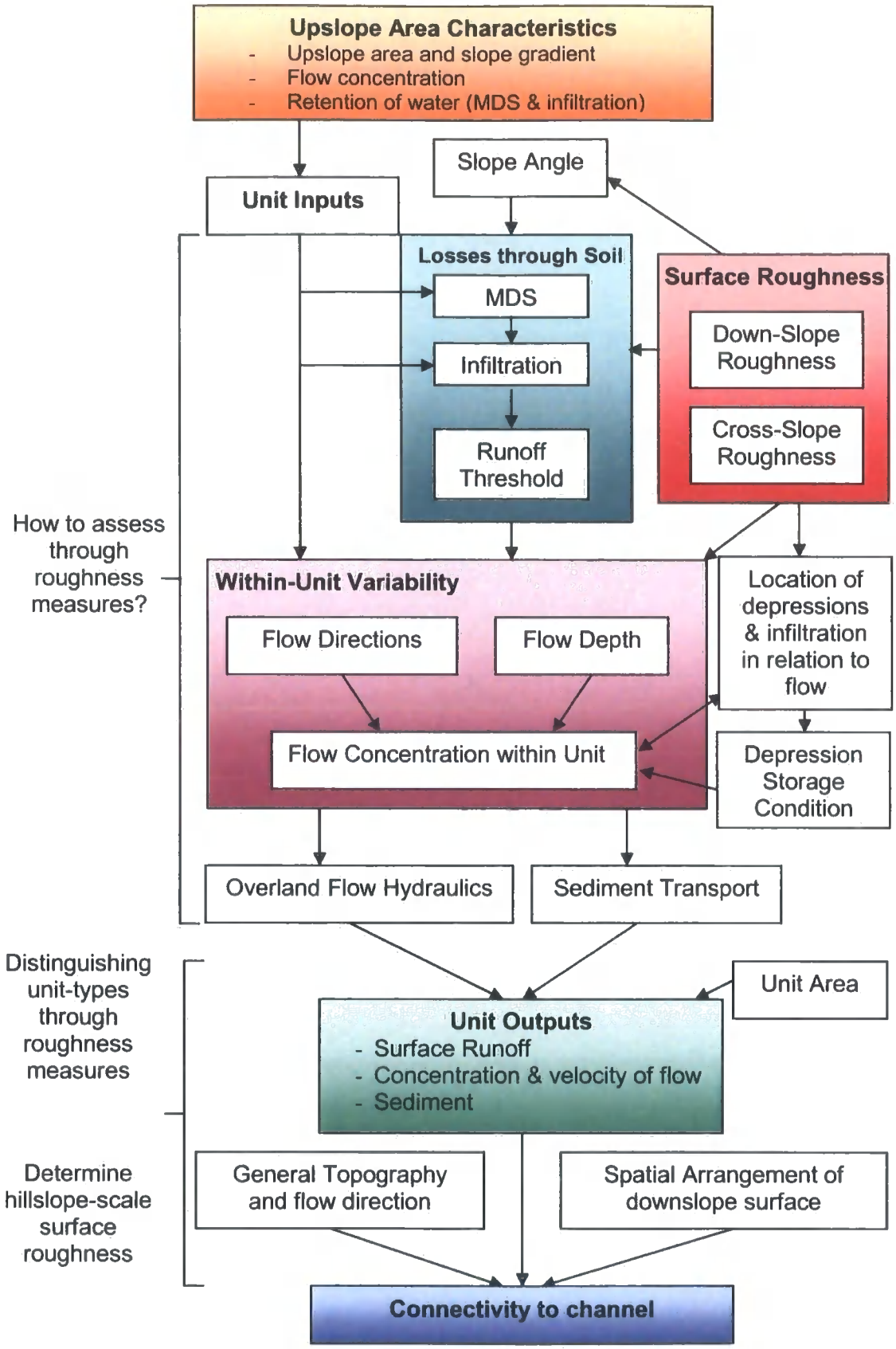

Figure 6.1. How measures of surface roughness can be used to assess hydrological processes operating over a hillslope. Each plot-type is considered a homogeneous 'unit'.

Section 6.3 describes how these plot-types (or 'units') are distributed across each hillslope and provides a discussion of the effects of the spatial configuration of surface roughness elements on the hydrological and sedimentological connectivity of the hillslopes. Finally, section 6.4 considers the limitations of the present study, suggesting potential directions for further research.

6.2 Relating Process to Form

As has already been noted, there are many ways in which to characterise a rough surface. Each will highlight or extract a specific attribute of that surface and must necessarily neglect others. This investigation has attempted to inductively compare the utility of numerous roughness measures in common usage for representing particular surface features relevant to several hydrological processes operating on soil surfaces. These results have been complicated by the realisation that, if we define microtopography as a measure of topographic deviation from a linear plane, this microtopography will have a different effect on any one surface hydrological process depending on the context of this deviation. For example, a 'positive' element of roughness (above the plane) may cause surface water ponding behind it if the local topographic conditions are appropriate. Alternatively, it may cause water to flow around it, leading to flow concentrations and eventually, surface incision. These two possibilities have directly opposing consequences for the hydrological response of the surface.

This is where the application of 'Morphological Runoff Zones' may prove crucial for further investigation. The categorisation of hillslopes into areas corresponding to the processes which can be seen to be operating on the soil surface is essential as this provides the context within which variations in soil surface roughness can be examined. Soil surface roughness on natural surfaces in semi-arid environments is quite different from that (intensively studied) roughness seen on tilled plots in America and north-western Europe (e.g. Currence & Lovely, 1970; Onstad, 1984). There, increased roughness generally suggests increased surface water storage, both because of the particular surface-context of that increased roughness and also because of the statistical treatments undertaken to divorce the surface roughness 'measurement' from the form of the actual surface (through the removal of 'oriented roughness' and effective rotation of

surfaces). Such a straight forward relationship between surface roughness and surface process has not been discovered on the natural surfaces investigated in this project.

On the semi-arid natural soil surfaces examined in this study, different processes are operating. Assuming Hortonian overland flow as the dominant process, rainfall is infiltrating into the soil surface, being stored in surface depressions, or both, or is becoming runoff and being routed downslope in a flowpath determined by surface topography (or roughness, depending on the scale of enquiry) at all scales (from individual grains to hillslope-scale variation). The width and depth of this flowing water and its velocity will mostly determine the sediment transport capacity of the runoff. As the concentration of water in linear channel features is of fundamental importance to these processes, the removal of 'oriented roughness' elements is an unwelcome step in this analysis.

Table 2.1 demonstrated that distinct surface features can be identified at each MRZ. Therefore, the spatial distribution of these robust descriptors over a hillslope surface may be easily mapped in a cost-effective and reproducible way (Le Bissonnais *et al.*, 2005). Moreover, an increased value of a surface roughness measurement within a MRZ is likely to produce a more consistent change in hydrological process (although this clearly depends on the roughness measure). For example, increased roughness at MRZ 4 is more likely to suggest increased flow incision (with enhanced flow concentration and decreased MDS) whereas increased roughness at MRZ 1 may signify greater topographic variability as a result of raindrop impact and grain roughness (and increased MDS). Although only 2-3 plots of each MRZ were considered, it appears that increased roughness leads to increased MDS at MRZ 1 and the ploughed plots, whereas the reverse is true for the other plot-types (with no obvious trend seen at the ploughed plots). Therefore, surface roughness measures are not immediately related to surface process when considered across a wide range of process environments.

Such an argument must also consider the different methods of characterising surface roughness. The 'downslope pit density' measures a property of the soil surface that is hardly unique to each 'process environment'. As such, this particular measure shows a strong relationship with MDS over the entire range of surfaces (and so is useful for examining surface process through analysis of surface form - see the top-half of Figure

6.1). This demonstrates an alternative approach to the measurement of soil surface roughness: the use of highly specific roughness measures that may be applied over a wide range of surfaces.

Relationships between surface roughness measures and surface hydrological processes were examined empirically using correlation analysis; the full results of this can be found in the Appendix (Tables A1 – A3). MDS was best correlated with the pit density as measured in the downslope direction (at $P < 0.005$) (Figure 6.2) followed by 5% trim mean Nearest Neighbour and downslope tortuosity (T_B) (both at $P < 0.01$). Similarly pit count downslope, mean NN and the 'standard deviation of T_B' showed significantly strong correlations with MDS. The correlation with the 'standard deviation of slope angles' measure was also significant ($P < 0.05$).

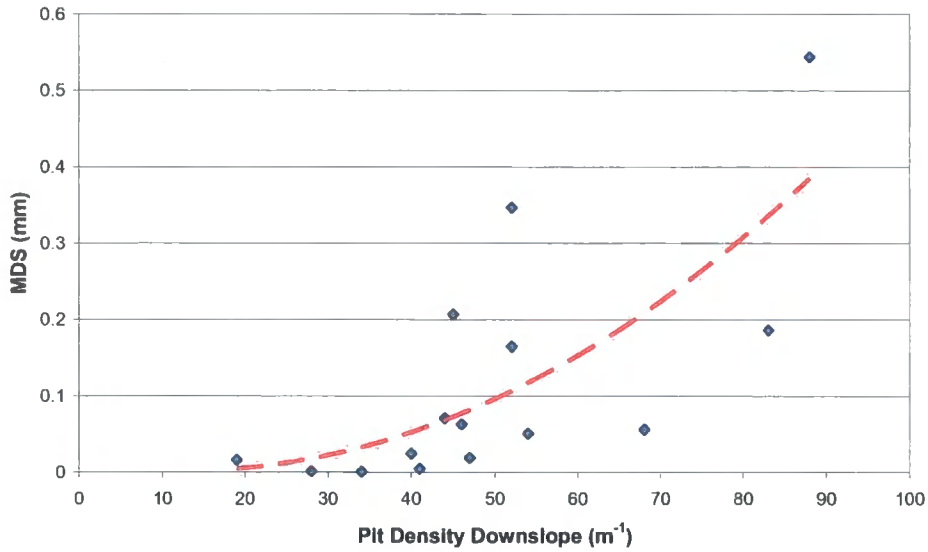

Figure 6.2. The relationship between Maximum Depressional Storage (mm) and pit density as measured in the downslope direction (m^{-1}).

The detrended *MDS* values showed very few significant correlations with the methods of surface characterisation emphasising its standing as an abstract property divorced from the actual surface form. Only pit count and density measured in the cross-slope direction ($P < 0.005$) displayed any significant correlation. This is likely to reflect the concentration of flow into small channels which fill upon surface rotation. Indeed whether to remove the general slope trend before calculation of roughness measures remains a problem. The percentage of flow in a downslope direction was, naturally, influenced by all the roughness measures encompassing the general plot slope (as general slope controls the anisotropy of local flow conditions). However, a strong

negative correlation exists between this and the percent of the surface morphometrically classified as a 'pass' (section 4.5.2). This simply represents the case that such a pass will interrupt downslope flowpaths. A ratio of general slope to local height variation, proposed by Darboux *et al.* (2002), would provide a useful tool to determine the dominant influence on flow direction.

The general plot slope also had an effect on the upslope area measurements which were particularly poorly correlated with the roughness measures used in this study. However, the increase in maximum upslope area (and percentage of the plot draining greater than 1 % of the area) with the filling of depressions was negatively related to all the slope-dependent terms (as increasing slope decreases the effect of depressions) and positively related to the percentage of the surface morphometrically identified as a peak, pass or pit (with $P < 0.005$). Each of these morphometric forms represents an interruption of linear channel, plane or ridge features. Such relationships present a dilemma: should the general slope be removed before the calculation of roughness measures, or should it be included to reflect its influence on MDS, flow patterns and other surface processes? The answer, as ever, depends on which particular element of surface roughness is of interest, but as the division between the slope-element and microtopographic-element of surface roughness is only a matter of scale, careful contemplation of the reasons and consequences is necessary before any such isolation of a specific 'wavelength' of roughness.

This study applied a combination of both profile-based and surface-based roughness measures to a wide range of soil surfaces. In general, the surface-based measures presented stronger associations with the hydrological properties of the surfaces than the measures taken from profiles. In particular the 'Nearest Neighbour' group of statistics provided many interesting relationships and so appeared to measure a hydrologically-relevant attribute of the surfaces. As the terrestrial laser scanner used in this investigation produces data in the form of point clouds, the calculation of such surface-based methods was relatively unproblematic as the resulting data can be exported directly into GIS, CAD or remote sensing software (Rosser *et al.*, in press).

However, the major shortcoming of a surface-based approach is that it fails to separate surface roughness into its directional components (down-stream and cross-stream,

approximated here by down-slope and cross-slope). Results displayed in chapter 4 suggest that this division is of the utmost importance, as each component considers separate elements of hillslope surface hydrology. Downslope-oriented transects are particularly relevant for the study of surface depression storage. This is reflected in the strong correlations between MDS and both tortuosity and pit density as measured in this direction (amongst others). Such relationships were not found for the cross-slope transects; these measures (particularly tortuosity and standard deviation of elevation) were well correlated (at $P < 0.025$ and < 0.005 respectively) with the percentage of flow that was not in a directly downslope direction. This provides an approximation of the degree of flow convergence occurring over a rough surface as the higher this value, the greater the organisation of surface runoff into flow concentrations.

The mean depth infiltrated and mean unsaturated hydraulic conductivity of the plots showed no significant relationships with any measures of surface roughness. However, the standard deviation of the amount infiltrated was related to the downslope pit density, the mean (and standard deviation of) downslope tortuosity and the mean 'combined direction' tortuosity with $P < 0.05$. This was irrespective of whether the general surface slope was removed. Each of the nearest neighbour measures and also the MDS of the surface were related to the standard deviation of the amount infiltrated with $P < 0.025$.

The square-root of semi-variance at 0.5 m, surface fractal dimension and surface tortuosity proved useful for an entirely different reason. Although not specifically related to any hydrological processes (beyond reasonably strong correlations with MDS), Figures 4.10, 4.21 and 4.24 show that they varied considerably and consistently between each plot-type examined. The progressive tendency for incision by Hortonian overland flow in the downslope direction is represented by a downslope increase in each of these surface roughness measures. Therefore, these roughness measures may be useful for distinguishing the distribution of plot-types across a hillslope (see the bottom-half of Figure 6.1). However, no universal 'surface tortuosity threshold' can be applied to quantitatively define MRZs across all semi-arid hillslopes, as each hillslope contains different soil-types which (as a function of soil texture, chemistry and surface rock fragment cover, for example) have individual thresholds of tortuosity at the transition between MRZs (Figure 4.21). Moreover, the variation within each unit (as seen, for example in the spread of profile tortuosity values in Figure 4.8) demonstrates the

difficulty of identifying a single threshold. The following section discusses the significance of identifying the spatial configuration of the different plot-types (or relatively homogeneous 'units') across a hillslope.

6.3 Hillslope Hydrological Response

The analysis presented above considers the effect of soil surface microtopography on runoff generation. Although it has been observed that soil microtopography influences surface water storage, infiltration patterns, flow patterns and the connectivity of runoff (Auzet *et al.*, 2005), thus far, the analysis has been restricted to the effect on the hydrological processes operating at the plot scale. However, in order to shed light on effective management strategies a broader perspective is necessary. An increase in scale from confined plots to the hillslope provides many challenges; assumptions of uniform distribution of depression storage down hillslopes have already been shown to be inaccurate. The question remains, how much of this observed hillslope-scale complexity and heterogeneity needs to be included in a predictive model? Although the one-dimensional water balance (limited to MDS and infiltration in this study) is particularly important in semi-arid areas, interactions and feedbacks in these processes occur over the hillslope.

An understanding of relationships between soil surface roughness and processes of runoff and sediment production at scales larger than the plot is absolutely necessary for the development of a process-based erosion model (Huang *et al.*, 2001). Therefore the soil surfaces of each hillslope were strategically sampled; each plot was located in a separate 'Morphological Runoff Zone' (as defined by Bracken & Kirkby, 2005) which therefore considers the entire range of surface conditions. In effect, this identified units of relatively homogenous soil surface morphology within each hillslope, providing a method of scaling-up to the hillslope through the consideration of fine-scale surface roughness. The analysis of each 'unit' has not been restricted to vertical water exchanges; in addition to MDS and infiltration, the propensity for flow convergence or divergence has been considered. Therefore, this provides some appreciation of the contribution of each unit to both the reduction (or increase) in water volume by the unit downslope boundary and how concentrated this unit outflow will become.

Reasonably consistent patterns between MRZs on different hillslopes have been observed (chapter 5), however this remains insufficient if we wish to effectively predict hillslope response. The overall interdependence of each unit is governed by their spatial configuration across a hillslope. The connection of each unit to the channel system will be a decisive factor in determining the geomorphic and hydrologic response of the hillslopes (Cammeraat, 2002).

Where a unit of low MDS and infiltration and high flow concentration is found adjacent to an area of concentrated flow (such as a small tributary), then a high percentage of the generated runoff will flow off the slope (the area is both 'active' and contributing to hillslope output). However, if an area of high MDS and infiltration which tends to cause run-on to disperse is found downslope of this unit (in the general flow direction), then the runoff will tend to be reabsorbed into the soil (the area is hydrologically 'active' yet remains spatially 'isolated') (Ambroise, 2003). Run-on and horizontal connections between units in the context of general slope morphology (particularly upslope contributing area) are critical to runoff generation. Depressions found near the top of slopes (or on microtopographic ridges) will take longer to fill and so the area contributing to runoff flux (i.e. connected to the defined 'outflow boundary' - Darboux *et al.*, 2001a) will rarely reach the very edge of the drainage divide.

Figure 6.3 demonstrates the relationship between the downslope distance from the drainage divide of each MRZ and the general slope for data combined from all three hillslopes. The superimposed parallel lines represent the upslope boundary of each MRZ (based on the general trend of the dataset). It is clear from this that each MRZ is found in a different sector of this graph. The only exception is that the MRZ 3 data is spread across the sector where MRZ 4 would be expected. This demonstrates a shortcoming of reducing the issue of MRZ threshold down to the distance from the drainage divide. As this study was not limited to areas within large-scale concavities, where little flow concentration from hillslope concavities occurs, rills are less likely to incise. This lack of appreciation of large-scale topographic roughness has the effect of increasing the scatter seen in Figure 6.3.

The scatter of points will also be influenced by the soil chemical and physical properties of each hillslope. Figure 6.4 separates the data into the three sites considered in this

study. The wide distribution of distance from the drainage divide for MRZs 2 and 3 seen for the Upper Nogalte site can partly be attributed to a ploughed band cutting across the hillslope disrupting the natural distribution of MRZs. Figure 6.4b shows that once flow concentration occurs at the Cardenas site, rill incision is fairly rapid (potentially as a result of strong surface crust formation). The Del Prado hillslope, however, shows strong zonation of the MRZs within the graph space.

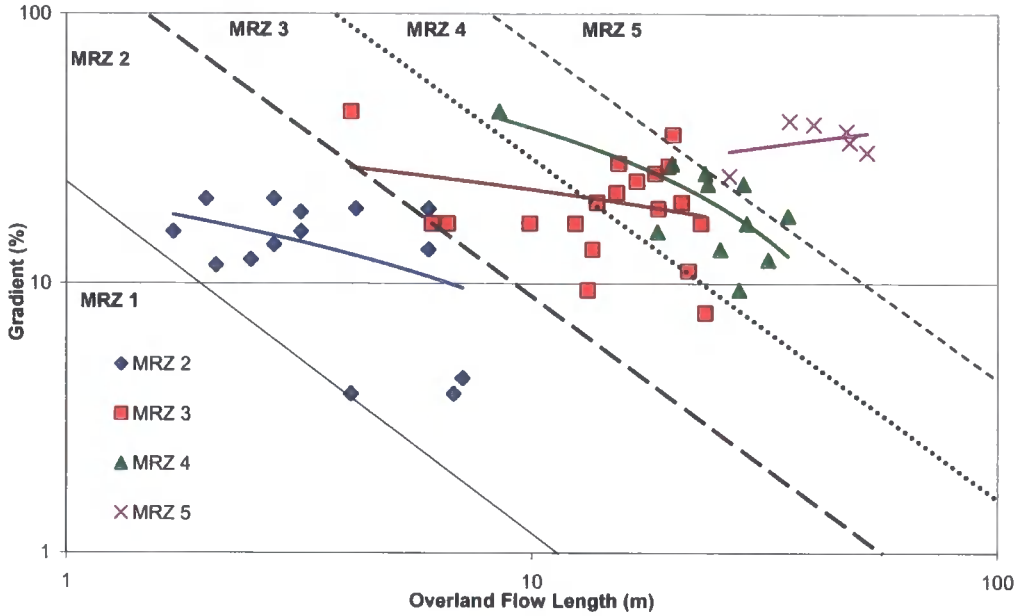

Figure 6.3. Thresholds of MRZs for the entire dataset, based on distance from the drainage divide (m) and slope gradient (%). Superimposed parallel lines are only an approximation for the purposes of clarity.

The slope-distance thresholds of each hillslope unit make no consideration of the spatial arrangement of these units. The distribution of each unit was mapped at each hillslope and can be seen in Figures 6.5-6.7. When analysed alongside general hillslope surface roughness (section 4.6) and flow patterns (found in Figure 5.45), and the individual unit hydrological characteristics, these maps provide a greater level of understanding of the responsiveness of each hillslope to a rainfall event. The planar area of each MRZ (as a percentage of the total hillslope area) is displayed in Table 6.1.

The next section provides a detailed analysis of the effect of the spatial configuration of units (MRZs and ploughed areas) on the connectivity of the Upper Nogalte hillslope to a tributary channel located at its base. The following sections discuss the key differences between the Cardenas and Del Prado hillslopes and this observed pattern.

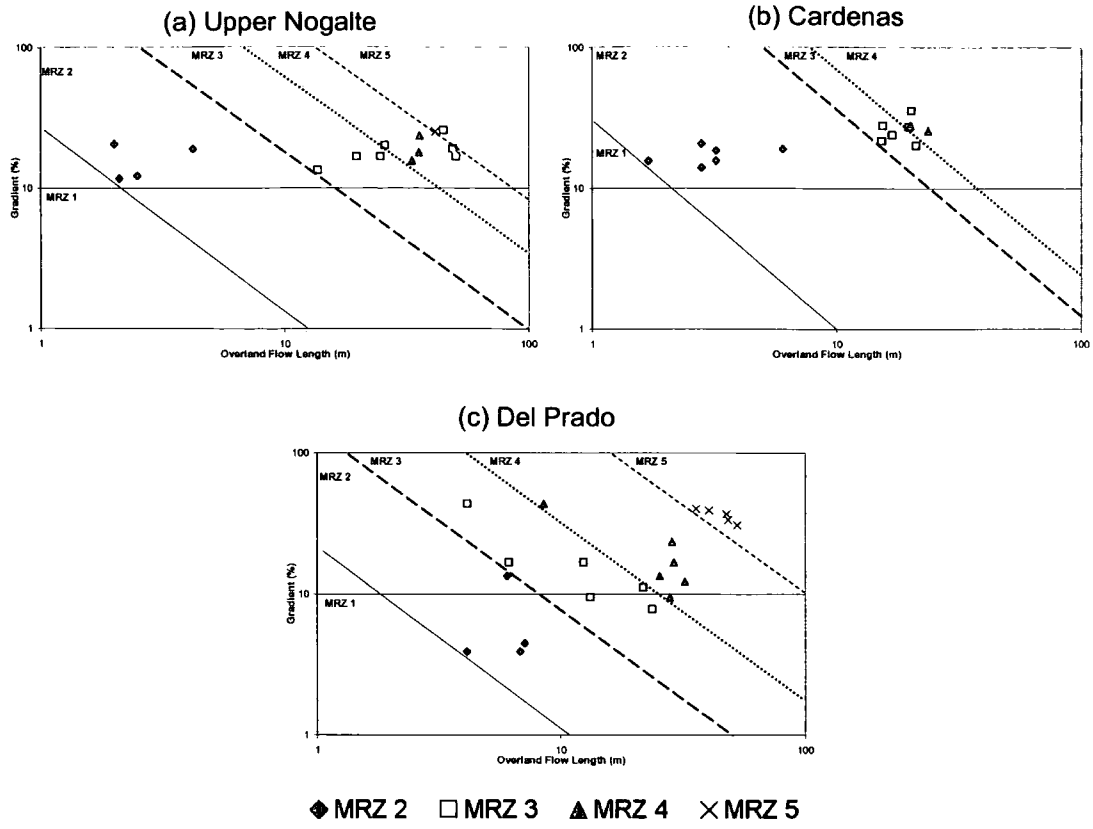

Figure 6.4. Thresholds of MRZs for each hillslope, based on distance from the drainage divide (m) and slope gradient (%): (a) Upper Nogalte, (b) Cardenas, (c) Del Prado.

	Upper Nogalte (%)	*Cardenas (%)*	*Del Prado (%)*
MRZ 1	5.45	4.70	17.12
MRZ 2	32.63	25.84	29.64
MRZ 3	22.52	12.56	20.80
MRZ 4	3.68	3.79	16.95
MRZ 5	3.24		15.49
Ploughed	32.48	53.12	

Table 6.1. Percentage planar area of each hillslope covered with each 'unit' or plot-type.

6.3.1 Upper Nogalte Hillslope

Figure 5.48a shows that the drainage network of this hillslope is linear as parallel flow lines show only few areas of convergence at the bottom edge of the slope. Therefore, very little topographic flow concentration occurs at this hillslope; the general flow direction is from the red area of MRZ 1 (top-right of Figure 6.5) to the tributary channel (bottom-left).

MRZ 1

From Figure 6.5 it is clear that only a thin band of plot-type MRZ 1 can be found at the very top of the slope (accounting for only 5 % of the total hillslope area). The relatively high MDS and low infiltration rate of this unit is not particularly important at the hillslope scale because of the dual characteristics of the low total area and distance of this area from the main channel. The low general slope of this unit causes the flow directions to be more evenly spread over 360°. Each roughness measure shows that this unit experiences only slight topographic variability, and so any flow over these areas will be of a relatively uniform depth. Although a moderate level of flow concentration was seen to take place through this unit, the resulting sediment transport capacity is balanced by the assumed low level of hillslope runoff at the drainage divide compared with the stabilising influence of diffusive rainsplash.

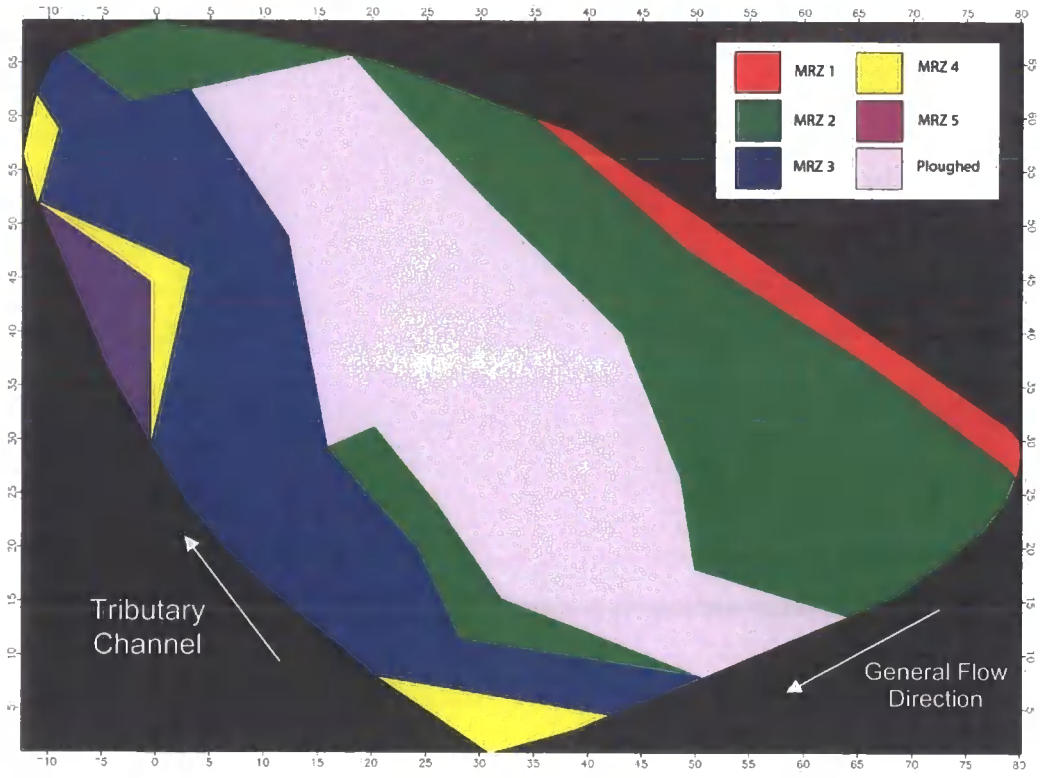

Figure 6.5. Spatial configuration of units over the Upper Nogalte hillslope.

MRZ 2

The MRZ 2 unit, on the other hand, comprises over 33 % of the hillslope area and will therefore have a larger influence on the hydrologic response of the hillslope. Over this unit MDS was negligible; therefore much of the Upper Nogalte hillslope traps no

surface water. This can be associated with the tendency for steep slopes (up to 20°) over this part of the hillslope. Despite the low capacity for surface storage, this unit infiltrated larger amounts of water than the rest of the hillslope (with a less dominant effect of the declining term). Indeed, the high unsaturated hydraulic conductivity distinguishes this unit from the remainder of the hillslope. The infiltration curve followed the pattern of Figure 5.29 with no major decline in infiltration rate after the first 30 s of infiltration.

Flow over the MRZ 2 unit was seen to be dominantly downslope (Figure 5.13b); unfortunately no maximum flow depths were recorded for this unit. A relatively low sediment transport rate (89 cm^3m^{-1}) was recorded, suggesting that little flow was occurring over this plot type (most likely a result of the low upslope area). While no single cell dominated the flow concentration (Figure 5.25) a large percentage area of the plot drained over 1 % of the plot (Figure 5.26). Therefore, much of the unit area will be in contact with any flow that occurs. Given the low MDS (which ponds water, increasing contact time for infiltration) and high infiltration rate, such spatial distribution of infiltration is particularly significant. Although roughness measures indicate that little topographic variability is present within this plot-type, total infiltration amount and k were lower on the wash deposit features characteristic of this unit (Figure 5.36). The remainder of the surface (which is relatively lower-lying and so more likely to encounter runoff) demonstrates a higher infiltration rate, increasing what could be considered the 'effective infiltration rate' of this unit. Despite the propensity of this unit for infiltration, the low MDS and reasonable capacity for concentrating flow suggest that it may act as an effective contributing area for the units further downslope.

Ploughed

The potential contributing area effect has been somewhat regulated at the Upper Nogalte hillslope by the presence of a large ploughed strip across the entire hillslope, which accounts for 32 % of the total slope area. At the widest point it extends for 25 m in the downslope direction. Most roughness measures record a moderate amount of surface topographic roughness for this unit, at a similar level to that at the onset of flow concentration. However, downslope-roughness was dominant over the cross-slope roughness component and so the major influence of this ploughed band is through a MDS which is over five times greater than any other unit. Much of the water received

from upslope areas will become trapped behind these ploughing ridges. Figure 5.6 shows that most water that is trapped on this surface is stored at an average depth of 10 mm (which is particularly deep in comparison to the other surfaces used in this study). As Figure 5.3 shows, this water storage is a direct result of ploughing ridges parallel to contour lines. This figure also shows that some ridges are more effective at holding back water against the general slope direction than others.

The ploughed unit showed a larger downslope flow direction percentage than other plots as little cross-slope flow concentration in small channels is taking place. This unit showed a large maximum upslope contributing area and percentage of the plot draining over 1 % of the area (Figures 5.25 and 5.26), but much of this was found to be an artefact of the depression filling (Figures 5.27 and 5.28), demonstrating the influence of the attainment of MDS on surface flow dynamics at this part of the hillslope.

Although MDS was high at this unit, the infiltration rate was the lowest recorded at this hillslope (Figure 5.33). In particular, both k and total amount infiltrated were much lower in the furrow bottoms. The low unsaturated hydraulic conductivity suggests the dominance of the declining term in equation 2.1, with a cumulative infiltration curve in the form of Figure 5.32. Obviously some property of the surface layer, potentially the depositional crust suggested by Fox *et al.* (1998a), causes a reduction of the infiltration rate within the first seconds of infiltration. Conversely, the high points within the plot experienced faster infiltration rates. Therefore, at this unit there is a definite relationship between microtopographic height and at-a-point infiltration. As a consequence, the effective infiltration rate of the unit will increase as flow depth increases and runoff overtops the plough ridges.

MRZ 3

Although at one side there is a thin strip of MRZ 2 below the ploughed area, in general the next area downstream is classified as MRZ 3. In some cases this unit extends to the tributary channel at the bottom of the slope. This downslope location combined with the large surface area (23 % of the hillslope) and generally steep slopes (around 20°) suggests that this unit is the most important for the hydrological response of the Upper Nogalte hillslope. Only a small depth of water storage (4.2×10^{-3} mm) was exhibited by this unit, but the infiltration rate is reasonably high (similar to MRZ 2). The total

amount infiltrated is higher out of the flow concentrations identified in the field; therefore, where most water will flow (and where most depressions have been identified), the infiltration rate is lowest.

Indeed, flow concentration is a characteristic of this unit as surface flow converges around microtopography. There is a much greater influence of the non-downslope flow directions (Figure 5.20), and over a third of the measured plot drains through one cell. This maximum upslope area is heavily influenced by the state of the depressions (Figure 5.27) and so these are mostly found in the flow concentrations themselves. There is also a large percentage of the plot draining over 1 % of its area, as no single area of flow concentration has dominated at this point of the hillslope.

As this unit of the hillslope demonstrates flow concentration, the spatial distribution of MDS and infiltration in relation to surface microtopography and flow depth (the microhydraulics of overland flow) becomes critical. The maximum runoff depth measured at this unit was 3 cm. This was measured in a flow concentration, but it is difficult to apply this single value to a field situation. Figure 6.6 interprets this maximum depth recording as the depth found from the bottom of each major flow concentration (although this generates an uneven flow depth across the surface). Figure 6.6a shows that near the top of the measured plot, a depth of approximately 3 cm in major flow concentrations inundates most of the surface (both elements of infiltration are submerged and therefore 'active'). Figure 6.6b, however, shows a second cross-slope transect (taken at the downslope boundary of the plot) and shows that significant 'micropiracy' has occurred over this short distance (Dunne *et al.*, 1995). One single flow concentration dominates the cross-profile, and only the very bottom of this channel experiences flow at 3 cm (and so the 'flow concentration' component of infiltration will be dominant). This transition has also been captured in Figure 5.24.

That a maximum flow depth of 3 cm was experienced in both transects is an assumption unlikely to hold true. However, from this example it is clear that there is much variability present within this unit. Flow incision is a gradual process and as such, the division of MRZ 3 and MRZ 4 is somewhat arbitrary. Figure 6.6a shows a much higher 'wet tortuosity' than Figure 6.6b and so the flow velocity will be retarded by the friction of the increased contact with the soil surface (Takken & Govers, 2000), increasing the

potential for infiltration. Moreover, this example demonstrates the relationship between a situation dominated by 'grain roughness' (Figure 6.6a) and one dominated by 'form roughness' (Figure 6.6b) and how these can both occur within a short distance of each other. Such rapid variability in the hydraulics of overland flow is of considerable importance in hydraulic and erosion models for the routing of runoff over the land surface, and for calculation of the erosivity and transport capacity of flow.

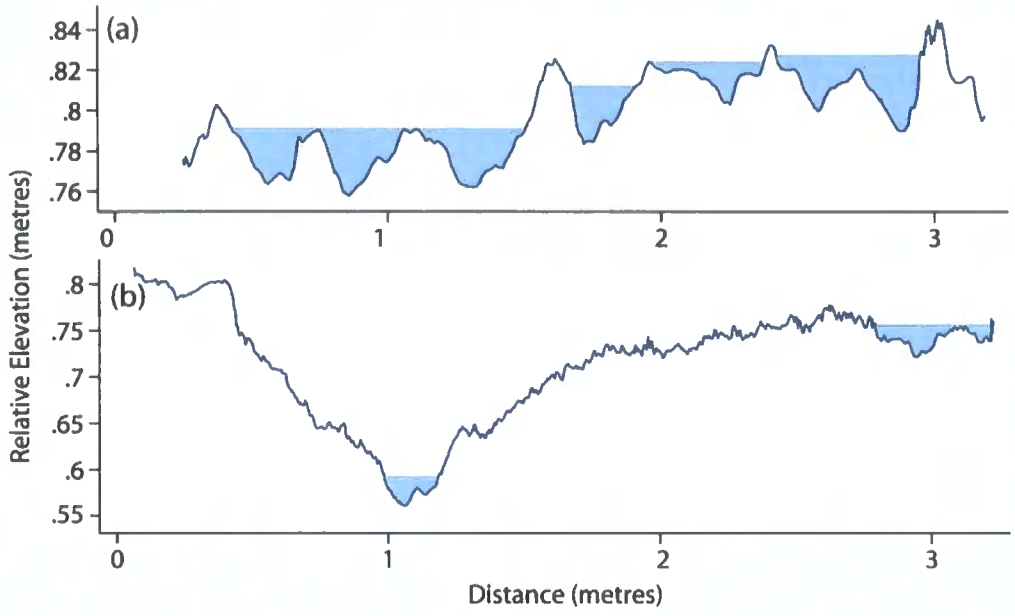

Figure 6.6. Variation in flow distribution on actual cross-slope profiles taken from the plot Upper Nogalte MRZ 3: (a) near the top of the plot; (b) near the bottom of the plot. The blue fill represents the 3 cm flow depth measured in the field (arbitrarily measured from the deepest point of significant cross-graded points on the transect).

Such rapid variation in hydraulic parameters might explain the large range of sediment transport values recorded for this unit. Considering the critical shear stress threshold for mobilisation, the local increase in maximum flow depth may be sufficient to render the flow competent for transport. Thus, the sediment transport equation is intimately related to soil microtopography and its effect on flow concentration (Dunne *et al.*, 1995). The sprayed line placed on the sidewall of a concavity experienced significantly more sediment movement than the other lines (Table 5.5). Bag sediment weight was high (for this hillslope), mostly comprising large particles but also a wide variety of particle-size

distributions (Figure 5.46a). This site also experienced a large range in weights trapped, most probably reflecting the range of process environments found within this unit.

MRZ 4

Only 4 % of the Upper Nogalte hillslope was classified as MRZ 4, but this is located by the downslope boundary of the hill. It would appear, from Figure 6.5, that the presence of the ploughed band combined with the parallel drainage pattern of the hillslope is actively preventing the incision of rills as the only areas where MRZ 4 (and 5) appear are where the ploughed unit is thinnest or is absent (as can be seen by the spread of the MRZ 3 boundaries in Figures 6.3 and 6.4). MRZ 4 holds back slightly more water than MRZ 2 or 3 despite demonstrating similar general slope angles. The unsaturated hydraulic conductivity is relatively low (fast initial infiltration), with a mid-range total amount infiltrated compared with the other units found on this hillslope. Although the sprayed line at this plot recorded a reasonably high sediment transport capacity (337 cm^3m^{-1}), only a low weight of sediment was trapped (mostly fines).

This unit demonstrates a high maximum upslope area but a low percentage area draining over 1 % of the plot. Therefore, flow is concentrated into a small area, suggesting a greater organisation of the surface. The strong influence of depression-filling on the maximum upslope area (Figure 5.27) suggests that much of the MDS is found at the rill bottoms. The generally high values of the roughness measures for this plot show that microtopography has a large influence in this unit. This is reflected in the distribution of infiltration rates. Both k and total amount infiltrated are considerably lower in the rill bottoms. Therefore, these areas experience fast initial infiltration, which slows dramatically after only a few seconds. The cross-sections of this plot reveal that the rill is deeper than 15 cm, whereas the maximum flow-depth seen over the monitoring period was just 5 cm, suggesting a situation resembling Figure 6.6b. Once again, a substantial proportion of the runoff contact with this surface will be made on a surface with a low infiltration rate but a reasonable capacity for surface water storage.

The downslope location of the MRZ 4 unit is determined in part by the slope-area threshold for rill incision, but also partly by upslope microtopography and its effect on MDS, infiltration and flow concentration. Although the unit itself has only a modest MDS and demonstrates low infiltration, it can be found over only a small area of the

hillslope. However, its tendency to further concentrate the flow from the MRZ 3 above (which was already fairly concentrated) and its connectivity to the tributary channel at the foot of the hillslope, suggests that this unit is extremely effective at transferring runoff downslope.

MRZ 5

Finally, evidence of gullying was found over only 3 % of the Upper Nogalte hillslope between areas of MRZ 4 and the downslope boundary. The reasonably high MDS at this unit was a result of a few depressions along the boundaries of the gully bottom. The contributing area measurements were disrupted by the poor data resolution in the gully bottoms; it would seem that flow was not as concentrated as at MRZ 4 due to the wide, flat gully bottom. However it is somewhat unreasonable to suggest that a 3 m by 3 m plot is a fair representation of the flow concentration caused by gullying. The extreme roughness measurements found at each of the MRZ 5 plots suggest that gullies represent morphological variation at a broader scale than that which has been considered at each of the other plot-types. Runoff over MRZ 5 only appears less organised than MRZ 4 at this scale of enquiry; such features exist at a scale larger than the plot.

High infiltration rates were found at this site, but greater infiltration occurred in the gully bottoms than on the surrounding soil surfaces. This is perhaps related to the deposition of fines by flowing water in the gully bottom, or loose poorly compacted soil as a result of sidewall collapse. Either way, such a high infiltration rate in the gully bottom will reduce the connectivity of water flowing from upslope to the tributary stream. However, such an effect will be limited by the depth (and velocity) of water flowing in the gully bottom. Unfortunately, no such measurements could be made at this plot.

6.3.2 Cardenas Hillslope

The spatial arrangement of each MRZ at the Cardenas hillslope can be seen in Figure 6.7. The first major difference between this slope and Upper Nogalte is that the hillslope is of a bowl-shape with a central flow concentration (as identified in Figure 6.7). Therefore, the dominant flow direction of this hillslope is towards this concavity (as seen in Figure 5.45). The slopes of this bowl-shaped hillslope are generally steeper than the other hillslopes (as reflected in the elevation range and general surface standard

deviation measures of Figure 4.34). One side of this bowl-shaped depression (53 % of the hillslope surface) has been ploughed for almond cropping, whereas the other side is natural matorral and displays a transition from MRZ 1 to MRZ 4 with increasing distance downslope.

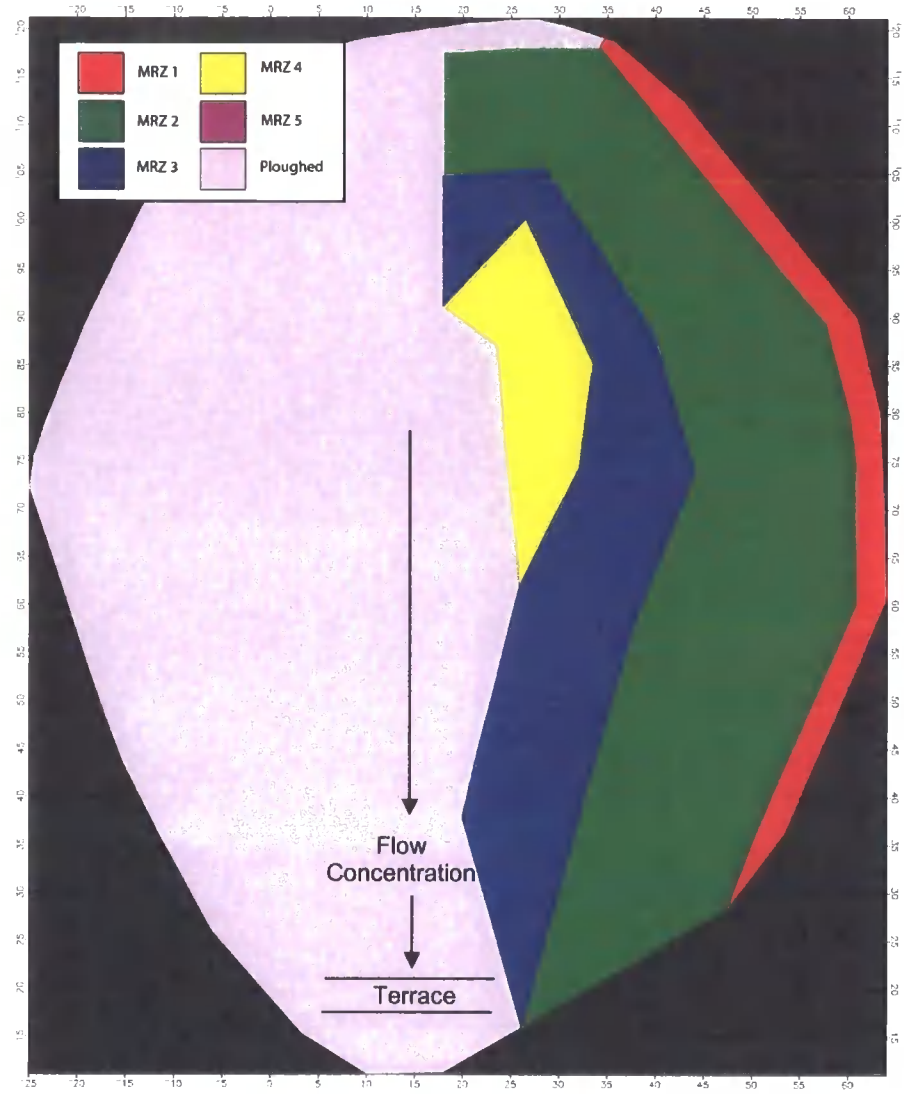

Figure 6.5. Spatial configuration of units over the Cardenas hillslope.

MDS and infiltration follow similar patterns downslope on the natural surface to those seen at Upper Nogalte: high MDS at MRZ 1, decreases at MRZ 2 and increases with further distance downslope (with the infiltration parameters experiencing the reverse trend). A major difference occurs at the MRZ 3 unit; each of the roughness measures shows that Cardenas displays more microtopographic roughness at both MRZ 3 and 4 than the other hillslopes. This is likely to be a function of incision brought about by the

deep flow recorded at this hillslope (12 cm at MRZ 3) which in turn is caused by the lower infiltration rates. This deep flow overtops the roughness elements so that the entire MRZ 3 unit is submerged at maximum flow depths (bearing greater resemblance to Figure 6.6a).

However, this submergence of the soil surface at deep flows has less of an effect than that demonstrated by the Upper Nogalte hillslope. The reason for this provides an explanation for the high levels of runoff experienced on this hillslope. The soil surface at the Cardenas hillslope is prone to crusting, and so infiltration rates (and hydraulic conductivity) are considerably lower than those found at the other sites. This explains the greater surface roughness found at both MRZ 3 and MRZ 4 of the Cardenas hillslope, as once flow incises through the crust the subsurface layer offers less resistance to flow and so all flow concentrations are relatively deep. Moreover, this is responsible for the opposite pattern of amount infiltrated across these roughness elements to that seen at the Upper Nogalte hillslope (Figures 5.37 and 5.38). Here, relatively more infiltration occurs inside the flow concentration than on the remainder of the soil surface. During small rainfall events, this may reduce the runoff from these units. However, despite this reverse pattern, the infiltration rates in the flow concentrations remain low compared with the rest of the catchment.

The ploughed side of the hillslope is not as effective at ponding runoff as the ploughed strip at Upper Nogalte. This is a result of steep slopes and the apparently long period of time that has elapsed since the hillslope was last ploughed. These ridges appear to route flow away from the general slope direction rather than store runoff (further suggested by the lack of any noticeable difference in infiltration rate between ridge and furrow). The ridges and furrows are becoming less effective with time (as suggested by Figure 2.1) and if they become abandoned then the propensity of the soil for crusting and the low infiltration rate of this steep slope will cause much runoff and erosion from this part of the hillslope (Lasanta *et al.*, 2000). Indeed Nicolau *et al.* (1996) showed that soils in the nearby province of Almeria tended to develop surface crusts after ploughing. This combined with the low recovery of vegetation may develop a positive feedback between infiltration, soil water content and vegetation cover.

The MRZ 4 unit has occurred below the area of greatest flow concentration, but this is at the top end of the bowl-shape. The flow output from the rills must travel some distance through a reasonably flat, ploughed area before coming off the hillslope. Despite the ineffectiveness of the ploughed areas on the steep slopes above, this flat area (which also contains an artificial terrace and several large bushes) severely reduces the connectivity of the upslope runoff-producing areas to the main channel. This buffer is fundamental to ensure that this area of high runoff and sediment transport remains relatively spatially isolated from the main channel.

6.3.3 Del Prado Hillslope

The general drainage of the Del Prado hillslope is in a dendritic pattern at the upper part of the hillslope (Figure 5.45). Figure 4.34 demonstrates that this hillslope displayed the highest surface tortuosity value; however this can not directly traced to either general surface slope (as seen from the elevation range and surface standard deviation measures also displayed in Figure 4.34) or soil surface microtopography (as the profile tortuosity values in Figure 4.33 are relatively low). Instead, it appears that the high surface tortuosity measures are related to the broad-scale concavity of the hillslope. Runoff accumulates from a large upslope area and is funnelled into a small area containing rills and gullies (Figure 6.8); the distribution of flowpath lengths is such that much of the runoff will reach the same point at about the same time allowing the mutual reinforcement of the flow. The hillslope shows the highest range of slope angles (Figure 4.34), but unlike the Cardenas hillslope, the distribution of slope angles is such that the slope becomes steeper closer to the outflow point (Figure 4.32). This prevents the runoff-producing areas from becoming spatially isolated from the main channel.

The patterns of MDS and infiltration between MRZs were similar to those seen at the other hillslopes. No ploughed areas interfere with the routing of water over the surface. Gullies (15 %) and rills (17 %) make up a considerably larger area of the hillslope than at the other sites, and as a result of the generally concave hillslope surface, the MRZ slope-distance thresholds display a linear trend (Figure 6.4c). The flow patterns of each plot are remarkably similar (Figure 5.24) with limited flow concentration by microtopography. Approximately 6 % of each Del Prado plot drains greater than 1 % of the area (Figure 5.26).

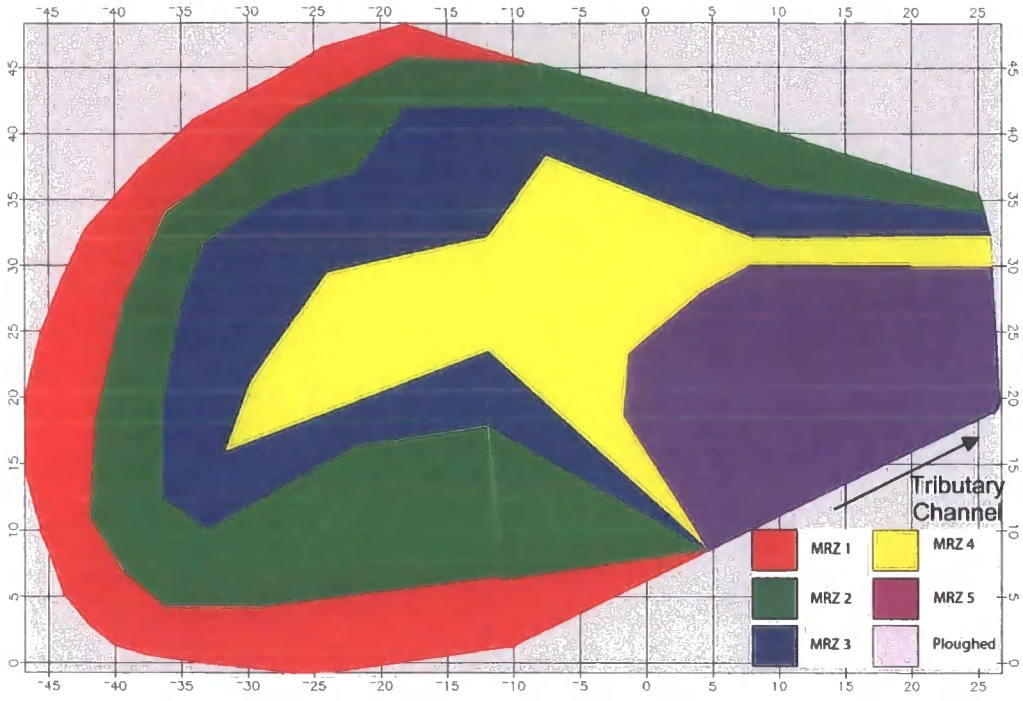

Figure 6.8. Spatial configuration of units over the Del Prado hillslope.

MDS and infiltration are high compared with the other hillslopes. Figure 5.49 suggests that larger depressions are more significant at storing water here than at the other hillslopes. This MDS is reflected in the downslope pit density and Nearest Neighbour roughness measures, but few other roughness measures were able to predict this high MDS. Indeed, from many of the roughness measures analysed in Chapter 4, it would seem that the soil surface of the Del Prado hillslope is smoother than the other hillslopes (however it has the highest pit density in both orthogonal directions). Despite this high MDS and infiltration, high flow depths and sediment transport rates were experienced over the hillslope; this reflects both the hydrological response of the hillslope and the erodibility of the marl surface. The sediment bags, however, trapped relatively little sediment (mostly dominated by fines; Figure 5.46c) except at the MRZ 4 site where the highest overall weight was trapped. This reflects the dendritic drainage pattern of this hillslope with many smaller flow concentrations joining into larger flow concentrations.

6.3.4 Summary

It seems from this analysis that the seemingly low runoff thresholds found at the Del Prado hillslope are not a result of a lower level of surface water or infiltration. Indeed, compared with the other hillslopes, the soil surface of Del Prado retained the most

water. Therefore, other factors must be responsible for the high runoff depth and sediment transport at this site. It seems that the influence of large-scale drainage patterns and the distribution of steep slope angles between runoff-generating areas and a major channel are responsible for the connectivity of large areas of this hillslope to the major flow concentration below. The large-scale surface roughness (general hillslope form) provides an important context for the runoff-response of the soil surfaces and should be considered alongside the effect of microtopography on hillslope connectivity (see the bottom-section of Figure 6.1). The integration of the rill network over the entire hillslope is a crucial factor in generating flow out of the hillslope (Kuhn & Yair, 2004). This integrated network ensures that flow will overcome transmission losses and propagate down flow concentrations. As flow depth increases with distance down the network this increases the strength of the 'delivery pathway', thereby enhancing hillslope connectivity (Bracken & Croke, in press).

The Cardenas hillslope was also particularly responsive to rainfall; it had the lowest values of MDS and infiltration and so recorded the deepest maximum overland flow of all the hillslopes. However, the sediment transport rates were generally lower than those of the Del Prado slope (Figure 5.41) and are probably a reflection of the surface crusting experienced at this site. Although considerable flow concentration occurs as a result of microtopography, such potentially runoff-generating features are found some distance from a major flow concentration. A buffer zone of a flat, ploughed area prevents this generated runoff from reaching the main runoff collecting network.

The Upper Nogalte hillslope is reasonably steep right to the small tributary at the foot of the slope, but it does not contribute large runoff amounts to the main channel. Three main reasons may be identified for this. First, the hillslope has reasonably high MDS and infiltration levels (and although infiltration is relatively lower in flow concentrations, these are generally where most MDS occurs). Second, the general drainage pattern is parallel in a downslope direction. The lack of integration of parallel rill networks prevents the generation of any mutually reinforcing, continuous overland flow as seen at the Del Prado site. Third, the ploughed band running across the hillslope prevents flow concentrations from forming further upslope and retains much of the runoff from further upslope. Should this ploughed band become abandoned (as seen at

Cardenas), then overland flow may begin concentrating further upslope and considerable soil erosion will occur as the hillslope re-adjusts.

The application of identical techniques over multiple scales has also demonstrated that similar processes operate at different scales. For example, the average depth of maximum depression storage is generally higher at the hillslope scale; this may be an artefact of DEM resolution. As Römkens & Wang (1986) divided surface roughness into four scale-dependent categories, it is useful to note that this is also true of surface water storage:

1. Grain roughness may bring about small amounts of surface water storage (as a result of water tension forces and fine scale topographic variation);
2. Water storage in small depressions formed by clods or aggregates. Summed over a large area, this may represent a considerable volume of water;
3. Linear roughness elements such as ploughing furrows or wheel tracks may impound water (Figure 6.9). Water may also be stored in local hillslope concavities. It is this level of storage which is included in the hillslope scans but not detected from plot-based studies;
4. At the landscape level, lakes may form in valley bottoms or man-made structures such as check-dams may impound small reservoirs.

Figure 6.9. Depression storage in a ploughing furrow, observed at the foot of the Cardenas hillslope.

6.4 Limitations & Further Study

The MDS values calculated in this study were considerably lower than those quoted in the literature (which may reach 30 mm on agricultural surfaces; Kamphorst *et al.*, 2000). The most obvious reason for this is that this study considered natural soil surfaces which store less water on the surface. Also, the runoff drained by the plot boundaries was allowed to drain freely off the surface as depressions located at the plot boundary were thought to be relatively minor as a result of the large plot area considered (9 m^2). MDS calculated from a DEM is also related to point resolution, however compared with much of the present literature, this investigation used a greater point density (Table 3.2) which is favourable to the calculation of greater MDS (Huang & Bradford, 1990a).

Many studies isolate the microtopography of interest through removing the general slope before calculating MDS. This technique will elevate MDS levels beyond the depths which naturally occur on these surfaces. Surface form is created in a particular process-environment; this method abstracts surface features from the environments in which they were formed (wash-deposits become peaks and flow concentrations become pits) (Figure 5.12). To isolate the effect of general slope, it would be preferable (albeit time-consuming) to examine a selection of plots for each MRZ demonstrating the full range slope angles found in the field (Figure 5.8 demonstrates this approach on an extremely limited dataset).

The method applied in this investigation would benefit from some form of field-calibration of the MDS value obtained from the GIS models. This could be achieved through direct measurement of MDS by making the surface impervious using polyester resin (Gayle & Skaggs, 1978), bitumen (Langford & Turner, 1972) or a plastic film (Mwendera & Feyen, 1992). Alternatively, Kamphorst & Duval (2001) created impermeable moulds of soil surfaces using polyester.

The application of a terrestrial laser scanner to studies of soil surface roughness has offered a considerable step forwards, allowing high-resolution topographic data to be obtained at the hillslope scale. Due to a lack of time, the resolution of these hillslope scans was not as high as desired. This problem can be easily overcome through a larger

number of strategically positioned scan locations. The variable resolution of hillslope-scale scans potentially affected the surface roughness measures and hydrological analysis presented in this investigation. In future, a method of standardising the resolution of such surfaces should be applied. Alternatively, Abedini *et al.* (in press) suggest that the determination of hydrological characteristics of such surfaces should be abandoned in favour of an analysis of the fractal characteristics of depression storage.

Lim *et al.* (2005) have recently developed a methodology for monitoring cliff-faces which integrates such laser scanning with photogrammetry. This approach provides a combination of qualitative and quantitative information sources and therefore records non-morphological information (such as the presence of rock fragments, vegetation or soil aggregates) so that the impact of such features upon surface roughness and surface processes can be analysed (Merel & Farres, 1998). Where there exists a strong variability of roughness within a single plot, this information may prevent the redistribution and averaging-out of distinct roughness components. Such local variability is often lost through a traditional approach of characterising surface roughness (Borselli, 1999).

Although the incorporation of photogrammetric techniques may prove problematic at the hillslope scale because of perspective problems on gentle slopes, such an approach would permit a more explicit treatment of vegetated areas. Indeed, the presence of vegetation on the soil surface has been ignored in this investigation and represents an obvious direction for further study. Vegetation has a major influence on surface roughness and the vertical water balance (through interception), but more importantly, the distribution of vegetated and bare patches on slopes has an important influence on the connectivity of runoff-producing areas to the main channel (Bergkamp, 1998).

The infiltration tests undertaken in this study produced interesting results which require further examination. It appears that the unsaturated hydraulic conductivity (calculated using the method proposed by Zhang (1997)) was sensitive to the initial infiltration rate, whereas the total amount infiltrated in 5 minutes measured a different property of the soil. The contribution of the different ranges of macroporosity to infiltration on a rough surface may shed some light on this matter. The pore-size distribution of the surface may be examined through repeated minidisk infiltrometer tests using a different level of

suction (Heddadj & Gascuel-Odoux, 1999). There may also be potential to harness the differential reflectance of moist surfaces recorded by the laser scanner (Lim *et al.*, 2005) and compare drying patterns of soil surfaces after wetting.

It would be especially interesting to relate the results of this study to soil physical and chemical characteristics. This would provide greater insight into the distribution of infiltration rates and sediment transport. Indeed, when combined with a more explicit treatment of the spatial distribution of soil surface crusting (through aggregate stability tests) and an assessment of how the soil surfaces change with simulated rainfall, the response of a hillslope to a particular rainfall event can be thoroughly analysed.

Long-term monitoring of microtopography with repeated mapping of flow concentrations, alongside recordings of runoff intensity and the distribution of runoff depths across the plot (from the clustering of mini crest-stage recorders in one area), would provide a clearer view of the interaction between surface roughness and overland flow hydraulics. While some limited analysis of the flow 'micro-networks' generated on soil surface has been carried out an examination of the fractal characteristics of the flow networks caused by fine-scale surface roughness may advance our understanding of overland flow hydraulics. The interaction between soil surface roughness and overland flow is important if runoff generation and soil erosion are to be predicted at the hillslope scale as it provides a clearer view of the process of channel formation (Dunne *et al.*, 1995).

Chapter 7 Conclusions

Surface runoff and soil erosion pose a major environmental threat to agriculture; these surface processes are affected by surface microtopography. Indeed, soil surface characteristics have been recognised as key parameters controlling surface hydrological processes on semi-arid hillslopes. The distribution of soil microtopography over these hillslopes dictates that its influence on the generation of runoff, the hydraulics of overland flow and the connectivity of this flow will be variable across each hillslope. Auzet *et al.* (2005: p.77) note that increasing our ability to characterise the soil surface "now emerges as a major and efficient step towards a better spatial assessment of processes and towards high-quality soil erosion forecasting".

This approach places greater emphasis on the description of the soil surface. However, it is not practical to attempt to represent every single component of a rough surface within a roughness measure. Surface description should be approached from the perspective of its purpose. This aim of this study was to examine the performance of several roughness measures in parameterising those properties of the soil surface that are most appropriate from the perspective of geomorphological process (more specifically, the processes related to the generation of Hortonian overland flow at the hillslope scale). Specific surface roughness measures, such as downslope pit density were most appropriate for predicting maximum depressional storage, although 5% trimmed mean nearest neighbour and downslope tortuosity also performed well across the wide range of surfaces examined in this study.

Cross-slope measures of roughness (such as cross-slope tortuosity and cross-slope standard deviation of elevations) were better able to identify the degree of flow convergence and organisation of the soil surface. Although mean infiltration rates could not be related directly to measures of surface form, the standard deviation of infiltration characteristics was related to the 'nearest neighbour' and tortuosity measurements. These relationships were discussed further in section 6.2. In all, the large range of soil surfaces and surface processes experienced at the hillslope scale limited the ability of general roughness measures to represent specific processes. If a larger dataset was put together, the performance of these measures within each MRZ could be considered as a greater number of slope angles could be considered.

Maximum depressional storage and infiltration demonstrated inverse trends in their distribution across the hillslopes. MDS was initially high at the drainage divide (partly a consequence of gentle slopes), decreased to a negligible value within several metres, before then increasing with further distance downslope. The depressions associated with this increase are generally found in the bottom of flow concentrations. Infiltration rates, on the other hand, began at a relatively low value at the drainage divide (possibly a consequence of surface crusting from raindrop impact), increased to a maximum within several metres, before decreasing with distance further downslope. The distribution of infiltration rates between flow concentrations and surrounding soil surfaces was inconsistent between the hillslopes, potentially as a consequence of surface crusting. Flow concentration generally increased with distance downslope, as did measures of maximum flow depth. Finally, sediment transport rates also increased with distance downslope, but were found to be very variable as a result of microtopographic context. Indeed, the range of 'process environments' found at each plot increased with distance downslope as a result of the increased levels of flow concentration. This was reflected in the wide range of sediment transport particle size distributions found at the mid-section of the hillslopes. The distribution of flow depths, MDS and infiltration-prone surfaces in relation to these flow concentrations is a key feature of soil surfaces and deserves further investigation.

The ploughing of a soil surface appeared to increase the general surface roughness. In particular, it increased that component of roughness that is related to MDS. Ploughing was found to increase MDS by 3-5 times, effectively reducing the amount of water flowing downslope. At the Upper Nogalte site, this effect has stabilised the soil surface downslope of a ploughing band through its influence on flow routing and hence the slope-area relationship. However, such an approach requires maintenance, as the ploughed area of the Cardenas hillslope is much less effective at storing water as the ridges have degraded over time. The removal of vegetation for almond cropping (which is practised over the majority of slope surfaces in the Rambla Nogalte catchment) also decreases infiltration rates (as found in this study) and the patchiness of runoff generation (Bull *et al.*, 2000). Once the effect on MDS has deteriorated, areas of abandoned agriculture demonstrate low runoff thresholds, high peak flows and rapid response to rainfall (Lasanta *et al.*, 2000). Should the ploughed band at the Upper

Nogalte hillslope become abandoned, soil erosion downslope would cause an upslope migration of flow concentrations and channel heads as each MRZ adjusts to the new upslope condition.

Therefore, soil surface roughness affects the organisation of the drainage pattern at the hillslope scale and so it helps determine the upslope supply of runoff and sediment at any point on a hillslope (Favis-Mortlock *et al.*, 2000). This will have important implications for the spatial distribution of sediment sources and sinks (Govers *et al.*, 2000). A natural consequence of the spatial variability of processes over a semi-arid hillslope is that soil surface morphology is also variable at the hillslope scale. An ability to determine the spatial configuration of these areas with regard to areas of major flow concentrations is of fundamental importance if we are to accurately assess the hydrological and sedimentological connectivity of these hillslopes. Several methods of surface characterisation ('surface tortuosity', 'surface fractal dimension' and semi-variance measures) were able to differentiate between each of five units of relatively homogeneous microtopography (MRZs). This is important because, as already demonstrated at the Cardenas site, the major runoff-generating areas may be disconnected from flow concentrations. The division of semi-arid hillslopes into 'Morphological Runoff Zones' also provides a suitable background knowledge of the nature of the soil surfaces through which subsequent fine-scale roughness measures can be considered, adding quantitative detail to this qualitative method of classifying hillslope surface conditions.

The large-scale topographic roughness is equally important in determining hillslope connectivity, as seen at the Del Prado site, where the form of the hillslope itself promotes the generation of an integrated drainage network, which increases the strength of the runoff delivery pathway. The Del Prado hillslope demonstrated the largest maximum upslope area measurements (of the 250 mm resolution scans; Figure 5.47a and c); the strong dependency of this with on the filling of depressions (Figure 5.47b and d) suggests that much surface storage occurs in areas of flow concentration. Analysis of this hillslope characteristic may help bridge the knowledge gap between storm inputs and connectivity (Bracken & Croke, in press). Further investigation of the relationships between microtopography and surface processes over different areas of the hillslopes, and an appreciation of the spatial configuration of these areas relative to

areas of major flow concentration in the context of the large-scale topographic variation of the hillslopes, may reveal suitable criteria for generalising from one hillslope to another.

It is important to realise that hillslope connectivity is only one small part of a larger problem. While this study has attempted to apply geomorphometry to plot surfaces and hillslopes, it is worth bearing in mind that the drainage basin has been frequently referred to as 'the fundamental geomorphic unit' (Chorley, 1969). The Cardenas and Del Prado hillslopes are situated in areas of gorge-like morphology which offer efficient flow routing beyond the hillslope, but the Upper Nogalte hillslope is disconnected from a major tributary of the Rambla Nogalte. Disconnection of hydrological pathways often occurs beyond the hillslope as a result of long travel distances with high transmission losses; therefore hillslope response is nested within a larger scale response. Nevertheless, it is the distribution of spatially variable hillslope responses across a catchment that determines the scale of the catchment response to a particular storm. Bull *et al.* (1999) note that the position and path of a storm cell over the Rambla Nogalte and Rambla de Torrealvilla catchments are major factors in determining the magnitude of the resulting discharge.

Therefore, catchment runoff production is a function of the interaction of topographic, surface and rainfall characteristics (Michaelides & Wainwright, 2002). As Auzet *et al.* (2005) suggest, the prevention of runoff and protection of soil has become a major challenge in reducing flood risk. In fragile semi-arid environments subject to uncertain future climate change, this task is particularly important, both environmentally and economically. Studies of palaeofloods in the Guadalentín basin suggest a recent increase in flood magnitude and frequency (Benito *et al.*, 2002). This is a result of the combined influences of land-use practices (such as widespread deforestation and land abandonment) and climate change (through increasing temperatures and changing storm characteristics) over the past few hundred years. A greater understanding of the contribution of land-use changes to this increased flood risk is necessary before policy makers can formulate effective flood-reduction strategies. The results of this study should therefore be placed in the wider context of the river basin to produce meaningful results at the catchment scale.

References

Abedini, M.J., Dickinson, W.T. & Rudra, R.P. in press. On depressional storages: the effect of DEM spatial resolution. *Journal of Hydrology.*

Abrahams, A.D. & Parsons, A.J. 1991. Resistance to overland flow on desert pavement and its implications for sediment transport modelling. *Water Resources Research*, 27, 1827-1836.

Abrahams, A.D., Parsons, A.J., & Hirsch, P. 1992. Field and laboratory studies of resistance to overland flow on semi-arid hillslopes, southern Arizona. In Parsons, A.J & Abrahams, A.D. (eds.) *Overland Flow*, UCL Press, London, 1-24.

Allen, T.F.H. & Star, T.B. 1982. *Hierarchy, Perspectives for Ecological Complexity.* University of Chicago Press, Chicago, 310pp.

Allmaras, R., Burwell, R., Larson, W. & Holt, R. 1966. Total porosity and random roughness of the interrow zone as influenced by tillage. *United States Department of Agriculture Conservation Research Report*, 7, 1-14.

Allmaras, R.R., Hallauer, E.A., Nelson, W.W. & Evans, S.D. 1977. Surface energy balance and soil thermal property modifications by tillage induced soil structure. *University of Minnesota Agricultural Experimental Station Technical Bulletin*, 306, 1-40.

Allmaras, R.R., Nelson, W.W. & Hallauer, E.A. 1972. Fall vs. spring ploughing and related soil heat balance in the western corn belt. *University of Minnesota Agricultural Experimental Station Technical Bulletin*, 283, 1-22.

Ambroise, B. 2003. Variable 'active' vs 'contributing' areas or periods: a necessary distinction. *Hydrological Processes*, 18, 1149-1155.

Auerswald, K. 1992. Changes in soil surface roughness during erosive rains. Internal report, Lehrstuhl für Bodenkd., TU München, D-8050 Freisning, Germany.

Auzet, A.V., van Dijk, P. & Kirkby, M.J. 2005. Surface characterisation for soil erosion forecasting, *Catena*, 62, 77-78.

Baird, A.J. 1997. Overland flow generation and sediment mobilisation by water. In Thomas, D.S.G. (ed) *Arid Zone Geomorphology – Process, Form and Change in Drylands*, Wiley, Chichester, 165-184.

Bartoli, F., Genevois-Gomendy, V., Royer, J.J., Niquet, S., Viver, H. & Grayson, R. 2005. A multiscale study of silty soil structure. *European Journal of Soil Science*, 56, 207-223.

Becker, A. & Braun, P. 1999. Disaggregation, aggregation and spatial scaling in hydrological modelling. *Journal of Hydrology*, 217, 239-252.

Benito, G., Rico, M., Sánchez-Moya, Y., Sopeña, A. & Thorndycraft, V.R. 2002. Magnitude and frequency of palaeofloods in the Upper Guadalentín Basin (SE-Spain) during the last 1000 years. EGS XXVII General Assembly, Nice, 21-26 April 2002, abstract #2345. Accessed 19 August 2005. (http://adsabs.harvard.edu/cgi-bin/nph-bib_query?bibcode=2002EGSGA..27.2345B&db_key=PHY&data_type=HTML&format=).

Bergkamp, G. 1998. A hierarchical view of the interactions of runoff and infiltration with vegetation and microtopography in semiarid shrublands. *Catena*, 33, 201-220.

Bertuzzi, P., Rauws, G. & Courault, D. 1990. Testing roughness indices to estimate soil surface roughness changes due to rainfall. *Soil & Tillage Research*, 17, 87-99.

Boiffin, J. 1984. Structural degradation of the soil surface by the action of rainfall. (In French). Ph.D. Dissertation. Institut Nationale d'Agronomie Paris-Grignon, Paris, France.

Borselli, L. 1999. Segmentation of soil roughness profiles. *Earth Surface Processes and Landforms*, 24, 71-90.

Bracken, L.J. & Croke, J. in press. The concept of connectivity and its application in geomorphology.

Bracken, L.J. & Kirkby, M.J. 2005. Differences in hillslope runoff and sediment transport rates within two semi-arid catchments in southeast Spain. *Geomorphology*, 68, 183-200.

Brough, D.L. & Jarrett, A.R. 1992. Simple technique for approximating surface storage of silt-tilled fields. *Transactions of the American Society of Agricultural Engineers*, 35 (3), 885-890.

Bull, L.J., Kirkby, M.J., Shannon, J. & Dunsford, H.D. 2003. Predicting Hydrologically Similar Surfaces (HYSS) in semi-arid environments. *Advances in Environmental Monitoring and Modelling,* 1 (2), 1-26.

Bull, L.J., Kirkby, M.J., Shannon, J. & Hooke, J.M. 1999. The impact of rainstorms on floods in ephemeral channels in SE Spain. *Catena*, 38, 191-209.

Burrough, P.A. 1983. Multiscale sources of spatial variation in soil. I. The application of fractal concepts to nested levels of soil variation. *Journal of Soil Science*, 34, 577-597.

Butler, J.B., Lane, S.N. & Chandler, J.H. 2001. Characterization of the structure of river-bed gravels using two-dimensional fractal analysis. *Mathematical Geology* 33 (3), 301-330.

Cammeraat, L.H. 2002. A review of two strongly-contrasting geomorphological systems within the context of scale. *Earth Surface Processes and Landforms*, 27, 1201-1222.

Campbell, I.A. & Honsaker, J.L. 1982. Variability in badlands erosion; problems of scale and threshold identification. In Thorn, C.E. (ed), *Space and Time in Geomorphology*, George Allen & Unwin, London, 59-79.

Carsel, R.F. & Parish, R.S. 1988. Developing joint probability distributions of soil water retention characteristics. *Water Resources Research*, 24, 755-769.

Chorley, R.J. 1969. The drainage basin as the fundamental geomorphic unit. In Chorley, R.J. (ed), *Water, Earth and Man*, Methuen & Co. Ltd., London, 77-99.

Chorley, R.J., Malm, D.E.G. & Pogorzelski, H.A. 1957. A new standard for measuring drainage basin shape. *American Journal of Science*, 255, 138-141.

Cogo, N.P., Moldenhauer, W.C. & Foster, G.R. 1983. Effect of crop residue, tillage-induced roughness, and runoff velocity on size distribution of eroded soil aggregates. *Soil Science Society of America Journal*, 47, 1005-1008.

Cox, N.J. 2004. Graphing categorical and compositional data. *Stata Journal*, 4, 2, 190-215.

Cremers, N.H.D.T., van Dijk, P.M., de Roo, A.J.P. & Verzandvoort, M.A. 1996. Spatial and temporal variability of soil surface roughness and the application in hydrological and soil erosion modelling. *Hydrological Processes*, 10 (3), 1035-1047.

Currence, H.D. & Lovely, W.G. 1970. The analysis of soil surface roughness, *Transactions of the American Society of Agricultural Engineers*, 13, 710-714.

Darboux, F. & Huang, C. 2003. An instantaneous profile laser scanner to measure soil surface microtopography, *Soil Science Society of America Journal*, 67, 92-99.

Darboux, F., Davy, P., Gascuel-Odoux, C. & Huang, C. 2001a. Effect of depression storage capacity on overland flow generation for rough horizontal surfaces: water transfer distance and scaling. *Earth Surface Processes and Landforms*, 27, 177-191.

Darboux, F., Davy, P., Gascuel-Odoux, C. & Huang, C. 2001b. Evolution of soil surface roughness and flowpath connectivity in overland flow experiments. *Catena*, 46, 125-139.

Darboux, F., Gascuel-Odoux, C. & Davy, P. 2002. Effects of surface water storage by soil roughness on overland-flow generation, *Earth Surface Processes & Landforms*, 27, 3, 223-233.

Dietrich, W.E. & Montgomery, D.R. 1998. Hillslopes, Channels and Landscape Scale. In Sposito, G. (ed), *Scale Dependence and Scale Invariance in Hydrology*, Cambridge University Press, Cambridge, 30-60.

Dunne, T., Zhang, W. & Aubry, B. 1991. Effects of rainfall, vegetation and microtopography on infiltration and runoff. *Water Resources Research* 27, 2271-2285.

Dunne, T., Whipple, K.X. & Aubry, B. 1995. Microtopography of hillslopes and initiation of channels by Horton overland flow. In Costa, J.E., Miller, A.J., Potter, K.W.

& Wilcock, P.R. (eds), *Natural and anthropogenic influences in fluvial geomorphology; the Wolman Volume*, Geophysical Monograph 89, American Geophysical Union, Washington D.C., 27-44.
Errea, M.P. 1996. La retirada de terras en el marco de la Política Agraria Comunitaria (1989-1994): incidencia en Aragón. *Revista Aragonesa de Administración Pública* 8, 67-109.

Evans, I.S. 1972. General geomorphometry, derivatives of altitude, and descriptive statistics. In Chorley, R.J. (ed) *Spatial Analysis in Geomorphology*, Methuen & Co. Ltd., London, 17-90.

Evans, I.S. 2003. Scale-Specific Landforms and Aspects of Land Surface. In Evans, I.S., Dikau, R., Tokunaga, E., Ohmori, H. & Hirano, M. (eds), *Concepts and Modelling in Geomorphology: International Perspectives*, Terrapub, Tokyo, 61-84.

Fardin, N., Feng, Q., & Stephanssen, O. 2004. Application of a new in situ 3D laser scanner to study the scale effect on the rock joint surface roughness. *International Journal of Rock Mechanics and Mining Sciences*, 41, 329-335.

Favis-Mortlock, D.T., Boardman, J., Parsons, A.J., & Lascelles, B. 2000. Emergence and erosion: a model for rill initiation and development. *Hydrological Processes*, 14, 2173-2205.

Fitzjohn, C., Ternan, J.L. & Williams, A.G. 1998. Soil moisture variability in a semi-arid gully catchment: implications for runoff and erosion control. *Catena*, 32, 55-70.

Flügel, W.A., 1995. Delineating hydrological response units by geographical information system analyses for regional hydrological modelling using PRMS/MMS in the drainage basin of the river Brol, Germany. *Hydrological Processes*, 9, 423-436.

Fox, D.M., Le Bissonais, Y. & Bruand, A. 1998a. The effect of ponding depth on infiltration in a crusted surface depression. *Catena*, 32, 87-100.

Fox, D.M., Le Bissonnais, Y. & Quétin, P. 1998b. The implications of spatial variability in surface seal hydraulic resistance for infiltration in a mound and depression topography. *Catena* 32, 101-114.

Gayle, G.A. & Skaggs, R.W. 1978. Surface storage on bedded cultivated lands. *Transactions of the American Society of Agricultural Engineers*, 21(1), 101-104, 109.

Gerits, J., Imeson, A.C., Verstraten, J.M., & Bryan, R.B. 1987. Rill development and badland regolith properties. In Bryan, R.B. (ed), *Rill Erosion: Processes and Significance*, Catena Supplement 8, 141-160.

Gilley, J.E. & Finkner, S.C. 1991. Hydraulic roughness coefficients as affected by random roughness. *Transactions of the American Society of Agricultural Engineers*, 34 (3), 897-903.

Gómez, J.A. & Nearing, M.A. 2005. Runoff and sediment losses from rough and smooth soil surfaces in a laboratory experiment. *Catena*, 59, 253-266.

Govers, G., Takken, I. & Helming, K. 2000. Soil roughness and overland flow, *Agronomie*, 20, 131-146.

Hansen, B. 2000. Estimation of surface runoff and water-covered area during filling of surface microrelief depressions, *Hydrological Processes*, 14, 1235-1243.

Hansen, B., Schjønning, P. & Sibbesen, E. 1999. Roughness indices for estimation of depression storage capacity of tilled soil surfaces, *Soil & Tillage Research*, 52, 103-111.

Hastings, H.M. & Sugihara, G. 1993. *Fractals: A User's Guide for the Natural Sciences*, Oxford University Press, New York, 235pp.

Heddadj, D. & Gascuel-Odoux, C. 1999. Topographic and seasonal variations of unsaturated hydraulic conductivity as measured by tension disc infiltrometers at the field scale, *European Journal of Soil Science*, 50, 275-283.

Helming, K., Römkens, M.J.M. & Prasad, S.N. 1998. Surface roughness related processes of runoff and soil loss: a flume study, *Soil Science Society of America Journal*, 62, 243-250.

Helming, K., Roth, C.H., Wolf, R. & Diestel, H. 1993. Characterization of rainfall - microrelief interactions with runoff using parameters derived from Digital Elevation Models (DEMs). *Soil Technology*, 6, 273-286.

Helming, K., Jeschke, W. & Storl, J. 1992. Surface reconstruction and change detection for agricultural purposes by close range photogrammetry. In Fritz, W. & Lucas, J.R. (eds), *Int. archives for photogrammetry and remote sensing*, Vol. 29, part B5. Int. Congr. For Photogrammetry and Remote Sensing, 17th. ISPRS, Washington, D.C., p.610-617.

Hooke, J.M. & Mant, J.M. 2000. Geomorphological impacts of a flood event on ephemeral channels in SE Spain. *Geomorphology* 34, 163-180.

Hosking, J.R.M. 1992. Moments or L moments? An example comparing two measures of distributional shape. *The American Statistician*, 46, 3, 186-189.

Huang, C. & Bradford, J.M. 1990a. Depressional storage for Markov-Gaussian surfaces. *Water Resources Research*, 26, 2235-2242.

Huang, C. & Bradford, J.M. 1990b. Portable laser scanner for measuring soil surface roughness. *Transactions of the American Society of Agricultural Engineers*, 54 (5), 1402-1406.

Huang, C. & Bradford, J.M. 1992. Application of a laser scanner to quantify soil microtopography. *Soil Science Society of America Journal*, 56, 14-21.

Huang, C. & Bradford, J.M. 1993. Applications of a laser scanner to quantify properties of soil crusts. In Poesen, J.W.A. & Nearing, M.A. (eds) *Soil Surface Sealing and Crusting*, Catena Supplement, 24, 129-139.

Huang, C., Gascuel-Odoux, C. & Cros-Cayot, S. 2001. Hillslope topographic and hydrologic effects on overland flow and erosion, *Catena*, 46, 177-188.

Hypanen, H. 1996. Spatial autocorrelation and optimal spatial resolution of optical remote sensing data in boreal forest environment. *International Journal of Remote Sensing*, 17, 3441-3452.

Jetten, V., De Roo, A. & Guérif, J. 1998. Sensitivity of the model Lisem to variables related to agriculture. In Boardman, J. & Favis-Mortlock, D. (eds.), *Modelling soil erosion by water*, NATO ASI Series, vol. I 55.
Jetten, V., de Roo, A. & Favis-Mortlock, D. 1999. Evaluation of field-scale and catchment-scale soil erosion models. *Catena*, 37, 521-541.

Kamphorst, E.C. & Duval, Y. 2001. Validation of a numerical method to quantify depression storage by direct measurements on moulded surfaces. *Catena*, 43, 1-14.

Kamphorst, E.C., Chadœuf, J., Jetten, V. & Guérif, J. 2005. Generating 3D soil surfaces from 2D height measurements to determine depression storage. *Catena*, 62, 189-205.

Kamphorst, E.C., Jetten, V., Guérif, J., Pitkänen, J., Iversen, B.V., Douglas, J.T. & Paz, A. 2000. Predicting depressional storage from soil surface roughness. *Soil Science Society of America Journal*, 64, 1749-1758.

Kersten, T., Sternberg, H., Mechelke, K. & Acevedo Pardo, C., 2004. Terrestrial laser scanning system Mensi GS100/GS200 - accuracy tests, experiences and projects at the Hamburg University of Applied Sciences. *International Archives of the Photogrammetry, Remote Sensing and Spatial Information Sciences*, 34(5W16). 8 pages on CD-ROM.

Kirkby, M. 2001. Modelling the interactions between soil surface properties and water erosion. *Catena*, 46, 89-102.

Kirkby, M.J. & Bracken, L.J. in press. Modelling hillslope connectivity and channel interactions in semi-arid areas: implications for hillslope restoration following land abandonment.

Kirkby, A. & Kirkby, M.J. 1974. Surface wash at the semi-arid break in slope. *Zeitschrift für Geomorphologie*, Supplement Band 21, 151-176.

Kirkby, M.J., Imeson, A.C., Bergkamp, G. & Cammeraat, L.H. 1996. Scaling up processes and models from the field plot to the watershed and regional areas. *Journal of Soil and Water Conservation*, 51, 5, 391-396.

Kirkby, M.J., Bracken, L.J. & Reaney, S. 2002. The influence of land use, soils, and topography on the delivery of hillslope runoff to channels in SE Spain. *Earth Surface Processes and Landforms*, 27, 1457-1473.

Kirkby, M.J., Bracken, L.J. & Shannon, J. 2005. The influence of rainfall distribution and morphological factors on runoff delivery from dryland catchments in SE Spain, *Catena*, 62, 136-156.

Kuhn, N. & Yair, A. 2004. Spatial distribution of surface conditions and runoff generation in small arid watersheds, Zin Valley Badlands, Israel. *Geomorphology*, 57, 183-200.

Kuipers, H. 1957. A relief meter for soil cultivation studies. *Netherlands Journal of Agricultural Science*, 5, 255-262.

Lal, R. 1997. Soil degradative effects of slope length and tillage methods on alfisols in western Nigeria. III. Soil physical properties. *Land Degradation & Development*, 8, 325-342.

Lane, S.N. 2005. Roughness – time for a re-evaluation?, *Earth Surface Processes & Landforms*, 30, 251-253.

Langford, K.J. & Turner, A.K. 1972. Effects of rain and depression storage on overland flow. *Transactions of the Institution of Engineers, Australia* 14(2), 137-141.

Larson, W.E. 1962. Tillage requirements for corn. *Journal of Soil Water Conservation*, 17, 3-7.

Lasanta, T., García-Ruiz, J.M., Pérez-Rontomé, C. & Sancho-Marcén, C. 2000. Runoff and sediment yield in a semi-arid environment: the effect of land management after farmland abandonment. *Catena*, 38, 265-278.

Le Bissonnais, Y. 1996. Experimental study and modelling of soil surface crusting processes, *Catena Supplement*, 17, 13-28.

Le Bissonnais, Y., Cerdan, O., Lecomte, V., Benkhadra, H., Souchère, V. & Martin, P. 2005. Variability of soil surface characteristics influencing runoff and interrill erosion. *Catena*, 62, 111-124.

Li, X.Y., González, A. & Solé-Benet, A. 2005. Laboratory methods for the estimation of infiltration rate of soil crusts in the Tabernas Desert badlands, *Catena*, 60, 255-266.

Lichti, D.D. & Harvey, B.R., 2002. The effects of reflecting surface material properties on time-of-flight laser scanner measurements. *Symposium on Geospatial Theory, Processing and Applications, Ottawa*. On CD-ROM. 9 pages.

Lim, M., Petley, D.N., Rosser, N.J., Allison, R.J., Long, A.J. & Pybus, D. 2005. Combined Digital Photogrammetry and Time-of-Flight Laser Scanning for Monitoring Cliff Evolution. *Photogrammetric Record*, 20(110), 109-129.

Linden, D.R. & Van Doren Jr., D.M. 1986. Parameters for characterising tillage-induced soil surface roughness, *Soil Science Society of America Journal*, 50, 1560-1565.

Linden, D.R., Van Doren, Jr., D.M. & Allmaras, R.R. 1998. A model of the effects of tillage-induced soil surface roughness on erosion. In *Tillage and traffic in crop production*. Proc. ISTRO Conf. 11th. Edinburgh, UK. 11-15 July 1998. ISTRO, Haren, the Netherlands, p.373-378.

Magunda, M.K., Larson, W.E., Linden, D.R. & Nater, E.A. 1997. Changes in microrelief and their effects on infiltration and erosion during simulated rainfall. *Soil Technology*, 10, 57-67.

Mandelbrot, B.B. 1982. *The Fractal Geometry of Nature*, Freeman, San Francisco, 460pp.

Mark, D.M. 1975. Geomorphometric parameters: a review and classification, *Geografiska Annaler* 57 A, 165-177.

Martínez-Mena, M., Albaladejo, J. & Castillo, V.M. 1998. Factors influencing surface runoff generation in a Mediterranean semi-arid environment: Chicamo watershed, SE Spain. *Hydrological Processes* 12, 741-754.

McBratney, A.B. & Webster, R. 1986. Choosing functions for semi-variograms of soil properties and fitting them to sampling estimates. *European Journal of Soil Science* 37 (4), 617-639.

Merel, A.P. & Farres, P.J. 1998. The monitoring of soil surface development using analytical photogrammetry. *Photogrammetric Record*, 16(92), 331-345.

Merril, D. 1998. Comments on the chain method for measuring soil surface roughness: Use of the chain set. *Soil Science Society of America Journal*, 62, 1147-1149.

Michaelides, K. & Wainwright, J. 2002. Modelling the effects of hillslope-channel coupling on catchment hydrological response. *Earth Surface Processes and Landforms*, 27, 1441-1457.

Moore, I.D. & Larson, C.L. 1979. Estimating micro-relief surface storage from point data, *Transactions of the American Society of Agricultural Engineers*, 22, 1073-1077.

Moore, D.C. & Singer, M.J. 1990. Crust formation effects on erosion processes. *Soil Science Society of America Journal*, 54, 1117-1123.

Morgan, R.P.C., Quinton, J.N., Smith, R.E., Govers, G., Poesen, J.W.A., Auerswald, K., Chisci, G., Torri, D., Styczen, M.E. & Folly, A.J.V. 1998a. *The European soil erosion model and user guide version 3.6.* Silsoe College, Cranfield University, U.K.

Morgan, R.P.C., Quinton, J.N., Smith R.E., Govers, G., Poesen, J.W.A., Auerswald, K., Chisci, G., Torri, D. & Styczen, M.E. 1998b. The European soil erosion model (EUROSEM): a dynamic approach for predicting sediment transport from fields and small catchments, *Earth Surface Processes & Landforms*, 23, 527-544.

Mosteller, F. & Tukey, J.W. 1977. *Data Analysis and Regression: A Second Course in Statistics*, Addison-Wesley, Reading, MA, 588pp.

Mwendera, E.J. & Feyen, J. 1992. Estimation of depression storage and Manning's resistance coefficient from random roughness measurements. *Geoderma* 52, 235-250.

Nagihara, S., Mulligan, K.R. & Xiong, W., 2004. Use of a three-dimensional laser scanner to digitally capture the topography of sand dunes in high spatial resolution. *Earth Surface Processes and Landforms*, 29(3), 391-398

Nicolau, J.M., Solé-Benet, A., Puigdefábregas, J., & Gutiérrez, L. 1996. Effects of soil and vegetation on runoff along a catena in semi-arid Spain. *Geomorphology* 14, 297-309.

Oelze, M.L., Sabatier, J.M. & Raspet, R. 2003. Roughness measurements of soil surfaces by acoustic backscatter. *Soil Science Society of America Journal*, 67, 241-250.

Oliver, M. & Webster, R. 1986. Semi-variograms for modelling the spatial pattern of landform and soil properties. *Earth Surface Processes and Landforms*, 11, 491-504.

Onstad, C.A. 1984. Depressional storage on tilled soil surfaces, *Transactions of the American Society of Agricultural Engineers*, 27, 729-732.

Pardini, G. & Gallart, F. 1998. A combination of laser technology and fractals to analyse soil surface roughness, *European Journal of Soil Science*, 49, 197-202.

Patton, P.C. & Schumm, S.A. 1975. Gully erosion, Northwestern Colorado: a threshold phenomenon. *Geology*, 3, 88-90.

Phillips, J.D. 2004. Independence, contingency & scale linkage in physical geography. In Sheppard, E. & R.B. McMaster (eds) *Scale & Geographic Enquiry*. Blackwell, Oxford: 86-100.

Planchon, O., Estèves, M. & Silvera, N. 1998. Micro-relief induced by ridging: Measurement modelling consequences on overland flow and erosion. P.1-7. poster no. 477. In *Proc. 16th World Congr. Soil Sci. August 1998*, Montpellier, France. (CD-ROM). CIRAD, Montpellier, France.

Podmore, T.H. & Huggins, L.F. 1980. Surface roughness effects on overland flow. *Transactions of the American Society of Agricultural Engineers*, 23, 1434-1439.

Poesen, J., Vandekerckhove, L., Nachtergaele, J., Oostwoud Wijdenes, D., Verstraeten, G. & Van Wesemael, B. 2002. Gully erosion in dryland environments. In Bull, L.J. & Kirkby, M.J. (eds), *Dryland Rivers: Hydrology and Geomorphology of Semi-arid Channels*, John Wiley & Sons, Chichester, 229-261.

Pringle, C. 2003. What is hydrologic connectivity and why is it ecologically important? *Hydrological Processes*, 17, 2685-2689.

Reaney, S.M. 2003. Modelling runoff generation and connectivity for semi-arid hillslopes and small catchments. Ph.D. Thesis: School of Geography, University of Leeds.

Richardson, L.F. 1961. The problem of contiguity: An appendix of statistics of deadly quarrels, *General Systems Yearbook*, 6, 139-187.

Rodríguez-Iturbe, I. & Rinaldo, A. 1997. *Fractal River Basins: Chance and Self Organisation*, Cambridge University Press, New York, 547pp.

Römkens, M. & Wang, J. 1986. Effects of tillage on surface roughness. *Transactions of the American Society of Agricultural Engineers*, 29 (2), 429-433.

Römkens, M. & Wang, J. 1987. Soil roughness changes from rainfall. *Transactions of the American Society of Agricultural Engineers*, 30 (1), 101-107.

Römkens, M.J.M., Prasad, S.N. & Whisler, F.D. 1990. Surface sealing and infiltration. In Anderson, M.G. & Burt, T.P. (eds), *Process Studies in Hillslope Hydrology*, Wiley, New York, 127-172.

Römkens, M.J.M., Helming, K. & Prasad, S.N. 2001. Soil erosion under different rainfall intensities, surface roughness and soil water regimes, *Catena*, 46, 103-123.

Rosser, N.J., Petley, D.N., Lim, M., Dunning, S.A. & Allison, R.J. in press. Terrestrial laser scanning for monitoring the process of hard rock coastal cliff erosion. *Quarterly Journal of Engineering Geology and Hydrogeology*.

Saleh, A. 1993. Soil roughness measurement, chain method. *Journal of Soil Water Conservation*, 48, 527-592.

Schroeder, M. 1991. *Fractal, Chaos and Power Laws*, Freeman, New York.

Skidmore, E.L. 1997. Comment on chain method for measuring soil roughness. *Soil Science Society of America Journal*, 61, 1532-1533.

Smith, T.R. & Bretherton, F.P. 1972. Stability and the conservation of mass in drainage basin evolution. *Water Resources Research*, 8, 1506-1529.

Solé-Benet, A., Calvo, A., Cerdà, A., Làzaro, R., Pini, R. & Barbero, J. 1997. Influences of micro-relief patterns and plant cover on runoff related processes in badlands from Tabernas (SE Spain), *Catena*, 31, 23-38.

Takken, I. & Govers, G. 2000. Hydraulics of interrill overland flow on rough, bare soil surfaces. *Earth Surface Processes & Landforms*, 25, 1387-1402.

Takken, I., Jetten, V., Govers, G., Nachtergaele, N. & Steegen, A. 2001. The effect of tillage-induced roughness on runoff and erosion patterns. *Geomorphology*, 37, 1-14.

Takken, I., Govers, G., Jetten, V., Nachtergaele, J., Steegen, A. & Poesen, J. 2005. The influence of both process descriptions and runoff patterns on predictions from a spatially distributed soil erosion model, *Earth Surface Processes & Landforms*, 30, 213-229.

Van Deursen, W.P.A. & Wesseling, C.G. 1992. *The PCRaster package*. Department of Physical Geography, Utrecht University, the Netherlands.

Van Wesemael, B., Poesen, J., de Figueiredo, T. & Govers, G. 1996. Effects of rock fragments on soil surface roughness evolution during rainfall. *Earth Surface Processes and Landforms*, 21, 399-411.

Wood J., 1996. *The geomorphological characterisation of digital elevation models* Unpublished PhD Thesis, Department of Geography, University of Leicester (http://www.soi.city.ac.uk/~jwo/phd/) Accessed 18 July 2005

Woolheiser, D.A. 2002. Infiltration and runoff on a hillslope. In Smith, R.E., Smettem, K.R.J., Broadbridge, P. & Woolhiser, D.A. *Infiltration Theory for Hydrologic Applications*, Water Reseources Monograph 15, AGU, Washington DC, 159-183.

Zhang, R. 1997. Determination of soil sorptivity and hydraulic conductivity from the disk infiltrometer, *Soil Science Society of America Journal*, 61, 1024-1030.

Zobeck, T.M. & Onstad, C.A. 1987. Tillage and rainfall effects on random roughness: a review. *Soil & Tillage Research*, 9, 1-20.

	MDS (mm)	*Detrended MDS (mm)*	*% flow downslope direction*	*% pit (PC Raster)*	*% not downslope (detrended)*	*Depressions Filled Max Upslope Area (%)*	*Depressions Filled % draining >1%*	*Max Upslope Area (%)*	*% draining >1%*	*Increase in Max Upslope Area (%)*	*Increase in %draining >1%*	*Mean Total Depth Infiltrated (cm)*	*Mean k (cmS^{-1})*	*Standard Deviation of Total Depth Infiltrated (cm)*	*Standard Deviation of k (cmS^{-1})*
Mean T_B down	$0.592^{\Diamond}$	-0.031	0.114	-0.141	0.478^{Δ}	-0.345	-0.328	0.074	0.035	-0.329	-0.220	0.184	0.168	0.471^{Δ}	-0.022
Sd of T_B Down	$0.589^{\Diamond}$	-0.085	0.008	-0.039	$0.505^{\square}$	-0.313	-0.418	0.012	-0.076	-0.267	-0.135	0.251	0.230	0.519	-0.009
Mean T_B across	$0.499^{\square}$	0.063	0.032	-0.103	$0.547^{\square}$	-0.257	-0.505	0.133	-0.058	-0.289	-0.204	0.186	0.155	0.407	-0.049
Sd of T_B across	0.319	0.045	0.001	-0.144	$0.562^{\square}$	-0.156	$-0.565^{\square}$	0.114	-0.076	-0.194	-0.215	0.158	0.162	0.227	-0.069
Mean T_B Comb	$0.543^{\square}$	0.022	0.068	-0.120	$0.521^{\square}$	-0.297	-0.432^{Δ}	0.108	-0.019	-0.309	-0.212	0.186	0.162	0.438^{Δ}	-0.038
Mean T_A down	0.470^{Δ}	0.126	0.258	-0.338	$0.498^{\square}$	-0.320	-0.277	0.215	0.187	-0.388	-0.376	0.047	0.054	0.281	-0.044
Mean T_A across	0.435^{Δ}	0.264	0.126	-0.230	$0.550^{\square}$	-0.211	$-0.505^{\square}$	0.274	0.024	-0.331	-0.303	0.035	0.021	0.253	-0.080
Mean T_A comb	0.450^{Δ}	0.212	0.192	-0.287	$0.535^{\square}$	-0.265	-0.403	0.255	0.105	-0.365	-0.345	0.037	0.032	0.262	-0.068
T_A down predicted MDS	0.481^{Δ}	0.112	0.243	-0.320	$0.499^{\square}$	-0.323	-0.285	0.202	0.172	-0.383	-0.362	0.060	0.065	0.297	-0.043
T_A across predicted MDS	0.441^{Δ}	0.251	0.117	-0.218	$0.552^{\square}$	-0.214	$-0.509^{\square}$	0.263	0.015	-0.327	-0.294	0.047	0.031	0.265	-0.079
T_A comb predicted MDS	0.458^{Δ}	0.198	0.179	-0.271	$0.537^{\square}$	-0.267	-0.410	0.243	0.091	-0.360	-0.333	0.050	0.043	0.276	-0.066
Detrended Mean T_B down	$0.593^{\Diamond}$	-0.044	0.068	-0.112	0.480^{Δ}	-0.307	-0.383	0.046	-0.024	-0.281	-0.179	0.195	0.185	0.468^{Δ}	-0.004
Detrended Sd of T_B Down	0.543	-0.077	-0.003	-0.053	$0.525^{\square}$	-0.295	-0.450^{Δ}	0.019	-0.082	-0.256	-0.146	0.247	0.235	0.476^{Δ}	-0.015
Detrended Mean T_B across	$0.498^{\square}$	0.064	0.031	-0.103	$0.547^{\square}$	-0.256	$-0.507^{\square}$	0.134	-0.060	-0.288	-0.203	0.186	0.155	0.406	-0.049
Detrended Sd of T_B across	0.325	0.043	0.002	-0.143	$0.562^{\square}$	-0.159	$-0.563^{\square}$	0.113	-0.076	-0.196	-0.214	0.160	0.163	0.232	-0.068
Detrended Mean T_B Comb	$0.536^{\square}$	0.024	0.045	-0.107	$0.525^{\square}$	-0.276	-0.463^{Δ}	0.101	-0.047	-0.287	-0.195	0.190	0.167	0.431^{Δ}	-0.032
Detrended Mean T_A down	$0.528^{\square}$	0.086	0.159	-0.242	0.487^{Δ}	-0.275	-0.362	0.138	0.061	-0.307	-0.270	0.084	0.090	0.333	-0.008
Detrended Mean T_A across	0.437^{Δ}	0.266	0.124	-0.227	$0.548^{\square}$	-0.209	$-0.506^{\square}$	0.274	0.020	-0.329	-0.299	0.036	0.022	0.254	-0.077
Detrended Mean T_A comb	0.473^{Δ}	0.205	0.140	-0.237	$0.531^{\square}$	-0.236	-0.454	0.226	0.038	-0.325	-0.292	0.054	0.045	0.284	-0.052
Detrended T_A down predicted MDS (m)	$0.535^{\square}$	0.074	0.148	-0.229	0.488^{Δ}	-0.278	-0.366	0.128	0.051	-0.304	-0.261	0.095	0.100	0.345	-0.009
Detrended T_A across predicted MDS (m)	0.442^{Δ}	0.253	0.115	-0.216	$0.550^{\square}$	-0.212	$-0.510^{\square}$	0.263	0.011	-0.326	-0.291	0.048	0.032	0.266	-0.076
Detrended T_A comb predicted MDS (m)	0.478^{Δ}	0.191	0.130	-0.224	$0.533^{\square}$	-0.239	-0.459^{Δ}	0.215	0.028	-0.321	-0.283	0.066	0.056	0.297	-0.051

Table A.1. Correlation matrix of profile tortuosity roughness measures and hydrological characteristics ($^{\Delta}$ = significant at 5 % level, $^{\square}$ = 2.5 % level, $^{\Diamond}$ = 1 % level, * = 0.5 % level and ** = 0.05 % level).

	MDS (mm)	*Detrended MDS (mm)*	*% flow downslope direction*	*% pit (PC Raster)*	*% not downslope (detrended)*	*Depressions Filled Max Upslope Area (%)*	*Depressions Filled % draining >1%*	*Max Upslope Area (%)*	*% draining >1%*	*Increase in Max Upslope Area (%)*	*Increase in %draining >1%*	*Mean Total Depth Infiltrated (cm)*	*Mean k (cmS^{-1})*	*Standard Deviation of Total Depth Infiltrated (cm)*	*Standard Deviation of k (cmS^{-1})*
Sd down (m)	0.013	0.210	0.699*	-0.756**	0.450$^{\Delta}$	-0.351	0.158	0.534$^{\square}$	0.737$^{\square}$	-0.595$^{\square}$	-0.805**	-0.076	-0.041	-0.020	-0.153
Sd across (m)	0.320	-0.118	-0.010	-0.161	0.622$^{\Diamond}$	-0.256	-0.497$^{\Delta}$	0.074	0.019	-0.255	-0.293	0.194	0.198	0.328	-0.098
Sd comb (m)	0.150	0.095	0.484$^{\Delta}$	-0.600	0.589$^{\Diamond}$	-0.358	-0.109	0.406	0.524$^{\square}$	-0.528$^{\square}$	-0.691*	0.032	0.059	0.131	-0.150
IQR down (m)	0.007	0.214	0.715*	-0.771**	0.421	-0.346	0.191	0.533$^{\square}$	0.752**	-0.590$^{\Diamond}$	-0.805**	-0.097	-0.056	-0.043	-0.146
IQR across (m)	0.371	-0.143	0.007	-0.136	0.573$^{\square}$	-0.308	-0.448$^{\Delta}$	0.060	0.019	-0.290	-0.266	0.229	0.232	0.374	-0.065
Detrended Sd (m)	0.375	-0.007	0.004	-0.144	0.648*	-0.150	-0.583$^{\Diamond}$	0.116	-0.069	-0.191	-0.233	0.221	0.186	0.364	-0.026
Detrended Sd down (m)	0.303	0.145	0.077	-0.235	0.613$^{\Diamond}$	-0.148	-0.538$^{\square}$	0.176	0.010	-0.223	-0.304	0.070	0.077	0.163	-0.094
Detrended Sd across (m)	0.392	-0.057	-0.021	-0.110	0.646*	-0.147	-0.589$^{\Diamond}$	0.092	-0.096	-0.175	-0.203	0.267	0.220	0.423	-0.004
Detrended IQR down (m)	0.308	0.111	0.071	-0.231	0.608$^{\Diamond}$	-0.156	-0.524$^{\square}$	0.147	0.008	-0.213	-0.294	0.077	0.089	0.167	-0.087
Detrended IQR across (m)	0.433$^{\Delta}$	-0.086	-0.039	-0.078	0.608$^{\Diamond}$	-0.183	-0.559$^{\square}$	0.062	-0.105	-0.188	-0.177	0.277	0.227	0.462$^{\Delta}$	-0.012
Pit Count Downslope	0.595$^{\Diamond}$	-0.001	-0.282	0.227	0.349	0.186	-0.758*	-0.212	-0.567$^{\square}$	0.275	0.274	0.171	0.165	0.378	0.137
Pit Density Downslope (m^{-1})	0.699*	0.022	-0.257	0.229	0.268	0.048	-0.607$^{\Diamond}$	-0.209	-0.505$^{\square}$	0.158	0.281	0.124	0.082	0.452$^{\Delta}$	0.171
Pit Count Cross-Slope	0.132	0.629*	0.162	-0.218	0.187	0.392	-0.412	0.358	-0.123	0.122	-0.075	-0.251	-0.192	-0.154	0.110
Pit Density Cross-Slope (m^{-1})	0.171	0.661*	0.241	-0.299	0.166	0.331	-0.374	0.432$^{\Delta}$	-0.034	0.030	-0.162	-0.288	-0.253	-0.145	0.096
Downslope root of SV at 0.5 m (m)	0.168	0.215	0.549$^{\square}$	-0.629*	0.546$^{\square}$	-0.359	-0.059	0.482$^{\Delta}$	0.555$^{\square}$	-0.573$^{\square}$	-0.702*	-0.015	-0.014	0.106	-0.122
Downslope root of SV at 1 m (m)	0.138	0.239	0.615$^{\square}$	-0.685*	0.479$^{\Delta}$	-0.375	0.057	0.513$^{\square}$	0.639*	-0.603$^{\square}$	-0.741*	-0.074	-0.057	0.055	-0.122
Cross-Slope root of SV at 0.5 m (m)	0.411	-0.023	0.023	-0.137	0.647*	-0.212	-0.543$^{\square}$	0.132	-0.032	-0.251	-0.256	0.230	0.177	0.421	-0.031
Cross-Slope root of SV at 1 m (m)	0.415	-0.151	0.013	-0.133	0.612$^{\square}$	-0.250	-0.482$^{\Delta}$	0.061	-0.009	-0.242	-0.251	0.255	0.230	0.441$^{\Delta}$	-0.028

Table A.2. Correlation matrix of profile standard deviation, pit density and semi-variance roughness measures and hydrological characteristics ($^{\Delta}$ = significant at 5 % level, $^{\square}$ = 2.5 % level, $^{\Diamond}$ = 1 % level, * = 0.5 % level and ** = 0.05 % level).

	MDS (mm)	*Detrended MDS (mm)*	*% flow downslope direction*	*% pit (PC Raster)*	*% not downslope (detrended)*	*Depressions Filled Max Upslope Area (%)*	*Depressions Filled % draining >1%*	*Max Upslope Area (%)*	*% draining >1%*	*Increase in Max Upslope Area (%)*	*Increase in %draining >1%*	*Mean Total Depth Infiltrated (cm)*	*Mean k (cmS^{-1})*	*Standard Deviation of Total Depth Infiltrated (cm)*	*Standard Deviation of k (cmS^{-1})*
Slope (%)	-0.003	0.328	0.724*	-0.776**	0.451^{Δ}	-0.300	0.151	0.627*	0.742*	$-0.605^{\Diamond}$	-0.814**	-0.097	-0.116	-0.021	-0.079
Elevation Range (m)	-0.042	0.116	$0.537^{\square}$	-0.673*	$0.554^{\square}$	-0.284	-0.078	$0.478^{\square}$	$0.619^{\Diamond}$	$-0.507^{\square}$	-0.790**	-0.067	-0.075	-0.043	-0.229
Elevation Sd (m)	0.020	0.222	$0.606^{\Diamond}$	-0.709*	$0.520^{\square}$	-0.336	0.022	$0.528^{\square}$	0.657*	$-0.579^{\Diamond}$	-0.781**	-0.059	-0.043	-0.004	-0.170
Elevation Variance (m^2)	0.071	0.180	0.497^{Δ}	$-0.560^{\square}$	$0.519^{\square}$	-0.407	0.004	0.425	$0.566^{\square}$	$-0.580^{\Diamond}$	-0.681*	-0.017	-0.031	0.036	-0.230
Detrended Elevation Sd (m)	0.315	-0.165	-0.209	-0.058	$0.523^{\square}$	-0.206	$-0.532^{\square}$	-0.021	-0.096	-0.160	-0.173	0.129	0.157	0.314	-0.128
Detrended Elevation Variance (m)	0.344	-0.195	-0.154	-0.032	$0.514^{\square}$	-0.224	$-0.526^{\square}$	-0.032	-0.127	-0.168	-0.133	0.243	0.252	0.365	-0.076
Mean NN (mm)	$0.578^{\Diamond}$	-0.093	0.048	-0.075	0.496^{Δ}	-0.285	-0.428^{Δ}	0.046	-0.054	-0.264	-0.167	0.258	0.217	$0.516^{\square}$	-0.008
Trim Mean NN (mm)	$0.611^{\Diamond}$	-0.047	0.100	-0.110	0.480^{Δ}	-0.284	-0.398	0.086	-0.019	-0.285	-0.194	0.224	0.171	$0.523^{\square}$	-0.004
NN Sd (mm)	$0.540^{\square}$	-0.146	-0.008	-0.036	$0.509^{\square}$	-0.283	-0.453^{Δ}	-0.002	-0.092	-0.234	-0.135	0.290	0.264	$0.506^{\square}$	-0.013
D	$0.540^{\square}$	0.165	0.102	-0.192	$0.539^{\square}$	-0.209	-0.486^{Δ}	0.161	-0.022	-0.266	-0.238	0.079	0.063	0.349	-0.020
Surface Tortuosity	$0.527^{\square}$	0.114	0.152	-0.221	$0.542^{\square}$	-0.277	-0.408	0.173	0.056	-0.329	-0.289	0.111	0.096	0.372	-0.047
Standard Deviation of Slope Angles (°)	0.445^{Δ}	0.398	0.374	-0.452^{Δ}	0.386	-0.129	-0.316	0.370	0.182	-0.317	-0.391	-0.142	-0.162	0.120	0.033
Plane (%)	0.217	-0.028	0.045	0.072	-0.023	-0.403	0.091	0.154	0.203	-0.423	-0.196	0.010	-0.267	0.231	-0.196
Channel (%)	-0.225	0.027	0.016	-0.136	0.045	0.356	-0.042	-0.123	-0.133	0.366	0.138	-0.002	0.287	-0.225	0.214
Ridge (%)	-0.212	0.034	-0.088	-0.035	0.014	0.442	-0.140	-0.166	-0.252	0.461^{Δ}	0.228	-0.024	0.245	-0.239	0.178
Pass (%)	0.124	-0.242	$-0.593^{\Diamond}$	0.891**	-0.460^{Δ}	0.246	-0.026	-0.659*	-0.721*	$0.579^{\Diamond}$	0.856**	0.179	0.077	0.093	-0.024
Peak (%)	0.111	-0.241	$-0.533^{\square}$	0.864**	-0.380	0.287	-0.075	-0.632*	-0.727*	$0.597^{\Diamond}$	0.838**	0.292	0.140	0.172	0.025
Pit (%)	0.104	-0.248	$-0.513^{\square}$	0.832**	-0.382	0.258	-0.029	-0.663*	-0.686*	$0.592^{\Diamond}$	0.812**	0.241	0.141	0.125	0.009

Table A.3. Correlation matrix of surface-based roughness measures and hydrological characteristics ($^{\Delta}$ = significant at 5 % level, $^{\square}$ = 2.5 % level, $^{\Diamond}$ = 1 % level, * = 0.5 % level and ** = 0.05 % level).